^{13}C AND ^{15}N LABELLING OF ALAMETHICIN AND ITS CONFORMATION IN METHANOL AND DETERGENT SOLUTION BY ^{13}C, ^{15}N, AND ^{1}H NMR SPECTROSCOPY

BY

ADELINDA A. YEE

A Thesis
Submitted to the Faculty of Graduate Studies
in Partial Fulfillment of the Requirements
for the Degree of

DOCTOR OF PHILOSOPHY

Department of Chemistry
University of Manitoba
Winnipeg, Manitoba

National Library
of Canada

Acquisitions and
Bibliographic Services Branch

395 Wellington Street
Ottawa, Ontario
K1A 0N4

Bibliothèque nationale
du Canada

Direction des acquisitions et
des services bibliographiques

395, rue Wellington
Ottawa (Ontario)
K1A 0N4

Your file *Votre référence*

Our file *Notre référence*

ISBN 0-612-13589-6

Canada

Name _____

Dissertation Abstracts International and *Masters Abstracts International* are arranged by broad, general subject categories. Please select the one subject which most nearly describes the content of your dissertation or thesis. Enter the corresponding four-digit code in the spaces provided.

CHEMISTRY

SUBJECT TERM

0487

SUBJECT CODE

UMI

Subject Categories

THE HUMANITIES AND SOCIAL SCIENCES

COMMUNICATIONS AND THE ARTS

- Architecture 0729
- Art History 0377
- Cinema 0900
- Dance 0378
- Fine Arts 0357
- Information Science 0723
- Journalism 0391
- Library Science 0399
- Mass Communications 0708
- Music 0413
- Speech Communication 0459
- Theater 0465

EDUCATION

- General 0515
- Administration 0514
- Adult and Continuing 0516
- Agricultural 0517
- Art 0273
- Bilingual and Multicultural 0282
- Business 0688
- Community College 0275
- Curriculum and Instruction 0727
- Early Childhood 0518
- Elementary 0524
- Finance 0277
- Guidance and Counseling 0519
- Health 0680
- Higher 0745
- History of 0520
- Home Economics 0278
- Industrial 0521
- Language and Literature 0279
- Mathematics 0280
- Music 0522
- Philosophy of 0998
- Physical 0523
- Psychology 0525
- Reading 0535
- Religious 0527
- Sciences 0714
- Secondary 0533
- Social Sciences 0534
- Sociology of 0340
- Special 0529
- Teacher Training 0530
- Technology 0710
- Tests and Measurements 0288
- Vocational 0747

LANGUAGE, LITERATURE AND LINGUISTICS

- Language
  - General 0679
  - Ancient 0289
  - Linguistics 0290
  - Modern 0291
- Literature
  - General 0401
  - Classical 0294
  - Comparative 0295
  - Medieval 0297
  - Modern 0298
  - African 0316
  - American 0591
  - Asian 0305
  - Canadian (English) 0352
  - Canadian (French) 0355
  - English 0593
  - Germanic 0311
  - Latin American 0312
  - Middle Eastern 0315
  - Romance 0313
  - Slavic and East European 0314

PHILOSOPHY, RELIGION AND THEOLOGY

- Philosophy 0422
- Religion
  - General 0318
  - Biblical Studies 0321
  - Clergy 0319
  - History of 0320
  - Philosophy of 0322
- Theology 0469

SOCIAL SCIENCES

- American Studies 0323
- Anthropology
  - Archaeology 0324
  - Cultural 0326
  - Physical 0327
- Business Administration
  - General 0310
  - Accounting 0272
  - Banking 0770
  - Management 0454
  - Marketing 0338
- Canadian Studies 0385
- Economics
  - General 0501
  - Agricultural 0503
  - Commerce-Business 0505
  - Finance 0508
  - History 0509
  - Labor 0510
  - Theory 0511
- Folklore 0358
- Geography 0366
- Gerontology 0351
- History
  - General 0578
  - Ancient 0579
  - Medieval 0581
  - Modern 0582
  - Black 0328
  - African 0331
  - Asia, Australia and Oceania 0332
  - Canadian 0334
  - European 0335
  - Latin American 0336
  - Middle Eastern 0333
  - United States 0337
- History of Science 0585
- Law 0398
- Political Science
  - General 0615
  - International Law and Relations 0616
  - Public Administration 0617
- Recreation 0814
- Social Work 0452
- Sociology
  - General 0626
  - Criminology and Penology 0627
  - Demography 0938
  - Ethnic and Racial Studies 0631
  - Individual and Family Studies 0628
  - Industrial and Labor Relations 0629
  - Public and Social Welfare 0630
  - Social Structure and Development 0700
  - Theory and Methods 0344
- Transportation 0709
- Urban and Regional Planning 0999
- Women's Studies 0453

THE SCIENCES AND ENGINEERING

BIOLOGICAL SCIENCES

- Agriculture
  - General 0473
  - Agronomy 0285
  - Animal Culture and Nutrition 0475
  - Animal Pathology 0476
  - Food Science and Technology 0359
  - Forestry and Wildlife 0478
  - Plant Culture 0479
  - Plant Pathology 0480
  - Plant Physiology 0817
  - Range Management 0777
  - Wood Technology 0746
- Biology
  - General 0306
  - Anatomy 0287
  - Biostatistics 0308
  - Botany 0309
  - Cell 0379
  - Ecology 0329
  - Entomology 0353
  - Genetics 0369
  - Limnology 0793
  - Microbiology 0410
  - Molecular 0307
  - Neuroscience 0317
  - Oceanography 0416
  - Physiology 0433
  - Radiation 0821
  - Veterinary Science 0778
  - Zoology 0472
- Biophysics
  - General 0786
  - Medical 0760

EARTH SCIENCES

- Biogeochemistry 0425
- Geochemistry 0996
- Geodesy 0370
- Geology 0372
- Geophysics 0373
- Hydrology 0388
- Mineralogy 0411
- Paleobotany 0345
- Paleoecology 0426
- Paleontology 0418
- Paleozoology 0985
- Palynology 0427
- Physical Geography 0368
- Physical Oceanography 0415

HEALTH AND ENVIRONMENTAL SCIENCES

- Environmental Sciences 0768
- Health Sciences
  - General 0566
  - Audiology 0300
  - Chemotherapy 0992
  - Dentistry 0567
  - Education 0350
  - Hospital Management 0769
  - Human Development 0758
  - Immunology 0982
  - Medicine and Surgery 0564
  - Mental Health 0347
  - Nursing 0569
  - Nutrition 0570
  - Obstetrics and Gynecology 0380
  - Occupational Health and Therapy 0354
  - Ophthalmology 0381
  - Pathology 0571
  - Pharmacology 0419
  - Pharmacy 0572
  - Physical Therapy 0382
  - Public Health 0573
  - Radiology 0574
  - Recreation 0575
  - Speech Pathology 0460
  - Toxicology 0383
- Home Economics 0386

PHYSICAL SCIENCES

Pure Sciences

- Chemistry
  - General 0485
  - Agricultural 0749
  - Analytical 0486
  - Biochemistry 0487
  - Inorganic 0488
  - Nuclear 0738
  - Organic 0490
  - Pharmaceutical 0491
  - Physical 0494
  - Polymer 0495
  - Radiation 0754
- Mathematics 0405
- Physics
  - General 0605
  - Acoustics 0986
  - Astronomy and Astrophysics 0606
  - Atmospheric Science 0608
  - Atomic 0748
  - Electronics and Electricity 0607
  - Elementary Particles and High Energy 0798
  - Fluid and Plasma 0759
  - Molecular 0609
  - Nuclear 0610
  - Optics 0752
  - Radiation 0756
  - Solid State 0611
- Statistics 0463

Applied Sciences

- Applied Mechanics 0346
- Computer Science 0984
- Engineering
  - General 0537
  - Aerospace 0538
  - Agricultural 0539
  - Automotive 0540
  - Biomedical 0541
  - Chemical 0542
  - Civil 0543
  - Electronics and Electrical 0544
  - Heat and Thermodynamics 0348
  - Hydraulic 0545
  - Industrial 0546
  - Marine 0547
  - Materials Science 0794
  - Mechanical 0548
  - Metallurgy 0743
  - Mining 0551
  - Nuclear 0552
  - Packaging 0549
  - Petroleum 0765
  - Sanitary and Municipal 0554
  - System Science 0790
- Geotechnology 0428
- Operations Research 0796
- Plastics Technology 0795
- Textile Technology 0994

PSYCHOLOGY

- General 0621
- Behavioral 0384
- Clinical 0622
- Developmental 0620
- Experimental 0623
- Industrial 0624
- Personality 0625
- Physiological 0989
- Psychobiology 0349
- Psychometrics 0632
- Social 0451

^{13}C AND ^{15}N LABELLING OF ALAMETHICIN AND ITS CONFORMATION IN METHANOL AND DETERGENT SOLUTION BY ^{13}C, ^{15}N, AND ^{1}H NMR SPECTROSCOPY

BY

ADELINDA A. YEE

A Thesis submitted to the Faculty of Graduate Studies of the University of Manitoba in partial fulfillment of the requirements of the degree of

DOCTOR OF PHILOSOPHY

THESIS RECORD SHEET

Page Numbers 330

Name **YEE, ADELINDA A.**

Address

Expected Graduation Date **May/96**

Degree Ph.D.

(or practicum)

Title of Thesis:

"^{13}C and ^{15}N LABELLING OF ALAMETHICIN AND ITS CONFORMATION IN METHANOL AND DETERGENT SOLUTION BY ^{13}C, ^{15}N, AND ^{1}H NMR SPECTROSCOPY"

(Examiners and their Departments)

Advisor Dr. J. O'Neil Department: Chemistry

Dr. T. Schaefer

Dr. F. Hruska

Dr. J. Peeling - Department of Pharmacology & Therapeutics

External Examiner: Dr. Lan Lee
Department of Chemistry & Biochemistry
University of Windsor
Windsor, ON N9B 3P4

External's copy Distributed by student

Received: January 22, 1996 Copies 3 Sent: January 22, 1996

Reported Approved

Sent to Library

Acknowledgements

I would like to thank my research supervisor, Dr. Joe O'Neil, for financial assistance, advice, and discussions regarding my research. I would like thank the members of my Ph.D. advisory and examining committee, Dr. Frank Hruska, Dr. Jim Peeling, and Dr. Ted Schaefer for their advice and suggestions on some NMR experiments and for taking time to read my lengthy thesis. I would like to thank my external examiner, Dr. Lana Lee of the University of Windsor, Ontario for reading my thesis.

I would like to thank Mr. Terry Woloweic for the generous NMR times and for maintaining the spectrometer in top shape; Dr. Kirk Marat for his help in some of my NMR experiments; Dr. Leo Spyracopoulos for discussions on NMR and alamethicin; Dr. Tony Secco for lending us the autoclave; Dr. Frank Hruska for lending us the freeze dryer; and Dr. Harry Duckworth for letting us use their HPLC.

I would also like to thank all the members of Dr. O'Neil's laboratory, past and present, for making this laboratory a fun place to work in; Ayeda Ayed for all her help and friendship; and Dr. Lynda Donald for all the personal advice she gave and her friendship.

Finally, I thank my family, especially Aday and Benny, for their love, encouragement, and phone calls which make living in Winnipeg by myself easier to bear and their financial help which made my coming and staying in Canada possible.

ABSTRACT

Alamethicin is a 20 amino acid peptide secreted by the fungus *T. viride*. Methods were developed to label uniformly the peptide with ^{15}N and ^{13}C by growing *T. viride* in a basal medium containing $K^{15}NO_3$ and $^{13}C_6$-glucose as the nitrogen and carbon sources, respectively. The percentages of isotopic labelling were determined using spin echo difference spectroscopy, and were found to be 90% and 51% for ^{15}N and ^{13}C, respectively.

The previously unassigned ^{13}C nuclear magnetic resonances of carbons with no attached protons in alamethicin dissolved in methanol were assigned using ^{13}C-^{15}N correlation spectroscopy. The $^{1}H_{\alpha}$, $^{13}C_{\alpha}$, and $^{13}C'$ chemical shifts suggest that alamethicin is helical in methanol from Aib 1 up to Gly 11 and from Aib 13 up to Gln 19. It is suggested that the Gly 11/Leu 12 segment forms a flexible hinge joining the two helices and that Phol 20 is in an extended conformation. No intermolecular H_N-to-H_N nuclear Overhauser effects (nOe) were observed between ^{15}N-labelled and unlabelled peptide, suggesting that alamethicin exists as a monomer in methanol. The sensitivity of the carbonyl chemical shift to dimethyl sulfoxide concentration appeared to depend upon the hydrogen bonding state of the carbonyl and revealed that Aib 10 and Gly 11 in the middle of the peptide and the four residues at the C-terminus interact with the solvent. Measurements of $^{1}J_{C'N}$ revealed hydrogen bonding with solvent at residues 1 and

19 at the ends of the peptide and at Gly 11. A large one-bond deuterium isotope shift on the ^{15}N resonance of Aib 1 was observed. Taken together with the $^{1}J_{C'N}$ measurements, the one-bond deuterium isotope shift supports the thesis that intramolecular hydrogen bonds in proteins and peptides are weaker than hydrogen bonds to water and methanol. The strong correlation between the structure of crystalline alamethicin and that in methanol solution is noted. The remarkable stability of the peptide is confirmed in a temperature titration of the carbonyl chemical shift. Measurements of $^{3}J_{NH\alpha}$, as indicators of backbone ψ angles, did not correlate well with other indicators of backbone conformation such as $^{3}J_{HNH\alpha}$. Conformational flexibility and an unconfirmed Karplus relationship between $^{3}J_{NH\alpha}$ and ψ angle are offered as possible explanations.

The ^{1}H, ^{15}N, and ^{13}C nuclear magnetic resonances of alamethicin in sodium dodecyl sulfate (SDS) solution were assigned using heteronuclear multidimensional experiments. The nOe- and $^{3}J_{HNH\alpha}$-restrained distance geometry/simulated annealing-calculated structures of alamethicin in SDS solution converged to a common conformation from Aib 3 to Aib 10. The C-terminal half of the peptide did not converge to a common conformation, perhaps due to a lack of constraints; medium range nOes suggestive of a helical conformation were observed in the C-terminal part of the peptide. The $^{1}H_{\alpha}$ and $^{13}C_{\alpha}$ chemical shifts suggest that alamethicin in SDS solution is helical from Aib 1 to Gly 11 and from Aib 13 to Phol 20.

The Leu 12 conformation is undetermined due to a lack of consensus in the $^{1}H_{\alpha}$ and $^{13}C_{\alpha}$ chemical shifts. pH-dependent amide hydrogen exchange of alamethicin in SDS solution suggests that all amide hydrogens except Aib 1 are hydrogen bonded. The data also suggest that the Leu 12- Aib 16- Phol 20 face of the C-terminal α-helix of alamethicin interacts with the surface of the SDS micelle. The conformation of alamethicin in SDS solution is consistent with a voltage-gating model that involves reorientation of helical rods upon application of voltage similar to that originally proposed by Latorre and Alvarez (1981).

Table of Contents page

List of Symbols and Abbreviations

δ : chemical shift

$^2\Delta$: two bond deuterium isotope effect

ϕ, ψ, χ, ω: dihedral angles in the peptide bonds. Refer to Appendix C for nomenclature

γ : magnetogyric ratio

σ : isotopic shielding

σ_{ij} : cross relaxation rates

ρ_i : spin lattice relaxation rates

τ_{ij} : rotational correlation time of the interproton vector between i and j

τ_m : mixing time

ω_o : Larmor frequency

A : magnetization matrix

A : alanine

Ac : acetyl

AChR : acetylcholine receptor

Aib : α-aminoisobutyric acid

ATP : adenosine triphosphate

avg : average

B : α-aminoisobutyric acid

BPTI : basic pancreatic trypsin inhibitor

BSA : bovine serum albumin

CSI : chemical shift index

DG/SA : distance geometry/ simulated annealing

DMSO : dimethylsulfoxide

DQF-COSY : two dimensional Double Quantum Filtered Correlation Spectroscopy

DSS : 2,2-dimethyl-2-silapentane-5-sulfonate

E : hydrogen bond enthalpy

E. COSY : Exclusive Correlation Spectroscopy

EDAC : 1-ethyl-3-(3-dimethylaminopropyl)carbodiimide·HCl

FTIR : fourier transform infrared spectroscopy

Gd[DTPA] : gadolinium(III) diethylenetriaminepentaacetate

GIAO : gauge including atomic orbital

Gln : glutamine

G : glycine

Gly : glycine

h : Planck's constant.

HMQC : two dimensional Heteronuclear Multiple Quantum Coherence Spectroscopy

HPLC : High performance liquid chromatography

HSQC : two dimensional Heteronuclear Single Quantum Correlated spectroscopy

IGLO : individual gauge for localized orbital

INEPT : insensitive nuclei enhancement polarization transfer

IR : infrared

J : spin-spin coupling constant

K : 1×10^3

kDa : kiloDalton

L : leucine

NMR : nuclear magnetic resonance

NOe : nuclear Overhauser effect

NOESY : two dimensional Nuclear Overhauser Effect Spectroscopy

O : phenylalaninol

OCD : oriented circular dichroism

P : proline

PF : protection factor

Phe : phenylalanine

Phol : phenylalaninol

Pro : proline

Q : glutamine

r_{ij} : distance between i and j

R : cross relaxation matrix

RMSD : root mean square deviation

ROESY : two dimensional Rotating Frame Overhauser Effect Spectroscopy

SEDS : Spin Echo Difference Spectroscopy

SDS : sodium dodecyl sulfate

THF : tetrahydrofuran

TOCSY : two dimensional Total Coherence Transfer Spectroscopy

V : valine

Val : valine

List of Figures page

List of Tables page

Chapter 1
Introduction

In multicellular organisms, individual cells are separated from each other by the cell membrane. The membrane is composed of two layers of phospholipids oriented with their polar hydrophilic heads exposed at the aqueous surface and the non-polar hydrocarbon tails buried in the interior. The membrane acts as a diffusional barrier between the intracellular and extracellular fluids. Transmission of messages among living cells has been described by Katz (1966) and more recently by Matthews (1991) and this will be briefly described here. The membrane of any cell is polarized because of the unequal distribution of ions inside and outside the cell and the ion-selective permeability of the membrane. The intracellular fluids generally have a higher concentration of $K^+_{(aq)}$ and large anions like proteins, amino acids, inorganic anions, etc. whereas the extracellular fluids have higher concentrations of $Na^+_{(aq)}$ and $Cl^-_{(aq)}$. The membrane is permeable only to small ions like $K^+_{(aq)}$ and $Cl^-_{(aq)}$, is less permeable to $Na^+_{(aq)}$, and is not permeable to large anions. The value of the net membrane potential is a balance between the equilibrium potentials of all the ions (e.g., $Na^+_{(aq)}$, $K^+_{(aq)}$, $Cl^-_{(aq)}$, etc.), depending on the relative permeability of these ions. The equilibrium potential (Nernst potential) of a permeate ion is the potential difference across the membrane when the diffusion of the ion along a concentration

gradient is balanced out by the accumulation of charge. The concentration gradient(s) across the membrane is maintained by a specialized sodium pump "fueled" by ATP (this is referred to as the Na^+-K^+-ATPase). A resting membrane is polarized with the inside of the cell being more negative than the outside. The ions permeate the membrane through aqueous holes referred to as ion channels. Ion channels are transmembrane proteins that can exist in at least two conformational states, open or closed. Ion channels can be classified into two, namely, ligand-gated and voltage-gated (Miller, 1992). Ligand-gated channels, as the name implies, are proteins that open to allow passage of ions across the membrane when they bind a ligand. An example of a ligand-gated channel is the acetylcholine receptor (AChR) found in the end plate membrane of the postsynaptic cell (these are the information-receiving cells in, say, muscles). Acetylcholine is one of the neurotransmitter substances released at the synaptic terminal of a neuron. When two molecules of acetylcholine bind to AChR, the AChR alters its conformation, the channel opens and allows the passage of $K^+_{(aq)}$ and $Na^+_{(aq)}$ into the cell thereby depolarizing the membrane.

Voltage-gated channels, on the other hand, are opened when a depolarization stimulus reaches the voltage threshold of the channel. Voltage-gated ion channels are involved in the propagation of the action potential along the length of the axon in a neuron. The molecular mechanism of voltage-

gating is not understood at present. Native voltage-gated ion channels are big proteins, around 365 kDa for the Na^+ channel, 429 kDa for the Ca^{++} channel. These channels usually consist of several subunits, 4 for the Na^+ and 5 for the Ca^{++} channel (Caterall, 1988; Stuhmer, 1991). Today, there are two approaches taken to study the molecular basis of voltage-gating; one is by site-directed mutagenesis of the native protein to find out which amino acids are responsible for which function and the other is by using small peptides, synthetic or natural, to reconstitute the channel (Stuhmer, 1991). Some of the natural peptides used as models for voltage-gated ion channels include gramacidin, mellitin, and alamethicin.

1.1 Alamethicin as Model for Voltage-Gated Ion Channel

Alamethicin is a 20 amino acid antibiotic peptide secreted by the fungus *Trichoderma viride*. Natural alamethicins are microheterogeneous because they are enzymatically produced as opposed to ribosomally produced. They contain the achiral amino acid α-aminoisobutyric acid (Aib). The sequences of the major components of natural alamethicins are: Ac-Aib-Pro-Aib-Ala-Aib-Ala (or Aib)-Gln-Aib-Val-Aib-Gly-Leu-Aib-Pro-Val-Aib-Aib-Gln (or Glu)-Gln-Phol, where Ac is acetyl and Phol is phenylalaninol. Another variation in the primary sequence found in the minor components of alamethicin includes the replacement of Aib with Val at residue 17 (Poppe-Schriemer, 1995). The voltage-

dependent ion conductance exhibited by alamethicin in lipid membrane was first reported by Mueller and Rudin (1968). Since then, several electrical conductance experiments have been reported and channel models have been suggested (see Figure 1-1). There are currently five channel models proposed for alamethicin: the helix-reorientation model of Latorre & Alvarez (1981); the funnel-like model of Fox and Richards (1982); the two-layered barrel model of Hall, et al. (1984); the helix dipole model of Mathew and Balaram (1983); and the helix flip-flop model of Boheim et al. (1983). Details of these models are described in the introduction to my M.Sc. thesis (Yee, 1991). All these models suggest a transmembrane, barrel-like channel in the open conducting state where each alamethicin molecule would be one stave in the barrel as opposed to a carrier that crosses the membrane, or "bracelet" structures stacked one on top of another. The barrel-stave model may be similar to the protein ion channels which are postulated to have several transmembrane helices arranged to form a barrel-like pore. The peptide models differ in their closed, non-conducting states. Knowledge of the structure of alamethicin in solution would provide some insight into the pre-conducting state of the channel which would be important for understanding the mechanism behind voltage-gating.

1.2 Structures of Alamethicin

The crystal structure of alamethicin was determined by Fox and Richards (1982) and its solution structure has been

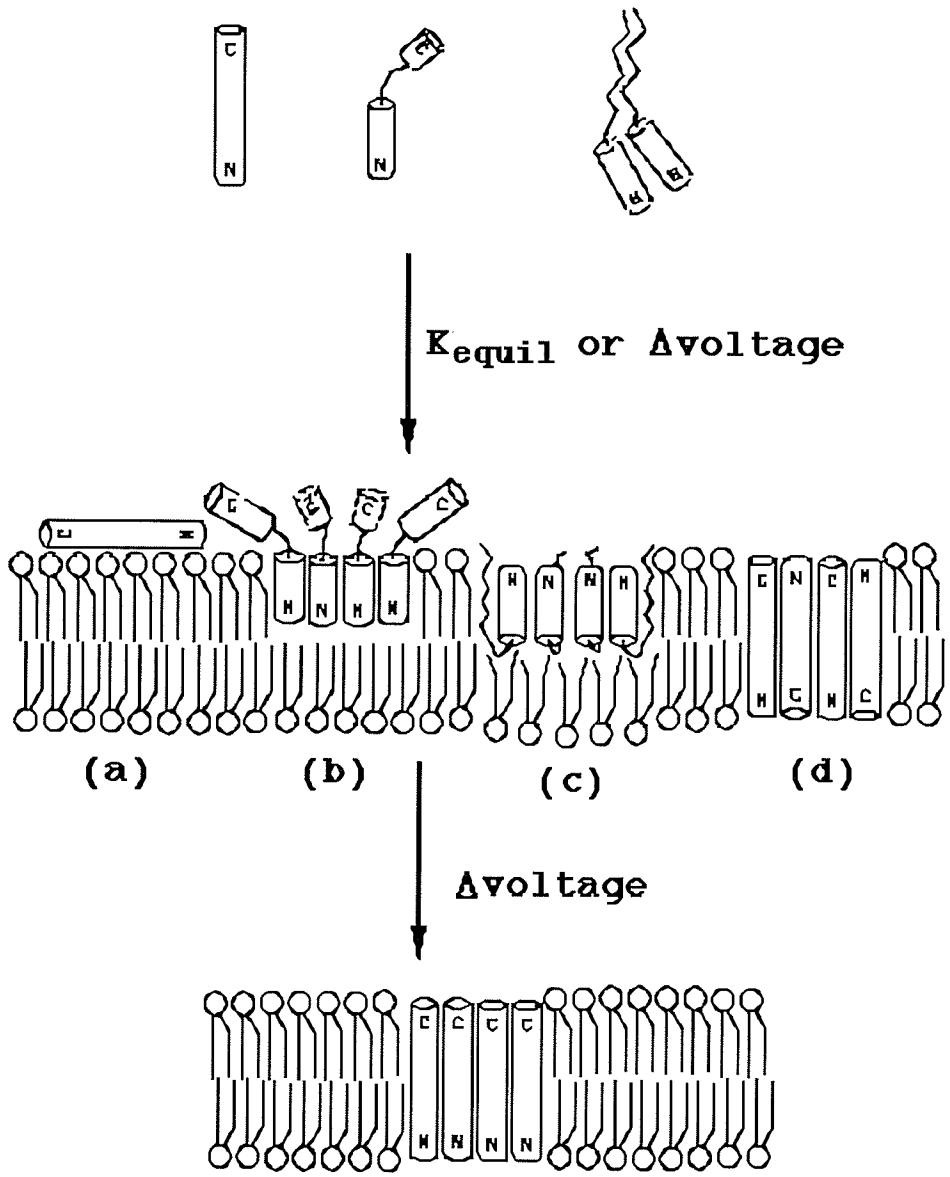

Figure 1-1: A cartoon of the proposed ion channel models for alamethicin. (a) Helix-reorientation model, (b) funnel-like model, (c) two-layered barrel, (d) helix flip-flop model. The helix-dipole model has the same structure as the open channel except that another molecule is clogging the channel.

studied using ^{1}H NMR spectroscopy by several groups. In the crystal (PDB file 1 AMT), there are three alamethicin molecules in the asymmetric unit existing in a predominantly α-helical conformation throughout their entire lengths and each helix axis is bent slightly to a different extent near the Pro 14 residue (Fox and Richards, 1982). The alamethicin was crystallized from a 90/10 acetonitrile/methanol solution. Based on the relaxation times of the N-terminal acetyl, Banerjee et al. (1983) suggested that alamethicin in methanol is a dimer. They proposed a structure in which residues 3 to 9 are in an α helical conformation, residues 10 to 14 are in an open non-hydrogen bonded conformation, and residues 15 to 20 are in an intermolecularly hydrogen bonded β-sheet conformation. Esposito et al. (1987) suggested, based on the NOESY experiment and coupling constants measured at -5°C, that the structure of alamethicin in methanol is as follows: residue 1 is in a non-helical conformation, residues 2 to 10 are in a regular helical structure, residues 11 to 13 are in a "tighter" helix making a bend from the main helical axis, residues 14 to 18 are in a helical conformation, and residues 19 to 20 are in an extended conformation. Our previous ^{1}H NMR study (Yee, 1991) suggested, based on the ROESY experiment and coupling constants, that the structure of alamethicin in methanol is as follows: residues 4 to 11 are in a helical conformation, residues 12, 15, and 18 are in a conformation that is neither α nor β, residues 19 to 20 are in an extended conformation, and residues 1 to 3 cannot be defined because

of lack of intraresidue nOe at the terminal and a lack of $^{3}J_{backbone}$ at these three residues. While the present work was in progress, Franklin et al. (1994) suggested that the structure of alamethicin in SDS detergent solution is as follows: residues 4 to 9 are in a helical conformation, residues 11 to 14 are in a flexible conformation forming a hinge, residues 14 to 18 are in a weakly helical conformation. This contrasts with their ^{13}C relaxation study of alamethicin in methanol in which they proposed a rigid helical rod (Kelsh et al., 1992).

1.3 Purpose of the Thesis

Each of the different NMR studies suggests a slightly different structure for alamethicin. The overall consensus is that residues 4 to 9 of the peptide are in a helical conformation; the terminals of the helix are difficult to determine using ^{1}H NMR alone because identification of a helix relies on medium range nOes, that is from residue i to i+3, sequential H_N and H_α nOes, and $^{3}J_{HNH\alpha}$. The absence of medium range nOes at the terminals is inherent in all peptides but the primary structure of alamethicin gave some added difficulty in determining its solution structure using ^{1}H NMR alone. The peptide has 8 α-aminoisobutyric acid residues which have α methyls in place of the usual α hydrogen found in the L-amino acids. The peptide also has 2 prolines which do not have amide hydrogens. These properties

reduce the number of measurable nOes and coupling constants ($^3J_{HNH\alpha}$).

The conformation of alamethicin in a membrane-mimetic environment in the absence of an applied voltage may add to our understanding of the mechanism of voltage-gating ion channels. The purpose of the work described herein was to label alamethicin with ^{13}C and ^{15}N, and to obtain ^{13}C and ^{15}N data to supplement the structural information from ^1H NMR. In addition, the structure of alamethicin in detergent solution was determined using ^1H NMR spectroscopy and hydrogen exchange chemistry.

Chapter 2
Isotopic Labelling of Alamethicin

2.1 Introduction

Isolation of alamethicin from the soil fungus *Trichoderma viride* was first reported by Meyer & Reusser (1967). Alamethicins are produced enzymatically in the fungal mycelia by a 480 kDa enzyme complex, alamethicin synthetase (Rindfleisch & Kleinkauf, 1976). This complex has been isolated and the synthesis of alamethicin *in vitro* from its components was monitored using ^{14}C-labelled amino acids (Rindfleisch & Kleinkauf, 1976).

In the early years of the study of alamethicin, its primary structure was in dispute. In efforts to determine its true primary structure, several groups synthesized alamethicin using the solution phase method (Schmitt & Jung, 1985; Slomczynska et al., 1992; Balasubramanian et al., 1981) and the solid phase method (Gisin et al., 1981).

The incorporation of ^{14}C-labelled amino acids in the *in vitro* studies clearly suggests that the same method can be used to label alamethicin with ^{13}C. Chemical synthesis can also be used to label alamethicin with ^{13}C. However, no ^{13}C- or ^{15}N-labelled Aib is commercially available at present and purified ^{13}C-labelled amino acids are expensive, making labelling of alamethicin by these methods very costly.

An alternative to these approaches would be to label the peptide using *in vivo* methods. *In vivo* labelling of proteins

involves growing the organism in medium containing simple carbon and nitrogen sources. For organisms which fail to grow or produce the desired protein on minimal defined media, cloning of the gene in *E. coli* is an alternative since some *E. coli* strains are able to grow on glucose or acetate (Venters et al., 1991). Both of these are commercially available in ^{13}C-labelled form. In the case of alamethicin, it can not be expressed in *E. coli* because it is enzymatically produced, i.e., there is no mRNA template for the peptide. Other organisms capable of growing on minimal media are the *Anabaena* sp. (blue green algae). Using $^{13}CO_2$ or $NaH^{13}CO_3$ and these organisms provide the least expensive source of labelled amino acids (Sailer et al., 1993).

The original complex Upjohn medium for *T. viride* uses molasses and dextrin as the main carbon source, and fishmeal and pharmamedia as the nitrogen source. Brewer et al. (1987) systematically studied the fermentation conditions for *T. viride* and were able to define a minimal medium for *T. viride* consisting of vitamins and mineral supplements (for the list see the Methods section), KNO_3 or/and amino acids as the nitrogen source, and carboxymethyl cellulose as the carbon source. This allowed us to label alamethicin with ^{15}N using $K^{15}NO_3$ although we had to use dextrin as carbon source (Yee, 1991; Yee & O'Neil, 1992). ^{13}C-Labelled carboxymethyl cellulose and dextrin are commercially unavailable, so ^{13}C labelling of alamethicin is not as straightforward as ^{15}N labelling.

Trichoderma spp. belongs to the Division *Amastigomycota*, and the Form-Subdivision *Deuteromycotina*. They are referred to as *Deuteromycetes* or formerly as the *Fungi Imperfecti*. *Deuteromycetes*, together with *Ascomycetes* and *Basidiomycetes*, are saprophytes in their natural environment. They are able to decompose cellulose, occurring abundantly in plant cell walls, by excreting cellulases that hydrolyze cellulose extracellularly into disaccharide units and then to glucose. The simpler sugars are then absorbed by the cells (Moore-Landeker, 1990). Since *T. viride* is able to grow on carboxymethyl cellulose, an alternative way of labelling alamethicin would be to grow the fungus in a ^{13}C-labelled glucose medium.

2.2 Determination of Extent of Isotopic Labelling by NMR Spectroscopy.

The common way to determine the extent of isotopic labelling by NMR spectroscopy is to use the Spin Echo Difference Spectroscopy (SEDS) experiment as suggested by Griffey et al. (1985). In each SEDS experiment, two spectra are acquired according to the pulse sequences given in Figure 2-1. In the spectrum from the first pulse sequence, all protons are of the same phase, while in the spectrum from the second pulse sequence, the protons bound to ^{13}C are antiphase to those bound to ^{12}C and nitrogen because of the 180° flip pulse applied to ^{13}C. The difference spectrum between the first and second spectra gives the ^{13}C-bound protons because

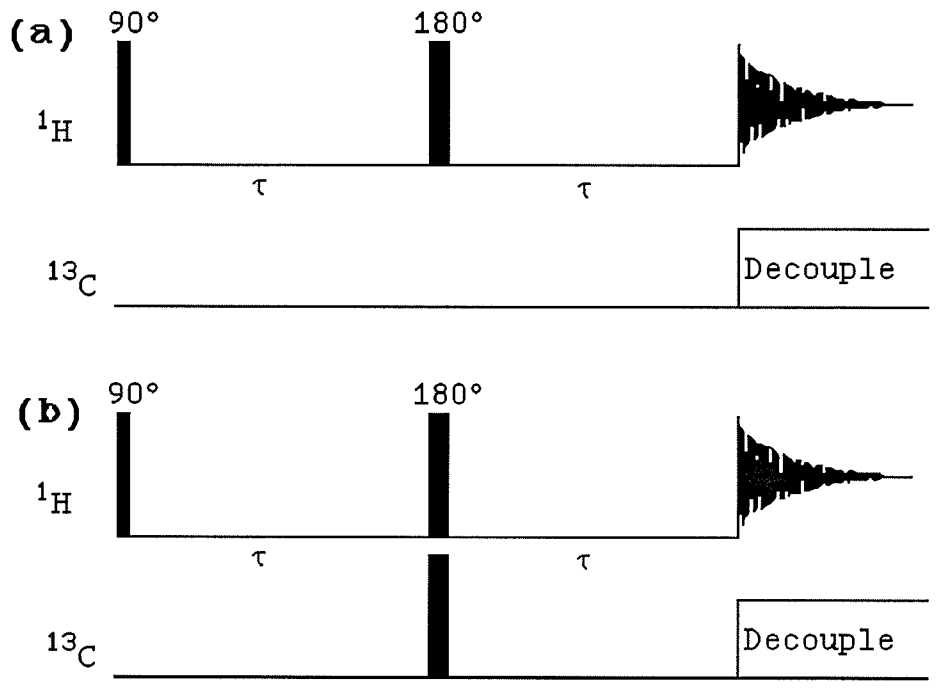

Figure 2-1: Pulse sequence for Spin Echo Difference Spectroscopy (SEDS) as suggested by Griffey et al. (1985).

the ^{12}C- and nitrogen-bound protons cancel out. The sum spectrum gives the ^{12}C- and nitrogen-bound protons as the ^{13}C-bound protons cancel out.

2.3 Experimental Procedures

2.3.1 Materials

Trichoderma viride (NRRL 3199) was purchased from the American Type Culture Collection (USA), catalogue number 38631. *T. viride* was grown on various media containing glucose, sucrose, and KNO_3 (all obtained from Fisher Scientific Co., USA), and dextrin (Matheson, Coleman and Bell, USA). All the vitamins added to the minimal medium were

purchased from Sigma Chemical Co., USA. The salts and minerals added to the minimal medium were NaCl; $CaCl_2$; $ZnSO_4 \cdot 7H_2O$; NH_4MoO_4 (all obtained from Fisher Scientific Co., USA); $CuSO_4 \cdot 5H_2O$; $MnSO_4 \cdot H_2O$; Boric acid (from Mallinckrodt, Missouri, USA) and $FeSO_4 \cdot nH_2O$ (from Science Borealis Ltd., Ontario, Canada).

$K^{15}NO_3$ (99% atom) and D-glucose-$^{13}C_6$ (98% atom) purchased from Cambridge Isotope Laboratories (Massachusetts, USA) were used in the labelling of the peptides. The NMR solvents used were CD_3OD, CD_3OH, and D_2O (from Aldrich Chemical Co., Wisconsin, USA). 2,2 Dimethyl-2-silapentane-5-sulfonate (DSS) from Sigma Chemical Co., Missouri, USA was used as an internal reference for ^1H NMR spectra. $^{15}NH_4Cl$ (99.5% atom) from Isotec Inc., Ohio, USA was used as an external reference for ^{15}N NMR spectra.

2.3.2 Methods

2.3.2.1 ^{13}C- and ^{15}N-Labelling of Alamethicin

^{15}N-Labelling of alamethicin was accomplished by using $K^{15}NO_3$ as the nitrogen source in the semi-basal medium (see Yee (1991) for a more detailed description of this medium). The ^{13}C-labelling required some modification of the medium because the carbon source in the semi-basal medium is dextrin, a complex carbohydrate.

In modifying the medium, the semi-basal medium was used as a control medium. The minimal medium consists of glucose (1 g), KNO_3 (0.125 g), vitamins and minerals solution (2.5

Table 2-1: List of ingredients and the amount added to make the vitamins and minerals solution. Water was added to make 1 L of solution.

NaCl	2.00	g
$CaCl_2$	2.00	g
$CuSO_4 \cdot 5H_2O$	7.86	mg
Boric acid	1.14	mg
NH_4MoO_4	0.74	mg
$Mn_2SO_4 \cdot H_2O$	1.22	mg
$ZnSO_4 \cdot 7H_2O$	0.18	g
$FeSO_4 \cdot nH_2O$	0.02	g
Biotin	200	µg
Thiamine·HCl (Vit B_1)	2.00	mg
Niacin (Nicotinic Acid)	2.00	mg
Ca Pantothenate	2.00	mg
Riboflavin	2.00	mg
Pyridoxine (Vit B_6)	2.00	mg
Folic Acid	2.00	mg
4-Aminobenzoic acid	1.00	mg
Vitamin B_{12}	80.0	µg
Inositol	60.0	mg

mL), and water to give a total volume of 50 mL. The vitamins and minerals solution was prepared by mixing the ingredients listed in Table 2-1. The pH of the solution was not adjusted. The solution is clear after sterilization.

The inoculum was a piece of agar with dense fungal growth (1 cm x 1 cm) or a fungal spore dispersion in water. A spore dispersion in water was prepared by putting 1 to 3 mL of sterile water onto a petri dish with dense fungal growth and the surface of the agar was swept with the aid of a sterile glass rod. The spore dispersion would look greenish. The inoculated medium was incubated at 25°C and shaken at 75 rpm. It took 50 days before the solution turned light brown indicating the culture is ready for harvesting (Yee, 1991). This compares with 15 days for the control medium. No growth was observed in medium inoculated with spore dispersions. All solutions were harvested after 50 days. In the ^{13}C-labelling experiment, $^{13}C_6$-glucose (0.5 g) was substituted for unlabelled glucose in the medium and the inoculum used was the solid mass of fungus grown in the medium containing unlabelled glucose instead of starting from a new piece of agar inoculum.

2.3.2.2 Purification of Alamethicin

The solid mass of fungus was removed from the medium using a sterile inoculating stick if it was needed to inoculate the next medium; otherwise the fungus was filtered and washed with a small amount of water. The filtrate was then acidified to pH 4.5 using dilute HCl solution. This was then diluted with 100 mL methanol and extracted with 100 mL and then 50 mL of chloroform. The methanol-chloroform-water mixture was shaken and the phases allowed to separate. The

chloroform-methanol phase was collected and evaporated in a rotary evaporator (Buchi Rotavapor RE111). Liquid that had not evaporated was transferred to a freeze-drying flask, the rotary evaporator flask was rinsed with a small amount of methanol and the methanol solution was transferred to the same freeze-drying flask.

The extract was partially air dried to remove the methanol and then was freeze dried (Virtis Lyophilizer, New York) at -56°C and <700 millitorr. The lyophilized solid was off-white in color. The lyophilized solid was dissolved in methanol and centrifuged to remove the undissolved particles and then was purified by HPLC (Perkin Elmer, USA). A reverse phase column (Beckman Ultrasphere 5 μ, 10 mm x 15 cm) was used and the detector was set to 210.6 nm. The eluting solvents were similar to those used by Balasubramanian et al. (1981): the mobile phase A was 0.05 N acetic acid adjusted to pH 3.5 with triethylamine and the mobile phase B was a mixture of tetrahydrofuran (THF), acetonitrile, and mobile phase A in a ratio of 8:1:2, respectively. The HPLC solvent gradient is shown in Table 2-2.

Eluates from several HPLC runs were collected and organic solvents were evaporated from the pooled eluates by blowing air into the solution. When most of the volatile organic solvents had evaporated, the remaining solution was freeze dried. The alamethicin yield was approximated from the height of the HPLC peak as follows: Crude alamethicin from a 50 mL culture was dissolved in 1 mL of methanol and a 50 μL

Table 2-2: Solvent program used in the HPLC purification of crude alamethicin.

Step	time (min)	flow (mL/min)	flow* gradient	percentage solvent A	B	solvent methanol	solvent* gradient
equil.	20	1.0	0	60	40	0	0
1	5	2.0	0	60	40	0	0
2	5	1.0	1	51	49	0	1
3	15	1.0	0	51	49	0	0
4	5	1.5	0	0	100	0	0
5	5	2.0	0	0	0	100	0

* Gradient of 0 means no gradient was used while a gradient of 1 means a linear gradient was used.

aliquot of this solution was diluted to 1 mL with methanol. 400 µL of the final crude solution gave an HPLC peak height of 8.7 cm which is approximated at 45 µg of alamethicin (see Figure 9 of Yee (1991) for the calibration curve). This gave a total yield of 2.25 mg alamethicin per 50 mL of minimal medium. The control medium gave a yield of 16 mg alamethicin per 50 mL semi-basal medium.

2.3.2.3 NMR Spectroscopy

NMR samples were prepared by dissolving alamethicin in 0.6 to 0.8 mL of CD_3OD or CD_3OH. All NMR spectra were acquired on a Bruker AMX500 NMR spectrometer and ^2H was used to lock

the spectrometer. The SEDS experiments (Griffey et al., 1985) were done using a 5 mm inverse broadband probehead with the inner coil tuned to ^{1}H and the outer coil tuned to ^{13}C. One dimensional ^{13}C observe spectra were done using a 5 mm triple resonance probehead with the inner coil tuned to ^{1}H and the outer coil tuned to ^{15}N and ^{13}C. All ^{1}H decoupling was done using WALTZ-16 composite pulse decoupling (Shaka et al., 1983), and ^{13}C and ^{15}N decoupling were done using the GARP sequence (Shaka et al., 1985), unless otherwise stated in the figure legends. Other acquisition and processing parameters are given in the figure legends.

2.4 Results

The HPLC chromatogram of the crude alamethicin extracted from the ^{13}C-labelled glucose-containing medium is shown in Figure 2-2 and it is similar to the one from the dextrin-containing medium (Yee, 1991). This suggests that the number and types of alamethicin components produced by *T. viride* are unaffected by the lack of dextrin. However, the total alamethicin yield, in the absence of dextrin, was only about 14% of the dextrin-containing medium suggesting that the fungi do not grow as well in the absence of a solid carbon source.

The fully coupled ^{1}H NMR spectrum of the extracted alamethicin in CD_3OD is shown in Figure 2-3. The alamethicin studied corresponds to the fraction containing Ala at residue 6 and Gln at residue 18. The peaks at ~1.5 ppm corresponding

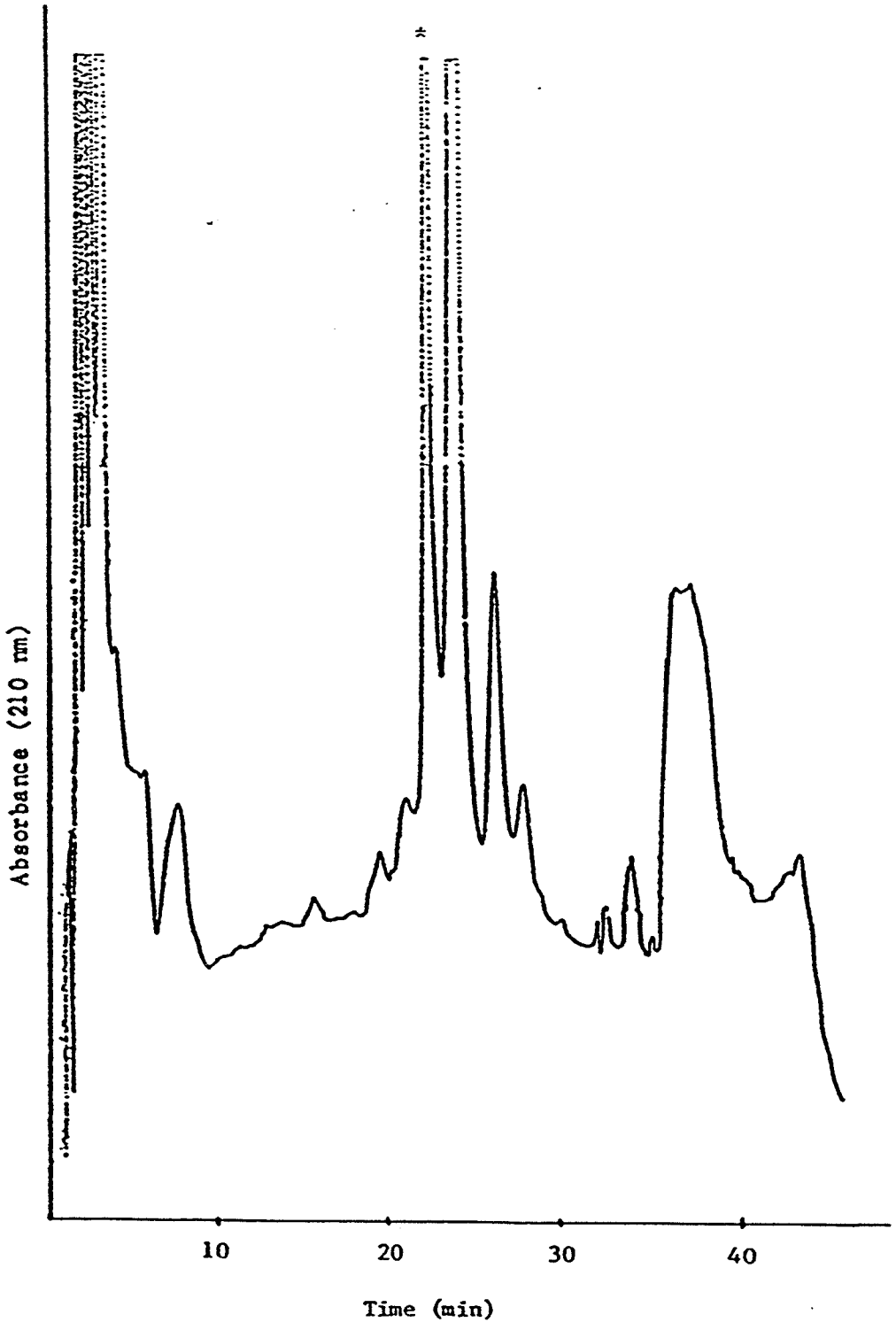

Figure 2-2: HPLC chromatogram of the crude alamethicin. The peak marked with * was isolated and used for subsequent studies. The HPLC solvents and gradient elution are given in the text.

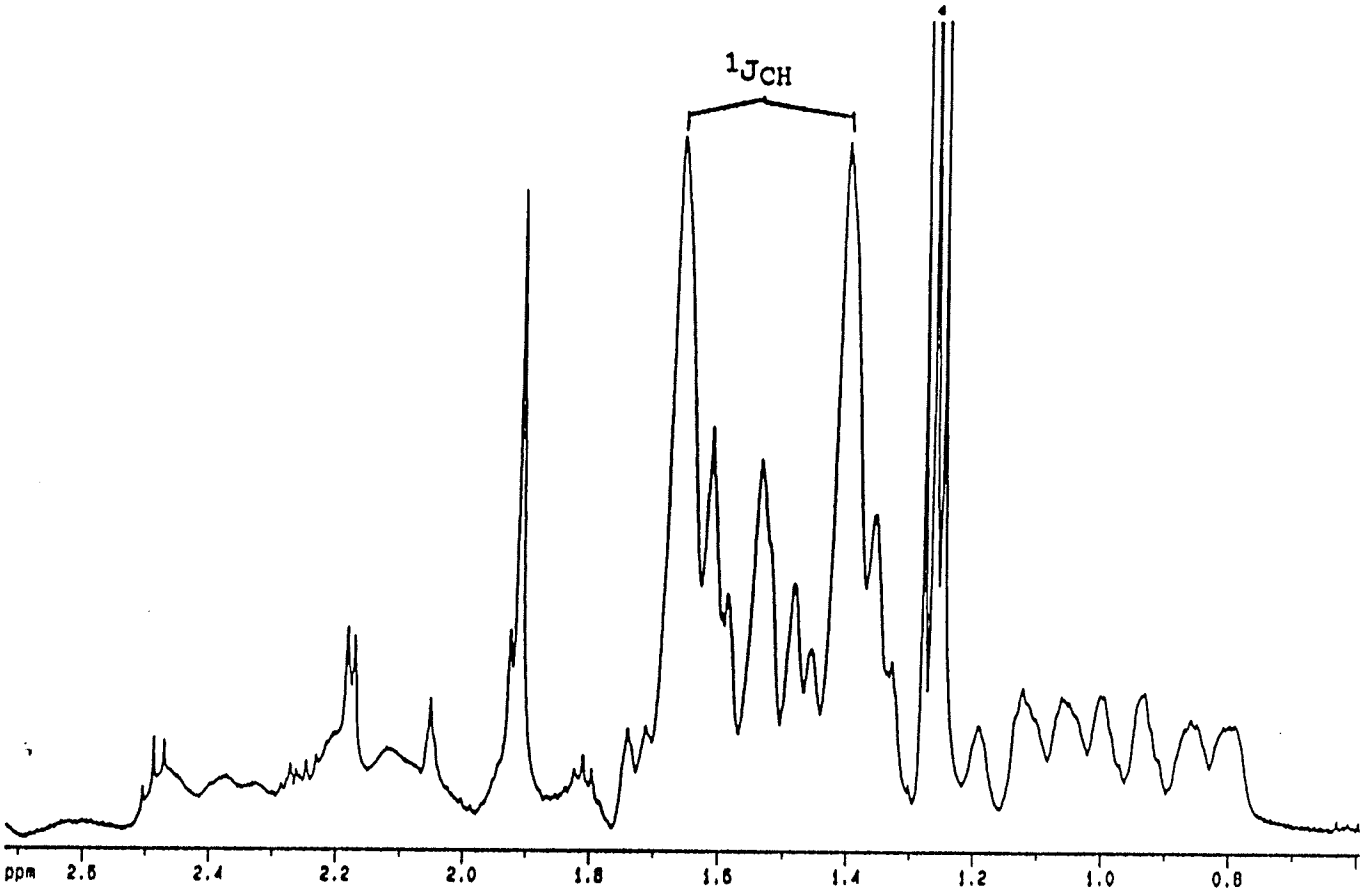

Figure 2-3: β methyl region of the ^1H NMR spectrum of approximately 1 mM ^{13}C-^{15}N labelled alamethicin in CD_3OD. 16K data points were acquired and zero filled to 32K; the total number of scans was 256. The peak marked with * is an impurity from the HPLC eluant.

to the methyl resonances of the α-aminoisobutyric acid and alanine residues are split by 128 Hz. The same splitting is observed on the peaks of the phenyl ring protons of the C-terminal phenylalaninol. This separation is due to the $^{1}J_{13C-1H}$ coupling indicating that the fungus has incorporated ^{13}C into the peptide. The 90 Hz splitting of the amide proton resonances (not shown) also indicates the incorporation of ^{15}N into the peptide. The ^{15}N incorporation is also evident in the carbonyl ^{13}C spectra acquired with and without ^{15}N decoupling (Figure 2-4 b and c). The fully coupled carbonyl ^{13}C spectrum of alamethicin in CD_3OD is shown in Figure 2-4a. This spectrum shows two groups of poorly-resolved resonances at low field and some better resolved resonances to high field. When protons are decoupled, the resonances appear as doublets of doublets in Figure 2-4b. The smaller separation of 15 Hz corresponds to the $^{1}J_{15N-13C}$ coupling confirming that the peptide is labelled with ^{15}N. When both ^{1}H and ^{15}N are decoupled, the peaks collapse into doublets separated by 53 Hz and a smaller peak in the middle. This is clearly seen at the 174 ppm peak in Figure 2-4c. The 53 Hz separation is the typical $^{1}J_{13C-13C}$ coupling and the small peak is due to the carbonyl carbons that do not have a neighboring ^{13}C.

The extent of ^{13}C incorporation was measured using the SEDS experiment (Griffey et al., 1985). Figure 2-5 shows some of the regions of the SEDS spectra. The percentage of ^{13}C labelling for alamethicin was found by integrating the peak areas to be 51% to 57%.

Figure 2-4: ^{13}C carbonyl spectra of alamethicin in CD_3OD (a) without decoupling (b) with ^{1}H decoupling (c) with ^{1}H and ^{15}N decoupling. The spectra were acquired with a spectral width of 1400 Hz, 4K data points and were zero filled to 32K; total number of scans was 1024. No window function was applied.

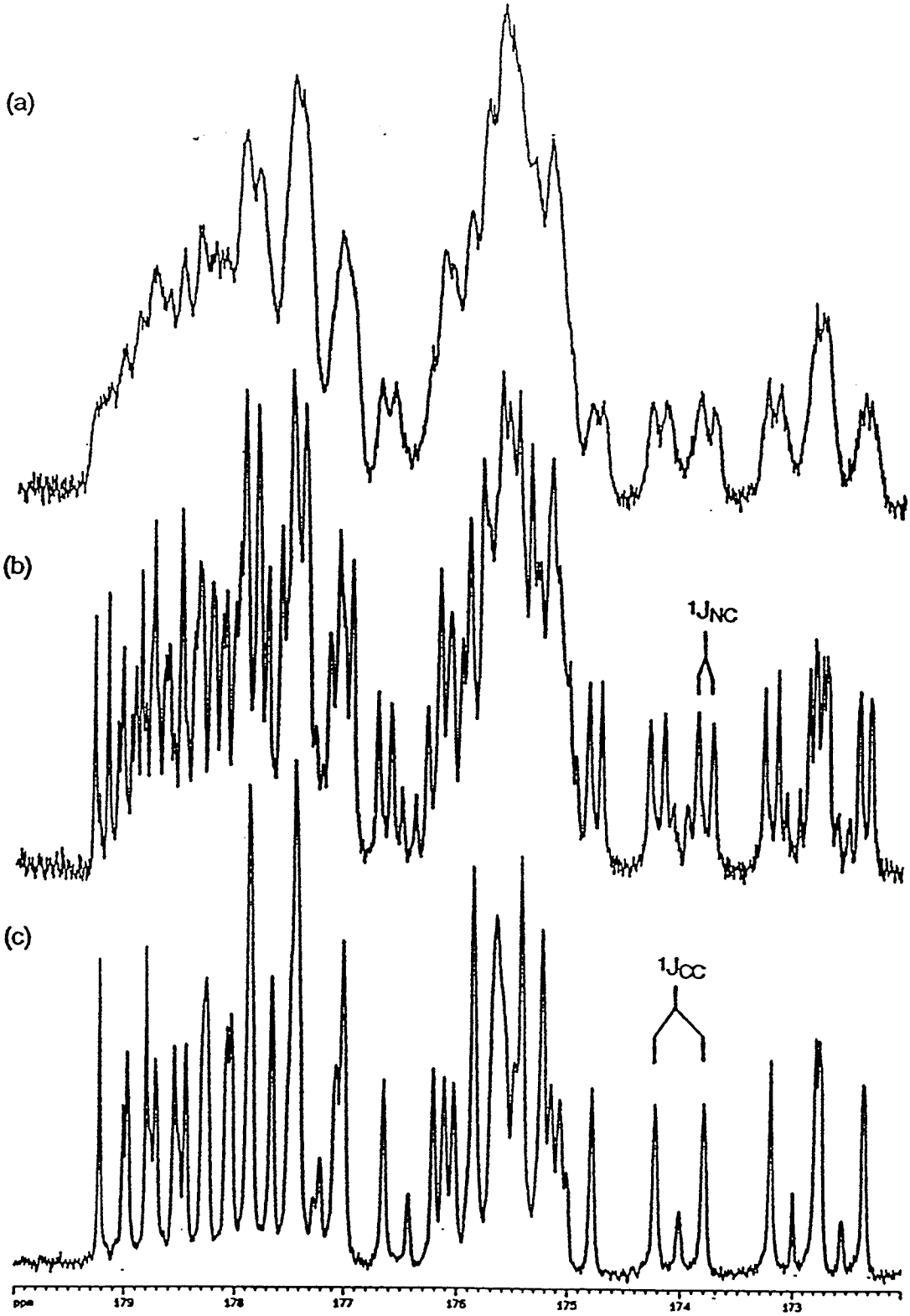
(a)
(b)
$^1J_{NC}$
(c)
$^1J_{CC}$
ppm
179
178
177
176
175
174
173
^{13}C

Figure 2-5: SEDS spectra of ^{13}C-^{15}N labelled alamethicin in CD_3OD with ^{13}C decoupling. The spectra show the methyl and the aromatic regions. The number of scans was 128, no window function was applied. The peaks marked * are impurities from the HPLC eluant. (a) Spin echo spectrum without 180° flip pulse to the ^{13}C, (b) spin echo spectrum with a 180° flip pulse applied to the ^{13}C, (c) the sum spectrum of (a) and (b), (d) the difference spectrum of (a) and (b). Some of the peak assignments and percentage ^{13}C-labelling are given in (c) and (d), respectively.

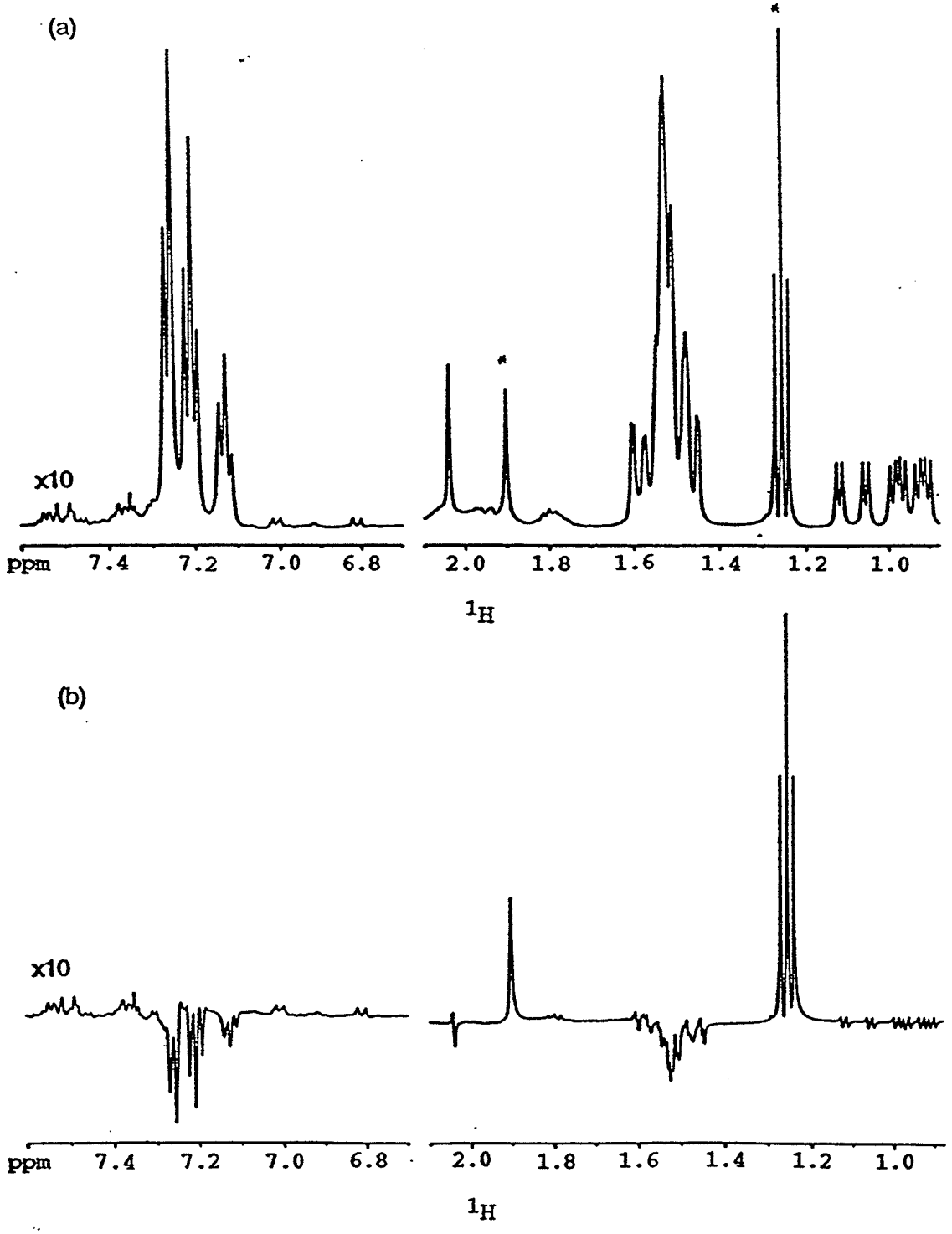
(a)
x10
ppm 7.4 7.2 7.0 6.8
2.0 1.8 1.6 1.4 1.2 1.0
^{1}H
(b)
x10
ppm 7.4 7.2 7.0 6.8
2.0 1.8 1.6 1.4 1.2 1.0
^{1}H

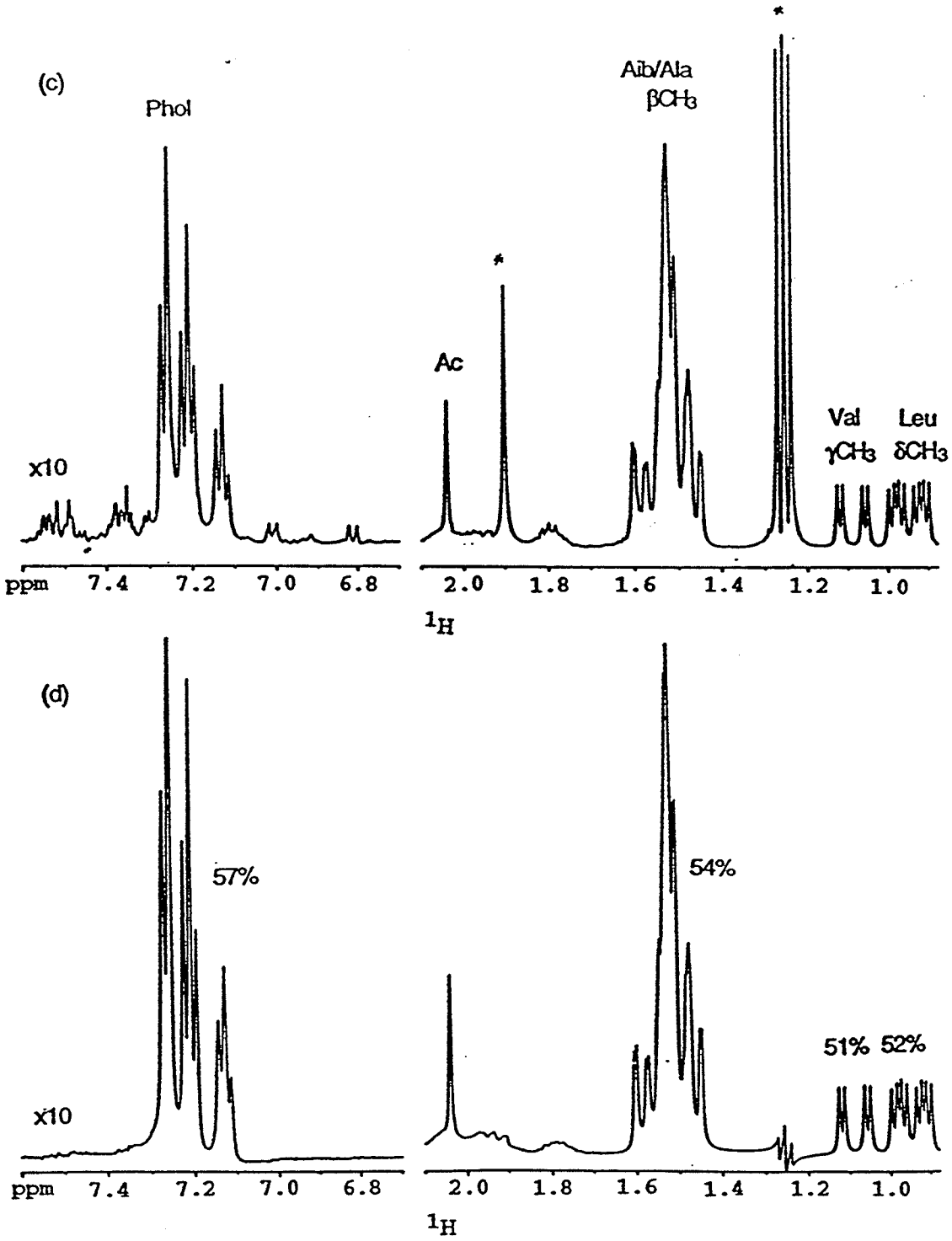
(c)
Phol
Aib/Ala
βCH3
Ac
Val
γCH3
Leu
δCH3
x10
ppm 7.4 7.2 7.0 6.8
2.0 1.8 1.6 1.4 1.2 1.0
1H
(d)
57%
54%
51%
52%
x10
ppm 7.4 7.2 7.0 6.8
2.0 1.8 1.6 1.4 1.2 1.0
1H

2.5 Discussion

In liquid culture, *T. viride* is usually grown in the presence of insoluble solids such as fish meal, dextrin (Reusser, 1967), and/or carboxymethyl cellulose (Brewer et al., 1987). This suggests that *T. viride* is able to metabolize cellulose which is in agreement with recent extractions of cellulases from *T. viride* culture media (Song et al., 1994). Brewer et al. (1987) reported that in the absence of such insoluble solids, growth of the fungus was observed but not the production of alamethicin. We showed previously (Yee, 1991) that the change of nitrogen source from fish meal to KNO_3 changes the relative proportions of the alamethicin types secreted by the fungus. In the present work, the change of carbon source from complex carbohydrate to simple glucose did not result in a marked change in the relative abundances of alamethicin types. These results are in agreement with the way *T. viride* utilizes carbon; since it only absorbs monosaccharides and possibly disaccharides, replacing the carbon source with glucose would not be detected intracellularly as a change in starting material for the alamethicin production.

When we used spore dispersions in water as inoculum for the glucose medium, no visible growth of fungus was observed even after 50 days of incubation. However, when we used a piece of agar containing growing fungus as inoculum, growth of fungus and production of alamethicin were observed. Mandels and Darby (1953) showed that spore germination in

Myrothecium verrucaria and possibly *T. viride* (no quantitative data were presented for *T. viride* in their paper) involves considerable swelling of the spores before protrusion of the germ tube. They showed that swelling is slow in the presence of glucose alone but that yeast extract stimulates swelling. So the difference we observed in fungal growth between the spore and vegetative mycelium as inoculum may be due to a lack of germination stimuli. Nevertheless, the isolation of ^{13}C-labelled alamethicin indicates that the fungus is able to absorb soluble glucose and use it in the production of alamethicin.

From the SEDS experiment, the percentage of ^{13}C-bound protons in our peptide is determined to be 51 to 57%. This result may indicate either that all of the molecules are approximately 50% labelled, or that approximately half of the molecules are 100% labelled. From the carbonyl ^{13}C spectrum (Figure 2-4c), it is evident that a large fraction of ^{13}C carbonyl atoms are coupled to $^{13}C_{\alpha}$ atoms suggesting that a high proportion of the ^{13}C label is in molecules that are nearly 100% labelled.

The ^{13}C-glucose that was used is 98%+ labelled but the labelling in alamethicin is only 51 to 57%. Possible sources of ^{12}C in alamethicin are the stored ^{12}C in the vegetative mycelium used as inoculum since these were previously grown in a ^{12}C-glucose medium. It is also possible that the fungus digests the remaining agar in the inoculum. If the stored ^{12}C in the mycelium is the main source of ^{12}C in alamethicin, then

the percentage of ^{13}C labelling may be increased by using those mycelium grown in ^{13}C medium as inoculum for subsequent labelling. For the purposes for which the present labelling was done, the 51 to 57% labelling is sufficient.

Chapter 3
Alamethicin in Methanol

3.1 ^{13}C Chemical Shifts and Secondary Structures in Peptides

Isotopic labelling and multidimensional heteronuclear NMR pulse schemes have made it easier to assign the ^{13}C resonances in proteins. The ^{13}C chemical shifts of the C_α, C_β, and carbonyl have been shown to be sensitive to conformation. For example, in solution the C_α and carbonyl carbons in a helical conformation resonate at a higher frequency than the random coil whereas those in a β sheet conformation resonate at a lower frequency than the random coil. The opposite trend is observed for C_β carbons (Wishart & Sykes, 1994).

The first attempt to explain the trends in ^{13}C chemical shift was based on substituent effects, that is, the substituent when gauche to the observed nucleus is predicted to exert more shielding than when it is in the trans conformation similar to that observed in paraffinic hydrocarbons (Tonelli, 1984). This empirical rule would explain the observed trend for C_β but this would give the opposite trend in the carbonyl carbon resonances and cannot explain the trend in C_α resonances. Semiempirical molecular orbital (MO) approximations were used to calculate the carbonyl chemical shift in the solid state of N-acetyl-N'methylglycinamide (Ando et al., 1988) and N-acetyl-N'methylalaninamide (Asakawa et al., 1992). They showed that

a decrease in hydrogen bond length ($R_{N\cdots O}$) causes a shift to the higher frequency. They also showed that the isotropic shielding constant for the carbonyl carbon is affected by changes in electronic distributions effected by formation of a hydrogen bond (C=O···H-N) and by conformational changes (ϕ and ψ). For short $R_{N\cdots O}$ up to 2.6Å, the hydrogen bond effect predominates although the conformational effect is still present. Beyond this, the conformational effect becomes dominant. An *ab initio* GIAO calculation on N-acetyl-N'methylglycinamide suggested that the carbonyl chemical shift is sensitive to the dihedral angle ω (Sulzbach et al., 1995). Non-planarity of the amide bond affects the chemical shift; as the angle ω becomes smaller than 180°, the carbonyl becomes deshielded. Jiao et al. (1993) used the *ab initio* IGLO method to calculate the conformational dependence of the C_α chemical shifts in N-acetyl-N'methylglycinamide. They showed that conformational dependence of the C_α shift in peptides can be explained at least qualitatively as due to changes in electronic structure as the backbone angles ϕ and ψ are varied without having to include hydrogen bonding effects. A series of GIAO calculations from Oldfield's group also examined the effect of conformation on the chemical shielding of ^{13}C, ^{15}N, and $^{1}H_N$ (de Dios et al., 1993a,b; de Dios & Oldfield, 1994; Le et al., 1995). They showed that the conformational dependence of the shieldings in proteins can be predicted by separating the short and long range contributions to shielding and doing *ab initio* calculations

only on the short range effects instead of doing *ab initio* calculations on the entire protein. The long range effects, which are mostly electrostatic in origin, are calculated using the charge field approach. They examined the effect of local geometry on the C_α shieldings for glycine, alanine, and valine fragments and found it to be dominated by torsion angle ϕ and ψ effects and less affected by bond angle N-C_α-C' and bond lengths (de Dios et al., 1993b). For alanine and valine a χ_1 effect influenced chemical shift to a small extent (de Dios & Oldfield, 1994). The C_α shielding is found to be only slightly affected by hydrogen bonding (de Dios et al., 1993a). The C_β shielding in the alanine and valine fragments is also dominated by ϕ and ψ effects and between the alanine and valine fragments, the valine is more affected by χ_1 effects.

3.2 Hydrogen Bonding in Peptides

Hydrogen bonding is said to exist if one hydrogen atom is bonded to more than one other atom (Lippert, 1976). The hydrogen bond is an attractive force between a neighboring acceptor atom A and a hydrogen that is already bonded to a donor atom X (Perrin, 1994). It arises from the stabilizing electrostatic interaction between dipoles. Hydrogen is favored because it is very small and so the dipoles can approach closely (Perrin, 1994). Hydrogen bonds with bond energy greater than 40 kJ/mol are considered very strong and those with bond energy less than 20 kJ/mol are said to be

weak (Jeffrey & Saenger, 1991). Strong hydrogen bonds usually involve charged acceptors or very electronegative atoms like fluorine. Very strong hydrogen bonds are usually linear with the hydrogen located midway between the two electronegative atoms and typical hydrogen bond lengths vary from 1.2 to 1.5 Å. On the other hand, weak hydrogen bonds may deviate from linearity with hydrogen bond angles of 160±20° and hydrogen bond lengths typically from 1.5 to 3.0 Å. Weak hydrogen bonds may also be involved in three-center hydrogen bonding (i.e., bifurcated configuration with two acceptor atoms).

Most hydrogen bonding in peptides and proteins involves weak hydrogen bonds involving main chain peptide groups with the N-H as a hydrogen bond donor and the C=O as an acceptor. Polar side chains and solvent molecules may also participate in hydrogen bonding. Hydrogen bonding helps to stabilize the structure of proteins. Common secondary structures found in proteins are the helices which are stabilized by short range intrachain hydrogen bonding and β pleated sheets which are stabilized by long range intrachain hydrogen bonding. The two commonly observed helices are the 3.6_{13} (α) helix and the 3_{10} helix (see Figure 3-1). The α helix is stabilized by a series of hydrogen bonding interactions between the C=O of the ith residue and the N-H of the (i+4)th residue whereas the 3_{10} helix is stabilized by a series of hydrogen bonds between the C=O of the ith residue and the N-H of the (i+3)th residue.

NMR, infrared, and Raman spectroscopy are commonly used to study hydrogen bonding in solution. For studying hydrogen

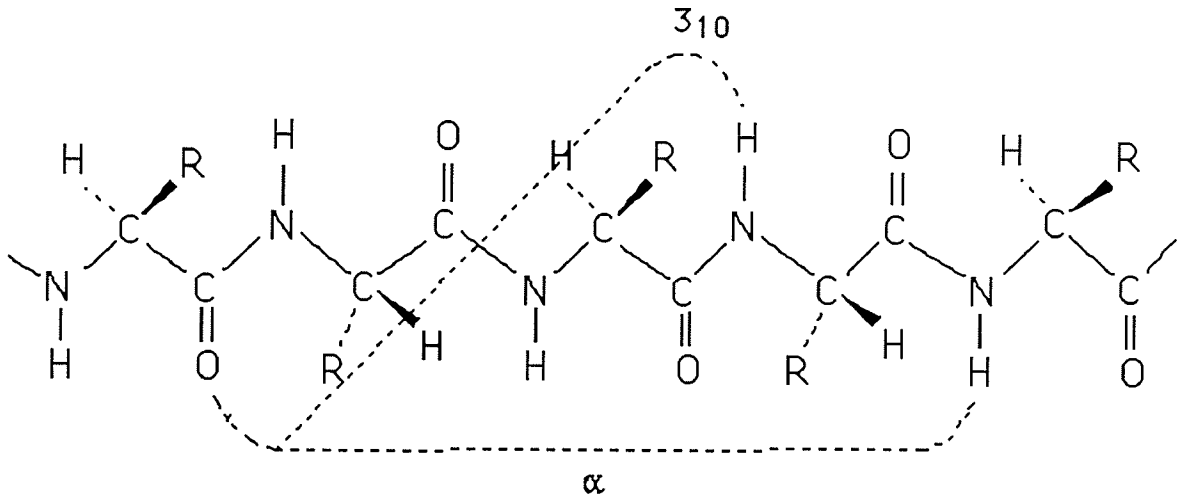

Figure 3-1: Different mainchain hydrogen bonding in a peptide in the α and 3_{10} helical conformations.

bonding in small molecules containing one or a few hydrogen bonds, infrared spectroscopy has an advantage over NMR in that absorption bands corresponding to the hydrogen bonded and non-hydrogen bonded states are observable because of the shorter time scale in the IR measurements, whereas in NMR, only a single average resonance may be observed (Gellman et al., 1991). For studying hydrogen bonding in peptides and proteins, NMR has an advantage over IR or Raman in that a large number of individual N-^{1}H or ^{13}C=O can be resolved and studied.

3.2.1 $^{1}H_{N}$ Chemical Shift and Hydrogen Bonding

Hydrogen bonded protons resonate at a higher frequency than non-hydrogen bonded ones. Theoretical calculations on an

O-H···O dimer system showed that, upon hydrogen bonding, there is a loss of electron density around the proton. The net effect is due to a deshielding and shielding, respectively, of the perpendicular ($\sigma_\perp$) and the parallel ($\sigma_\parallel$) components of the ^1H shielding tensor by the oxygen in the acceptor molecule, and a deshielding of the $\sigma_\perp$ and a shielding or deshielding of the $\sigma_\parallel$ of the ^1H shielding tensor by the oxygen of the donor molecule. Since the isotropic shielding (σ) has a stronger dependence on $\sigma_\perp$ (i.e., $\sigma = (2/3)\sigma_\perp + (1/3)\sigma_\parallel$), then the above mentioned influences are predicted to lead to a net deshielding of the ^1H (Ditchfield & McKinney, 1976; Rohling et al., 1983).

In proteins, Pardi et al. (1983) were the first to show a correlation between the H_N chemical shift and the O···H distance ($r_{O\cdots H}$) ($\Delta\delta_{HN} = a\ r_{O\cdots H}^{-3} + b$, where $\Delta\delta_{HN}$ is corrected for ring current shift). Their data were based on three homologous proteins with a total of 163 non-proline residues. Recently, Wishart et al., (1991) compiled ^1H chemical shift data from 76 proteins representing a total of 4888 H_N resonances. Like Pardi et al. (1983), they showed a correlation between the $\Delta\delta_{HN}$ (corrected with random coil values) and $r_{O\cdots H}^{-1}$. They also suggested that, because of the short range of $r_{O\cdots H}$ distances involved, both $r_{O\cdots H}^{-1}$ and $r_{O\cdots H}^{-3}$ give a reasonable correlation with $\Delta\delta_{HN}$ (no correlation coefficient was given). The $r_{O\cdots H}^{-1}$ dependence of chemical shift in small organic and inorganic molecules had been explained in terms of the predominance of the effect of

polarization of the O-H bond by the neighboring hydrogen bond donor oxygen as opposed to the predominance of the through space shielding on the hydrogen by the donor oxygen which would lead to a $r_{O\cdots H}^{-3}$ dependence (Sternberg & Brunner, 1994). The H_N in a helical conformation resonates at a lower frequency than that in a β sheet conformation and this was rationalized as due to the average hydrogen bond lengths in helices being longer than those in β sheets as opposed to the actual backbone ϕ and ψ conformational effect (Wishart et al., 1991).

3.2.2 Temperature Coefficient of ^1H_N and Hydrogen Bonding

The effects of vibration and centrifugal stretching on the magnetic shielding of a nucleus was first predicted by Ramsey (1952). Evidence for this effect is the observation that deshielding of the nucleus occurs as temperature increases in isolated molecules (Jameson, 1980). In an anharmonic vibration, the average internuclear distance increases with increase in vibrational quantum number, whereas in a harmonic vibration, the average internuclear distance remains the same for all vibrational quantum numbers (Figure 3-2). An increase in internuclear distance will decrease shielding. As the temperature increases, the fraction of molecules occupying the higher vibrational and also rotational states increases. Since the observed nuclear shielding is a population-weighted average over all the

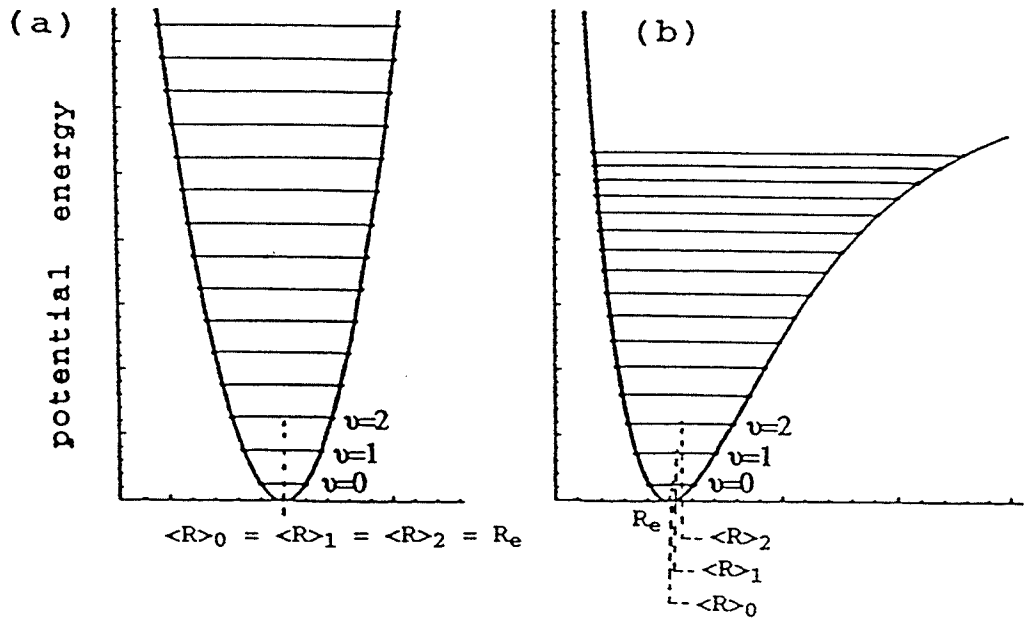

Figure 3-2: Hypothetical potential curves for showing the effect of anharmonic vibration on the average internuclear distance. (a) harmonic vibration and (b) anharmonic vibration.

occupied vibrational and rotational states, deshielding is expected to be observed at higher temperatures (Muller & Reiter, 1965; Jameson, 1980).

In proteins, Kopple et al. (1969) were the first to use the temperature coefficients of the amide protons (H_N) to identify the intramolecularly hydrogen bonded H_N. Hydrogen bonded H_N showed smaller temperature coefficients than the non-hydrogen bonded ones. Ohnishi & Urry (1969) showed that in methanol non-hydrogen bonded H_N in gramacidin S and valinomycin, both cyclic peptides, have temperature coefficients close to those observed in N-methyl-acetamide. This difference in temperature coefficient in a hydrogen

bonding solvent is thought to be due to the ease of breaking hydrogen bonds between peptide and solvent compared with breaking peptide intramolecular hydrogen bonds (Deslauriers & Smith, 1980). This is because solvent molecules have more mobility while the different parts of the peptide are restricted by covalent bonding. However, not all small temperature coefficients can be interpreted as hydrogen bonded H_N especially for molecules dissolved in non-hydrogen bonding solvents (Gellman et al., 1991).

3.2.3 Solvent Perturbation and Hydrogen Bonding

The changes in chemical shift of the carbonyl ^{13}C and amide ^{1}H upon solvent perturbation have been used to determine the solvent-exposed amides and carbonyls in peptides (Urry et al., 1974; Khaled et al., 1979). The peptide groups that are exposed to the solvent experience the greatest shift provided that the conformation of the peptide does not change upon solvent change. The change in solvent from a good proton donor to a poor proton donor can affect the chemical shift of a solute via a change in through-space shielding and/or a change in charge distribution of the solute (Howarth and Lilley, 1978). For small peptides, the insensitivity of the chemical shift to solvent is expected to be due mainly to intramolecular hydrogen bonding.

3.2.4 Deuterium Isotope Effect and Hydrogen Bonding

The isotope effect on nuclear shielding is additional

evidence for the rotational and vibrational effects predicted by Ramsey (1952). The isotope effect is influenced by a dynamic and an electronic factor (Jameson & Osten, 1986). The dynamic factor contributes to the isotope effect by the small change in the average geometry of the molecule upon substitution of a heavier isotope. The lighter atom would have a larger average bond displacement because the amplitude of motion for the heavier atom is smaller than that of the lighter one. Because the vibrational frequencies for a heavier isotopomer are lower than those of a lighter one, the higher vibrational states are more populated in the heavier isotopomer. The electronic factor contributes to the isotope effect by the small change in the sensitivity of the shielding with the change in molecular geometry.

The two-bond deuterium isotope effect on carbon ($^2\Delta$) in several localized hydrogen bonding systems has been correlated with hydrogen bonding strength. In a series of phenol derivatives (see Table 3-1), the $^2\Delta$ showed a very good correlation with the H_O chemical shifts which in turn are correlated with hydrogen bond energies (Reuben, 1986). In a series of aniline derivatives, the $^2\Delta$ showed a very good correlation with the H_N chemical shifts (Reuben, 1987). In a series of enamine derivatives, the $^2\Delta$ also showed a very good correlation with the H_N chemical shift (Hansen et al., 1990). In the compounds just mentioned the carbons where the isotope effect was measured are along a π-conjugated pathway and are not necessarily appropriate models for proteins. In some

Table 3-1: Equations relating deuterium isotope effect on carbon with intramolecular hydrogen bond enthalpy based on model compounds.

Compounds	Calibration Equation	Reference
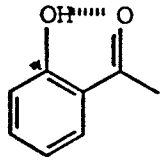	$\ln(^2\Delta) = 2.783+1.48E$ R=0.988	Reuben (1986)
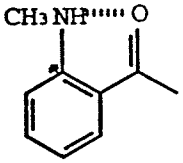	$^2\Delta = -133.9+31.8\delta_{HN}$ R=0.998	Reuben (1987)
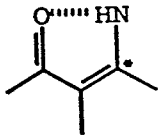	$^2\Delta = \text{const}+0.028\delta_{HN}$ R=0.83	Hansen et al. (1990)
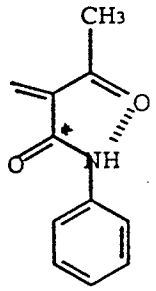	$-E = 0.224^2\Delta+1.72$ R=0.87	Hansen et al. (1992)

Deuterium isotope effects ($^2\Delta$) were measured from the carbon labelled with *. R is the correlation coefficient. The y-intercept for the equation for the enamine derivatives was not given. $^2\Delta$ are in ppb except in the enamine derivatives where it is in ppm; δ_{HN} is the chemical shift of ^1H_N (ppm); E is the hydrogen bond enthalpy (kJ/mol).

acetamido compounds, the $^2\Delta C{=}O(ND)$ correlate with $^2\Delta C_{ar}(ND)$ (R = 0.85) which are strongly correlated with hydrogen bonding at the H_N. On this evidence Hansen et al. (1992) have proposed that large $^2\Delta C{=}O(ND)$ are diagnostic of hydrogen bonding in proteins.

3.2.5 ^1H_N Exchange Rate and Hydrogen Bonding

Amide proton exchange can be used to identify hydrogen bonded secondary structures in proteins (Wagner, 1983; Englander & Kallenbach, 1984). Amides involved in α helix and β sheet hydrogen bonding have been found to exhibit very slow amide exchange. In BPTI, hydrogen exchange is observed to be 10^3-fold slower in hydrogen bonded amides than in those not involved in hydrogen bonding (Wagner & Wuthrich, 1982). In order for exchange to occur, hydrogen bonds must be broken (Englander et al., 1972). pH dependent exchange experiments allow the measurement of the base (k_{OH}) and acid (k_H) catalyzed exchange rate constants. A more thorough description of the hydrogen exchange chemistry is presented in Section 4.2. In BPTI, k_H values have been correlated with the static solvent accessibility of the carbonyl oxygen (Tuchsen & Woodward, 1985). In alanine-based peptides, protection from base catalyzed exchange was shown to be a measure of the extent of hydrogen bonding of the peptide H_N (Rohl & Baldwin, 1994).

3.3 Heteronuclear Coupling Constants in Peptides

In protein NMR structure determination, homonuclear coupling constants provide information on the backbone torsion angle and the stereospecific assignment of the sidechain protons. By far the most useful coupling constant employed in protein structure determination is the $^{3}J_{HNH\alpha}$ and its Karplus-type relationship with the backbone angle ϕ is the best calibrated (see Table 3-2). But in alamethicin, because of the presence of prolines and some unusual amino acid residues like Aib, the number of measurable $^{3}J_{HNH\alpha}$ diminishes. ^{1}H couplings to ^{15}N and ^{13}C can supplement the information available from homonuclear coupling constants, nOes, and chemical shifts. The Karplus-type dependence of $^{1}H/^{15}N$ and $^{1}H/^{13}C$ vicinal coupling constants in model dipeptides was reviewed by Bystrov (1976). Among these couplings, only the $^{3}J_{H\alpha N}$ can provide information about the backbone angle ψ. For amino acid residues that do not have an α proton, the $^{3}J_{HNC'}$ and $^{3}J_{HNC\beta}$ can provide information on the backbone ϕ angle.

Lately, uniform labelling of proteins with ^{13}C and ^{15}N has become common practice and several new heteronuclear pulse sequences have been developed. In large proteins, measurement of small ^{3}J values is difficult but the large one bond couplings can be easily measured. The large number of high resolution protein structures determined by NMR has generated enough data to be able to correlate these ^{1}J values with relevant dihedral angles.

Table 3-2: Karplus-type relationships between coupling constant and intervening dihedral angles.

$$^3J_{ij} = a\ Cos^2\theta_{ij} + b\ Cos\theta_{ij} + c.$$

ij	a	b	c	θ_{ij}	Reference
$H_\alpha H_\beta{}^2$	9.5	-1.6	1.8	χ_1-120[a]	[c]Guntert et al., 1989
$^{15}NH_\beta{}^2$	-4.4	1.2	0.1	χ_1+120[b]	[c]DeMarco et al., 1978
$H_N H_\alpha$	6.4	-1.4	1.9	ϕ-60	[c]Pardi, et al., 1984
$H_\alpha{}^{15}N_{(i+1)}$	-5.1	2.2	0.9	ψ-120	[e]Bystrov et al., 1975

[a]for $H_\alpha H_\beta{}^3$, $\theta_{ij}=\chi_1$; [b]for $NH_\beta{}^3$, $\theta_{ij}=\chi_1$-120; [c]obtained from correlation with experimental ^3J; [e]obtained from correlation with calculated ^3J.

The $^1J_{C'N}$ values in model amides were shown to increase upon protonation of the amide oxygen, but were insensitive to the cis or trans conformation of the amide (Berger, 1978). In a small cyclic peptide, the $^1J_{C'N}$ were observed to be higher by at least 1 Hz for those peptides involved in intramolecular hydrogen bonding at the amide hydrogen (Walter and Wright, 1979). They attributed this increase in $^1J_{C'N}$ to an increase in hybridization of the amide bond through the transfer of electron charge density from the nitrogen to the carbonyl. This results in shortening of the C-N bond and the lengthening of the C=O and N-H bonds. This effect of hydrogen bonding was also studied in N-acetylglycine in different

solvents. The $^{1}J_{C'N}$ was found to increase with the proton-donating ability of acidic protic solvents and to decrease with the proton attracting ability of basic aprotic solvents. Thus, $^{1}J_{C'N}$ increases as hydrogen bonding goes from hydrogen bonding in the amide hydrogen to hydrogen bonding in the amide oxygen (Juranic et al., 1995).

In *Staphylococcal* nuclease, it was found that the $^{1}J_{C'N}$ are smaller for helices and β sheets than in the unstructured regions of the protein (Delagio et al., 1991). It has been suggested that the $^{1}J_{C'N}$ indicate that intramolecular amide hydrogen bonds are weaker than hydrogen bonds between the amides and water (Juranic et al., 1995). The $^{1}J_{C'N}$ and were correlated with dihedral angles ϕ and ψ. In human ubiquitin, the $^{1}J_{C'N}$ were found to be highest in peptide bonds preceded by small ψ angles but not all $^{1}J_{C'N}$ preceding a small ψ angle are high which would suggest that ψ angle is not the only determining factor in $^{1}J_{C'N}$ in proteins (Juranic et al., 1995).

3.4 Experimental Procedures

For the measurement of long range ^{1}H-^{15}N coupling constants ($^{3}J_{H\alpha N}$), HPLC-purified ^{15}N-labelled alamethicin was dissolved in 0.6 mL of CD_3OH to a concentration of about 2.5 mM without adjustment of the pH, and the sample was placed in a 10 mm NMR tube. The experiments were done using a 10 mm inverse broadband probehead with the inner coil tuned to ^{1}H and ^{2}H (lock) and the outer coil tuned to ^{15}N. The selective

heteronuclear 2D J experiment with INEPT polarization transfer was used (Bax & Freeman, 1982; Davis et al., 1983). The pulse sequence used for these experiments is shown in Figure 3-3.

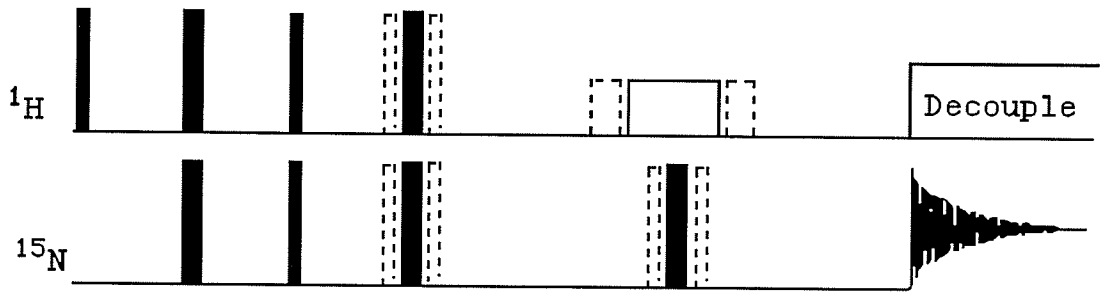

Figure 3-3: 2D-J pulse sequence used for determining $^3J_{H\alpha N}$ in ^{15}N-labelled samples. The dashed bars are 90° pulses added to correct imperfect 180° pulses. Filled bars are hard pulses and the open bar is a selective 180° pulse.

The refocusing π pulse on ^{15}N was replaced by a composite π pulse and full EXORCYCLE phase cycling (Bodenhausen et al., 1977) was employed in combination with the CYCLOPS phase cycling to eliminate the "ghost" peaks arising from imperfect ^{15}N π pulses. A composite π pulse was also used in place of the selective π "proton flip" pulse in order to eliminate F_1 artifacts (Bodenhausen & Turner, 1980). Likewise, a composite π pulse was used in the middle of the refocusing delay to make sure that phase shifts are eliminated when the antiphase components of the ^{15}N magnetization come into phase.

For the ^{1}H-^{13}C correlation experiments, HPLC-purified unlabelled alamethicin was initially dissolved in CD_3OD with no adjustment of the pH. The experiment was done using a 5 mm inverse broadband probehead with the inner coil tuned to ^{1}H and ^{2}H (lock) and the outer coil tuned to ^{13}C. The ^{1}H-^{13}C correlation experiments were done via heteronuclear single quantum correlated spectroscopy (HSQC) with ^{13}C decoupling during acquisition (Bodenhausen & Ruben, 1980).

For the ^{13}C-^{15}N correlation experiments, HPLC-purified ^{13}C-^{15}N labelled alamethicin was initially dissolved in CD_3OD with no adjustment of the pH. The amount of doubly labelled sample was too small to be weighed accurately. Comparing the intensity of the ^{1}H signals of the doubly labelled solution with that from a different alamethicin solution of known concentration acquired under the same conditions, the concentration of the doubly labelled sample was approximated at 1 mM. The experiments were done using a 5 mm triple resonance probehead with the inner coil tuned to ^{1}H and ^{2}H (lock) and the outer coil tuned to ^{13}C and ^{15}N. The ^{13}C-^{15}N correlation experiments were done via heteronuclear zero and double quantum coherence with ^{1}H decoupling throughout the experiment and ^{15}N decoupling during acquisition unless otherwise specified (Mooberry et al., 1989). After these experiments, the NMR sample was placed in a beaker of hot water until half the volume of the solvent had evaporated. Then the sample was filled back to its original volume with CD_3OH for the deuterium isotope effect experiment. After

these experiments, the solvent was again evaporated to 20% of its original volume and then filled with a CH_3OH/DMSO (3:1) mixture to give an initial DMSO concentration of 20%. CH_3OH and unlabelled DMSO were used so that the DMSO concentration in solution could be determined by integration of the ^1H methyl signals from DMSO and CH_3OH without having to redissolve the sample in fresh solvent. After a spectrum was acquired, the solvent in the same sample was partially evaporated and the sample was filled to its original volume with the CH_3OH/DMSO mixture. The final concentration of the DMSO was determined from the ratio of the ^1H methyl signals from methanol and DMSO, assuming that CD_3OD, CD_3OH, and CH_3OH all evaporated at the same rate so that their ratio remained the same. This increased the DMSO concentration to approximately 80% because the boiling point of methanol (64.7°C) is lower than that of DMSO (189°C). A slight precipitate was observed upon addition of DMSO but it was not removed from the NMR tube. After the solvent perturbation experiment was completed, the sample was repurified by HPLC to eliminate the DMSO.

Circular dichroic (CD) spectra of HPLC-purified alamethicin in methanol at a concentration of 5.8 μM were acquired using a JASCO J500A spectropolarimeter. The following spectropolarimeter settings were used: sensitivity is 1 m°/cm, time constant is 4 sec, chart speed is 1 cm/min, and wavelength expansion is 5 nm/cm. The temperature of the sample in a 0.5 cm pathlength cell was controlled by a Haake

D1-G waterbath. Mean residue ellipticities [Θ] were calculated using the equation (Freifelder, 1976):

$$[\Theta]_{222} = M\ \Theta_{222}/(10\ d\ c)$$

where M is the mean residue mass of alamethicin (97.9); Θ_{222} is the observed ellipticity at 222 nm in deg; d is the cell pathlength in cm (0.5); and c is concentration in g/mL (1.16×10^{-5}). The concentration of the samples used in the CD studies were obtained by dilution of an alamethicin stock solution of known concentration.

3.5 Results

3.5.1 Resonance Assignments

The ^{1}H and ^{15}N resonances of alamethicin in methanol had been assigned previously (Yee, 1991). The assignment of the ^{13}C resonances of the atoms with attached protons was done using an HSQC ^{1}H-^{13}C correlation experiment (Figure 3-4) using the known ^{1}H assignments. The assignment of the carbonyl carbons was done using an HMQC ^{13}C-^{15}N correlation experiment (Figure 3-5). The ^{15}N of residue (i) is directly bonded to the carbonyl of the preceding residue (i-1) and to its own $C_{\alpha}(i)$, and in the case of prolines, it is also bonded to its $C_{\delta}(i)$. Since all the ^{15}N resonances had been assigned, except for the two prolines, the assignment of the carbonyls as indicated in Figure 3-5 is straightforward. Although the ^{15}N resonances for the two prolines had not been assigned, the $^{13}C_{\alpha}$ and $^{13}C_{\delta}$ resonances were assigned based on the ^{1}H-^{13}C correlation spectrum (Figure 3-4), so from the $^{13}C_{\delta(i)}$-$^{15}N_{(i)}$ correlation

Figure 3-4: Aliphatic region of the ^{13}C-^{1}H HSQC (Bodenhausen & Ruben, 1980) spectrum of unlabelled alamethicin in CD_3OH with ^{13}C decoupling. (a) C_β region (b) C_α region. The number of scans was 128 for each of 512 t_1 increment of 4K data points each. Only the F_1 dimension was zero filled to 1K points. A $\pi/2$-shifted sine-squared filter was applied in both dimensions before fourier transformation.

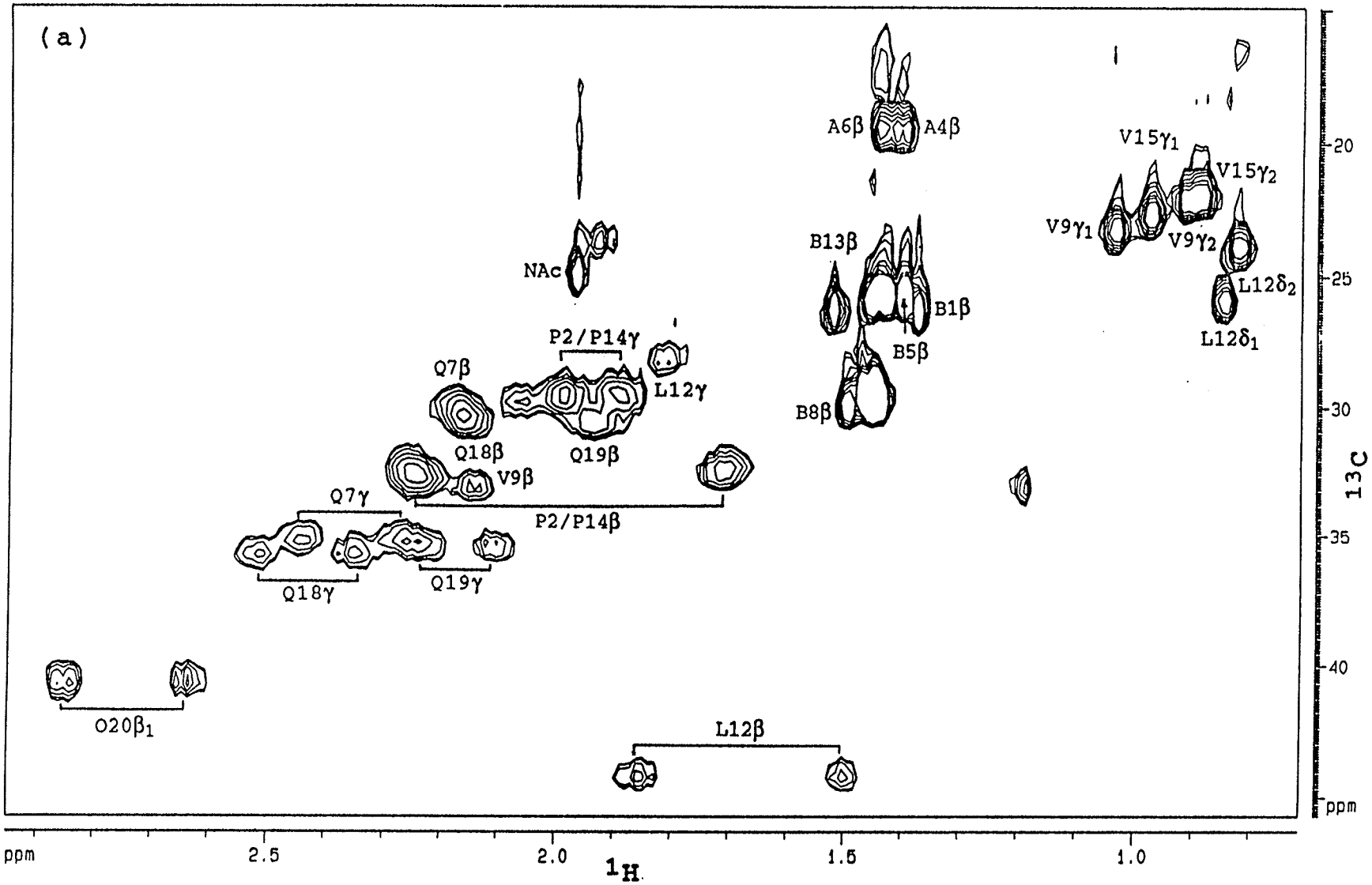
(a)
A6β
A4β
V15γ1
V15γ2
V9γ1
V9γ2
L12δ2
L12δ1
NAc
B13β
B1β
B5β
B8β
P2/P14γ
Q7β
L12γ
Q18β
Q19β
V9β
Q7γ
P2/P14β
Q18γ
Q19γ
O20β1
L12β
20
25
30
35
40
13C
ppm
2.5
2.0
1.5
1.0
1H

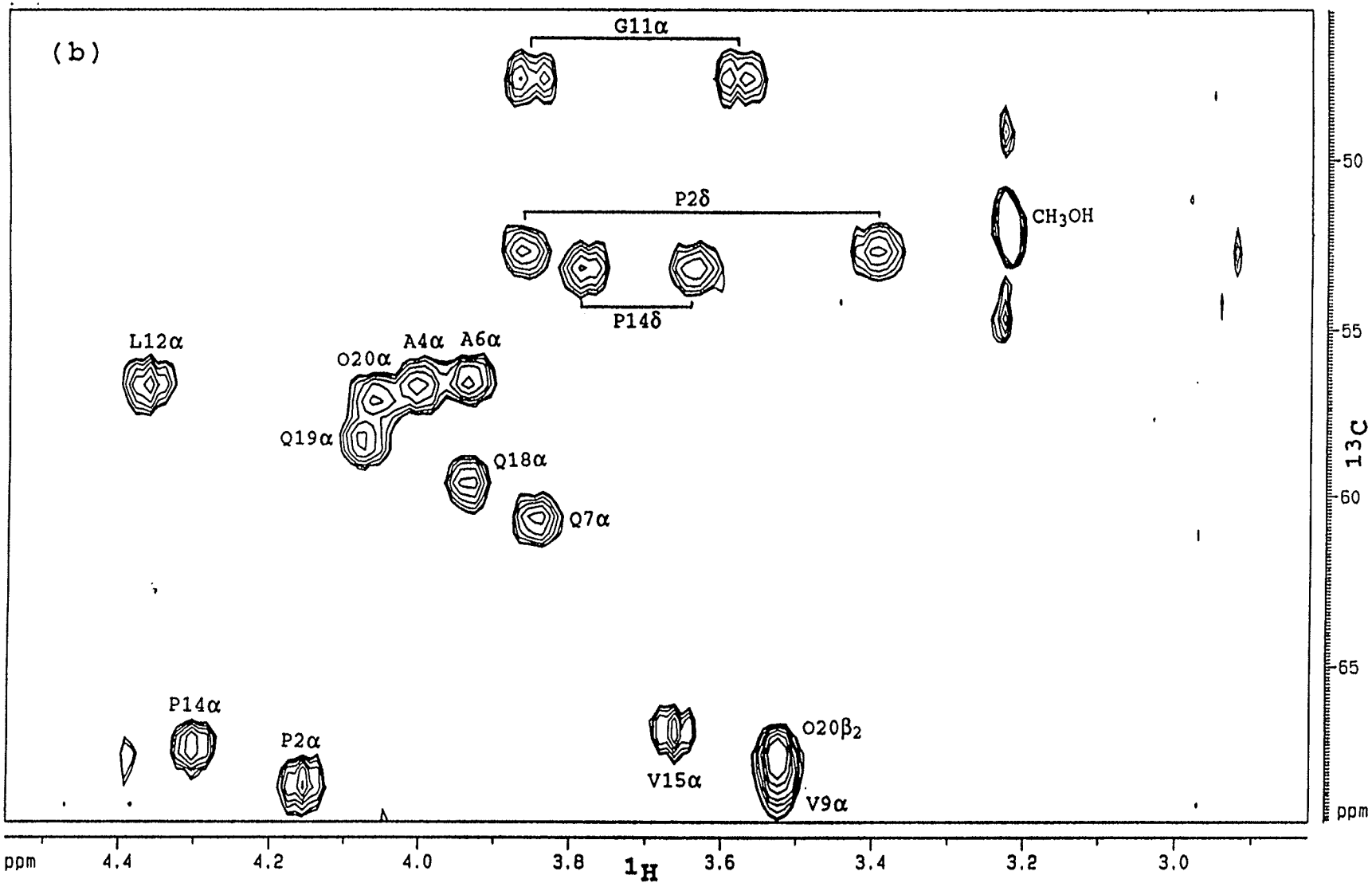
(b)
G11α
P2δ
P14δ
CH3OH
L12α
A4α
A6α
O20α
Q19α
Q18α
Q7α
P14α
P2α
V15α
O20β2
V9α
50
55
60
65
13C
ppm
ppm
4.4
4.2
4.0
3.8
1H
3.6
3.4
3.2
3.0

Figure 3-5: The carbonyl region of the ^{13}C-^{15}N correlation spectrum (Mooberry et al., 1989) of ^{13}C-^{15}N labelled alamethicin in CD_3OD with ^{1}H and ^{15}N decoupling. The carbonyl of residue (i) is correlated with the amide nitrogen of residue (i+1). The assignments given are for the $^{13}C'(i)$. The number of scans was 160 for each of 64 t_1 increments of 2K data points each. The F_1 and F2 dimensions were zero filled to 4K and 128 points, respectively and a $\pi/2$-shifted sine-squared filter was applied in both dimensions before fourier transformation.

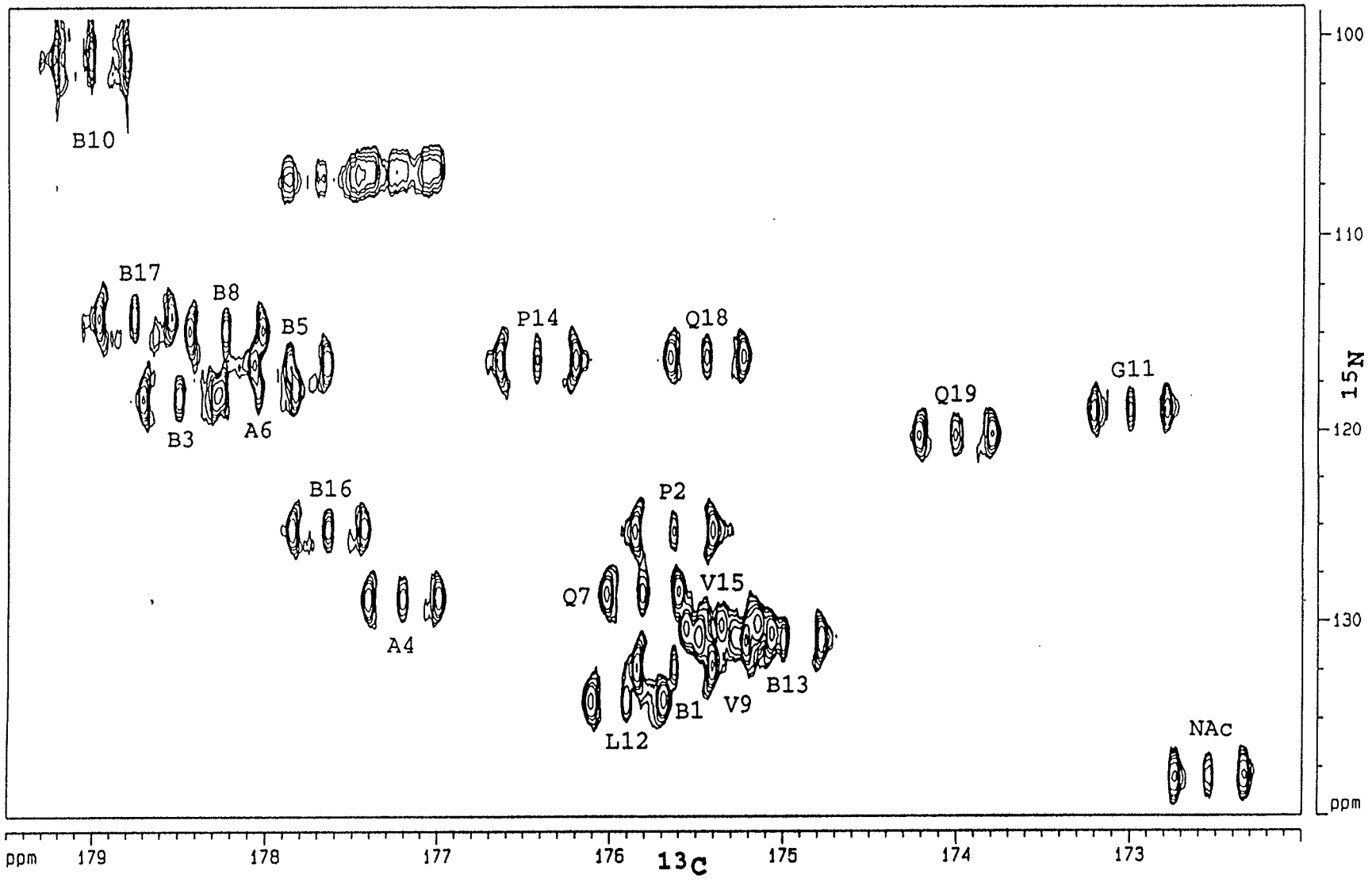
B10
B17
B8
B5
B3
A6
B16
A4
P14
Q18
Q19
G11
P2
Q7
V15
B13
B1
V9
L12
NAc
100
110
120
130
15N
ppm
ppm
179
178
177
176
175
174
173
13C

(Figure 3-6), the nitrogens at 131 ppm and at 132.3 ppm were assigned to Pro 2 and Pro 14, respectively. From this followed the assignment of the ^{13}C carbonyls of residues 1 and 13 shown in Figure 3-5. The proline $C\delta$ crosspeaks are more intense than the $C\alpha$ crosspeaks because they are only split by coupling to the $C\gamma$ whereas the $C\alpha$ are split by coupling to both the $C\beta$ and the carbonyl carbon. Six of the 8 Aib carbonyls resonated from 177.6 ppm to 178.7 ppm. The carbonyls of Aib 1 and Aib 13 resonated at a lower frequency because they precede a proline. A similar observation was reported for amino acids preceding proline (Tuchsen & Hansen, 1988; Breitmaier & Voelter, 1987). The lowest frequency carbonyl belongs to the N-acetyl at 172.5 ppm followed by Gly 11 at 173.0 ppm. The rest of the carbonyls resonate between 174.0 ppm and 177.2 ppm. This pattern of chemical shift is attributable to the β-effect on the chemical shift of the carbonyl whereby an increase in the number of substituents on the $C\alpha$ causes a decrease in shielding of the carbonyl. A similar effect is observed for the ^{15}N resonances of alamethicin (Yee, 1991).

The quarternary α carbons of all of the Aibs could not be assigned unambiguously using the 2D ^{13}C-^{15}N correlation experiment because the signal is barely above the noise level (see Figure 3-6). The carbonyl and each of the β carbons split the α carbon resonances making the signal very weak. The Aib α carbons were assigned using a 3D $^{1}H_N$-^{15}N-$^{13}C\alpha$ correlation experiment because in this experiment, the

Figure 3-6: The aliphatic carbon region of the ^{13}C-^{15}N correlation spectrum (Mooberry et al., 1989) of ^{13}C-^{15}N labelled alamethicin in CD_3OD with ^{1}H and ^{15}N decoupling. The α carbon of residue (i) is correlated with its own amide nitrogen. The number of scans was 160 for each of 64 t_1 increments of 2K data points each. The F_1 and F2 dimensions were zero filled to 4K and 128 points, respectively and a $\pi/2$-shifted sine-squared filter was applied in both dimensions before fourier transformation.

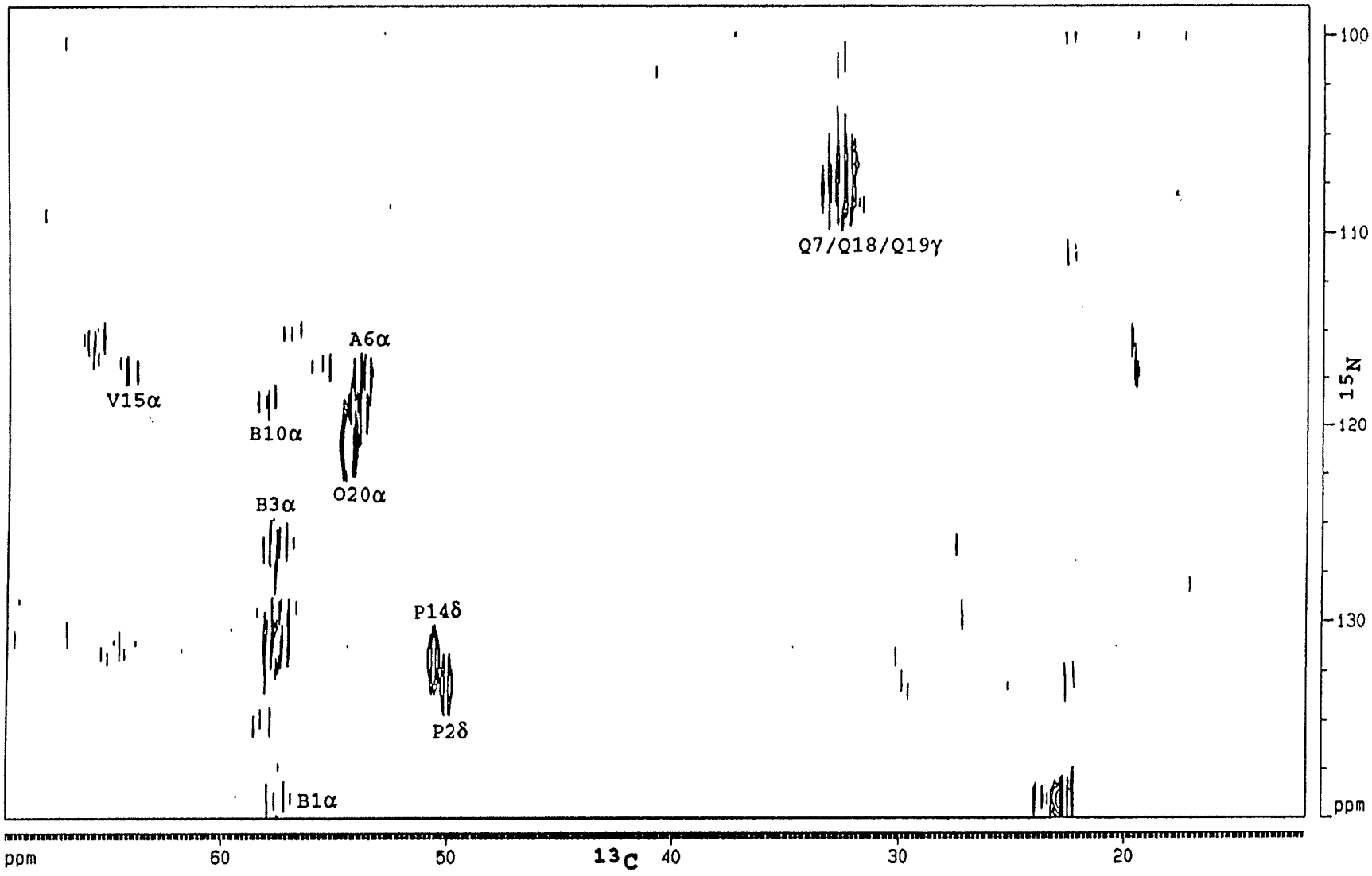
Q7/Q18/Q19γ
A6α
V15α
B10α
O20α
B3α
P14δ
P2δ
B1α
100
110
120
130
ppm
15N
ppm
60
50
40
30
20
13C

observed nucleus is ^{1}H and so the one bond couplings to the α carbons from the β and carbonyl carbons can be eliminated by ^{13}C decoupling during acquisition. The $C_{\alpha(i)}$ to $N_{(i)}$ correlation slices along the amide ^{1}H dimension for all the Aibs are shown in Figure 3-7. The 3D $^{1}H_{N}$-^{15}N-$^{13}C_{\alpha}$ correlation experiment also confirmed the non-Aib α carbon assignments. All the Aib α carbons resonate in a very narrow range from 57.3 to 58.1 ppm suggesting that the conformations of all the Aib residues are very similar. A summary of the ^{1}H, ^{15}N, and ^{13}C resonance assignments of alamethicin in methanol are given in Appendix A.

3.5.2 Alamethicin Exists as a Monomer in Methanol

Banerjee & Chan (1983) previously suggested that alamethicin exists as dimers in methanol based on the relaxation properties of the N-acetyl group at the N-terminus of alamethicin. The monomers in the suggested dimer are parallel and symmetric, so that only one signal is observed for all the ^{1}H resonances. If such dimers exist, some of the nOes assigned to be intrapeptide may be interpeptide. One way to distinguish between an inter- and intramolecular nOe is to mix labelled and unlabelled molecules as they would give separate signals for the ^{1}H resonances for each molecule. The signals from the ^{15}N-attached protons would be split by the $^{1}J_{NH}$ of 90 Hz and the signals from the ^{14}N-attached protons would be in the middle. The nOes between ^{14}N- and ^{15}N-attached protons would be diagnostic of intermolecular contacts. A

Figure 3-7: Slices along the ^{1}H dimension of the 3D HNCA correlation experiment (Kay et al., 1990; Bax & Ikura, 1991) of ^{13}C-^{15}N labelled alamethicin in CD_3OH. Each panel is a ^{1}H slice at the indicated chemical shift and shows the C_α to N correlation. The total number of scans was 16 for each increment and 512 data points were collected along the observed ^{1}H dimension. A total of 64 increments were acquired along the ^{13}C dimension and 128 increments were acquired along the ^{15}N dimension. All three dimensions were processed with a $\pi/2$-shifted sine-squared window function. No zero filling was applied to the ^{1}H and ^{15}N dimensions and forward linear prediction was applied to the ^{13}C dimension; 64 points were predicted and zero filled to 256 points. This experiment is courtesy of K. Marat.

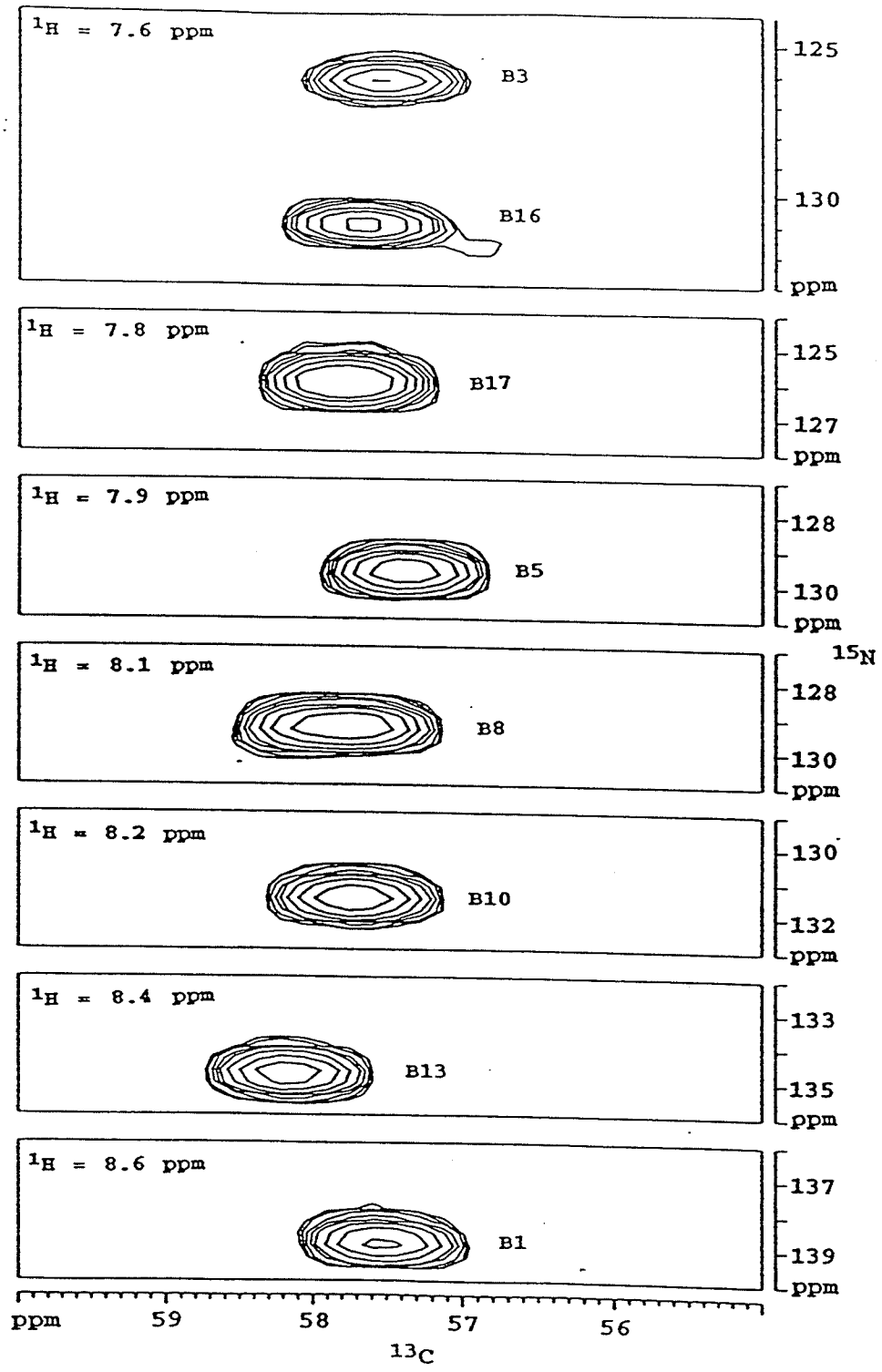
^{1}H = 7.6 ppm
B3
B16
125
130
ppm
^{1}H = 7.8 ppm
B17
125
127
ppm
^{1}H = 7.9 ppm
B5
128
130
ppm
^{1}H = 8.1 ppm
B8
^{15}N
128
130
ppm
^{1}H = 8.2 ppm
B10
130
132
ppm
^{1}H = 8.4 ppm
B13
133
135
ppm
^{1}H = 8.6 ppm
B1
137
139
ppm
ppm 59 58 57 56
^{13}C

SEDS experiment of the ^{15}N-labelled alamethicin showed that it is 85% to 94% labelled (spectra not shown). The amide region of a ROESY spectrum of a mixture of ^{15}N-labelled and unlabelled alamethicin in CD_3OH is shown in Figure 3-8. This region of the spectrum shows that all the crosspeaks originated as $H_{^{14}N}$-$H_{^{14}N}$ and $H_{^{15}N}$-$H_{^{15}N}$ interactions. No intermolecular H_N to H_N nOes between the labelled and unlabelled molecules were observed.

3.5.3 Heteronuclear Coupling Constants in Alamethicin

In homonuclear experiments like NOESY and TOCSY, only the ^1H is pulsed, so in an ^{15}N-labelled or ^{13}C-labelled sample, the heteronuclear coupling is passive and the cross peaks appear as E.COSY-type (Montelione et al., 1989). The cross peak from the H_N to another ^1H is split by heteronuclear coupling in addition to the homonuclear couplings. For example, in an ^{15}N-labelled sample, a TOCSY cross peak from H_N to H_α would be split by the $^3J_{HNH\alpha}$ similar to that observed in an unlabelled sample; the cross peak will be split further into two by the heteronuclear couplings. The resulting cross peaks are displaced by the large $^1J_{NH}$ along one dimension and by the smaller $^3J_{NH\alpha}$ along the other dimension. The homonuclear and heteronuclear couplings may then be measured by the displacement of the two cross peaks.

Figure 3-9 shows the H_N to β methyl region of a high resolution homonuclear ROESY spectrum of ^{15}N-labelled alamethicin in methanol; some of the well resolved Aib β

Figure 3-8: The amide region of a ROESY spectrum of a mixture of unlabelled and ^{15}N-labelled alamethicin in CD_3OH. The mixing time was 300 msec. The number of scans was 64 for each of the 512 t1 increments, 1K data points each. Zero filling was applied in the F_1 dimension only and $\pi/2$-shifted sine-squared filter was applied to both dimensions before fourier transformation. Some of the intramolecular crosspeaks are labelled (between ^{14}N-attached protons). Dashed lines connect sets of nOe peaks between the ^{15}N-attached protons. An nOe between the ^{15}N-attached protons of Aib 5 and Ala 6 is marked with an *. No nOe between the ^{14}N-attached protons of these two residues were observable previously because their amide protons resonate at the same frequency.

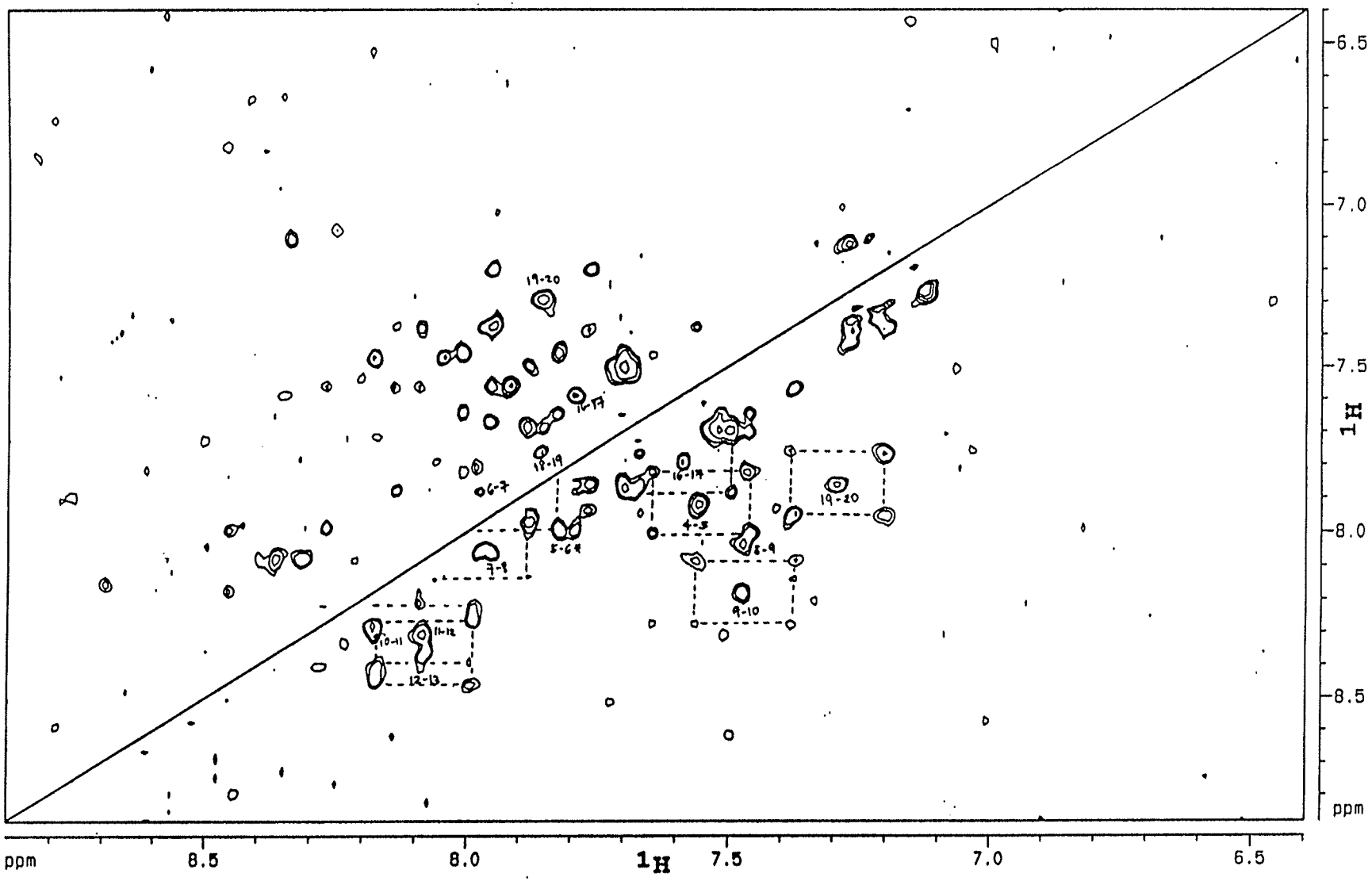
19-20
17-18
18-19
6-7
16-17
19-20
4-5
5-6
8-9
7-9
9-10
10-11
11-12
12-13
6.5
7.0
7.5
8.0
8.5
ppm
1H
ppm
8.5
8.0
1H
7.5
7.0
6.5

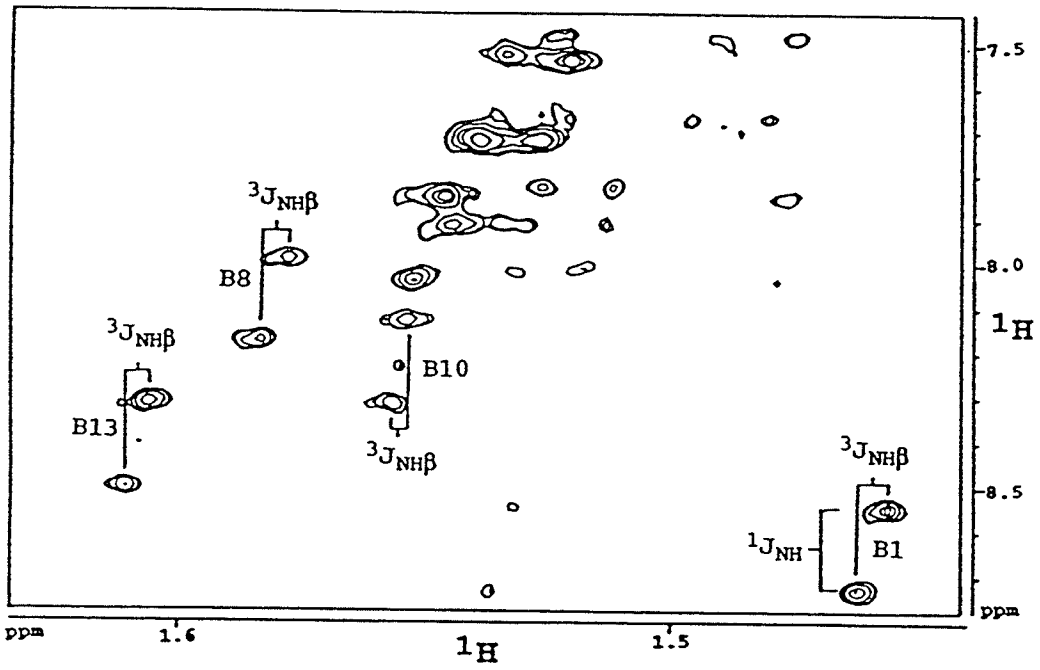

Figure 3-9: H_N to $H\beta$ region of the ROESY spectrum of an ^{15}N-labelled alamethicin in CD_3OH. The number of scans was 64 for each of the 512 increments with 8K data points each. No zero filling was applied and a $\pi/4$-shifted sine-bell window function was applied to both dimensions before fourier transformation.

methyls are labelled. In this spectrum, the cross peaks from the H_N to the $H\beta$ of the Aib residues are displaced by the $^1J_{NH}$ of 90 Hz in the F_1 dimension and by the $^3J_{NH\beta}$ in the F_2 dimension. The H_N to $H\alpha$ region of the ROESY spectrum of ^{15}N-labelled alamethicin is too crowded to measure the $^3J_{NH\alpha}$ from the figure (not shown). This is because the ROESY spectrum contains intraresidue and interresidue rOe crosspeaks.

A TOCSY spectrum will contain only intraresidue cross peaks and $^3J_{NH\alpha}$ might be measured from this experiment. Figure

3-10 shows the H_N to $H\alpha$ and $H\beta$ regions of a homonuclear TOCSY spectrum of ^{15}N-labelled alamethicin in methanol. From Figure 3-10, it is evident that the $^3J_{NH\alpha}$ are too small to be measured from this experiment.

Figure 3-11 shows a 2D-J spectrum. In this experiment, only the ^{15}N that is coupled to the selectively inverted proton is split and this splitting is due to the long range heteronuclear coupling. Figure 3-12 shows some slices along the F_1 dimension of the 2D-J spectrum acquired with selective inversion of different $H\alpha$ and $H\beta$. Table 3-3 gives the $^3J_{NH\beta}$ measured from the 2D-J experiments and the $^3J_{H\alpha H\beta}$ measured from DQF-COSY (Yee, 1991). The couplings measured were corrected for peak overlap using Figure 3-13. The largest $^3J_{NH\alpha}$ obtained is only 1.8 Hz. Based on the equation given in Table 3-2, for every $|^3J_{NH\alpha}|$ value less than or equal to 1.1 Hz, there are eight corresponding possible ψ angles. Figure 3-14 shows the dependence of $^3J_{NH\alpha}$ on the dihedral angle ψ. Also indicated in the figure are the expected $^3J_{NH\alpha}$ values for an ideal α helix and β sheet. The calculated ψ angles for alamethicin are closer to the β-strand conformation than the α helix. These values are given in Table 3-4.

Figure 3-15 shows the ^{13}C-^{15}N correlation spectrum of alamethicin in CD_3OH acquired with protons decoupled but ^{15}N coupled. The observed splitting is due to coupling of $^{13}C'$ to $^{13}C_\alpha$ and to ^{15}N. The long range J_{CC} are too small to be observed even in the ^{15}N decoupled spectrum (Figure 3-5). The $^1J_{C'N}$ are listed in Table 3-4. The average value is 15.3 ± 1.1

Figure 3-10: H_N to aliphatic region of the TOCSY spectrum of an ^{15}N labelled alamethicin in CD_3OH. The number of scans was 32 with 4K data points for each of the 256 t_1 increments. The F_1 and F_2 data were zero filled to 512 and 8K respectively and a $\pi/2$-shifted sine bell window function was applied before fourier transformation. Inset shows the F_2 slices of the H_N to H_α crosspeak components of Gly 11 showing that the displacement along F_2 due to $^3J_{NH\alpha}$ is almost nil.

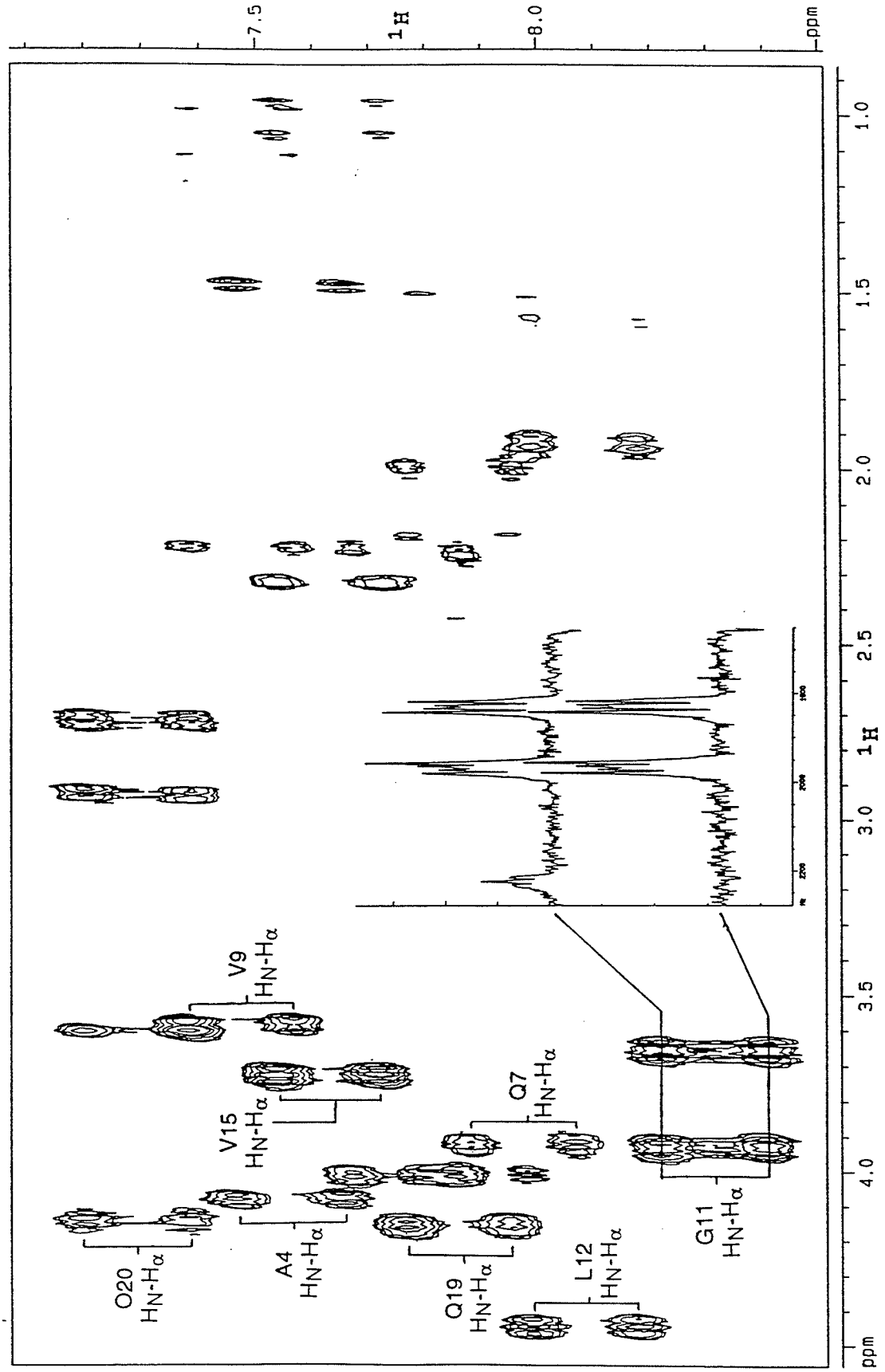
7.5
1H
8.0
ppm
1.0
1.5
2.0
2.5
3.0
3.5
4.0
ppm
V9 HN-Hα
V15 HN-Hα
A4 HN-Hα
O20 HN-Hα
Q7 HN-Hα
Q19 HN-Hα
L12 HN-Hα
G11 HN-Hα

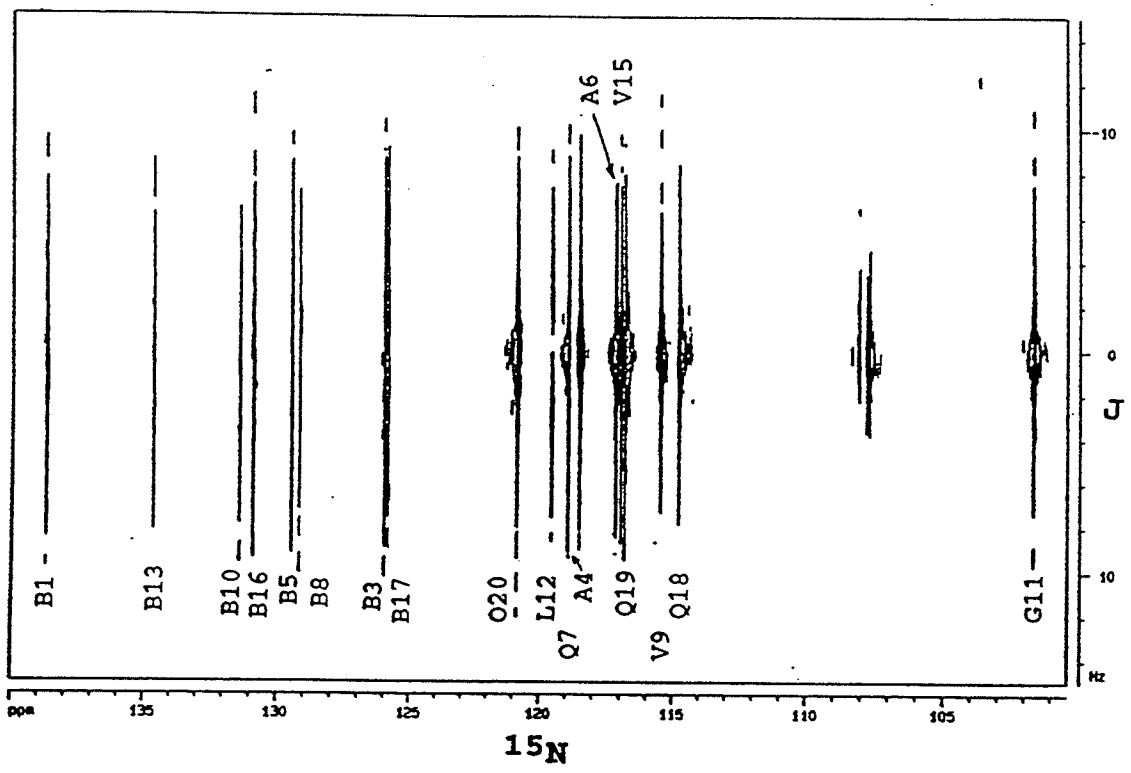

Figure 3-11: A 2D-J spectrum of ^{15}N-labelled alamethicin in CD_3OH acquired using the pulse sequence given in Figure 3-3. In this spectrum, the Hβ of Leu 12 at 1.9 ppm was selectively inverted with a 22 msec square, selective π pulse. A total of 32 increments of 4K data points each, over a spectral width of 40 Hz in the F_1 dimension were acquired. The data were zero filled to 8K by 256 points and processed using a gaussian linebroadening of 0.7 and exponential linebroadening of -0.5 in F_1. The F1 slice at Leu 12 is shown in Figure 3-12 c.

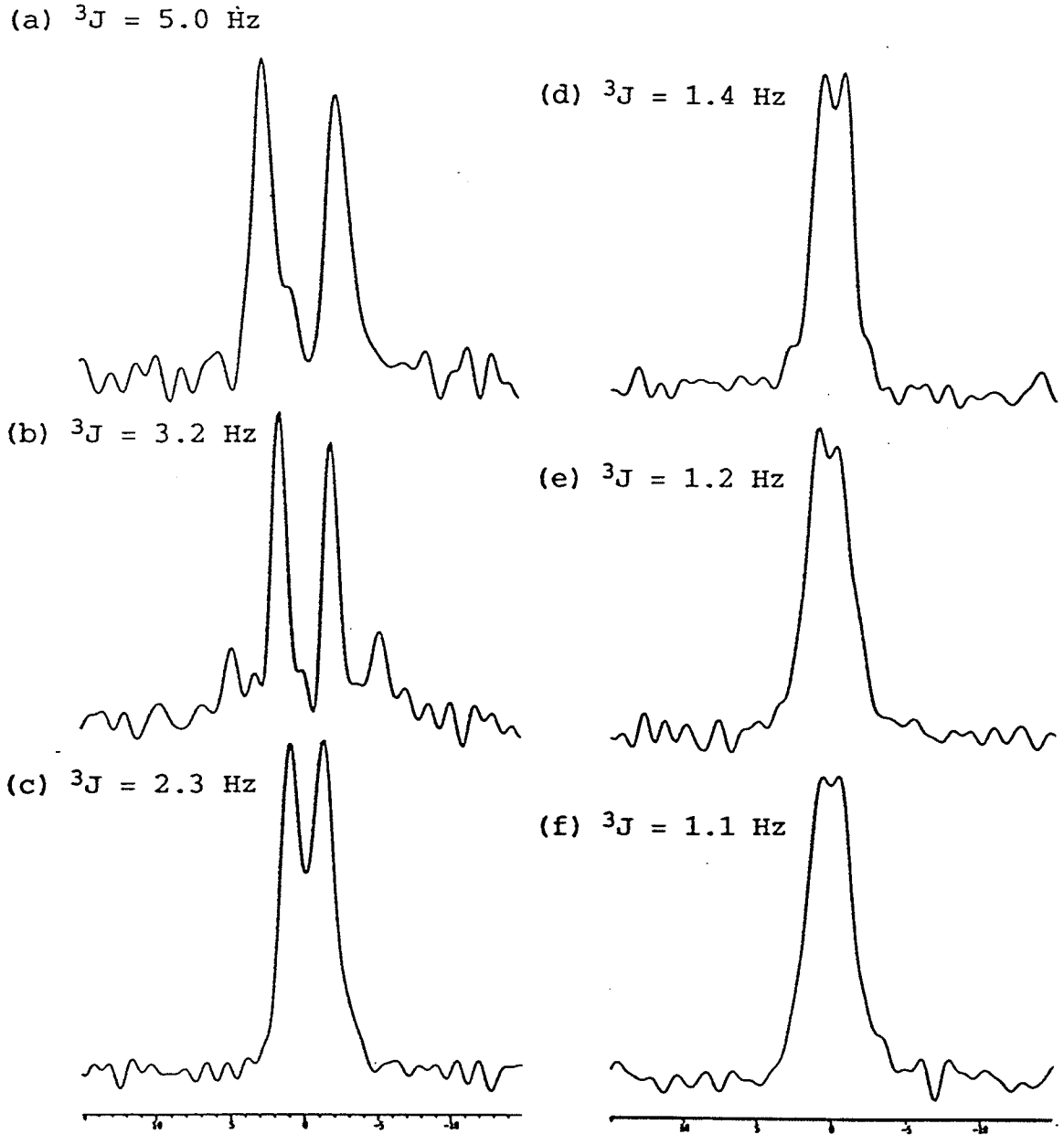

Figure 3-12: F_1 slices taken from the selective 2D-J experiments (see Figure 3-11) showing the peak separation due to $^3J_{NH\beta}$ for (a) Leu 12 (b) Ala 4 (c) Val 9 and the peak separation due to $^3J_{NH\alpha}$ for (d) Pro 14 (e) Val 9 (f) Ala 4. The J values given above are the apparent J (uncorrected).

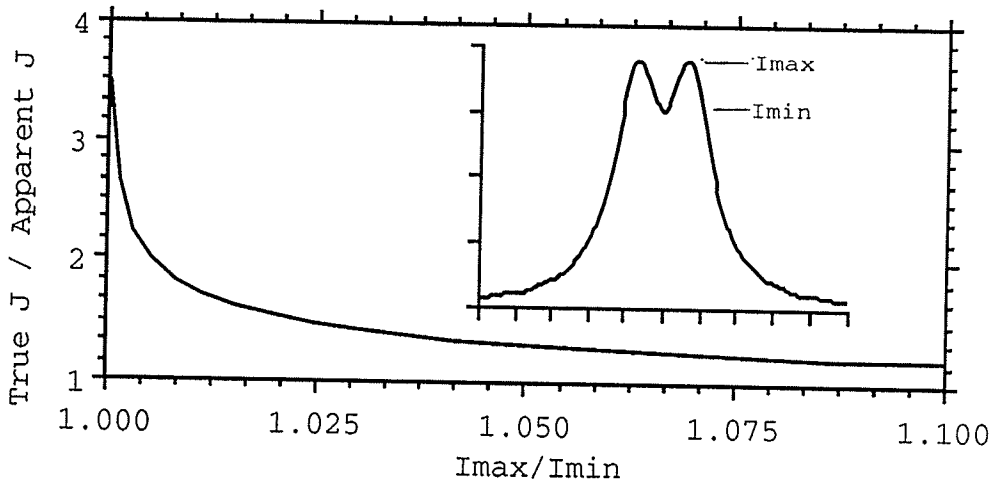

Figure 3-13: Correction for the observed coupling constant in overlapping doublets based on the peak-to-trough ratio (Bystrov, 1976). The curve was calculated based on the sum of two Lorentzian peaks with a width at half-height of 2 Hz.

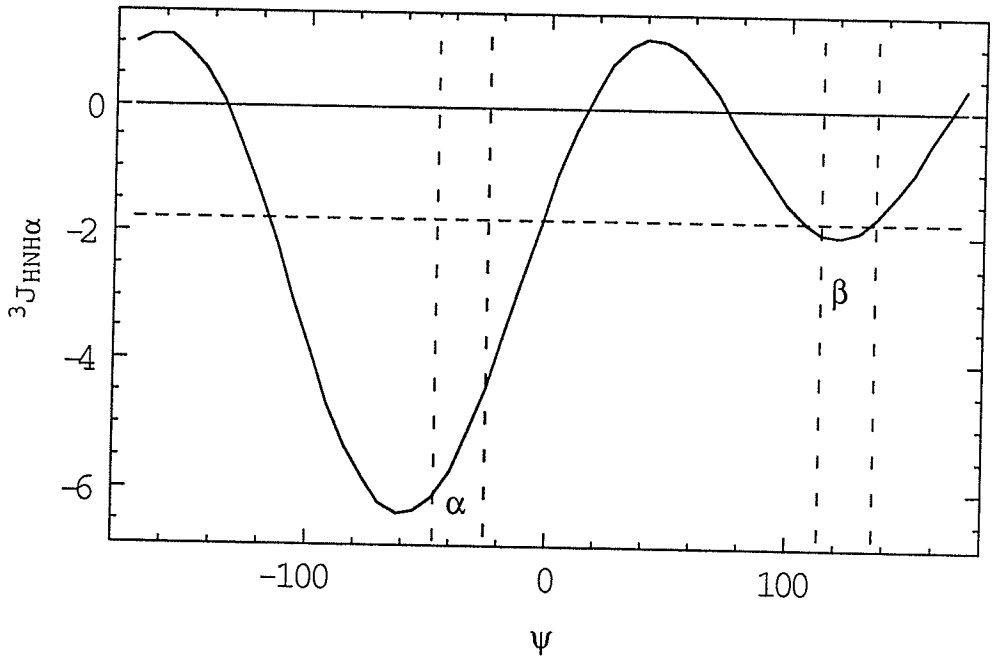

Figure 3-14: Plot of the $^3J_{NH\alpha}$ dependence on the ψ angle according to the equation given in Table 3-2 (Bystrov et al., 1975). The expected ranges of $^3J_{NH\alpha}$ for the ideal helix and β strand are shown. The largest value obtained is 1.8 Hz.

Table 3-3: χ_1 angles of alamethicin in solution as calculated from $^3J_{H\alpha H\beta}$ and $^3J_{NH\beta}$ using equations from Table 3-2. X-ray structure χ_1 angles are shown for comparison (Fox & Richards, 1982).

Residue	δ Hβ (ppm)	$^3J_{H\alpha H\beta}$[a] (Hz)	χ_1	$^3J_{NH\beta}$ (Hz)	χ_1	X-ray χ_1 A	B	C
Gln 7	2.28	nd	-	3.3	-101.1	-76.1	-71.4	-180.0
	2.15	nd	-	nd	-			
Val 9[b]	2.23	10.2	149.3	2.3	147.5	173.1	177.7	175.1
Leu 12	1.92	6.1	-79.7	5.0	-78.4	-64.8	-74.1	-96.3
	1.59	10.6		1.6	-80.6			
Val 15[b]	2.32	10.0	148.1	1.9	154.5	164.5	172.4	175.9
Gln 18[c]	2.23	6.3	-81.0	1.6	-80.6	-69.1	-60.0	-178.2
Gln 19[c]	2.02	6.9	-85.3	3.9	-94.2	-41.6	-178.8	-71.4
Phol 20	2.73	5.6	-76.2	3.7	-96.6	-65.3	-65.7	59.9
	2.94	8.8		1.7	-82.2			

[a]from M.Sc. Thesis; [b]χ_1 is the dihedral angle N-Cα-Cβ-Cγr, [c]degenerate; nd is not determined due to noise or overlap.

Table 3-4: ψ angles of alamethicin in solution as calculated from $^{3}J_{N(i+1)H\alpha(i)}$ coupling constants using equation from Table 3-2. $^{1}J_{C'-N}$ measured from Figure 3-19 and x-ray ψ angles are shown for comparison (Fox & Richards, 1982).

Residue (i)	$^{3}J_{NH\alpha}$ (Hz)	Calculated ψ from $^{3}J_{NH\alpha}$				$^{1}J_{C'-N}$ (Hz)	X-ray ψ A	X-ray ψ B	X-ray ψ C
N-Acetyl	1.6					13.3			
Aib 1	-					14.3	-45.9	-48.7	-41.2
Pro 2	1.8	-117	-3	107	133	14.3	-32.9	-35.8	-30.1
Aib 3	-					15.4	-50.1	-49.7	-50.7
Ala 4	1.6	-119	-1	101	138	15.1	-49.2	-46.4	-40.8
Aib 5	-					14.8	-44.2	-47.3	-44.5
Ala 6	b	-124→-152; 150→-172; 4→33; 52→90				15.7	-35.7	-37.7	-34.9
Gln 7	nd					14.7	-44.7	-48.1	-43.5
Aib 8	-					15.8	-49.3	-49.1	-42.7
Val 9	1.7	-117	-2	104	136	nd	-41.4	-49.0	-61.5

Aib 10	-					15.3	-35.9	-40.9	-52.6
Gly 11	b	same as Ala 6				17.0	-27.0	-29.7	-31.3
Leu 12	b	same as ala 6				16.1	-36.8	-46.7	-1.7
Aib 13	-					14.2	-32.8	-46.6	-36.6
Pro 14	1.7	-117	-2	104	136	14.9	-30.4	-29.0	-25.6
Val 15	1.8	-117	-3	107	133	nd	-60.5	-41.8	-53.1
Aib 16	-					15.6	-55.0	-51.0	-52.6
Aib 17	-					16.1	-39.1	-26.3	-33.1
Gln 18	b	same as Ala 6				15.8	-4.2	-24.3	-29.7
Gln 19	b	same as Ala 6				18.0	-7.2	-49.6	-39.5

b, less than 1 Hz, shows only broadening of the peak.

Figure 3-15: ^{13}C-^{15}N correlation spectrum (Mooberry et al., 1989) of ^{13}C-^{15}N labelled alamethicin in CD_3OH with ^{1}H decoupling only. The number of scans was 160 for each of 64 t_1 increments of 2K data points each. The F_1 and F2 dimensions were zero filled to 4K and 128 points, respectively and a $\pi/2$-shifted sine-squared filter was applied in both dimensions before fourier transformation. The splitting of the crosspeaks is due to the direct coupling of $^{13}C'(i)$ to $^{13}C_\alpha(i)$ and to $^{15}N(i+1)$. The assignments given are for the C'(i). The cross peaks in the middle arise from $^{13}C'(i)$-$^{15}N(i+1)$ correlations of molecules with $^{12}C_\alpha$ adjacent to $^{13}C'$.

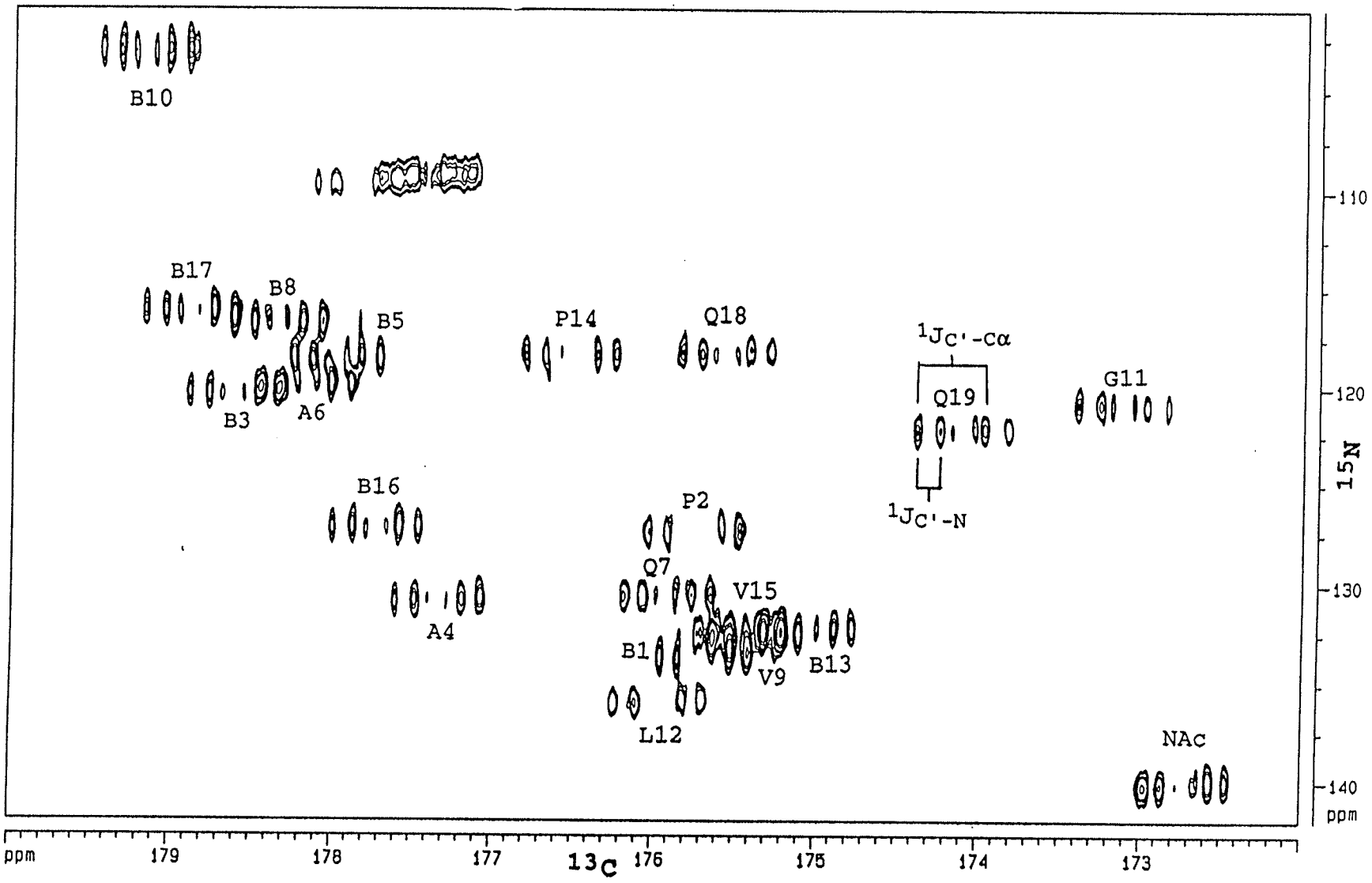
B10
B17
B8
B5
B3
A6
P14
Q18
$^1J_{C'-C\alpha}$
Q19
$^1J_{C'-N}$
G11
B16
A4
P2
Q7
V15
B1
V9
B13
L12
NAc
110
120
130
140
^{15}N
ppm
179
178
177
176
175
174
173
^{13}C

Hz. The lowest value is for the N-acetyl (13.3 Hz) and the highest value is for Gln 19 (18.0 Hz).

3.5.4 Deuterium Isotope Effect in Alamethicin

When alamethicin was dissolved in 50/50 CD_3OD/CD_3OH solvent, doubling of the cross peaks was observed in the ^{13}C-^{15}N correlation spectrum, except for the cross peaks assigned to Aib 1, Aib 13, and the sidechain carbonyls (Figure 3-16). The sidechain carbonyls are split into unresolved multiplets. The sidechain carbonyl is expected to be a triplet in 50/50 CD_3OD/CD_3OH because a primary amide has two exchangeable protons, each of which gives a different deuterium isotope shift on the adjacent carbonyl. The deuterium isotope effect is usually written as: $^n\Delta X(YD) = \delta_X(YD) - \delta_X(YH)$ where n is the number of bonds between atom X and the exchanging H; $\delta_X(YH)$ and $\delta_X(YD)$ are the chemical shifts of X when Y is bonded to H and D respectively (Hansen, 1988). In Figure 3-16, the peaks are shifted along the F_2 dimension by the $^2\Delta C{=}O(ND)$ and possibly by $^3\Delta C{=}O(ND)$, and along the F_1 dimension by $^1\Delta N(ND)$. For Pro 2, Pro 14, and for the N-acetyl the shift along F_2 is the $^2\Delta C{=}O(ND)$ only as there are no amide hydrogens three bonds away. For Aib 1 and Aib 13 the shift along F_2 is the $^3\Delta C{=}O(ND)$ as these residues are bonded to Pro residue. The shift was negligible in the Aib 1 and Aib 13 crosspeaks confirming the observations of Tuchsen and Hansen (1991) that $^3\Delta C{=}O(ND)$ are small except in strongly hydrogen bonded antiparallel β sheet residues.

Figure 3-16: Correlation of the ^{13}C carbonyls of residue (i) with the amide ^{15}N of residue (i+1) for ^{13}C-^{15}N labelled alamethicin in ~50/50 CD_3OH/CD_3OD. The acquisition and processing parameters are the same as those of Figure 3-5. The peak at the higher frequency corresponds to the $\delta_{C'}(NH)$ and the one at lower frequency to the $\delta_{C'}(ND)$. No doubling of peaks was observed in Aib 1 and Aib 13 because they are followed by Pro residues which do not contain amide hydrogens.

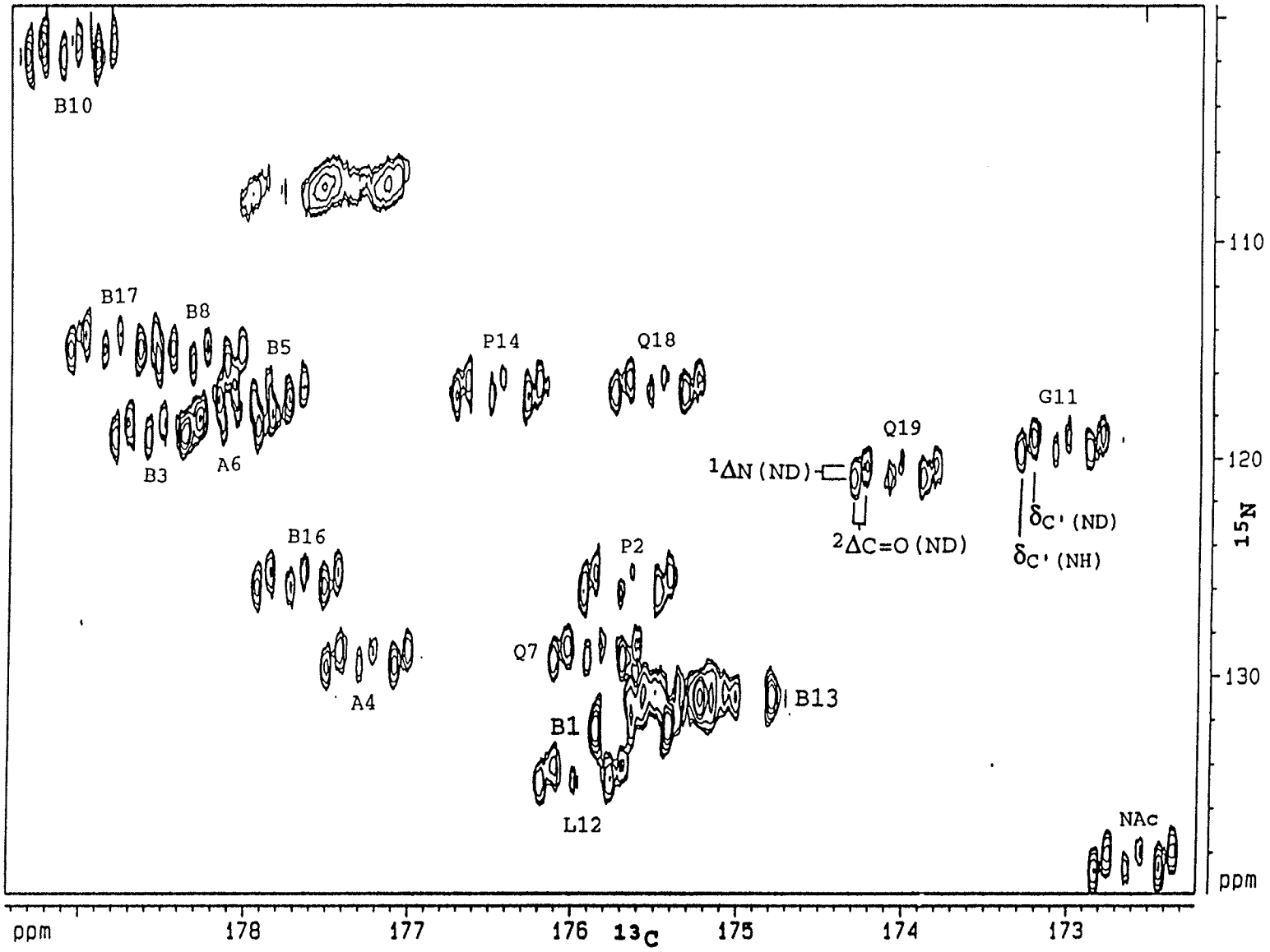
B10
B17
B8
B5
B3
A6
P14
Q18
Q19
G11
$^1\Delta N(ND)$
$^2\Delta C{=}O(ND)$
$\delta_{C'}(ND)$
$\delta_{C'}(NH)$
B16
P2
A4
Q7
B13
B1
L12
NAc
110
120
130
^{15}N
ppm
ppm
178
177
176
^{13}C
175
174
173

Table 3-5: Deuterium isotope shifts observed in alamethicin dissolved in 50/50(v/v) CD_3OD/CD_3OH. All values were measured from the $^{13}C(i-1)-^{15}N(i)$ correlation spectrum (Figure 3-16).

Residue (i)	$^{2}\Delta C{=}O(ND)$ ppm	$^{1}\Delta N(ND)$ ppm
Aib 1	0.085	0.92
Pro 2	na[a]	na
Aib 3	0.069[b]	0.70
Ala 4	0.083	0.70
Aib 5	0.082	0.77
Ala 6	0.090	0.61
Gln 7	0.087	0.55
Aib 8	0.085	0.77
Val 9	0.090	0.77
Aib 10	0.081	nd
Gly 11	0.090	0.63
Leu 12	0.080	0.73
Aib 13	0.079	0.73
Pro 14	na[a]	na
Val 15	0.070[b]	0.64
Aib 16	0.075	nd
Aib 17	0.084	0.68
Gln 18	0.090	0.78
Gln 19	0.085	0.66
Phol 20	0.076	0.76

na, no amide H; nd, not determined due to spectral overlap; [a] $^{3}\Delta C{=}O(ND)$ only; [b] $^{2}\Delta C{=}O(ND)$ only.

The $^{2}\Delta C{=}O(ND)$ in alamethicin range from 0.07 to 0.09 ppm (Table 3-5). The values obtained for alamethicin are in the same range as those reported for BPTI (Tuchsen & Hansen, 1991). The lowest values are those of Pro 2 and Pro 14. In model compounds, the $^{2}\Delta C(ND)$ values increase with increasing amide hydrogen bond strength (Reuben, 1986; 1987; Hansen et al., 1990; 1992). In the model acetamides, a non-hydrogen bonded $^{2}\Delta C{=}O(ND)$ has a value of 0.06 ppm (Hansen et al., 1992). The values in alamethicin are all greater than 0.06 ppm suggesting that all the H_N are hydrogen bonded either intramolecularly or with the solvent. Correlation of the $^{2}\Delta C{=}O(ND)$ values with δ_{HN} gave a very low correlation coefficient of 0.09 (Figure 3-17). Correcting the δ_{HN} values with the random coil values obtained from Wishart & Sykes (1994) gives a better correlation (0.35), but this is still small compared with those reported for model amides (> 0.8). (Table 3-1)

The $^{1}\Delta N(ND)$ values were also measured from Figure 3-16 and are listed in Table 3-5. The one-bond isotope effect is much larger than the two-bond isotope effect. The largest and smallest $^{1}\Delta N(ND)$ in alamethicin are for Aib 1 and Gln 7 respectively. A graph of $^{1}\Delta N(ND)$ vs $\Delta\delta_{HN}$ shows very little correlation between the two measurements (Figure 3-17).

Figure 3-17: Correlation of deuterium isotope effects in alamethicin with the chemical shift of the amide hydrogen. Filled circles are Aib residues and open circles are non-Aib residues. The random coil chemical shifts for non-Aib residues were obtained from Wishart & Sykes (1994) and the chemical shift of Aib 1 was used for the Aib residues.

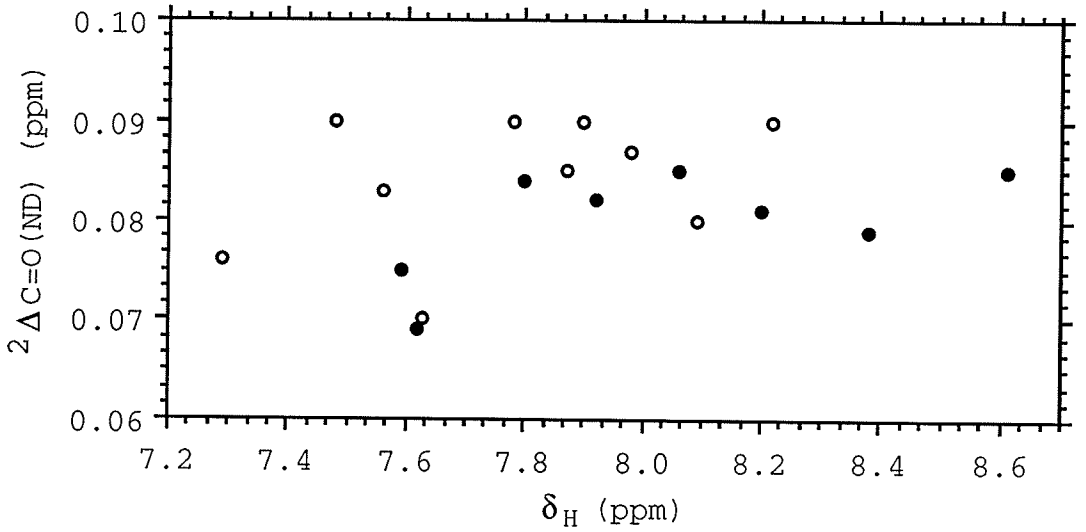
0.10
0.09
0.08
0.07
0.06
$^2\Delta$ C=O (ND) (ppm)
7.2
7.4
7.6
7.8
8.0
8.2
8.4
8.6
δ_H (ppm)

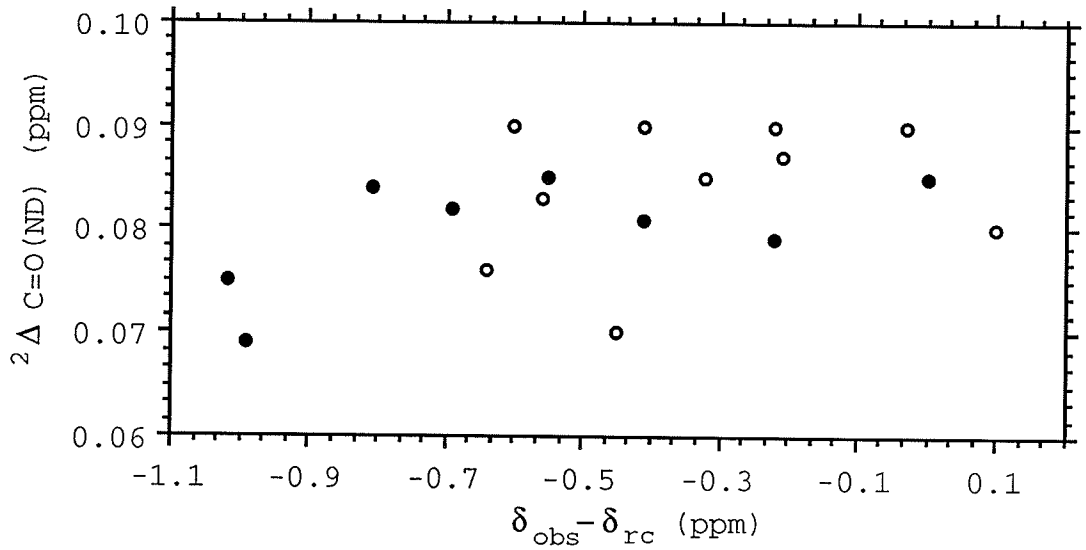
0.10
0.09
0.08
0.07
0.06
$^2\Delta$ C=O (ND) (ppm)
-1.1
-0.9
-0.7
-0.5
-0.3
-0.1
0.1
$\delta_{obs} - \delta_{rc}$ (ppm)

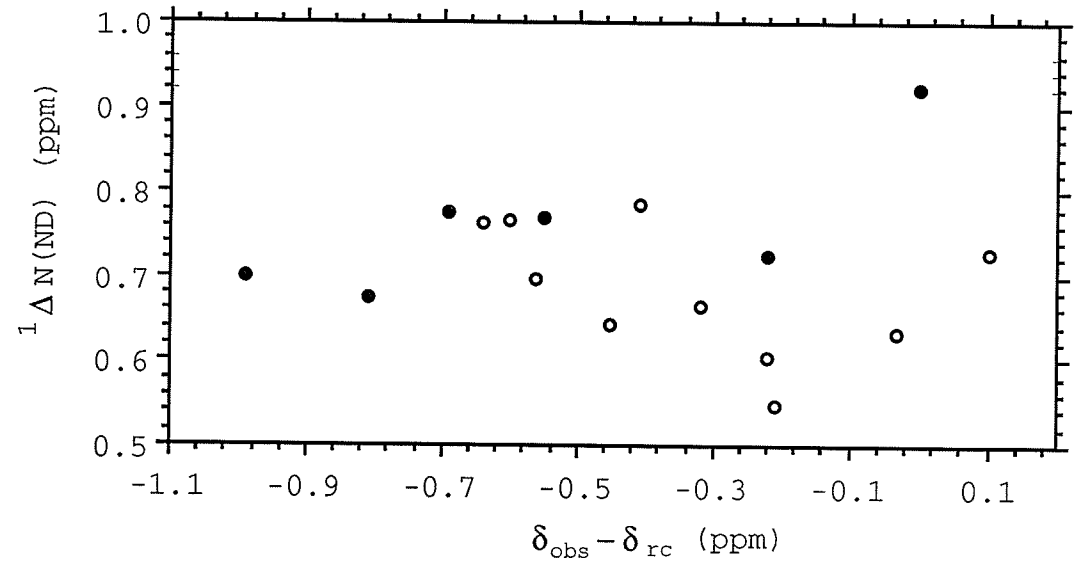
1.0
0.9
0.8
0.7
0.6
0.5
$^1\Delta$ N (ND) (ppm)
-1.1
-0.9
-0.7
-0.5
-0.3
-0.1
0.1
$\delta_{obs} - \delta_{rc}$ (ppm)

3.5.5 Solvent Dependence of the ^{1}H and ^{13}C Carbonyl Resonances in Alamethicin

Figure 3-18 shows sections of the ^{13}C-^{15}N correlation spectra of alamethicin at different DMSO concentrations. As the DMSO concentration was increased, the shielding on all the carbonyls increased except for those of Aib 1, Pro 2, and Leu 12 which were slightly deshielded (see Figure 3-19c). No data are reported for Val 9 and Val 15 because of resonance overlap in the mixed methanol-DMSO solvent. The largest shifts observed are for the ^{13}C carbonyl resonances of Aib 10, Gly 11, Aib 17, Gln 18, and Gln 19. Figures 3-19a,b show the static solvent accessibility of the carbonyl oxygens and carbons in the crystal structure. These were calculated following the method of Lee and Richards (1971) which is incorporated into the Xplor 3.1 software (Brunger, 1992). The probe radius used was 1.6 Å. The coordinates of the crystal structures were obtained from the Brookhaven protein data bank (Fox & Richards, 1982). The carbonyl oxygens of Gly 11, Gln 18, Gln 19, and the O_H of Phol 20 are solvent accessible in all three molecules in the crystal. The intramolecular hydrogen bonding pattern for each of the molecules in the crystal (Fox & Richards, 1982) shows that the carbonyls of Gly 11 and Gln 18 are not intramolecularly hydrogen bonded in any of the molecules, whereas the carbonyl of Aib 10 and Gln 19 is not hydrogen bonded in two of the three molecules. The carbonyl of Aib 17 is hydrogen bonded to the H_O of the Phol

Figure 3-18: Sections of the ^{13}C-^{15}N correlation spectra of ^{13}C-^{15}N labelled alamethicin in CD_3OD/DMSO mixture at (a) 0% DMSO, (b) 20% DMSO, and (c) 80% DMSO. Acquisition and processing parameters are the same as those of Figure 3-5. The doubling of the peaks is a result of isotope effects on $^{13}C'$ and ^{15}N because of residual CD_3OH (see Section 3.4).

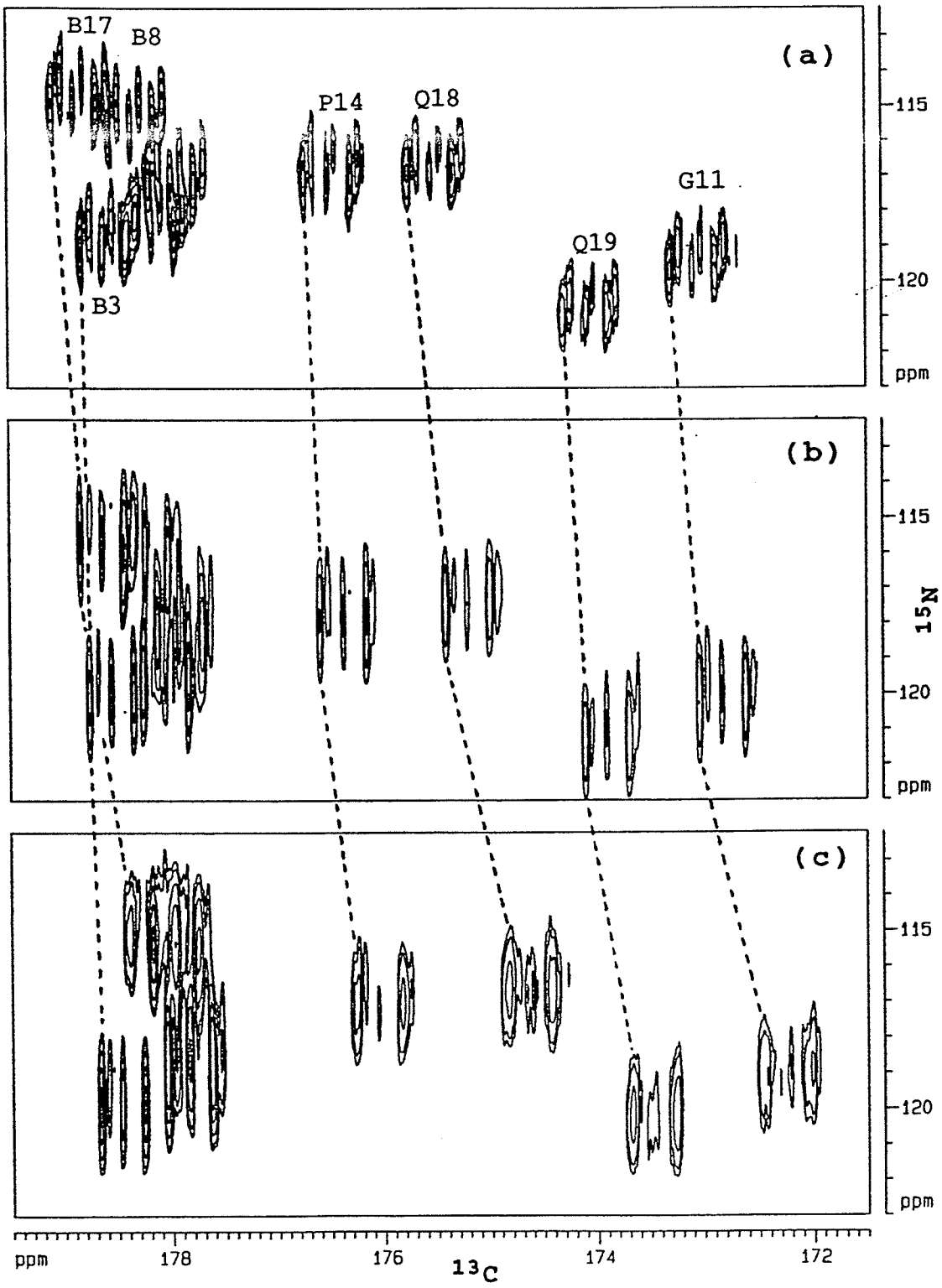
B17
B8
B3
P14
Q18
Q19
G11
(a)
(b)
(c)
115
120
ppm
^{15}N
ppm
178
176
174
172
^{13}C

Figure 3-19: Panels (a) and (b) are the static solvent accessibilities of the carbonyl O and C', respectively, in the three molecules (A, B, C) in the crystal structure (Fox & Richards, 1982). Panel (c) is the change in chemical shift of the carbonyl C' upon addition of DMSO. The chemical shifts were measured from Figure 3-18. Residue 0 is the carbonyl of the N-terminal acetyl group. The value for Val 9 and Val 15 in panel (c) was plotted as zero because this cannot be determined due to spectral overlap in the methanol-DMSO mixture. No value was determined for Phol 20 because it does not have a carbonyl C' but rather a CβOH and further there is no N(i+1) to correlate it with.

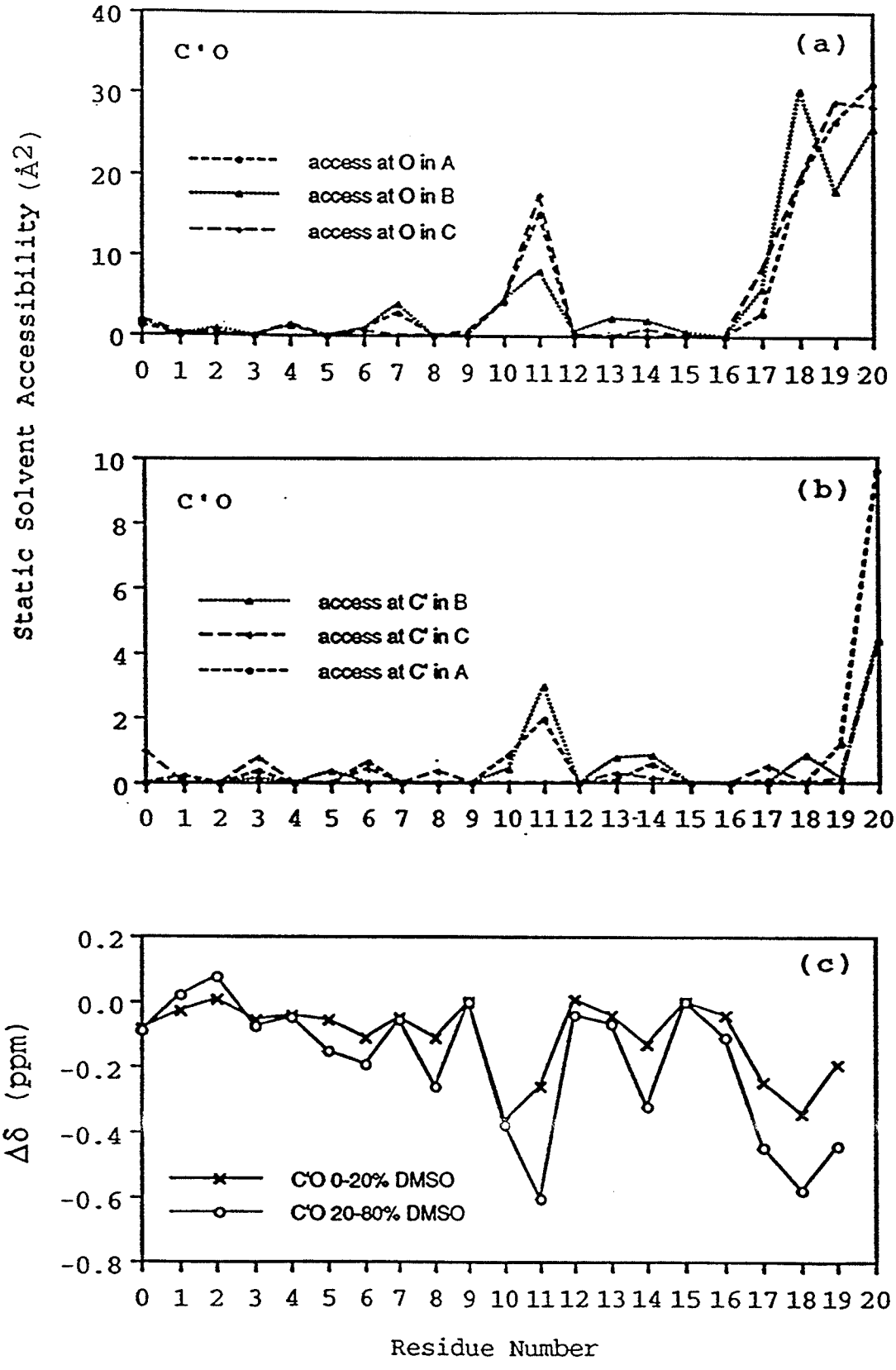
C'O
(a)
access at O in A
access at O in B
access at O in C
Static Solvent Accessibility (Å2)
C'O
(b)
access at C' in B
access at C' in C
access at C' in A
(c)
C'O 0-20% DMSO
C'O 20-80% DMSO
Δδ (ppm)
Residue Number

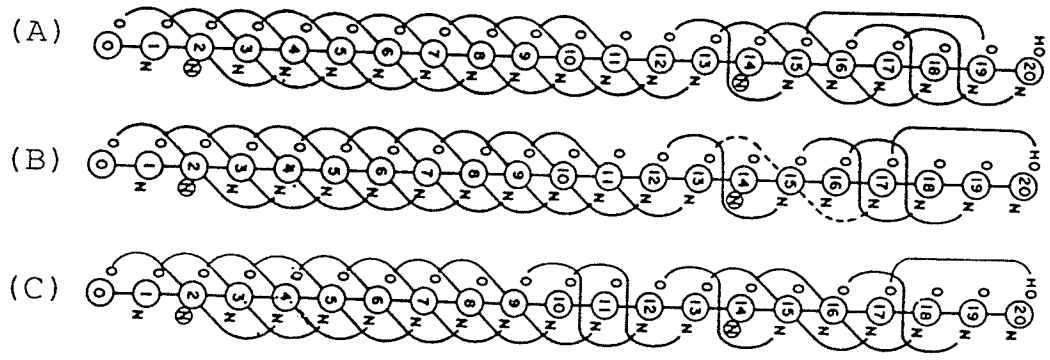

Figure 3-20: The intramolecular hydrogen-bonding pattern for the three alamethicin molecules deduced from the crystal structure (Fox & Richards, 1982). Residue 0 is the N-acetyl group. This diagram was photocopied from Fox & Richards (1982).

20 in two structures and to the H_N of Phol 20 in the other (see Figure 3-20).

One major assumption in interpreting the solvent perturbation results is that the local conformation of the peptide remains the same in going from pure methanol to a methanol-DMSO mixture. FTIR studies of the effect of DMSO on some proteins suggested that DMSO disrupts peptide intramolecular hydrogen bonding (Jackson & Mantsch, 1991). Figure 3-21 shows the amide region of ^1H spectra at two different DMSO concentrations. Addition of DMSO may induce aggregation of alamethicin as shown by the precipitates in the sample and also the increased linewidths in the ^1H spectra. To ensure that the addition of DMSO did not induce a drastic change in conformation, the $^3J_{HNH\alpha}$ of some residues

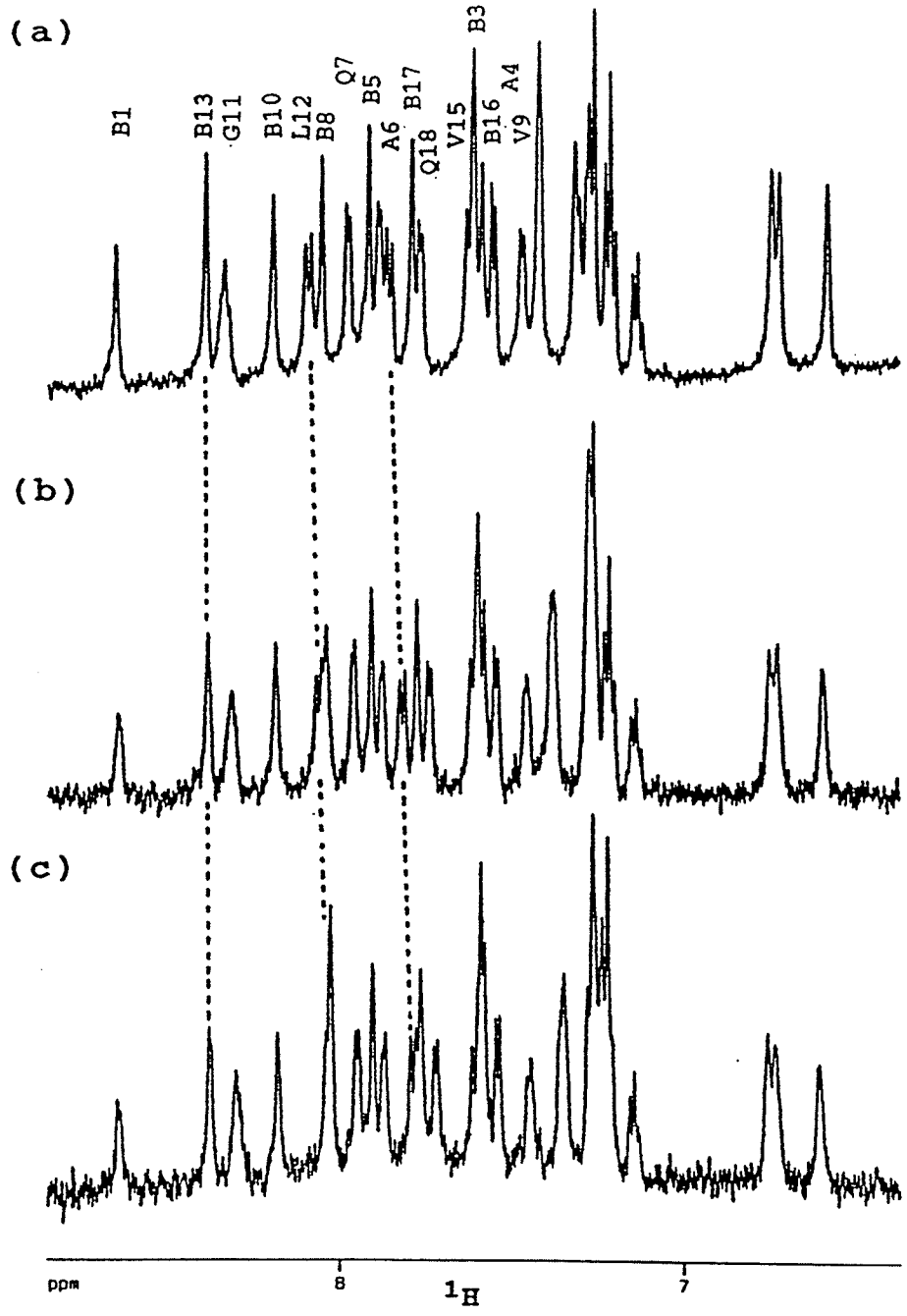

Figure 3-21: Amide regions of ^{1}H spectra of ^{15}N-labelled alamethicin in CD_3OH/DMSO-d_6 mixtures with ^{15}N decoupling during acquisition. (a) 0% DMSO, (b) 8.3% DMSO, and (c) 15.4% DMSO. The number of scans was 512 and no window function was applied.

Table 3-6: Measurable $^3J_{HNH\alpha}$ of alamethicin in CD_3OH/DMSO-d_6 solvent mixtures.

Residue	0% DMSO	8.3% DMSO	15.4% DMSO
Ala 4	5.7	6.0	5.2
Ala 6	4.5	a	a
Gln 7	5.1	3.7	2.9
Val 9	5.1	a	a
Leu 12	7.6	8.2	b
Gln 18	5.1	5.7	5.2
Gln 19	7.7	7.2	7.2

a, cannot be determined due to broad peaks; b, cannot be determined due to overlap.

were monitored from the 1D ^1H spectra and they are given in Table 3-6. The biggest observed change in coupling was in Gln 7 which went from 5.1 Hz to 2.9 Hz. Based on the equation given in Table 3-2 for $^3J_{HNH\alpha}$, this corresponds to a 24° change in the dihedral angle ϕ. Nevertheless, the measured $^3J_{HNH\alpha}$ suggest that the peptide is still in a helical conformation after the addition of DMSO. The changes in $^3J_{HNH\alpha}$ of all the other residues are less than one Hz.

Figure 3-22 c gives a summary of the DMSO solvent effect on the H_N chemical shifts. The largest changes observed are for Leu 12 and Gln 19 followed by Gln 18 and Phol 20. The H_N

Figure 3-22: Panels (a) and (b) are the static solvent accessibility of amide N and H_N in the three molecules in the crystal structure (Fox & Richards, 1982), respectively. Panel (c) is the change in amide ^1H chemical shift upon addition of DMSO. The ^1H chemical shifts were obtained from Figure 3-20 except for Phol 20 which was obtained from a ^1H-^{15}N correlation spectrum. The H_N value at Pro 2 and Pro 14 in panels (b) and (c) were plotted as zero because Pro residues do not have amide hydrogens.

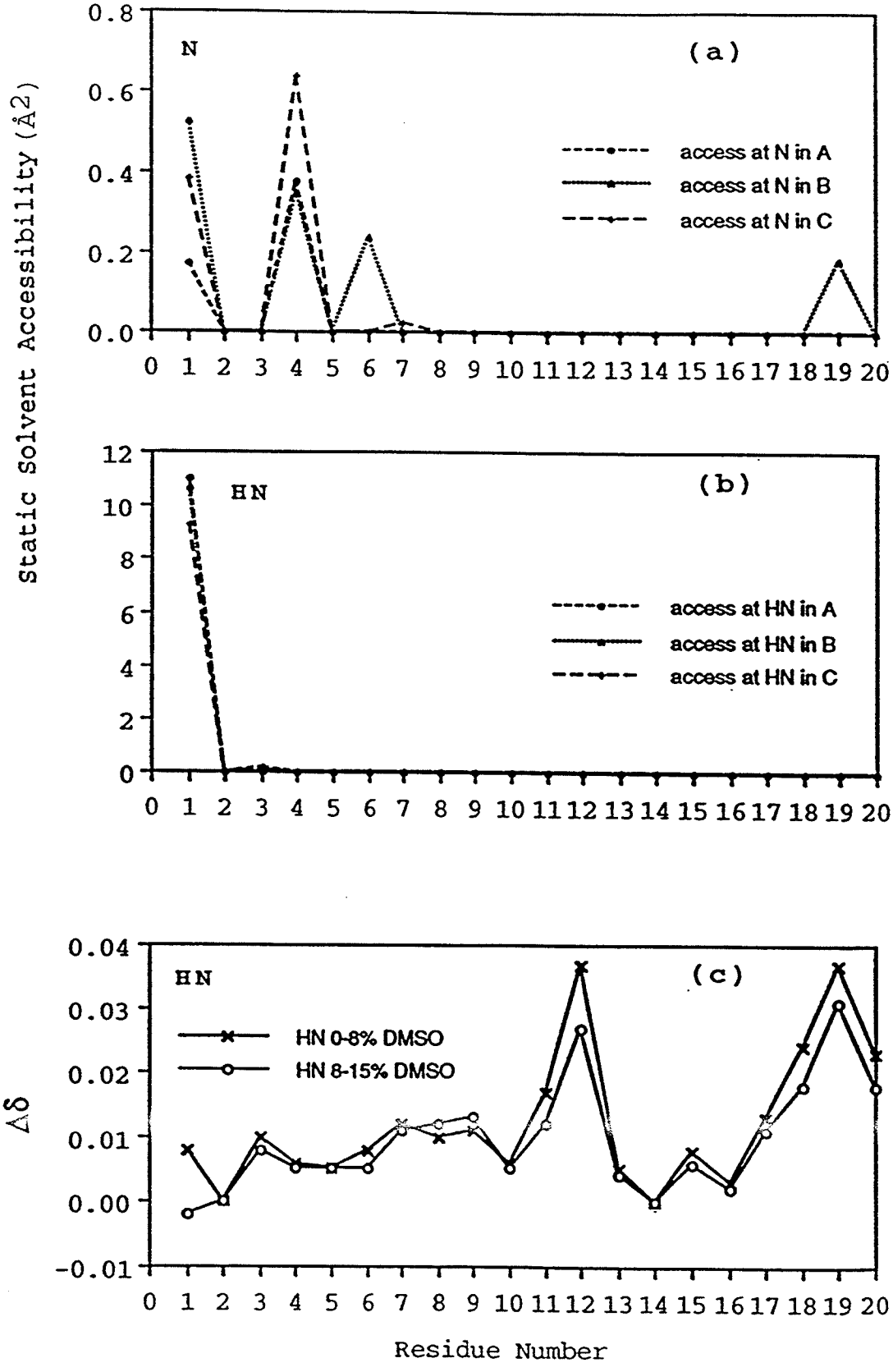
Static Solvent Accessibility (Å2)
N
(a)
access at N in A
access at N in B
access at N in C
HN
(b)
access at HN in A
access at HN in B
access at HN in C
HN
(c)
HN 0-8% DMSO
HN 8-15% DMSO
Δδ
Residue Number

of Aib 1 seems to be inaccessible to solvent in solution (see Figure 3-22 c). The static solvent accessibility of the amide nitrogens and hydrogens in the crystal structure are also shown in Figure 3-22 a, b. In the crystal structures, only the amide nitrogens of Aib 1 and Ala 4 are relatively solvent accessible in the three molecules and all the amide hydrogens with the exception of Aib 1 are inaccessible to solvent. (Note the difference in scale for the two measurements shown in a and b.)

3.5.6 Temperature Dependence of the Molar Ellipticity

Temperature dependence of the CD spectrum and the molar ellipticity is shown in Figure 3-23. The CD spectrum of alamethicin in methanol shows minima at 208 nm and 222 nm, typical of peptides containing helical conformations. The low thermal dependence of the molar ellipticity suggests stability toward helix unfolding of alamethicin.

3.5.7 Temperature Dependence of the Carbonyl Chemical Shifts

All carbonyl resonances exhibited a linear dependence on temperature from -23 to +57 °C. Figure 3-24 shows the temperature dependence for the chemical shifts of the carbonyl resonances. The temperature coefficients ($\Delta\delta/\Delta T$) for the carbonyls of all residues are summarized in Figure 3-25. The carbonyls of the N-terminal acetyl and Aibs 1, 3, 5, and 13 moved to higher frequency as the temperature was raised

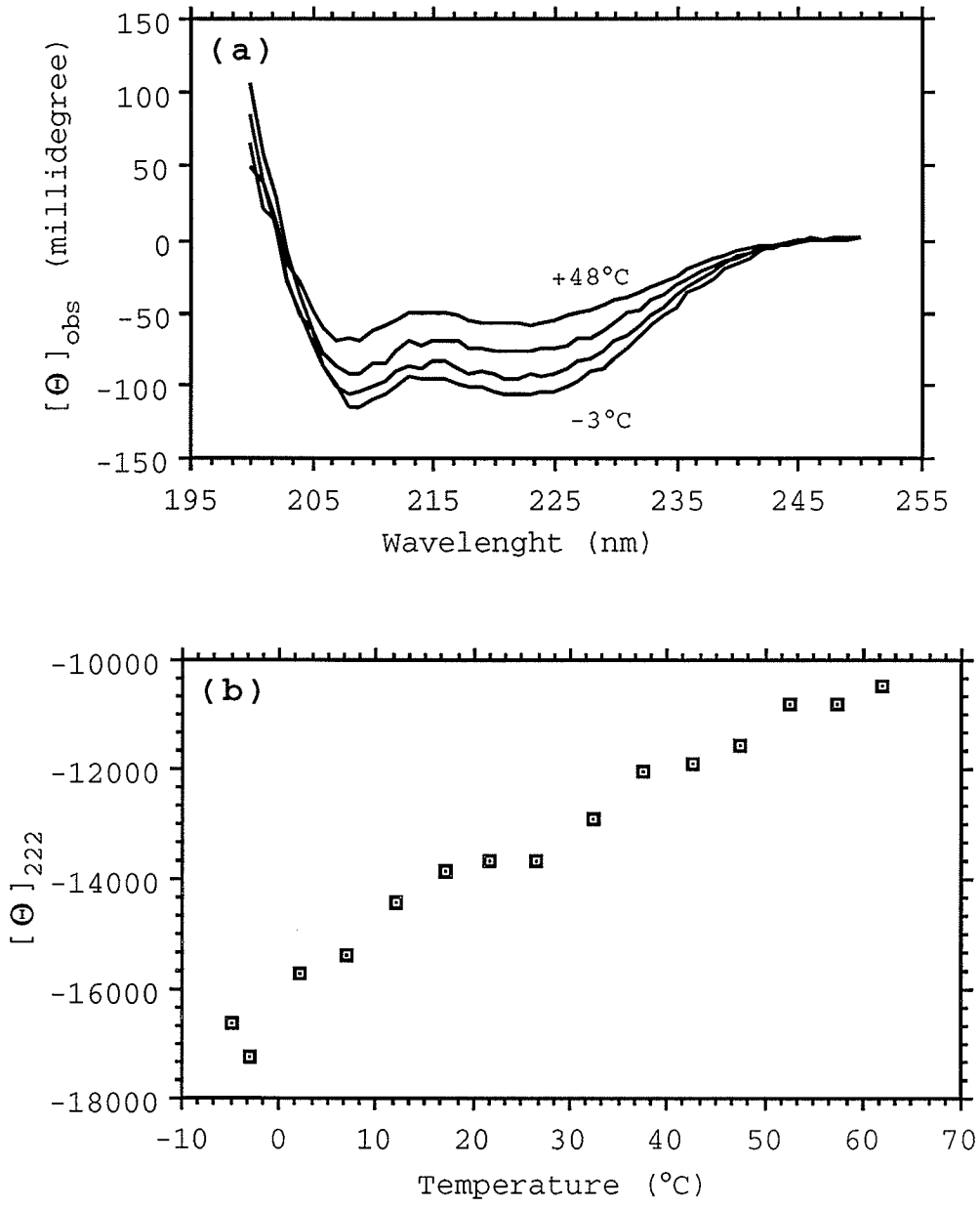

Figure 3-23: Variation with temperature of the (a) CD spectrum of alamethicin in methanol and (b) mean residue ellipticity measured at 222 nm. The CD spectra shown are for temperatures: -3°C, 16°C, 32°C, and 48°C.

Figure 3-24: Changes in ^{13}C carbonyl chemical shifts of residues in ^{13}C labelled alamethicin from -23°C to +57°C. The chemical shifts were measured from ^{13}C-^{15}N correlation spectra.

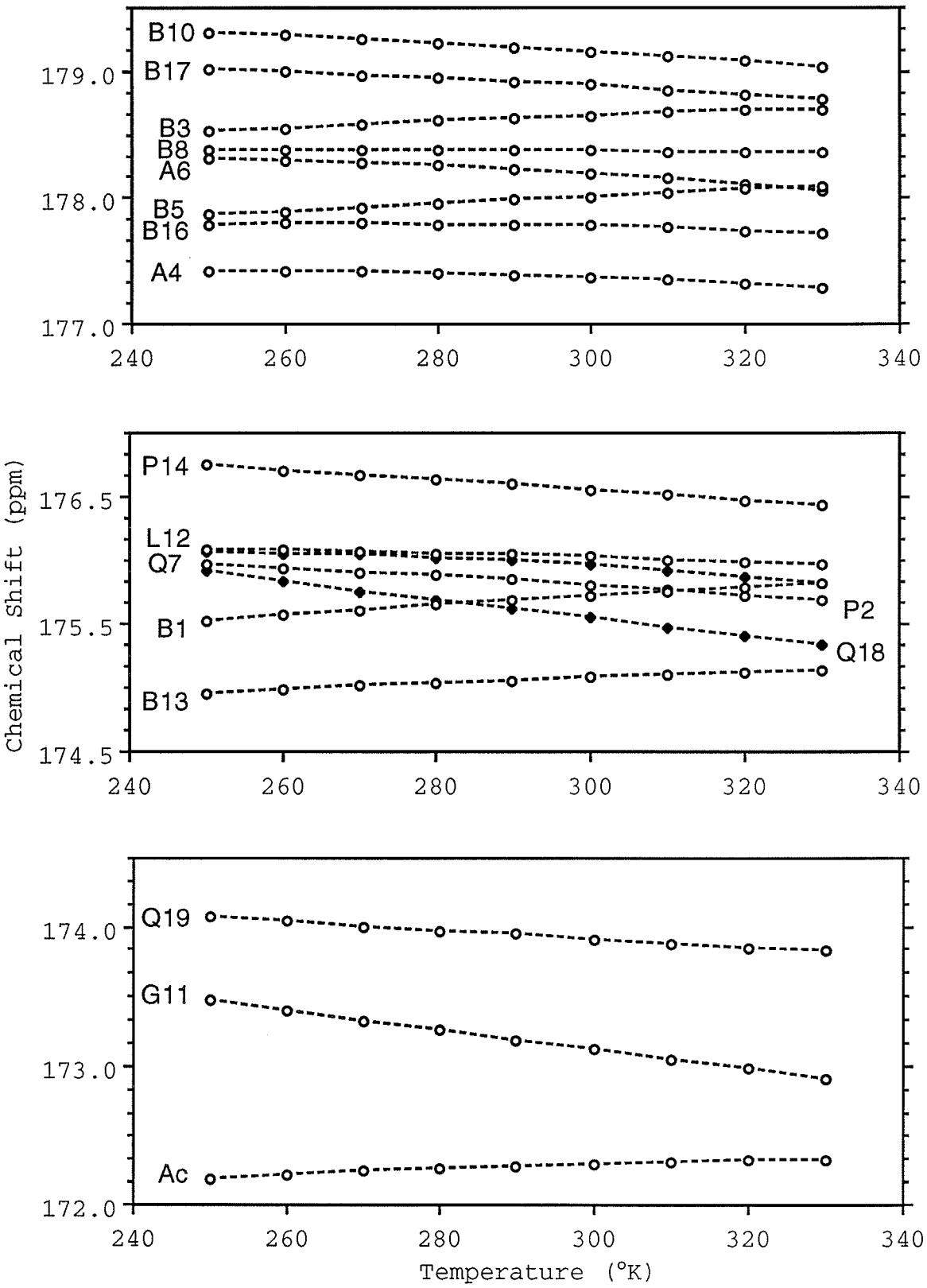
B10
B17
B3
B8
A6
B5
B16
A4
179.0
178.0
177.0
240
260
280
300
320
340
P14
L12
Q7
B1
B13
P2
Q18
176.5
175.5
174.5
Chemical Shift (ppm)
Q19
G11
Ac
174.0
173.0
172.0
Temperature (°K)

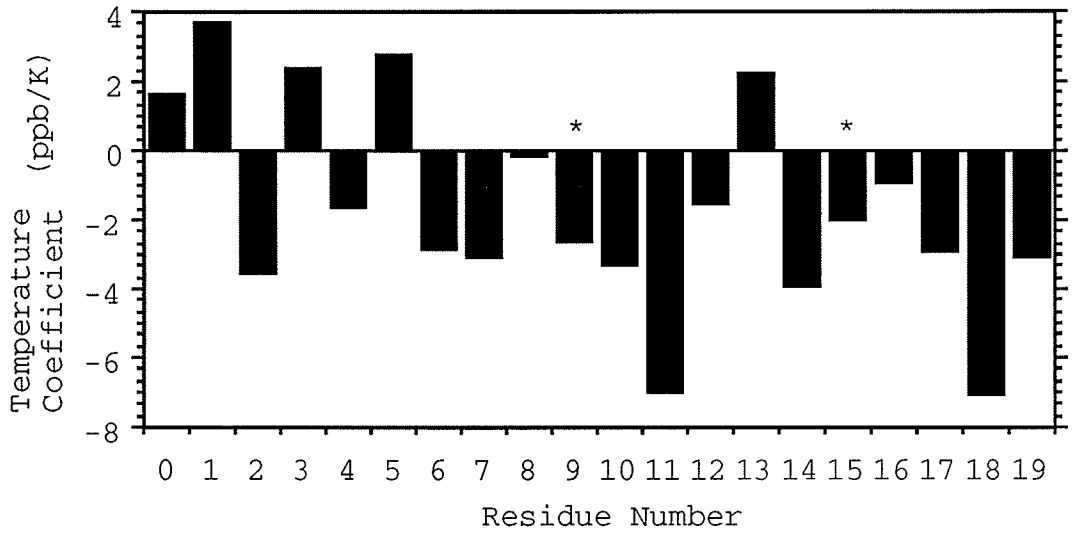

Figure 3-25: Temperature coefficients of the carbonyls of alamethicin in methanol. *Coefficients were calculated only from 276.7°K to 330°K because of resonance overlap at lower temperatures.

while all non-Aib residues and Aibs 8, 10, 16, and 17 moved to lower frequency. Both negative and positive $\Delta\delta/\Delta T$ were also reported in BPTI (Tuchsen & Hansen, 1988). The largest temperature coefficients observed are for Gln 18 and Gly 11, residues which are also the most sensitive to DMSO perturbation (Figure 3-19c).

3.6 Discussion

3.6.1 Conformation of Alamethicin in Methanol Based on ^{13}C and ^{1}H Chemical Shifts

Residue specific assignment of the ^{13}C resonances (Section 3.5.1) provides information about the secondary structure in alamethicin as the ^{13}C chemical shifts are

sensitive to backbone secondary structure (Spera & Bax, 1991; Wishart et al, 1991; Wishart and Sykes, 1994). Figure 3-26 shows the chemical shifts of the α carbons, carbonyl carbons, and α protons of the non-Aib residues of alamethicin relative to their random coil chemical shifts calculated from the data compiled by Wishart and co-workers (Wishart et al., 1992; Wishart & Sykes, 1994). The carbonyl and α carbons of residues 2, 4, 6, 7, and 18 resonate at a frequency higher than their random coil values by more than 0.5 ppm and 0.7 ppm, respectively, while the αH resonate at a frequency lower than their random coil values by more than 0.1 ppm, all suggesting that these residues are in a helical conformation. The chemical shifts for these residues agree with the observed coupling constants $^{3}J_{HNH\alpha}$ for residues 4, 6, 7, and 18 which are all less than 6.0 Hz indicating a helical conformation (Wuthrich, 1986). The terminal Phol does not have a carbonyl carbon but its α carbon resonates at a frequency lower than the random coil suggesting that it is in an extended conformation, in agreement with the observed $^{3}J_{HNH\alpha}$ of 9.9 Hz. The chemical shift of the α proton does not support this as it resonates at a lower frequency than the random coil value suggesting a helical conformation. An extended conformation at Phol 20 in solution however would explain the apparent lack of hydrogen bonding, as determined by solvent perturbation, between the Aib 17 carbonyl and the Phol 20 amide or hydroxide which is observed in the crystal structure. The carbonyl carbon of residue 19 suggests that it

Figure 3-26: The chemical shifts of the non-Aib residues in alamethicin in methanol relative to their random coil values used in the chemical shift indexing (CSI) as described by Wishart & Sykes (1994). 1.6 ppm was added to the ^{13}C chemical shifts reported in Appendix A before indexing to account for the difference in reference between TMS for the sample and DSS for the random coil values.

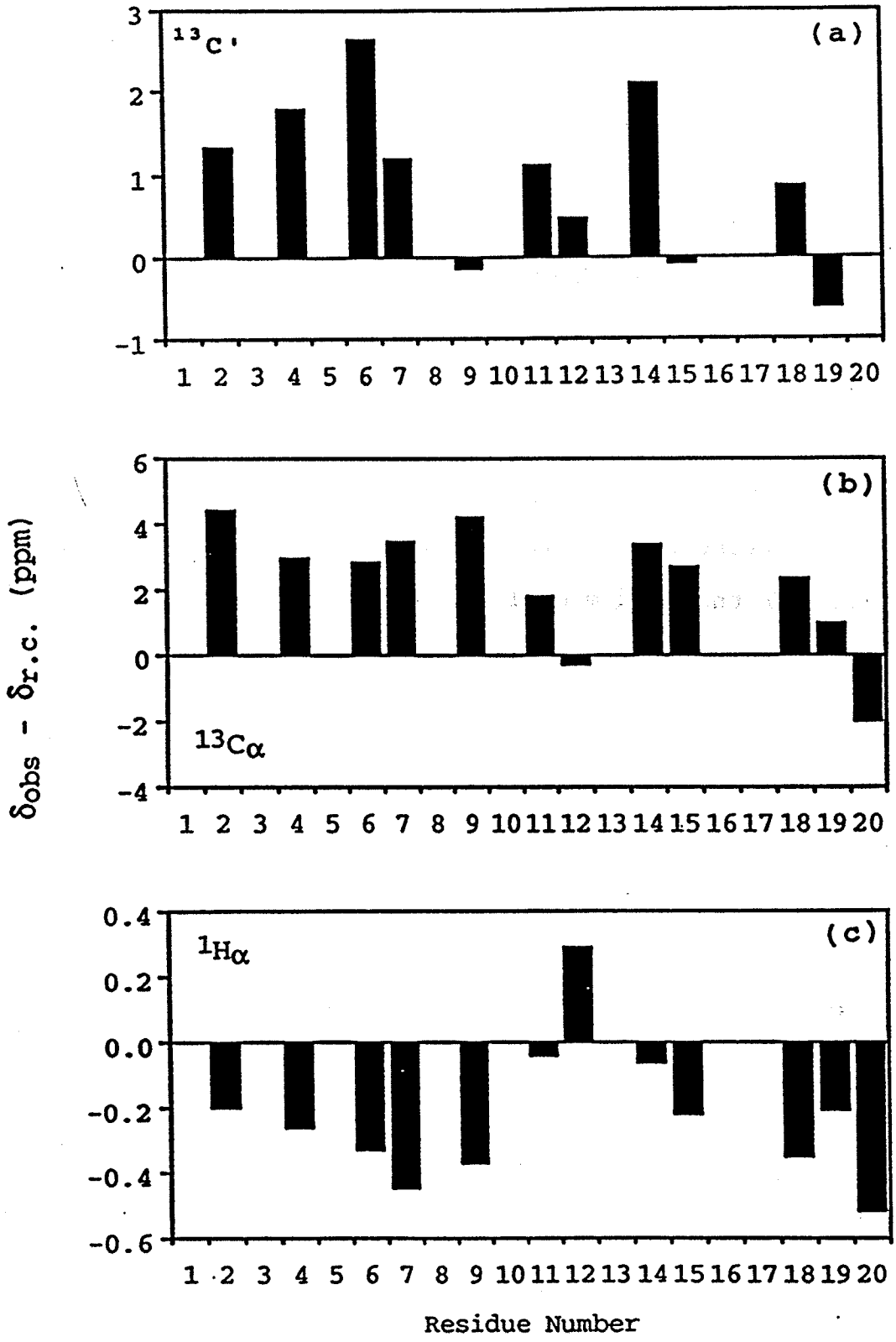
(a)
$^{13}C'$
(b)
$^{13}C\alpha$
(c)
$^{1}H\alpha$
$\delta_{obs} - \delta_{r.c.}$ (ppm)
Residue Number

is in an extended conformation because it resonates at a frequency lower than the random coil value by 0.6 ppm but its α carbon and α proton suggest that it is in a helical conformation. As pointed out by Wishart & Sykes (1994), the CSI method is a statistical technique and its accuracy for secondary structure prediction is better where there is a consensus among two of the three indices. Also the carbonyl shift is slightly less accurate than the C_α CSI because of its added sensitivity to solvent exposure and hydrogen bonding. So the chemical shifts in residue 19 suggest that it is in the helical conformation but its $^3J_{HNH\alpha}$ of 7.5 Hz suggests that it is conformationally averaged. The α and carbonyl carbon chemical shifts of Leu 12 fall within the random coil range but its H_α suggests that it is in an extended conformation, so again we follow the concensus CSI which would suggest that it is in the averaged conformation and would agree with the observed $^3J_{HNH\alpha}$ of 7.9 Hz. The α and carbonyl shifts of residues 11 and 14 suggest that they are in a helical conformation whereas the H_α shift suggests that both are in a random coil conformation. A helical conformation at Gly 11 is in agreement with the $^3J_{HNH\alpha}$ of 5.8 Hz but no $^3J_{HNH\alpha}$ value is available for Pro 14. The C_α and H_α CSI of Val 9 and 15 suggest that these are in a helical conformation whereas the C' CSI suggests that these are in a random coil conformation. The $^3J_{HNH\alpha}$ of Val 9 agrees with the helical conformation whereas the $^3J_{HNH\alpha}$ for Val 15 does not.

Thus, it appears that Val 9 is helical whereas the conformation of Val 15 is uncertain.

The eight Aib residues in alamethicin cannot be indexed because the chemical shifts of the α and carbonyl carbons in the random coil are not known. Aib residues have been shown to have a very high helix propensity (Basu and Kuki, 1993). In Aib-containing peptides, the chemical shift difference between the $^{13}C\beta$ of the Aib residues is at most 1.8 ppm for those peptides that are too short to form a helix. In longer peptides which form a helix, as judged from the Ala $C\alpha$ shifts, the difference between the $C\beta$ shifts of the Aibs increases to 3.2 ppm (Leibfritz et al., 1978). In alamethicin, the difference between the $^{13}C\beta$ shifts for all eight Aib is greater than 3 ppm (see Figure 3-4a) suggesting that they all adopt a helical conformation. All the Aib $^{13}C\alpha$ resonate over a very narrow range from 57.3 to 58.1 ppm (see Figure 3-7) suggesting that the conformation of all the Aib residues are very similar.

From the CSI of the non-Aib residues and the chemical shifts of the Aib residues, we conclude that (a) the N-terminus of alamethicin is helical from Aib 1 up to Gly 11, (b) Leu 12 is in an undefined or perhaps flexible conformation, (c) Aib 13 to Gln 19 form another helix although the coupling constants at Val 15 and Gln 19 suggest conformational averaging weakening the evidence for a helical C-terminus at these residues, and (d) Phol 20 is in an extended conformation.

3.6.2 Heteronuclear Coupling Constants in Alamethicin

The calculated ψ angles from the $^3J_{NH\alpha}$ of alamethicin are quite different from the ψ angles in the crystal structure (Table 3-4). One interpretation for the low $^3J_{NH\alpha}$ values observed in alamethicin in solution is that they reflect rotational averaging about ψ. The $^3J_{NH\alpha}$ coupling of the methyl protons of the terminal N-acetyl to the N of Aib 1 is 1.6 Hz which is close to the 2 Hz value reported for alumichrome (DeMarco et al., 1978) and the 1.3 Hz value reported for acetamide (Binsch et al., 1964). These coupling constants could be taken to represent the value for free rotation about the torsion angle ψ. All the measured $^3J_{NH\alpha}$ in alamethicin are within 1 Hz of the rotationally averaged values, which suggests that there is considerable rotation about the Cα-C' bonds in alamethicin. This is surprising since the $^3J_{HNH\alpha}$ for residues 4, 6, and 9 of alamethicin in CD_3OH are all less than 6 Hz suggesting that these residues are in a well-defined helical conformation (Yee, 1991; Esposito et al., 1987). Calculations on N-methylacetamide showed that the barrier to rotation around the ϕ angle ranges from about 1.2 to 2.3 kcal/mol while the barrier to rotation around the ψ angle range from about 0.4 to 1.3 kcal/mol depending on the empirical potential function used (Hagler et al., 1976). This difference in rotational barrier between the ϕ and ψ angles may possibly explain why the $^3J_{HNH\alpha}$ reports a

well-defined ϕ angle whereas the $^3J_{NH\alpha}$ suggest averaged ψ angles.

In the literature there are no reported $^3J_{NH\alpha}$ values larger than 2.1 Hz. The only evidence of large $^3J_{NH\alpha}$ values comes from HMBC experiments where a correlation cross peak between ^{15}N and the H_α of the preceding residue is observed in the helical regions of the proteins and this was attributed to the large $^3J_{NH\alpha}$ predicted for helices (5-6 Hz) (Bax et al., 1988). In larger proteins, the helical regions are less mobile because of hydrophobic interactions and hence might be expected to give larger $^3J_{NH\alpha}$. However, another interpretation is that the calculated Karplus equation does not adequately describe the relationship between the $^3J_{NH\alpha}$ and the ψ angle and that the cross peaks observed in the HMBC spectra arise from $^3J_{NH\alpha}$ of 2 Hz. In the cyclic peptide alumichrome, the ψ angle between Orn 1 and 2 is -38° in the crystal and so the calculated $^3J_{NH\alpha}$ should be -5.5 Hz but the measured $^3J_{NH\alpha}$ is less than 1 Hz (DeMarco et al., 1978). This discrepancy was partly explained as due to a distortion of the tetrahedral geometry of the C_α caused by the cyclic conformation of alumichrome (Llinas et al., 1977). Alamethicin is a linear peptide so distortions to the tetrahedral geometry of the C_α are less likely. Quantum mechanical calculations for N-methylacetamide and other small amides show that the correct experimental minima for the ϕ angle are predicted if an extended basis set is used in the calculation whereas a minimal basis set gives the wrong minima (Hagler et al.,

1976). Experimental minima were obtained from analysis of x-ray crystal structures of these compounds. For the ψ angles, however, neither basis set predicted the correct minima and it was postulated that the extended basis set (6-31G) that was used is not complete enough (Hagler et al., 1976). Clearly it would be helpful if more measurements of the $^{3}J_{HNH\alpha}$ could be obtained on larger proteins with known solution structures so that the Karplus equation could be verified.

The $^{1}J_{C'N}$ are interesting as they appear to reveal the hydrogen bonding state in proteins and small molecules (Juranic et al., 1995; Walter & Wright, 1979). In a short helix in human ubiquitin, the N-terminal residues show smaller than average $^{1}J_{C'N}$ (14 Hz) and the C-terminal residues have larger than average $^{1}J_{C'N}$ (16.5 Hz). The N-terminal residues are intramolecularly hydrogen bonded through their carbonyl oxygens and strongly hydrogen bonded to solvent through their amide hydrogens. The carbonyl oxygens are strongly hydrogen bonded to solvent at the C-terminus but their amide hydrogens are weakly hydrogen bonded intramolecularly. Strong hydrogen bonding through the carbonyl increases the $^{1}J_{C'N}$ whereas strong hydrogen bonding through the amide proton decreases the $^{1}J_{C'N}$. The same pattern is evident in alamethicin (Table 3-4). The N-acetyl has a smaller than average $^{1}J_{C'N}$ (13.3 Hz) which suggests that the H_N of Aib 1 is hydrogen bonded to the solvent, whereas Gln 19 has a larger than average value (18.0 Hz) which suggests that the C'O of Gln 19 is hydrogen bonded to the solvent. The

large $^{1}J_{C'N}$ at Gly 11 (17.0 Hz) supports the idea that the helical hydrogen bonding is interrupted in the middle of the molecule likely by intermolecular hydrogen bonding between solvent and the C'O of Gly 11.

3.6.3 Hydrogen Bonding in Alamethicin

The $^{2}\Delta C{=}O(ND)$, which show a very good correlation with δ_{H_N} in model compounds, show a very poor correlation with the H_N chemical shift in alamethicin (Figure 3-17). Tuchsen & Hansen (1991) suggested that the lack of correlation they observed in BPTI may be due to other effects aside from hydrogen bonding influencing the δ_{H_N} (e.g., ring current and residue type). In contrast Wishart et al. (1991) pointed out that in proteins, the δ_{H_N}, after correcting for residue type by subtracting the random coil value, mostly depend on $r_{NH\cdots O}^{-1}$ and that the ring current effect from aromatic sidechains is minimal. When the δ_{H_N} were corrected by the random coil values in alamethicin the $^{2}\Delta C{=}O(ND)$ vs δ_{H_N} correlation improved but it is still small (0.35) compared with that for the model compounds. This could be due to the presence of a helix macrodipole in alamethicin affecting the δ_{H_N}.

In the first three sets of model compounds used to calibrate $^{2}\Delta C(ND,OD)$, all the observed carbons belonged to a π-conjugated pathway (see Table 3-1 for structures). Hansen et al. (1992) used the acetamido compounds to calibrate the isotope effects ($^{2}\Delta C{=}O$) on carbons which are not conjugated by correlating them with the isotope effects on the aromatic

carbons ($^2\Delta C_{ar}$). They obtained a high correlation coefficient of 0.85 between $^2\Delta C{=}O$ and $^2\Delta C_{ar}$. They explained the small scatter in the data as due to added hydrogen bonding at the carbonyl oxygens of some of the compounds and to steric hindrance causing non-planarity of the amide groups in other compounds. The effect of the strength of hydrogen bonding at the carbonyl oxygen on $^2\Delta C{=}O$ is not known at present. Hydrogen bonding at both the amide hydrogen and the carbonyl oxygen is common in helical conformations. So another possible cause of the lack of correlation between $^2\Delta C{=}O$ and δ_{HN} in proteins is the presence of hydrogen bonding at the carbonyl oxygen which would affect the $^2\Delta C{=}O$ but not the δ_{HN}. Hydrogen bonding at the carbonyl oxygen would likely affect the $^2\Delta C{=}O$ via a change in the electronic distribution in the C'-N bond. The magnitude of the $^2\Delta C(ND)$ in the E-enamines (the non-hydrogen bonded form) is related to the double bond character of the C-N bond (Hansen et al., 1990). The $^2\Delta C_2(C_1D)$ in naphthalene and phenanthrene increase with the increase in the π-bond order of the C_1-C_2 bond (Martin et al., 1974). The $^1J_{C'-N}$ value was shown to be affected by hydrogen bonding at both the amide hydrogen and carbonyl oxygen in an opposing manner by changing the electronic distribution in the C'-N bond (perhaps changing the s character of the bond) (Juranic et al., 1995; Walter & Wright, 1979). If the same electronic pathway is taken to transmit the $^2\Delta C{=}O$ effect, then the effect of hydrogen bonding on the carbonyl oxygen will likely be opposite to that on the amide hydrogen, masking any

correlation between $^{2}\Delta C{=}O$ and δ_{HN}. Clearly, the effect of hydrogen bonding at the carbonyl oxygen could be studied by repeating the experiment of Juranic et al. (1995) and monitoring the $^{2}\Delta C'(ND)$ together with the $^{1}J_{C'-N}$.

Unlike the $^{2}\Delta C{=}O(ND)$, the $^{1}\Delta N(ND)$ in model compounds have not been correlated with hydrogen bond enthalpy. The $^{1}\Delta N(ND)$ in alamethicin is largest at Aib 1. In model enamine derivatives hydrogen bonded H_N (Z-enamines) show larger $^{1}\Delta N(ND)$ than non-hydrogen bonded H_N (E-enamines). The temperature coefficient of the H_N resonances (Babiuk, 1995; Yee et al., 1995) and the hydrogen exchange of the H_N (Dempsey, 1995) of alamethicin in methanol indicate that the Aib 1 H_N is not involved in intramolecular hydrogen bonding and must therefore be interacting with the solvent. This suggests that the large $^{1}\Delta N(ND)$ observed for Aib 1 compared to the rest of the residues indicates that the hydrogen bonding with solvent at Aib 1 is stronger than the intramolecular hydrogen bonding which all the rest of the H_N experience.

The results from the DMSO solvent perturbation of the carbonyl carbons agree well with the static solvent accessibilities of the carbonyl oxygens at the last two Glns (Figure 3-19). The large shifts in Aib 10 and Gly 11 suggest that both of these are solvent-exposed in solution; in the crystal, only Gly 11 is exposed in each molecule but the carbonyl of Aib 10 is not hydrogen bonded in two of the three molecules (Figure 3-20). The large DMSO-induced shift

observed at the Aib 17 carbonyl carbon suggests that its carbonyl is not hydrogen bonded. The $^{3}J_{HNH\alpha}$ and $^{13}C_{\alpha}$ CSI suggest that Phol 20 is in an extended conformation in solution and this could explain the apparent absence of hydrogen bonding between the carbonyl of Aib 17 and either of the Phol 20 amide or hydroxyl groups. Thus, the hydrogen bonding interaction with Phol 20 observed in the crystal structure is not present in solution.

The carbonyls of the N-acetyl and Aib 1 show a very small solvent perturbation which suggests that these are solvent shielded, most likely by hydrogen bonding. ROe and homonuclear coupling constant data on alamethicin suggested that its N-terminus is predominantly helical in methanol (Yee, 1991; Esposito et al., 1987; Franklin et al., 1994). In the crystal, the carbonyls of N-acetyl and Aib 1 are suggested to be in an α helical hydrogen bonding arrangement (Fox & Richards, 1982). However, the temperature dependence of the amide chemical shifts suggests that the amide hydrogens of Aib 3 and Ala 4 are hydrogen bonded to the carbonyls of the N-acetyl and Aib 1, respectively (Babiuk, 1995; Yee et al., 1995). Moreover, in alanine-based peptides, it has been suggested that, when the carbonyl of an acetyl at the N-terminus participates in backbone hydrogen bonding, it is likely to be in a 3_{10}- rather than in an α-helical arrangement (Rohl and Baldwin, 1994). The presence of a 3_{10} interaction in alamethicin has been suggested based on FTIR spectroscopy (Harris and Chapman, 1988). The conclusion is

that the carbonyl of the N-acetyl is shielded from solvent by interaction with the H_N of Aib 3 in a 3_{10} interaction and that the peptide is stably folded up to the end of the amino terminus of the peptide.

The solvent perturbation on the H_N is interesting in that it seems to correlate better with the static solvent accessibility of the carbonyl oxygens than with the static accessibility of the amide hydrogens or nitrogens. An exception is the sensitivity to solvent of the Leu 12 amide hydrogen which correlates with the accessibility of neither the O nor the N. The three C-terminal amide protons are solvent shielded in all the crystal molecules but these are very sensitive to solvent perturbation. Also the Aib 1 H_N, which is very accessible in the crystal structure, is relatively insensitive to solvent perturbation. If the solvent-induced chemical shifts of the H_N resonances are shifted to the N-terminus by one residue, the C' solvent perturbation pattern (Figure 3-19c) is nearly identical to the H_N pattern (Figure 3-21c). Since the carbonyl carbon of residue (i) belongs to the same amide group as the H_N of residue (i+1) this suggests that the solvent perturbation of the chemical shift of the amide hydrogen is sensitive to the solvent environment of the preceding carbonyl to which it is bonded.

Insensitivity to solvent perturbation of the H_N has previously been interpreted as due to solvent shielding on the H_N mostly by hydrogen bonding (Ausperger et al., 1995;

Urry et al., 1975). In gramacidin S and in a synthetic cyclic dodecapeptide, the solvent perturbation of the H_N and C' were observed to be complementary and were used to identify the hydrogen bonding partners (Urry et al., 1975; Khaled et al., 1979). However, this is not what we observe in alamethicin. It is possible that, if there is conformational mobility around Leu 12 and Gln 19, then their H_N or the CONH groups may have larger solvent exposure than when they are locked in a rigid helical conformation in the crystal. The Aib 1 H_N is insensitive to solvent perturbation but its temperature coefficient (Babiuk, 1995) and hydrogen exchange data (Dempsey, 1995) suggest that it is not intramolecularly hydrogen bonded in methanol. So the sensitivity to solvent perturbation of the H_N is more likely due to solvent accessibility of the CONH group that is reflected in the accessibility of the carbonyl oxygen but not the H_N.

From the carbonyl solvent perturbation results, we conclude that the carbonyls of N-acetyl and Aib 1 are hydrogen bonded presumably in a 3_{10}-type of interaction with the H_N of Aib 3 and Ala 4, respectively; the carbonyls of Aib 10 and Gly 11 are not hydrogen bonded; and the carbonyls from Aib 17 to Gln 19 are also not hydrogen bonded. The interaction between the carbonyl of Aib 17 and the Phol 20 amide or side chain is not observed in solution.

3.6.4 Stability of Alamethicin to Temperature Denaturation

The stability of the alamethicin helix, particularly in the N-terminal half of the peptide, is evident from the temperature dependence of the carbonyl chemical shifts. Increasing the temperature of an alamethicin solution by 80°C causes the carbonyl resonances of all the non-Aib residues to shift to a lower frequency. For the residues postulated to be in a helical conformation on the basis of $^{1}H_{\alpha}$, $^{13}C_{\alpha}$, and $^{13}C'$ CSI (2, 4, 6, 7, 18) the shift is in the direction expected if increasing temperature decreases the time spent in the helical conformation. However, the total change in carbonyl chemical shift over the entire temperature range is at most 0.6 ppm (Gly 11) for any residue. This compares to the difference in carbonyl chemical shift between the average random coil and α helix values which ranges from 1 to 2.2 ppm in the data compiled by Wishart et al. (1991) and ranges from 2 to 3 ppm for the residues studied by Shalongo et al. (1994a,b). Even at +57°C most of the non-Aib carbonyls resonate at a higher frequency than their random coil chemical shifts suggesting that they are significantly helical at the highest temperature studied. These results are supported by the CD data which indicate significant helicity over the entire temperature range.

In contrast to the non-Aib residues which shift to a lower frequency, several Aib residues (1, 3, 5, 13) shift to higher frequency as the temperature is increased. Shalongo et

al. (1994a) have pointed out that a major component of the observed temperature-dependence of peptide $^{13}C'$ chemical shifts is the temperature-dependence of the lock signal which is about +10 ppb/°C for D_2O (Glasel, 1974). In the peptide Ac(AAQAA)$_3$amide at low temperatures, where the helix is fully formed and stable, the thermal dependence of the carbonyl resonances is about +10 ppb/°C (Shalongo et al., 1994a). Conformational changes due to increased temperature were readily apparent from the CD spectra (Figure 3-27) and the non-linear shifts of $^{13}C'$ to lower frequency with slopes as high as -40 ppb/°C (Figure 3-28).

Alamethicin shows a very different behaviour with temperature (compare Figure 3-23 with Figure 3-27 and Figure 3-24 with Figure 3-28). The most thermal sensitive residue, Gly 11, exhibits linear shifts of only -7 ppb/°C. The small (+1 to +3 ppb/°C), linear thermal dependence of the N-acetyl carbonyl and the carbonyls of Aib residues 1, 3, 5, and 13 suggest that, over the 80°C temperature range studied, these residues are the most conformationally stable in the peptide. These small slopes suggest that alamethicin is more stable than alanine-based peptides. This is in agreement with the hydrogen exchange data for alamethicin in methanol (Dempsey, 1995) which showed that alamethicin is considerably more stable than alanine-based peptides (Figure 3-29). It had been suggested that Aib residues give conformational stability to helical peptides (Augsperger et al., 1995) and the presence of an N-acetyl group may also help to stabilize the N-

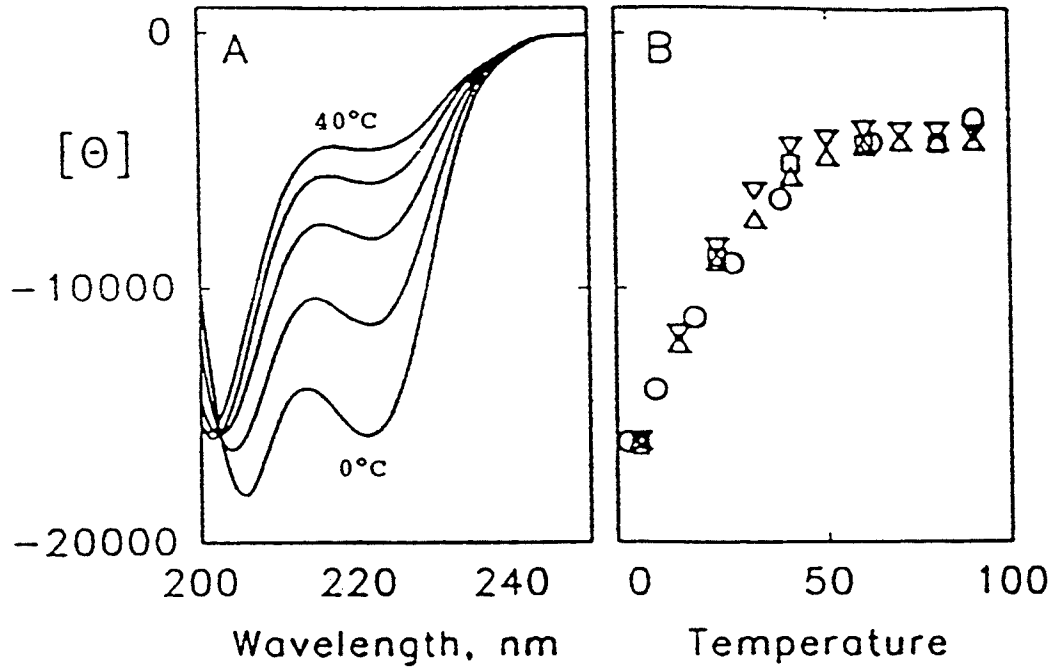

Figure 3-27: Variable temperature CD measurements of the peptide Ac(AAQAA)$_3$amide in water. The square symbols in panel B are for the peptide Ac(AAQAA)$_3$Yamide and the others are for different concentrations of the peptide Ac(AAQAA)$_3$amide ranging from 23 μM to 230 μM. This diagram was photocopied from Shalongo et al. (1994a).

terminus of the helix (Chakrabartty et al., 1993; Jung et al., 1983).

The transition from a helix to a coil conformation in alanine-based peptides was explained using a two state cooperative transition. Cooperative unfolding of a helix is characterized by sigmoidal CD versus denaturant or temperature plots (see Figure 3-27). In alamethicin we fail to see a sharp transition between helix and coil in the CD measurements. The cooperative transition is usually explained

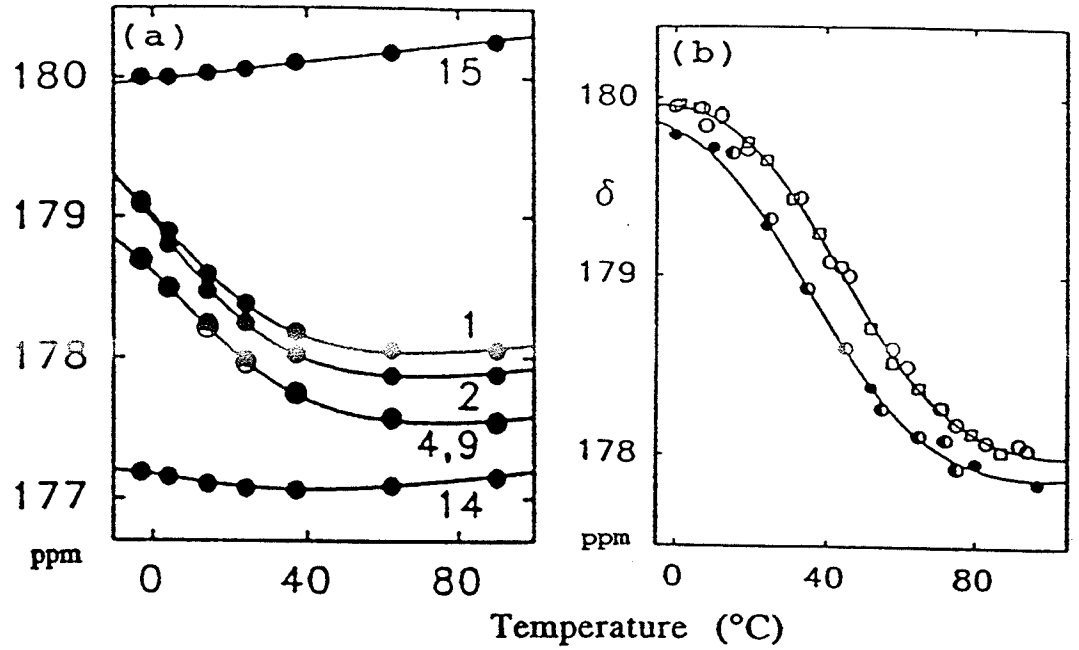

Figure 3-28: Changes in the carbonyl chemical shift of alanine residues of the different alanine-based peptides in water. (a) The residue number of different alanines in the peptide Ac(AAQAA)$_3$amide are indicated in the diagram. This panel was photocopied from Shalongo et al. (1994a). (b) The data are for Ala 9 of the peptide AcW(EAAAR)$_3$Aamide in water. Different symbols are for different solution pH. This panel was photocopied from Shalongo et al. (1994b).

in terms of the difficulty of initiation of the helix (Cantor & Schimmel, 1980). Formation of the first hydrogen bond in a α helix from a random coil requires fixing three (ϕ,ψ) pairs to a particular angle (see Figure 3-1 for the hydrogen bonding arrangement in α helix). This is entropically unfavorable but this will be compensated by the formation of a hydrogen bond. The formation of successive hydrogen bonds requires fixing of only one (ϕ,ψ) pair. So once the helix is initiated, elongation becomes much easier.

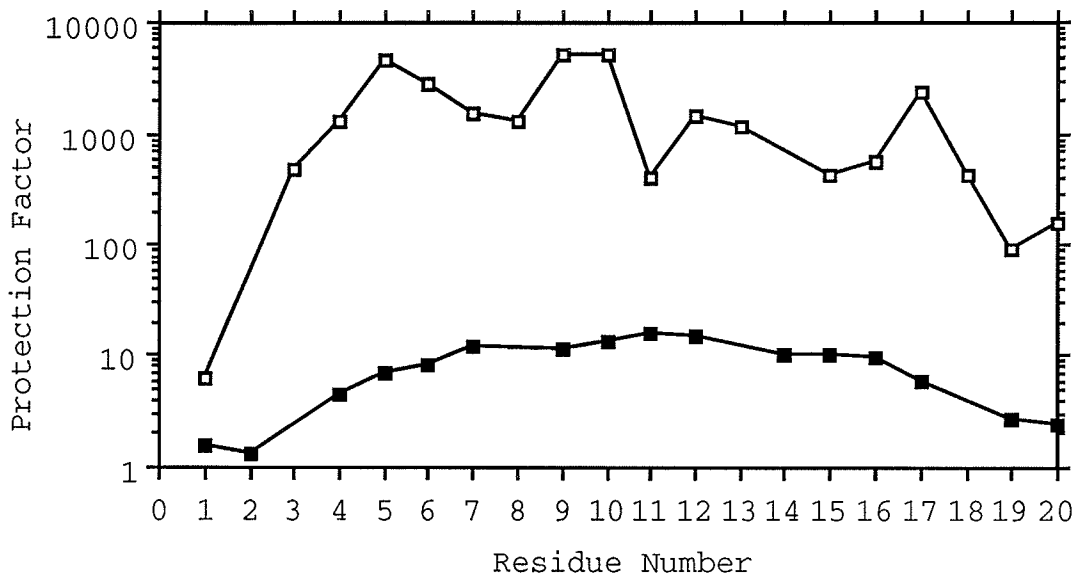

Figure 3-29: Comparison of the protection from hydrogen exchange of alamethicin in methanol and an alanine-based peptide. All protection factors are from exchange rates at the pH_{min}. Open squares are for alamethicin with data obtained from Dempsey (1995). Filled squares are for $Ac(AAKAA)_4Yamide$ with data obtained from Rohl and Baldwin (1994). The relationship between protection factor and peptide hydrogen bond stability is describe in more detail in Section 4.2 and Section 4.6.4.

The lack of cooperativity in alamethicin may be explained by the high helix propensity of the Aib residue (Basu & Kuki, 1993). The presence of a methyl group in place of a hydrogen in the α carbon of an Aib residue limits the allowed (ϕ,ψ) conformation of the Aib residue to helical angles; an extended chain conformation is disfavored because of steric interactions (Burgess & Leach, 1973). So the Aib

residues in alamethicin may be viewed as permanent helix initiators throughout the entire length. Synthetic Aib-rich peptides in DMSO and chloroform have been shown to be thermally stable in a 3_{10} helical conformation up to a temperature of 150°C (Augsperger et al., 1995).

Chapter 4
Alamethicin in Detergent Solution

4.1 Structure determination by NMR Spectroscopy

The strategy used for the determination of protein structure in solution using NMR involves three steps: The first step is to assign each proton resonance to specific protons in the molecule. The second step is interpreting the NMR observable parameters in terms of geometric constraints and the third step is producing molecular models consistent with the experimental constraints.

4.1.1 Resonance Assignment

Assignment of ^{1}H resonances in small peptides is usually done using the conventional Wuthrich method (1986) (sequential assignment) or more recently, by heteronuclear correlation experiments (Grzesiek & Bax, 1992).

The sequential assignment method involves two steps: First the ^{1}H spin systems are identified. This is done using J-correlated types of experiments sometimes called "through-bond" experiments. Examples of these are the COSY (Bax & Freeman, 1981; Jeener,1971), DQF-COSY (Marion & Wuthrich, 1983), and TOCSY (Bax & Davis, 1985) experiments. The cross peaks in a 2D J-correlated experiment result from coherence transfer between two J-coupled spins (Bax & Freeman, 1981; Jeener, 1971). The more bonds separating the two protons, the smaller the coupling, so this essentially makes each residue

an isolated spin system. The connectivities can be traced from the spectrum and different amino acids give characteristic cross peak patterns.

After the amino acid spin systems are traced, the second step is to assign the spin systems according to the protein sequence. This is done using a "through-space" experiment like NOESY or ROESY. In NOESY or ROESY, cross peaks are observed between protons that are close in space, 5 Å or less apart. The distance between $H_N(i)$ and $H_N(i+1)$ is farthest in a fully extended structure at only 4.8 Å (Wuthrich, 1986). Ideally, all 2° structures give a NOESY crosspeak between sequential H_N resonances. In this way, the protein sequence can be traced from $H_N(i)$ to (i+1) in the amide region of the NOESY spectrum. In the case of Pro residues that do not have H_N resonances, the H_δ can be used for sequential assignment. Other sequential nOes like the $H_N(i)$ to $H_\alpha(i+1)$ or $H_N(i)$ to $H_\beta(i+1)$ can be used to confirm the sequential assignment especially in proteins containing a large fraction of β strands where the $H_N(i)$ to $H_N(i+1)$ nOes are weak.

For proteins of more than 100 residues, the conventional sequential assignment method is less successful because of severe resonance overlap in homonuclear 2D ^1H spectra. In addition, the broader line widths compared with the homonuclear coupling constants makes the magnetization transfer via the homonuclear J-coupling mechanism inefficient since the amount of magnetization transfer between nuclei with coupling J at an increment t_1 is proportional to:

$\exp(-t_1/T_2)\ \sin(\pi J t_1)$ (Derome, 1987; Wagner et al., 1992; Boelens, et al., 1991; Bax & Grzesiek, 1993). An alternative is to use a heteronuclear third, or even fourth, dimension to increase spectral resolution. This involves the use of an ^{15}N and/or ^{13}C labelled protein. The heteronuclear one bond coupling constants are usually much larger than the $^{n}J_{HH}$ so that magnetization transfer is very efficient. Several pulse sequences have been developed making use of $^{1}J_{XH}$ (Bax & Grzesiek, 1993). By convention, these pulse sequences are named according to the observed resonances along the magnetization transfer path with those resonances which are not observed being enclosed in parenthesis. For example, in a pulse sequence named CBCA(CO)NH, the sequence is started by an INEPT sequence to transfer polarization from the $^{1}H_{\beta}$ and $^{1}H_{\alpha}$ to the $^{13}C_{\alpha}$ and $^{13}C_{\beta}$ using the $^{1}J_{CH}$ of ~140 Hz. The coherence is then transferred to the $^{13}C'$ using the $^{1}J_{C\alpha C'}$ of ~55 Hz. From the $^{13}C'$ the coherence is transferred to the ^{15}N of the next amino acid using $^{1}J_{C'N}$ of ~15 Hz and then to the $^{1}H_{N}$ using the $^{1}J_{NH}$ of ~90 Hz. The variable time delays in this experiment are such that the $^{13}C'$ chemical shift is not observed and the following chemical shift frequencies are observed: the $^{13}C_{\beta}$ and $^{13}C_{\alpha}$ in F_1, the ^{15}N in F_2, and the $^{1}H_{N}$ in F_3 (Grzesiek & Bax, 1992).

In this method, the assignment of resonances is done by tracing the correlation between backbone heteroatoms and their attached protons. For example, in the HNCO pulse sequence (Ikura et al., 1990) a correlation between $^{1}H_{N}(i)$,

$^{15}N(i)$, and $^{13}C'O(i-1)$ is observed. In the HCACO pulse sequence (Ikura et al., 1990) a correlation between the $^{1}H_{\alpha}(i)$, $^{13}C_{\alpha}(i)$, and $^{13}C'O(i)$ is observed. These 2 sequences allow for the sequential assignment of the H_N, H_{α}, and the backbone heteroatoms. The β protons may be assigned using the HBHA(CBCACO)NH pulse sequence (Grzesiek & Bax, 1992) or by an ^{15}N-edited TOCSY experiment (Marion et al., 1989).

4.1.2 Observable NMR parameters as Geometric Constraints

The nOe intensity obtained from a NOESY or ROESY spectrum is the source of most of the geometric constraints used for distance geometry calculations. For macromolecules, nOe crosspeaks are observed between protons that are separated by 5 Å or less. The nOe phenomenon arises from the cross relaxation between 2 nuclei as given by Solomon's equation (Solomon, 1955).

$$d\mathbf{A}/d\tau_m = -\mathbf{R}\cdot\mathbf{A}$$

where **A** is the magnetization matrix, τ_m is the mixing time, and **R** is the cross relaxation matrix where the spin lattice relaxation rates (ρ_i) are the diagonal elements and the cross relaxation rates (σ_{ij}) are the off-diagonal elements.

$$R_{ii} = \rho_i = (0.1\gamma^4h^2)\Sigma(1/r_{ij}^6)[J_o(\omega) + 3J_1(\omega) + 6J_2(\omega)]$$

$$R_{ij} = \sigma_{ij} = (0.1\gamma^4h^2/r_{ij}^6)[6J_2(\omega) - J_o(\omega)]$$

$$J_n(\omega) = \tau_{ij}/[1+(n\ \omega_o\ \tau_{ij})^2]$$

where r_{ij} is the distance between protons i and j; τ_{ij} is the rotational correlation time of the interproton vector between

i and j; ω_o is the Larmor frequency; γ is the magnetogyric ratio; h is Planck's constant.

The solution to Solomon's equation is given by the equation: $\mathbf{A}(\tau_m) = \exp(-\mathbf{R}\,\tau_m)\cdot\mathbf{A}(0)$. The exponential term is solved as $\exp(-\mathbf{R}\,\tau_m) = \chi\cdot\exp(-\lambda\,\tau_m)\cdot\chi^{-1}$ where χ and λ are the eigenvectors and eigenvalues of the matrix **R** (James et al., 1991; Baleja et al, 1990). Diagonalizing a large matrix **R** is computationally very time consuming. The exponential term may also be approximated by expanding it into a Taylor series as $\exp(-\mathbf{R}\,\tau_m) = 1 - \mathbf{R}\,\tau_m + 0.5\,\mathbf{R}^2\,\tau_m^2 + \cdots$ and truncating after the second term.

The nOe crosspeak intensities may be converted into distances by either of the following methods: At very short mixing times, we can write, $d\mathbf{A}/d\tau_m|_{\tau m=0} = -\mathbf{R}\cdot\mathbf{A}(\tau_m=0)$ or $(A_{ij})_{\tau m=0} = -R_{ij}\,A_{ij0}$. The R_{ij} are proportional to r_{ij}^{-6} so that the distance between protons i and j can be obtained from the intensity of a reference nOe crosspeak between protons k and l, provided that r_{kl} is known, using the ratio:

$$A_{ij}/A_{ref} = r_{ij}^{-6}/r_{ref}^{-6}$$

The reference distance used is usually the distance between 2 methylene protons which is set to 1.8 Å. This method may be used only at very short mixing times such that the initial rate approximation still holds.

An alternative is to use the slope of the nOe build-up curve because the cross peak intensity may be approximated by the linear term in the Taylor expansion series. At short mixing times, the slope of the initial build up of A_{ij} with

mixing time is equal to R_{ij}. NOESY experiments are acquired at different mixing times and nOe crosspeak intensity is plotted as a function of τ_m. The slopes are then converted into distances using the proportionality: $(slope)_{ij}/(slope)_{ref} = r_{ij}^{-6}/r_{ref}^{-6}$. Again the reference distance used is that between methylene protons. This has an advantage over the previous method in that spectral artifacts that may affect a crosspeak intensity in a single NOESY spectrum are averaged out by the linear fitting with intensities from NOESY experiments at several mixing times. The disadvantage of this approach is that the slope of each crosspeak build-up curve has to be determined before the calibration equation can be used.

Yet another alternative for converting nOe intensities to internuclear distances is the distance extrapolation method (Baleja et al., 1990). At very short mixing times, the nOe signal to noise ratio is low, but the nOe is a more reliable indicator of distance. At longer mixing times, the calculated distances may deviate from the correct values because of spin diffusion. So the idea is to calculate the distances at different mixing times using the first method and then extrapolate to zero mixing time.

A major assumption in any of the above methods is that the molecule is rigid. The distances obtained by neglecting internal motion are shorter than the average distance when motion is present (Neuhaus & Williamson, 1989; Wagner, 1990). The distances calculated from the nOe intensities should be considered as the minimum distance between the atoms. So to

err on the side of caution, the distances obtained from the nOe calibration are usually classified into conservative distance ranges instead of using the calculated numerical values (Jardetzky et al., 1991). Other precautions to keep in mind in using the calibration methods include inaccurate integration of the nOe crosspeaks due to limited digital resolution and the presence of spin diffusion so that the two-spin approximation is no longer applicable (Jardetzky et al., 1991).

Another NMR parameter which can be translated into a geometric constraint is the coupling constant. The vicinal coupling constant is related to the intervening dihedral angle via a Karplus-type equation (Wuthrich, 1986; Bystrov, 1976). The best calibrated Karplus equation used in proteins is the relationship between $^3J_{HNH\alpha}$ and the backbone ϕ angle shown in Figure 4-1. For a regular helical structure, the ϕ angle is -57° to -60° and corresponds to a coupling constant of 3.9 to 4.2 Hz whereas for a regular β sheet, the ϕ angle is -119° to -139° and corresponds to a coupling constant of 8.9 to 9.7 Hz. In practise, a coupling value of less than 6 Hz is usually taken as an indication of a helical backbone conformation while a value larger than 8 Hz is usually taken to indicate a β-sheet conformation. Coupling constants between 6 and 8 Hz are usually taken as an indication of conformational averaging. The distance between $H_\alpha(i)$ and $H_N(i)$ is constrained to 2.60 to 2.80 Å for a helix and 2.90 to 2.95 Å for a β sheet (Wuthrich, 1986). Another coupling

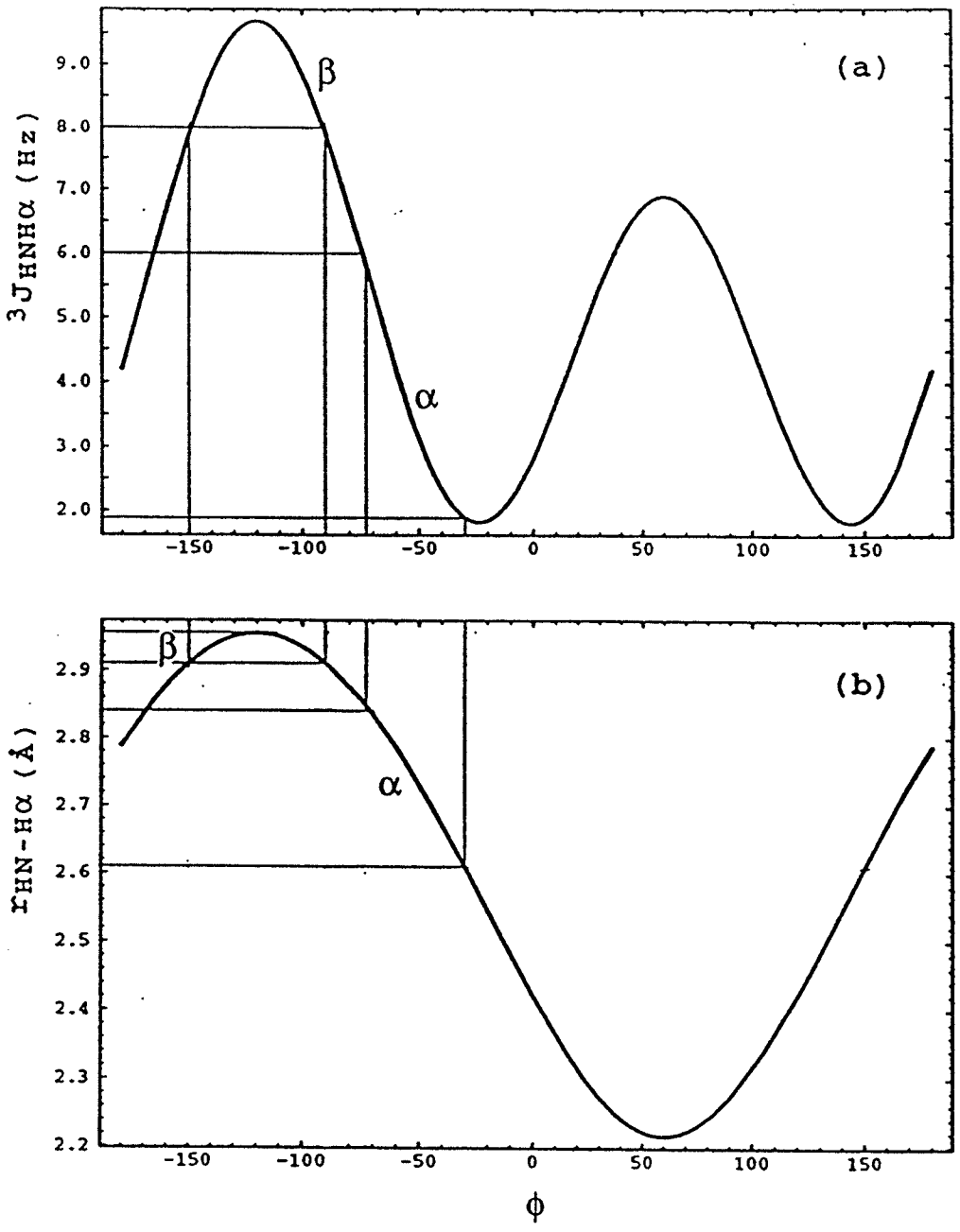

Figure 4-1: Relationship between the backbone ϕ angle and (a) $^3J_{HNH\alpha}$ based on the equation $^3J_{HNH\alpha} = 6.4\ Cos^2(\phi-60) - 1.4\ Cos(\phi-60) + 1.9$ (Pardi et al., 1984) and (b) distance between the H_N and H_α. The lines in (b) indicate the regions of the curve used to translate the $^3J_{HNH\alpha}$ values into distance constraints for α-helical and β-strand structures for use in distance geometry calculations.

constant which can be translated into a distance constraint is the $^3J_{H\alpha H\beta}$ which is related to the dihedral angle χ_1. For a sidechain *trans* conformation, the $H_\alpha(i)$ to $H_\beta(i)$ distance is constrained to 2.50 to 3.50 Å.

The other parameters translated into distance constraints are the H_N exchange rate and the temperature coefficient of the H_N chemical shift. H_N exchange rates are usually determined from an exchange-out experiment in D_2O and a slow H_N exchange rate is taken as an indication of the presence of hydrogen bonding (see Section 4.2). The temperature coefficient of the H_N chemical shift is determined from a variable temperature experiment and a small temperature coefficient is taken as an indication of the presence of hydrogen bonding (see Section 3.2.2). These two methods identify only the H-bond donor and not the acceptor. The hydrogen bonding acceptor is usually inferred from nOe patterns. For example, if the H_N involved in hydrogen bonding is among the residues showing a series of (i) to (i+3) nOes, then a regular α helix is assumed and the hydrogen bonding partner is assumed to be the carbonyl at position (i+4) (Wagner et al., 1992).

4.1.3 Distance Geometry

All the NMR-derived and covalent structure geometric constraints are used as lower (**L**) and upper (**U**) boundary distances between atoms in a bounds matrix. The molecular models that are consistent with the geometric constraints are

then calculated using a distance geometry algorithm like that found in DSPACE® and XPLOR®. The procedure involved in these algorithms has been fully described (DSPACE manual; Xplor 3.1 manual (Brunger, 1992); Kuntz et al., 1979; Crippen & Havel, 1978) and what follows is a brief summary of the method. The distance or bounds matrix is a symmetric matrix with N(N-1)/2 distances for an object with N points (atoms). The number of experimental constraints and covalent constraints is usually not enough to fill the N(N-1)/2 distances. To ensure that the input data are geometrically self-consistent, the bounds matrix is smoothed. The constraint applied is the triangle inequality. For the upper bounds in the matrix, the triangle inequality is defined as follows: For all atoms taken three at a time (i,j,k), the upper distance between the atoms i and j ($D_{ij}U$) must be less than the sum of the upper distances from i to k ($D_{ik}U$) and from k to j ($D_{kj}U$). $D_{ij}U$ = MIN($D_{ij}U$ or $D_{ik}U$ + $D_{kj}U$), i.e., whichever is smaller of the two distances will be the $D_{ij}U$ value. Once the upper bounds can be reduced no further, the triangle inequality is applied to the lower bounds (inverse triangle inequality) which is defined as follows: the lower distance from i to j ($D_{ij}L$) must be greater than the difference between the lower distance from i to k ($D_{ik}L$) and the upper distance from j to k ($D_{jk}U$) for all points (i,j,k). $D_{ij}L$ = MAX($D_{ij}L$ or $D_{ik}L$ - $D_{jk}U$), i.e., whichever is the larger of the two values will be the $D_{ij}L$ value. When the lower bounds can be raised no further, then smoothing is complete.

Distance geometry uses embedding to convert distances between points into Cartesian coordinates. The first step of the process is to define a distance matrix (**D**) to replace the upper and lower bounds matrix. The elements of the distance matrix are chosen at random with the constraint that the value must be between the lower and upper bounds. Then a reference point O, to which the atoms in the molecule can be related, is defined and distances (d) from all the atoms to this reference point are calculated. The next step is to define the (NxN) metric matrix (**G**). The elements of the metric matrix are the dot products of the vectors from atoms i to the origin O (u_i) and atoms j to O (u_j) and these can be solved from the distances:

$$g_{ij} \equiv u_i.u_j = 0.5(d_{i0}^2 + d_{j0}^2 - d_{ij}^2)$$

The unique property of the metric matrix is that the square roots of the eigenvalues of this matrix are the principal moments of the molecule with the origin of the coordinate system at the molecular centroid (reference point O). The eigenvectors are the distributions of the atoms along the axes. When the metric matrix is diagonalized, there are N eigenvalues (λ), but only the largest 3 are used. These eigenvalues are mutually orthogonal and their corresponding eigenvectors contain the x, y, and z coordinates of the atoms. If the distance matrix used is ideal and not derived from the bounds matrix (e.g., it is derived from a molecule of fixed and known conformation), then the corresponding metric matrix would have only three non-zero eigenvalues

corresponding to x, y, and z. The coordinates of the atoms in the molecule can be calculated from the eigenvalues and eigenvectors by $C_{ij} = \lambda_i^{(1/2)} w_{ij}$ where i is 1(x), 2(y), or 3(z); j ranges from atom 1 to N; w_{ij} are the elements of the (Nx3) eigenvector matrix (**W**).

4.1.4 Refinement of Structures

The initial coordinates of the embedded molecules are the best multidimensional fit to the trial distances which are chosen as randomly distributed between the upper and lower boundary conditions. The randomly-embedded structures are minimized using conjugate gradient minimization. The deviations between the experimental distances in the bounds matrix and the calculated distances in the current structure are minimized. Further refinement of the structure is done using simulated annealing to let the molecule escape out of local minima and sample more conformational space.

Usually, several starting structures are generated and refined. The resulting structures are either accepted or rejected based on a target function (penalty in DSPACE) and/or violations of constraints at an arbitrary cut-off value. Those structures that are accepted are then superimposed pairwise and the average of the root mean square deviation (RMSD) is reported.

4.2 Hydrogen Exchange Chemistry

For amides in free solution, hydrogen exchange is catalyzed by either H_3O^+, OH^-, or H_2O itself.

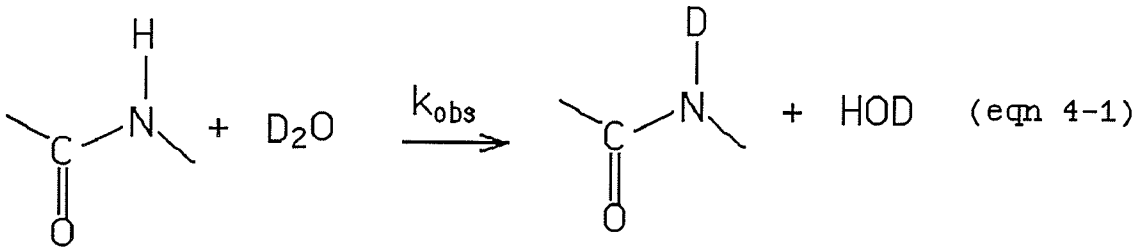

The mechanism for base catalyzed exchange is unambiguous and involves deprotonation of the amide nitrogen as given by equation 4-2 below (Englander & Kallenbach, 1984).

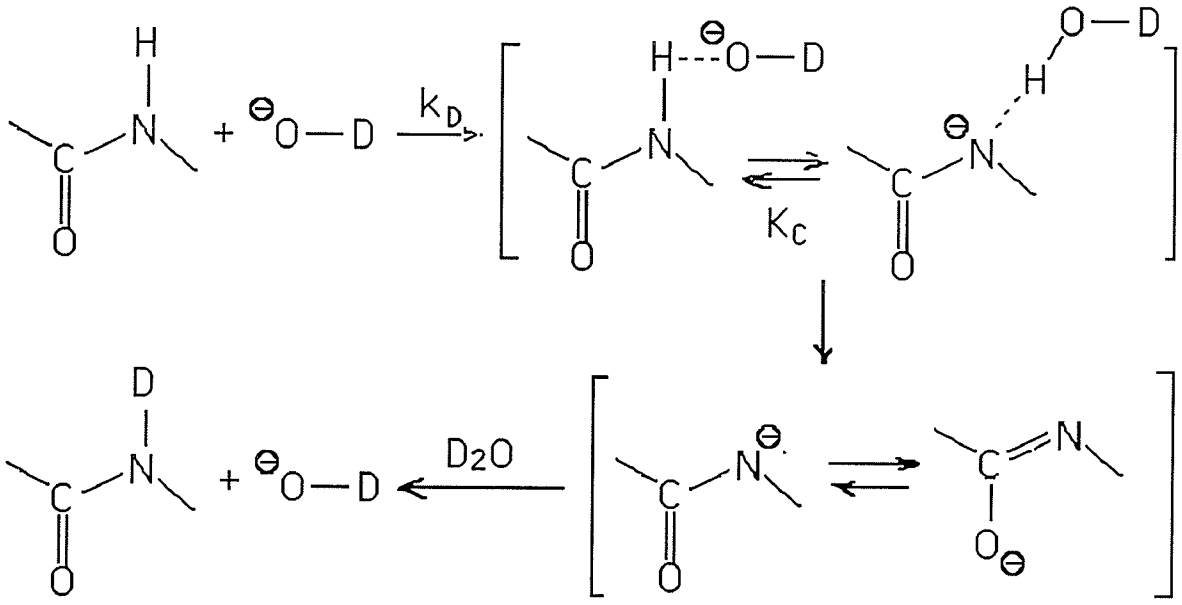

The formation of the hydrogen bonded complex occurs by diffusion-controlled collision between the proton donor (HN) and the acceptor (OD^-) (Eigen, 1964). The proton equilibriates between the two species in the H-bonded complex

and the equilibrium constant (K_c) depends on the relative acidity of the two acceptors as given by equation 4-3.

$$K_c = 10^{\Delta pK_a} = 10^{(pK_W - pK_{NH})} \qquad \text{(eqn 4-3)}$$

where pK_{NH} is the pK for the reaction: $NH \leftrightarrow N^- + H^+$ and pK_w is the pK for the reaction: $H_2O \leftrightarrow H^+ + HO^-$. The overall proton transfer rate (k_{OH}) is the product of the rate of diffusion-controlled collision (k_D) and the fraction of successful collisions. The fraction of successful collisions (f_c) is the fraction of species in the hydrogen bonded complex in which the proton has been transferred to OD^- and this is given in equation 4-4.

$$f_c = \frac{[\text{-CO-N}^-\cdots\text{H-OD}]}{[\text{-CO-N}^-\cdots\text{H-OD}] + [\text{-CO-NH}\cdots{}^-\text{OD}]} \qquad \text{(eqn 4-4)}$$

Since $K_c = [\text{-CO-N}^-\cdots\text{H-OD}]/[\text{-CO-NH}\cdots{}^-\text{OD}]$, then

$$f_c = K_c / (K_c + 1).$$

The specific base-catalyzed exchange rate can then be written as in equation 4-5.

$$k_{OH} = \frac{k_D\, 10^{(pK_W - pK_{NH})}}{10^{(pK_W - pK_{NH})} + 1} \qquad \text{(eqn 4-5)}$$

There are two mechanisms proposed for specific acid catalyzed exchange (k_H). The earlier suggested mechanism involves protonation of the amide nitrogen (equation 4-6) (Berger et al., 1959; Barksdale & Rosenberg, 1982; Leichtling & Klotz, 1966; Molday & Kallen, 1972) and the other mechanism involves protonation of the amide oxygen (equation 4-7) (Perrin & Arrhenius, 1982).

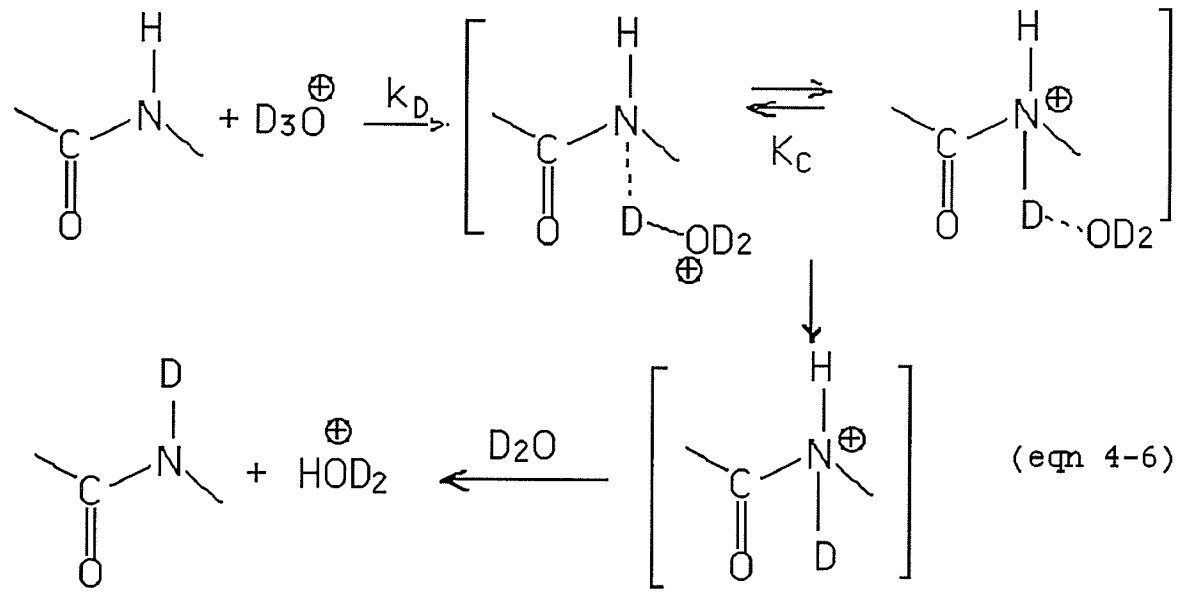

(eqn 4-6)

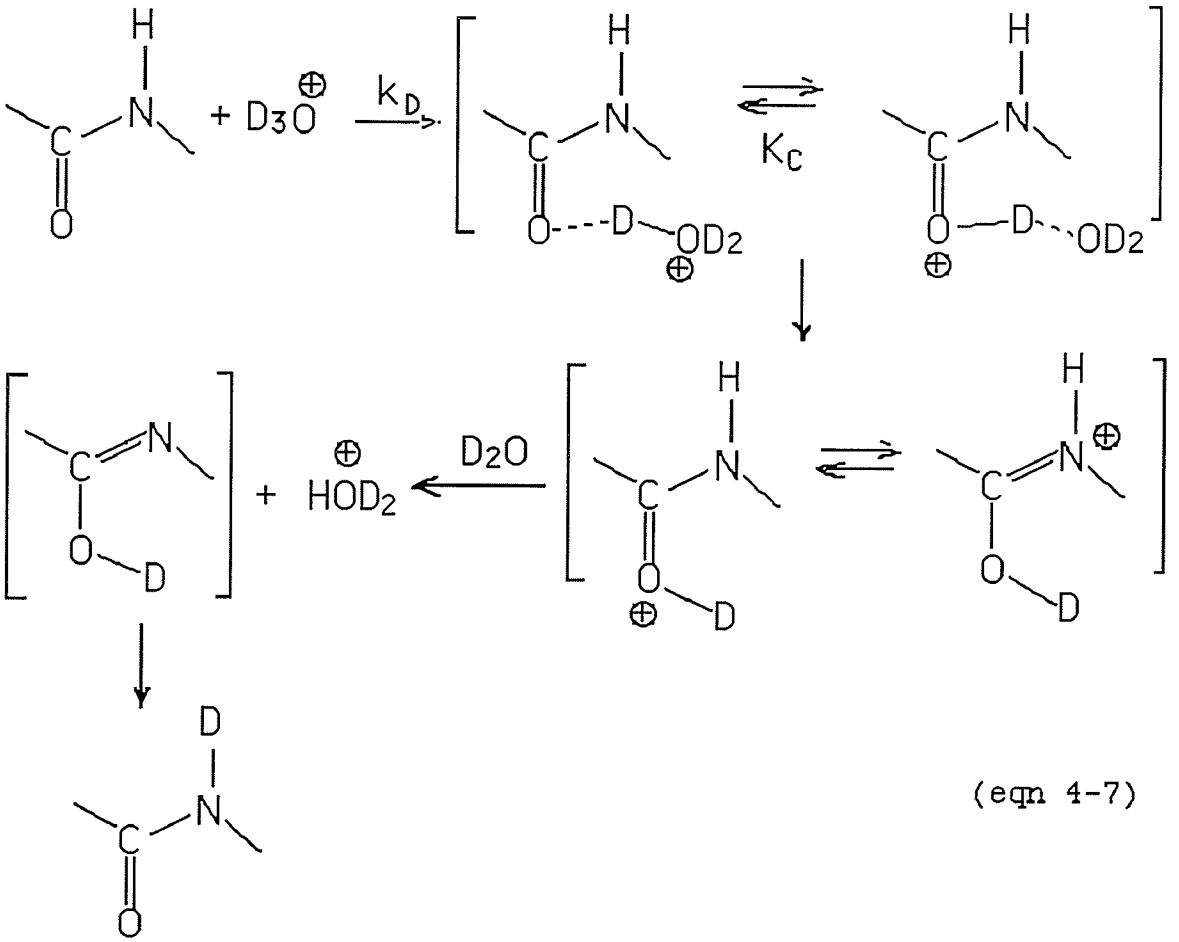

(eqn 4-7)

The specific acid-catalyzed exchange rate can be written as follows:

$$k_H = \frac{k_D\ 10^{(pK_a - pK_W^+)}}{10^{(pK_a - pK_W^+)} + 1} \qquad \text{(eqn 4-8)}$$

where pK_w^+ is the pK for the reaction: $H_3O^+ \leftrightarrow H_2O + H^+$ for both mechanisms, pK_a is the pK for the reaction: $NH_2^+ \leftrightarrow NH + H^+$ for the N-protonation mechanism and pK_a is the pK for the reaction: $C{=}OH^+ \leftrightarrow C{=}O + H^+$ for the O-protonation mechanism.

The mechanism of acid catalyzed exchange in peptides and proteins is still debated; recent hydrogen exchange papers discuss their results in terms of both mechanisms (e.g., see Connelly et al., 1993; Zhang et al., 1995). However, O-protonation mechanism seems to be preferred. The evidence for N-protonation is as follows (Perrin & Arrhenius, 1982): (1) A correlation was observed between the acid catalyzed exchange rates (k_H) and the pK_a values of the parent carboxylic acids (Molday & Kallen, 1972). It was suggested that an increase in the electron-withdrawing ability of the substituent would decrease the basicity of the amide nitrogen and decrease the k_H (e.g., N-Methylacetamide exchanges faster than N-Methylformamide because the CH_3 group is more electron donating than the H). N protonation was favored over O protonation because with electron donating substituents, the increase in basicity of the amide oxygen would be cancelled out by a decrease in acidity of the amide nitrogen making the proton a more difficult leaving group (see equation 4-7). O protonation would thus make the k_H insensitive to the

substituent effect (Molday & Kallen, 1972). (2) The substituent effects on k_H are similar in magnitude but opposite in direction to those on k_{OH} (Molday & Kallen, 1972; Leichtling & Klotz, 1966). (3) The behavior of the N-methyl resonance of N-methylacetamide as a function of pH parallels that of the N-methyl signal of N,N-dimethylacetamide. In solution, the N-methyl signals of N,N-dimethylacetamide are inequivalent due to the partial double bond character of the amide and so they appear as a doublet. At acidic pH, the amide N is protonated and free rotation around the C-N bond results in the collapse of the doublet. At nearly the same pH, the N-methyl signal of N-methylacetamide was also observed to collapse from a doublet to a singlet, the decoupling being due to acid-catalysed hydrogen exchange. This was taken to suggest that the mechanism involved in the acid catalyzed free rotation in the tertiary amide (N-protonation) is the same as that in the hydrogen exchange of secondary amides (Berger et al., 1959).

Some of the evidence for the O-protonation mechanism is as follows: (1) The correlation between the k_H and the pK_a of the parent carboxylic acid showed a very small slope suggesting that the mechanism does not involve a full positive charge in the transition state making it less sensitive to substituent effects in agreement with the explanation of Molday and Kallen (1972). They suggested that the increase in basicity of the amide oxygen with electron donating substituents is not completely cancelled out by the

decrease in acidity of the amide proton. This explanation was also supported by work on primary amides (Perrin & Arrhenius, 1982). (2) In measurements of the surface peptide protons of BPTI, a correlation was observed between the acid catalyzed exchange rate (k_H), but not the base catalyzed exchange rate (k_{OH}), and the static carbonyl accessibility calculated from the crystal structure. This suggested to Tuchsen & Woodward (1985) that acid catalysis occurs via O, and not N, protonation. (3) In a 21-residue alanine-based helical peptide, the two N-terminal H_N, which are not capable of helical hydrogen bonding, were not protected from base catalyzed exchange but were protected from acid catalyzed exchange (Rohl & Baldwin, 1994). In an O protonation mechanism, hydrogen bonding at the C'O would be expected to decrease k_H by hindering the protonation of the carbonyl oxygen and in a helical peptide the two N-terminal carbonyl oxygens will be hydrogen bonded.

The overall exchange rate (k_{obs}) in equation 4-1 is the sum of all possible pathways and is given by equations 4-9 (Leichtling & Klotz, 1966).

$$k_{obs} = k_H[H^+] + k_{OH}[OH^-] + k_{H2O}$$

$$k_{obs} = k_H[H^+] + k_{OH}K_w/[H^+] + k_{H2O} \qquad \text{(eqn 4-9)}$$

where k_{H2O} is the rate constant for direct exchange with water which is small compared with the first two terms and is often dropped from the equation; $[H^+]$ and $[OH^-]$ are the effective hydronium and hydroxide ion concentrations respectively; K_w is the ionization constant for water. A plot of $\log(k_{obs})$

versus solution pH yields the familiar V-shaped curve (see Section 4.5.2); the exchange rate constant and pH at exchange minimum are as follows:

$$k_{min} = k_H\ 10^{-pHmin} + k_{OH}\ 10^{-(pKw-pHmin)}$$

$$pH_{min} = 0.5\ pK_w + 0.5\ \log(k_H/K_{OH})$$

4.3 Hydrogen Exchange in Peptides

The proton transfer chemistry requires the exchanging amide group to come into contact with the catalysts (H_3O^+ or OH^-) and solvent for proton transfer to proceed. Thus, any factor that impedes this contact retards the observed hydrogen exchange rates. Likewise, any factor that affects the proton transfer chemistry will also alter the observed hydrogen exchange rates.

The factors affecting proton transfer chemistry at a certain temperature were enumerated by Barksdale and Rosenberg (1982) and will be briefly mentioned here as follows: (1) Proton transfer is catalyzed by H^+ and OH^- so the observed exchange rate will depend on the choice of solution pH. (2) Proton transfer proceeds via charged intermediates so substituents on the carbons bonded to the amide groups that stabilize these intermediates favor the forward reaction and therefore hasten the exchange. Amino acids with different sidechains thus exert different inductive and electrostatic influences on the H_N exchange. Englander's group (Molday et al., 1972; Molday & Kallen, 1972) studied the primary structure effects on peptide hydrogen exchange in peptide

derivatives. Their results showed that the addition of a peptide (amide) group on either side of the amide in N-methylacetamide increases the k_{OH} and decreases the k_H to a different extent relative to the same measurements in N-methylacetamide. They also calculated the sidechain inductive/electrostatic effects of the polar amino acid sidechains on the neighboring peptide group to the left or right of the sidechain. Electron withdrawing sidechains increase k_{OH} and decrease k_H by making the peptide groups more acidic so that abstraction of the amide proton is easier and protonation of the amide group is more difficult. Their study revealed several important principles governing hydrogen exchange in proteins: (i) They showed that the "Molday Effect" acts independently and is additive. (ii) They showed that only the nearest neighbor sidechain has a significant influence in determining the H_N exchange rates. (iii) They showed that hydrogen exchange rates are independent of the protein molecular mass. (iv) They showed that the sidechains do not act as general acid or base catalysts. The use of the Molday Effect allows the prediction of the exchange rate of any amide H_N in the protein provided the two neighboring sidechains are known.

(3) In the presence of ionizable groups like titratable side chains, the observed exchange rate (k_{obs}) at a given pH is actually the sum of the observed rate constants from the two species (neutral and charged) present weighted by the fraction of each species present. The fraction of each

species at a given pH depends on the ionization constant of the titratable group. The k_{obs} versus pH profile of H_N exchange follows the k_{obs}^0 (or k_{obs}^-) curve until the solution pH is comparable to the pK_a of the titratable group then it gradually shifts to follow the k_{obs}^+ (or k_{obs}^0) curve. This charge effect is also thought to affect the k_{obs} via stabilizing/destabilizing effects on the exchange intermediates (Kakuda et al., 1971). (4) A decrease in exchanging solvent polarity from pure D_2O to a DMSO mixture was first thought to affect k_{obs} by increasing pK_w (Klotz & Frank, 1965; Leichtling & Klotz, 1966; Englander & Kallenbach, 1984). The decrease in K_w would increase k_{OH}. Recently, a more detailed study of the effect of DMSO showed that it decreases the k_{OH} by increasing the pK_a of the amide H_N (Zhang et al., 1995). The increase in pK_w is less important because it is more than offset by the increase in pK_a of the amide H_N. (5) The presence of other acids and bases can increase the k_{obs} by catalysing the formation of the exchange intermediates (as general acid or base catalysts) but these are usually less efficient than the specific acid and base catalysts, OH^- and H_3O^+. Buffers do not usually participate in the exchange reactions because their pK_a values are low relative to the pK_a for peptide group protonation and deprotonation (Englander & Poulsen, 1969).

Interference in the encounter between the exchanging amide group and the catalyst can come either from the bulky sidechains or from the structure that the protein adopts. In

the earlier calibration of the sidechain Molday Effect, all the nonpolar sidechains were considered to have the same correction factor as the alanine residue (Molday et al., 1972). Recently a more complete sidechain calibration was done to account for the steric blocking effect of the sidechains (Bai et al., 1993). The inductive effect from polar sidechains shifts the rate-pH curve (V-curve) to the left lowering the pH_{min} but the k_{min} remains relatively unchanged. The sidechain blocking effect however, decreases both the k_H and k_{OH} shifting the V-curve downwards lowering the k_{min} but the pH_{min} remains relatively unchanged. The H_N to the left of the sidechain experiences a greater blocking effect than the one to the right and this is attributed to the geometric accessibility to the sidechain of the left H_N. Like the Molday Effect, the blocking effect of the sidechains to the left and right of an amide H_N were found to be additive despite the expected competition for the same space by two sidechains. This blocking effect additivity was taken to suggest that the sidechains retard the exchange not by spatially blocking the approach of the catalyst but by preventing the formation of the hydrogen bonded complex by interfering with the ordering of the complex's hydration shell (Bai et al., 1993). Knowledge of the electrostatic/inductive and blocking effect of each amino acid sidechain allows better predictions of the exchange rates in structureless (random coil) proteins.

Amide hydrogen exchange in folded, globular proteins is usually slower than that measured in structureless proteins. There are two mechanisms proposed which aim to explain how the catalysts can come in contact with the exchanging amide group in a folded protein. One mechanism is the breathing model (Linderstrom-Lang, 1955; Linderstrom-Lang & Schellman, 1959; Englander & Kallenbach, 1984) and the other is the penetration model (Woodward, 1977; Woodward & Hilton, 1979). Englander and Kallenbach (1984) reviewed evidence for and against both mechanisms and made a very convincing argument for the breathing model. Both mechanisms agree that the preexisting hydrogen bond has to be broken before exchange can occur. Both mechanisms also agree that under destabilizing conditions, such as high denaturant concentrations or at temperatures at or above the protein melting temperature, hydrogen exchange occurs via global cooperative unfolding. That is, hydrogen exchange occurs when the protein is in the "structureless denatured" state. The two mechanisms rationalize hydrogen exchange under non-denaturing conditions differently. In the breathing model, hydrogen exchange is thought to occur from the unfolded state. When part of the protein undergoes segmental unfolding, catalysts come into contact with the exchangeable amide hydrogens. Thus, exchange is slowed down because of the stability of the protein towards segmental unfolding. In the penetration model, hydrogen exchange is thought to occur from the folded state and the exchanging catalysts have to

penetrate into the protein interior to come into contact with the exchangeable amide hydrogen. Thus, exchange is slowed down because of inaccessibility to solvent.

In a folded protein, the observed hydrogen exchange rate (k_i^{obs}) is related to that of the predicted exchange rate for a structureless random coil (k_i) by equation 4-10.

$$k_i^{obs} = \beta_i \, k_i \qquad \text{(eqn 4-10)}$$

where β_i is the probability of exposure of an exchangeable proton to solvent and catalysts (Hvidt, 1973). The subscript i is H^+, OH^-, or H_2O. β is the inverse of the protection factor (PF_i) (Rohl & Baldwin, 1994). In the penetration model, β is reflective of the local accessibility to the solvent of the exchanging amide group (Tuchsen & Woodward, 1987). In the EX_2 limit of the breathing model, where the rate of chemical catalysis is slow compared with rate of refolding, β is equal to the opening equilibrium constant ($K_{op} = k_{op}/k_{cl}$) which is simply the ratio of the rate constants for opening and closing during cooperative segmental unfolding/refolding of the protein (Englander & Kallenbach, 1984). Thus, β is reflective of the fraction of the exchanging amide groups in the unfolded state.

4.4 Materials and Methods

4.4.1 Materials

^{15}N-labelled and unlabelled alamethicin were isolated as described in Section 1.2. Sodium dodecyl-D_{25} sulfate (98% atom) was purchased from Cambridge Isotope Laboratories,

Massachusetts, USA. Standard buffer solutions (Fisher Scientific Co., USA) were used to calibrate the pH meter. $^{15}NH_4Cl$ (99.5% atom) from Isotec Inc., Ohio, USA was used as external reference for ^{15}N NMR spectra. The reverse phase HPLC column used was a Beckman Ultrasphere 5μ, 10 mm x 15 cm.

N-acetyl amino acid N'-methyl amides were synthesized from the corresponding N-acetyl amino acid and methylamine·HCl (from ICN Biomedicals Inc., Ohio, USA) using 1-ethyl-3-(3-dimethylaminopropyl)carbodiimide·HCl (EDAC) (from Sigma Chemical Co., Missouri, USA) for coupling. N-acetyl glycine and N-acetyl alanine were purchased from Sigma Chemical Co., Missouri, USA. N-acetyl α-aminoisobutyric acid was synthesized from α-aminoisobutyric acid (from Sigma Chemical Co., USA) and acetic anhydride (from Fisher Scientific Co., New Jersey, USA). Citric acid, trisodium salt dihydrate (from Sigma Chemical Co., USA) and succinic anhydride (from Eastman Kodak Co., USA) were used as buffers in the measurements of hydrogen exchange of model dipeptides.

4.4.2 Methods

4.4.2.1 Synthesis and Purification of N-acetyl amino acid N'-methyl amide

N-acetyl α-aminoisobutyric acid was synthesized from α-aminoisobutyric acid and acetic anhydride (Means & Feeney, 1971). α-aminoisobutyric acid (1 g, 9.7 mmol) was dissolved in 5 mL of water and the pH was adjusted to 8-9 with NaOH solution. 10 mL (106 mmol) of acetic anhydride was added

dropwise to the Aib solution with constant stirring. At first, the acetic anhydride was immiscible but gradually it became dissolved. Acetylation was checked with a ninhydrin solution. That is, to a 0.1 mL aliquot of reaction mixture, 80 μL of 1% ninhydrin solution in acetone was added and the absorbance from 500 to 600 nm was recorded. Ninhydrin reacts with free NH_3^+ in the amino acid forming a complex that absorbs at 565 nm. As a control for this test, ninhydrin was added to a mixture of α-aminoisobutyric acid and glacial acetic acid in the same proportion as in the reaction mixture. Successful acetylation should show no absorbance at 565 nm, whereas the control solution should absorb (see Figure 4-2).

The products were purified using reverse-phase HPLC with pure H_2O as eluant and a flow rate of 3 mL/min. The HPLC chromatogram showed 3 major peaks at 4 mins., corresponding to unreacted acetic anhydride (acetic acid), 16 mins., and 21 mins. The 16 and 21 min. peaks were collected. ^1H NMR spectroscopy showed that the peak at 16 mins. corresponded to the N-acetyl α-aminoisobutyric acid (not shown).

The amidation reactions were done by reacting the N-acetyl amino acids with methylamine; amide formation was promoted by a water-soluble carbodiimide (Means & Feeney, 1971).

164.5 mg (1.3 mmol) of N-acetyl α-aminoisobutyric acid (HPLC peak number 16) and 190.7 mg (2.8 mmol) of methylamine·HCl were dissolved in 4 mL of H_2O and the pH of

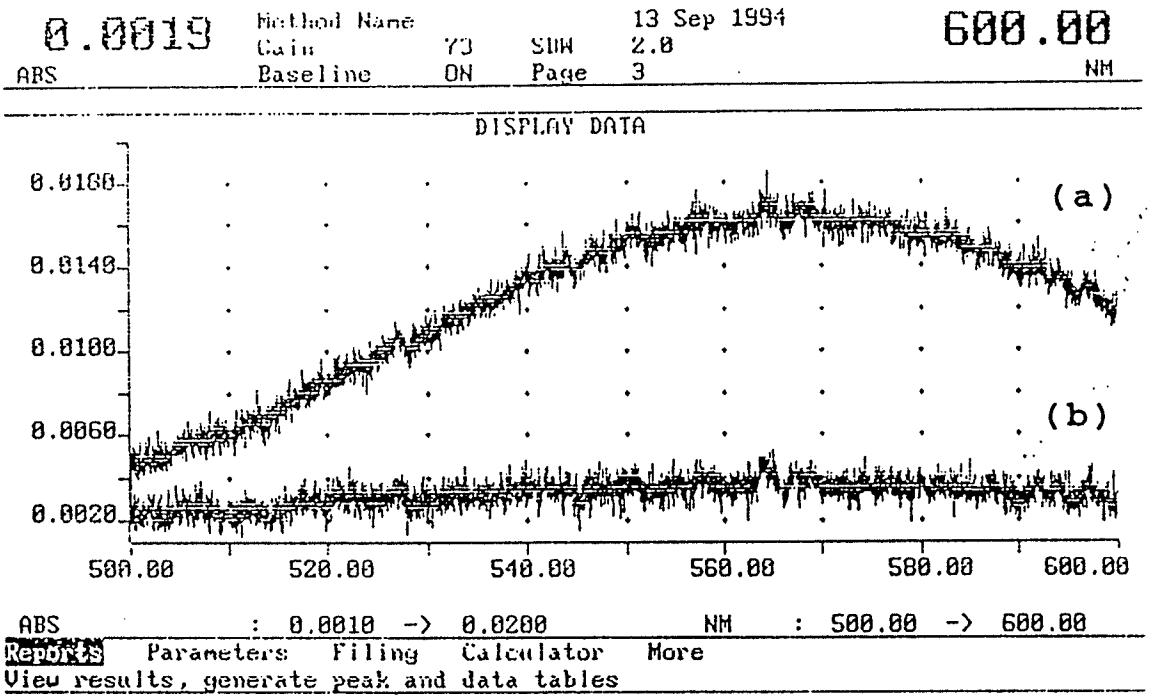

Figure 4-2: Sample absorbance spectra to check the acetylation reaction of α-aminoisobutyric acid by adding ninhydrin solution. (a) Control mixture containing Aib and acetic acid. (b) Reaction mixture containing Aib and acetic anhydride.

the solution was adjusted to 5.1 with NaOH solution. Then 269.4 mg (1.4 mmol) of EDAC were added to the resultant solution with constant stirring. The solution was left to react overnight and was then chromatographed on HPLC using 3 mL/min. of pure H_2O as eluant. The HPLC chromatogram showed 3 major peaks at 3, 7 and 9 mins. A ^1H NMR spectrum showed that the peak at 9 mins. corresponds to N-acetyl-α-aminoisobutyric acid-N'methyl amide. Eluates corresponding to the peak at 9 mins were collected and then freeze dried.

224.1 mg (1.7 mmol) of N-acetyl alanine, used as purchased without further purification, and 191.8 mg (2.9 mmol) of methylamine were dissolved in 5 mL H_2O. The pH of the solution was adjusted to 5.14 with NaOH solution. To this solution, 305.6 mg (1.6 mmol) of EDAC were added with continuous stirring. The mixture was left to react overnight at room temperature. The reaction mixture was chromatographed on the reverse phase column using 3 mL/min. of pure H_2O as eluant and the N-acetyl-alanine-N'-Methyl was freeze dried. Figure 4-3 shows the ^1H NMR spectra of the isolated dipeptides confirming their identity.

4.4.2.2 NMR Spectroscopy

All NMR experiments were done on a Bruker AMX500 NMR spectrometer using a 5 mm inverse broadband probehead with the inner coil tuned to ^1H and ^2H (lock), and the outer coil tuned to ^{15}N or ^{13}C. Details of the acquisition and processing parameters are given in the appropriate figure legends.

For the assignment of the ^1H resonances of alamethicin in detergent solution, HPLC-purified alamethicin was dissolved in 150 mM SDS-D_{25} and 20 mM phosphate as buffer in 95%/5% H_2O/D_2O. The D_2O was used for the deuterium lock signal. The pH was adjusted to approximately 5 with HCl. Because of the large HOD signal, solvent presaturation reduced the HOD signal but resulted in a very distorted baseline in the 1D ^1H spectrum. Better solvent suppression was achieved by using a combination of solvent presaturation

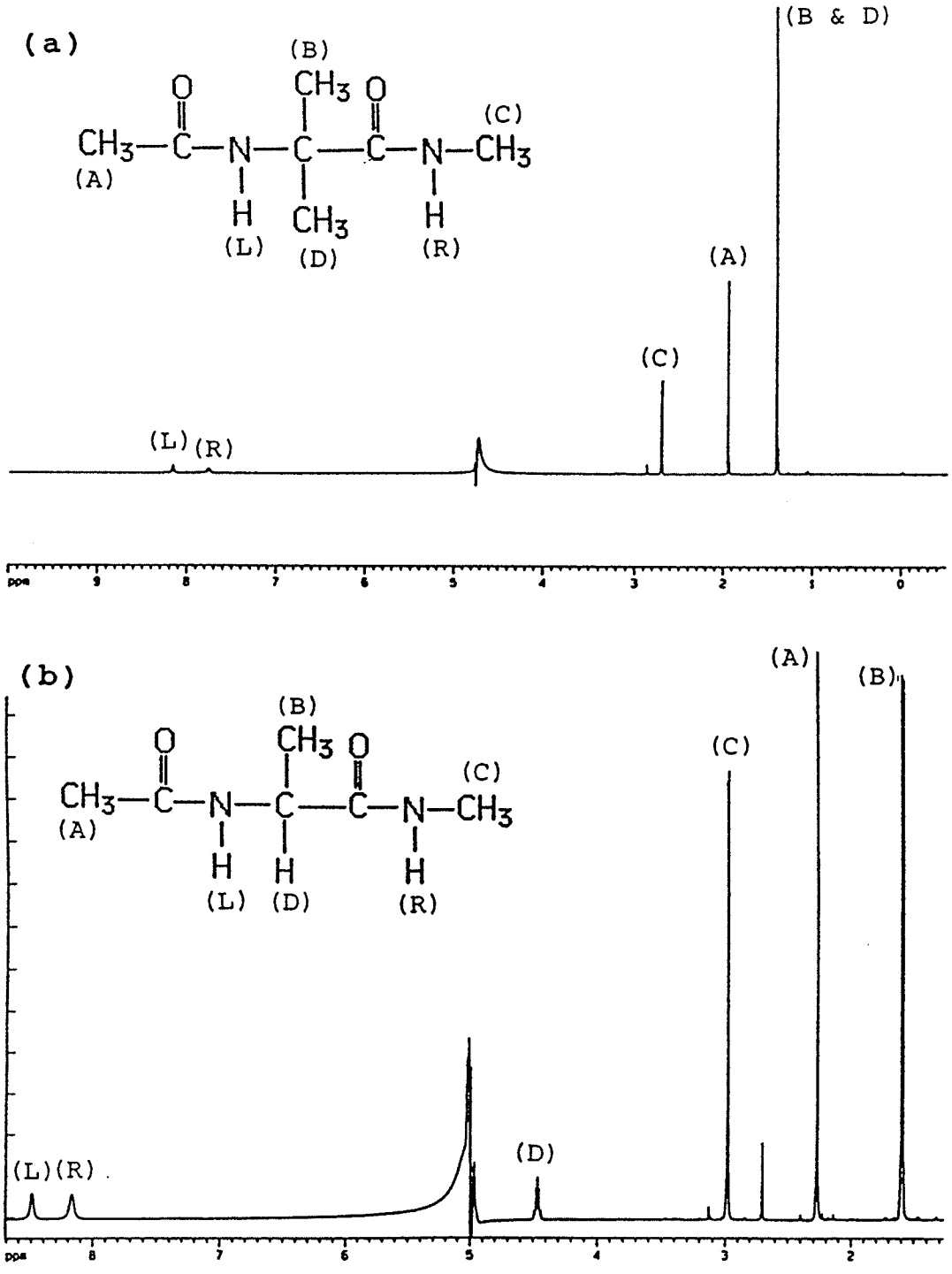

Figure 4-3: 1D ^{1}H NMR spectra of (a) N-acetyl α-aminoisobutyric acid-N'methyl amide and (b) N-acetyl alanine-N'methyl amide. The number of scans was 128, no window function was applied.

and the P1$\bar{1}$ pulse sequence (Plateau & Gueron, 1982). This pulse sequence gives a spectrum where the resonances at a higher frequency than the HOD are opposite in phase to those at a lower frequency than the HOD resonance (Figure 4-5).

For the measurement of H-D exchange of the N-acetyl amino acid N'-methyl amides, stock solutions were made by dissolving a weighed amount of the sample in 1 mL of a H_2O solution containing 50 mM buffer and 0.5 M KCl. The buffers were either succinate, for pH 4 to 6.5, or citrate, for pH 4 and below. 0.8 mL of a solution containing the same buffer and salt concentrations as the stock solution but in D_2O were used to dilute 0.1 mL of the stock solution at 5°C. The solution was shaken, and a series of 1D ^1H spectra were acquired at various times at 5°C. The amide proton intensities were integrated. In all H-D experiments, the pH values were measured at room temperature (20 to 22°C) after the experiment (H-D exchange) was completed. The pK_a values of citrate and succinate at 20°C are higher by 0.06 units relative to those at 5°C (Weast, 1987; Bai et al., 1993). Since the experiments were done at 5°C and the pH was read at 20°C, the pH at 5°C was calculated using the relation:

$$pH^{5°C} = pH^{20°C} - \Delta pK_a/2.$$

For the H-D exchange experiments on alamethicin, a solution containing 150 mM SDS-D_{25} and 20 mM Na_2HPO_4 solution in D_2O, the pH of which had been adjusted accordingly, was used to dilute a solution of alamethicin dissolved in H_2O containing the same SDS and buffer concentrations. Several

HMQC spectra were acquired at different times following the mixing. Each HMQC experiment took 20 mins to acquire. The cross peak volumes of the HMQC spectra were integrated. In the exchange experiments on alamethicin and the N-acetyl amino acid N'-methyl amides, the pHs measured after the experiment were different from the pH of the diluting D_2O solution because the pH of the stock solutions were not adjusted. The pH measured after the experiment is the one reported as the pD_{read}.

The peak integrals were then fit to a three parameter equation: $a = a_o exp(-k_{obs}t) + b$ using the software Passage® to determine the exchange rate constant at a particular pH. The pD_{read} was corrected for the pH meter reading in D_2O using the relation: $pD_{corr} = pD_{read} + 0.4$ (Glasoe & Long, 1960). The pD_{corr} was plotted versus k_{obs} and these were fit to a two parameter equation which is a modified form of equation 4-9 using the software Kaleidograph®.

$$k_{obs} = k_H\, 10^{-pD} + k_{OH}\, 10^{(pD-pK_D)} \qquad \text{(eqn 4-11)}$$

In the fitting procedure, the observed data were weighted by the reciprocal of their magnitude so as not to favor points far from the pD_{min} (Rohl & Baldwin, 1994; Robertson & Baldwin, 1991). Figure 4-4 gives a comparison of fitted data with and without weighting function. The pD is the pD_{corr}, K_D is the molar ionization constant of D_2O which is $10^{-15.65}$ at 5°C and $10^{-15.05}$ at 20°C (Bai et al., 1993). For the dipeptide models, the K_D at 5°C was used and k_{H2O} was assumed to be small and was dropped from equation 4-8. This was done so that the

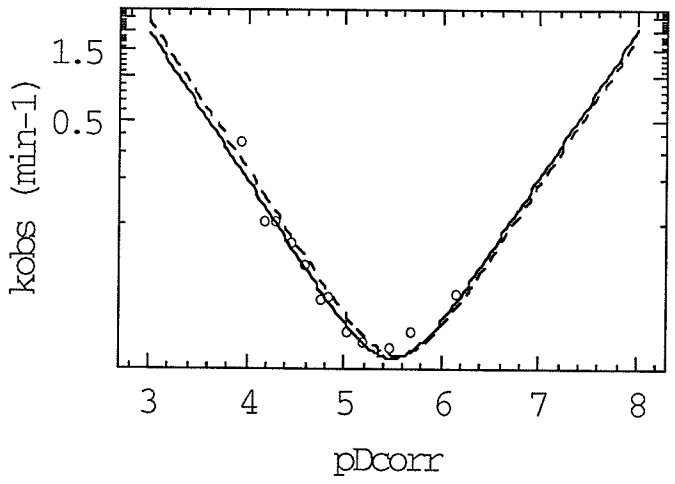

Figure 4-4: Sample hydrogen exchange data fitted to eqn 4-11 showing the effect of the weighting described in the text on the resulting fit. The dashed curve is the fit without weighting the data and the solid curve is the fit with weighted data.

sidechain correction (Molday and blocking effects) for the Aib residue was calculated similarly to those calculated for the other amino acid residues reported in Bai et al. (1993). For the predicted exchange rates in a random coil alamethicin, the K_D at 20°C was used. For the exchange rate of alamethicin in SDS solution (k_{rc}), the K_D at 27°C was used which has a value of $10^{-14.801}$ (Weast, 1987). Since the exchange experiments for alamethicin in SDS solution were conducted at 27°C, the predicted exchange rates (k_{rc}) at 20°C were extrapolated to 27°C to allow comparison with experimental k_{obs} using equation 4-12 (Bai et al., 1993):

$$k_{rc}(T) = k_{rc}(293)\exp[-E_a(1/T - 1/293)/R] \qquad \text{(eqn 4-12)}$$

where E_a is the activation energy which is 14, 17, and 19 kcal/mol for k_H, k_{OH}, and k_{H2O}, respectively; R is the gas constant.

4.5 Results

4.5.1 Determination of the Conformation of Alamethicin in SDS Solution

4.5.1.1 Spin System Identification of Alamethicin

The first step in the assignment of the ^1H resonances is spin system identification. In a ^1H 2D J-correlated experiment, no interresidue correlation cross peaks are observed because the homonuclear ^1H coupling across a peptide bond is too small. This makes each residue an isolated spin system and the geometric pattern of cross peaks observed depends on the kind of side chain in the residue (Wuthrich, 1986).

Identification of spin systems in alamethicin starting from the 1D amide ^1H resonances is difficult because the ^1H_N resonances of alamethicin are broad and overlapping (Figure 4-5). In a 2D TOCSY experiment, intraresidue correlations from the H_N to the sidechains can be observed. The H_N-aliphatic region of a TOCSY spectrum of alamethicin shows correlations between ten non-Aib H_Ns and their $H\alpha$ and $H\beta$ resonances (Figure 4-6). However, not all H_N to $H\gamma$ and $H\delta$ cross peaks are observed. In Figure 4-6, the H_N at 7.07 ppm can be easily identified as belonging to the Phol because of

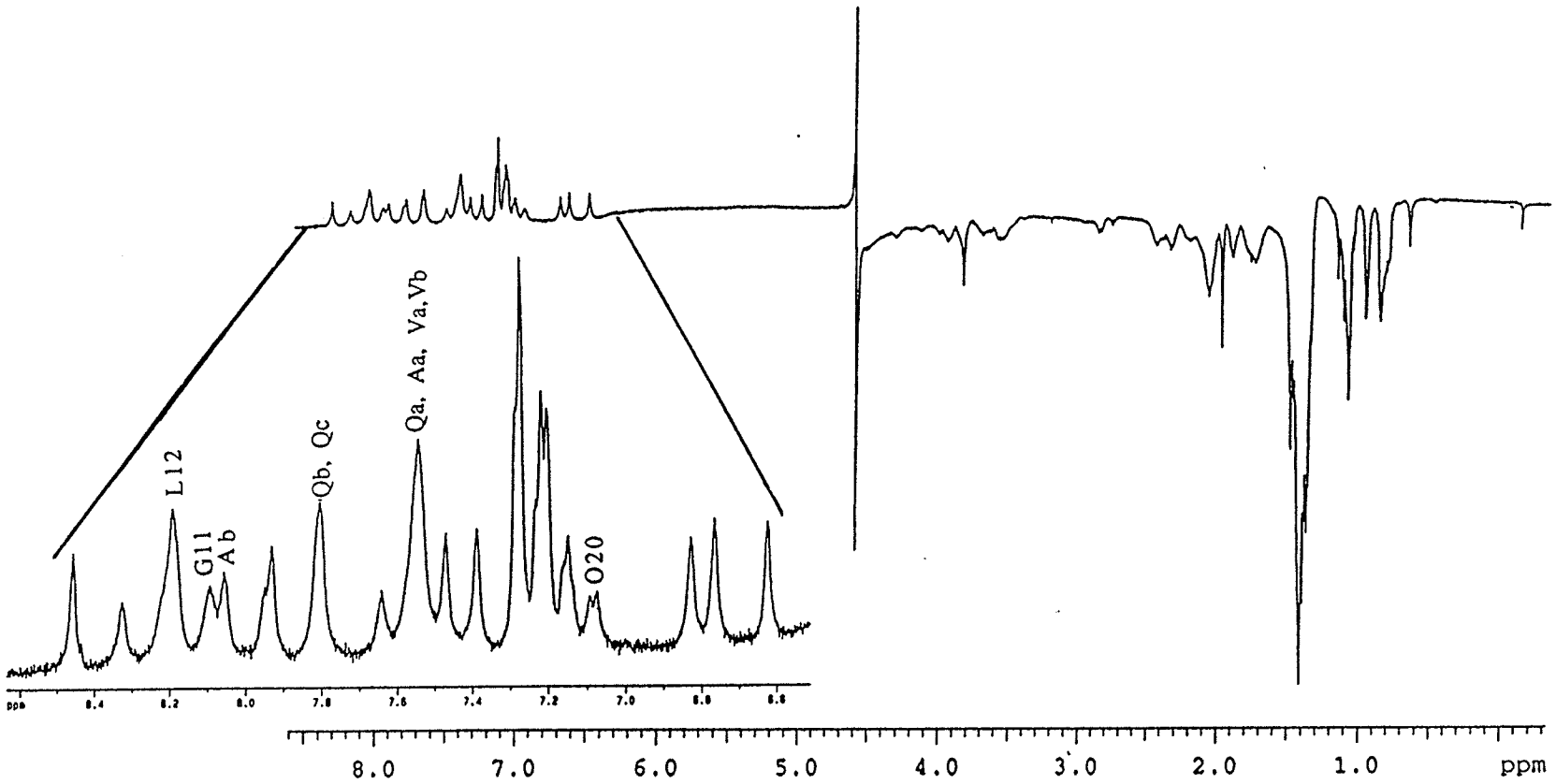

Figure 4-5: 1D ^1H NMR spectrum of unlabelled alamethicin in 150 mM SDS-D_{25}, 20 mM Na_2HPO_4 in 95/5 H_2O/D_2O, pH = 5.06 using the P1$\bar{1}$ pulse sequence (Plateau & Gueron, 1982) with 1 sec presaturation of HOD. The delay for binomial suppression was set to 196 µsec corresponding to a distance of 2550 Hz (5.1 ppm) between null signals. The number of scans was 512. The tentative peak labels for the non-Aib amide protons were from the TOCSY spectrum. No window function was applied.

the H_N cross peaks to two sets of $H\beta$ methylene cross peaks. The H_N at 8.08 ppm belongs to the lone Gly because of the characteristic cross peaks from the H_N to two $H\alpha$ resonances. Around 7.51 ppm, there are at least four H_N resonances overlapping each other and one of them is a Val which is recognized by the strong cross peak between H_N and the two γCH_3 resonances; another H_N belongs to an Ala which has a characteristic strong H_N to βCH_3 cross peak. The other Ala H_N was identified at 8.01 ppm also because of a strong H_N to βCH_3 cross peak. The other residues, including the two Pro, were identified from the aliphatic region of the TOCSY spectrum (Figure 4-7). The pattern of cross peaks for the different non-Aib residues are traced in Figure 4-7. At this point, 10 non-Aib H_N resonances had been identified from the TOCSY experiment (Figure 4-7). Five of the 8 Aib H_N are clearly resolved in the 1D spectrum of Figure 4-5, leaving 3 Aib H_N resonances to be resolved. At least one appears to be overlapped with the Leu 12 H_N.

4.5.1.2 Sequence-Specific Assignments

Residues that are unique in the peptide sequence like Gly, Leu, and Phol were assigned as described in section 4.5.1.1. These assignments served as starting points in the sequence-specific assignment using the amide region of a NOESY spectrum (Figure 4-8).

Starting with the H_N of Phol 20 at 7.08 ppm, an nOe crosspeak to a resonance at 7.81 ppm was identified as the H_N

Figure 4-6: The H_N to aliphatic region of the TOCSY spectrum (Bax & Davis, 1985) of unlabelled alamethicin in 150 mM SDS-D_{25}, 20 mM Na_2HPO_4 in 95/5 H_2O/D_2O, pH = 5.06. The mixing time was 70.6 msec. The number of scans was 64. A total of 512 increments of 1K data points each were acquired. The F_1 dimension was zero filled to 1K, no zero filling was applied to the F_2 dimension and a $\pi/2$-shifted sine-squared filter was applied to both dimensions before fourier transformation. Spin systems are identified by residue type (e.g., V_b) or by sequence position (e.g., G11).

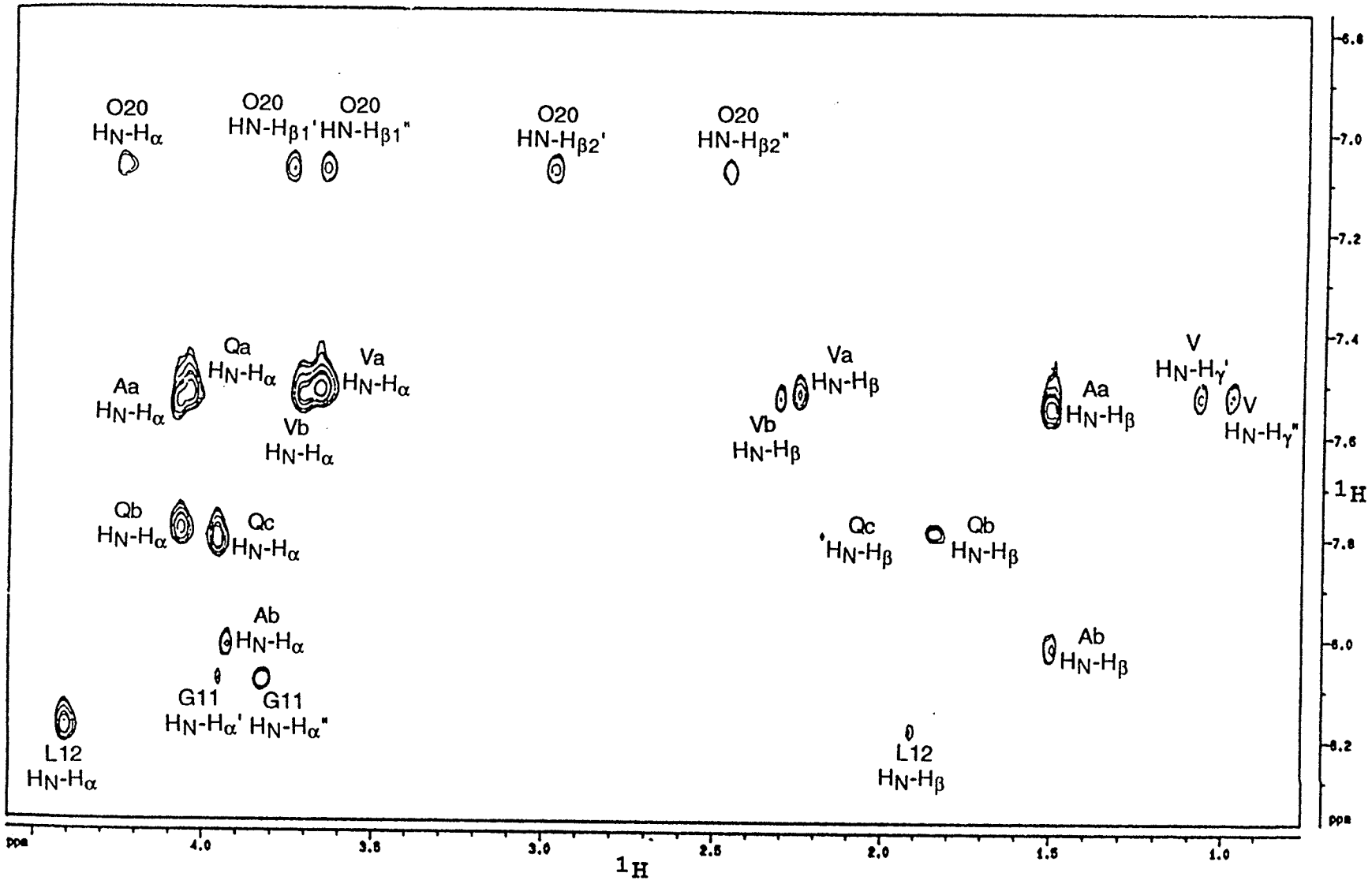
O20 HN-Hα
O20 HN-Hβ1'
O20 HN-Hβ1"
O20 HN-Hβ2'
O20 HN-Hβ2"
Aa HN-Hα
Qa HN-Hα
Va HN-Hα
Vb HN-Hα
Qb HN-Hα
Qc HN-Hα
Ab HN-Hα
G11 HN-Hα'
G11 HN-Hα"
L12 HN-Hα
Va HN-Hβ
Vb HN-Hβ
Aa HN-Hβ
V HN-Hγ'
V HN-Hγ"
Qc HN-Hβ
Qb HN-Hβ
Ab HN-Hβ
L12 HN-Hβ
ppm
4.0
3.5
3.0
2.5
2.0
1.5
1.0
1H
6.8
7.0
7.2
7.4
7.6
7.8
8.0
8.2
ppm
1H

Figure 4-7: The aliphatic region of a TOCSY spectrum (Bax & Davis, 1985) of unlabelled alamethicin in 150 mM SDS-D_{25}, 20 mM Na_2HPO_4 in 95/5 H_2O/D_2O, pH = 5.06. The acquisition and processing parameters were the same as those in Figure 4-6. The spin systems of the non-Aib residues in alamethicin are traced. (a) Val_b below the diagonal, Phol 20 (dashed line) and Pro_a above the diagonal. (b) Val_a and Ala_a (dashed line) below the diagonal, Leu 12 above the diagonal. (c) Ala_b below the diagonal, Gln_b and Pro_b (dashed line) above the diagonal. (d) Gln_c below the diagonal and Gln_a above the diagonal.

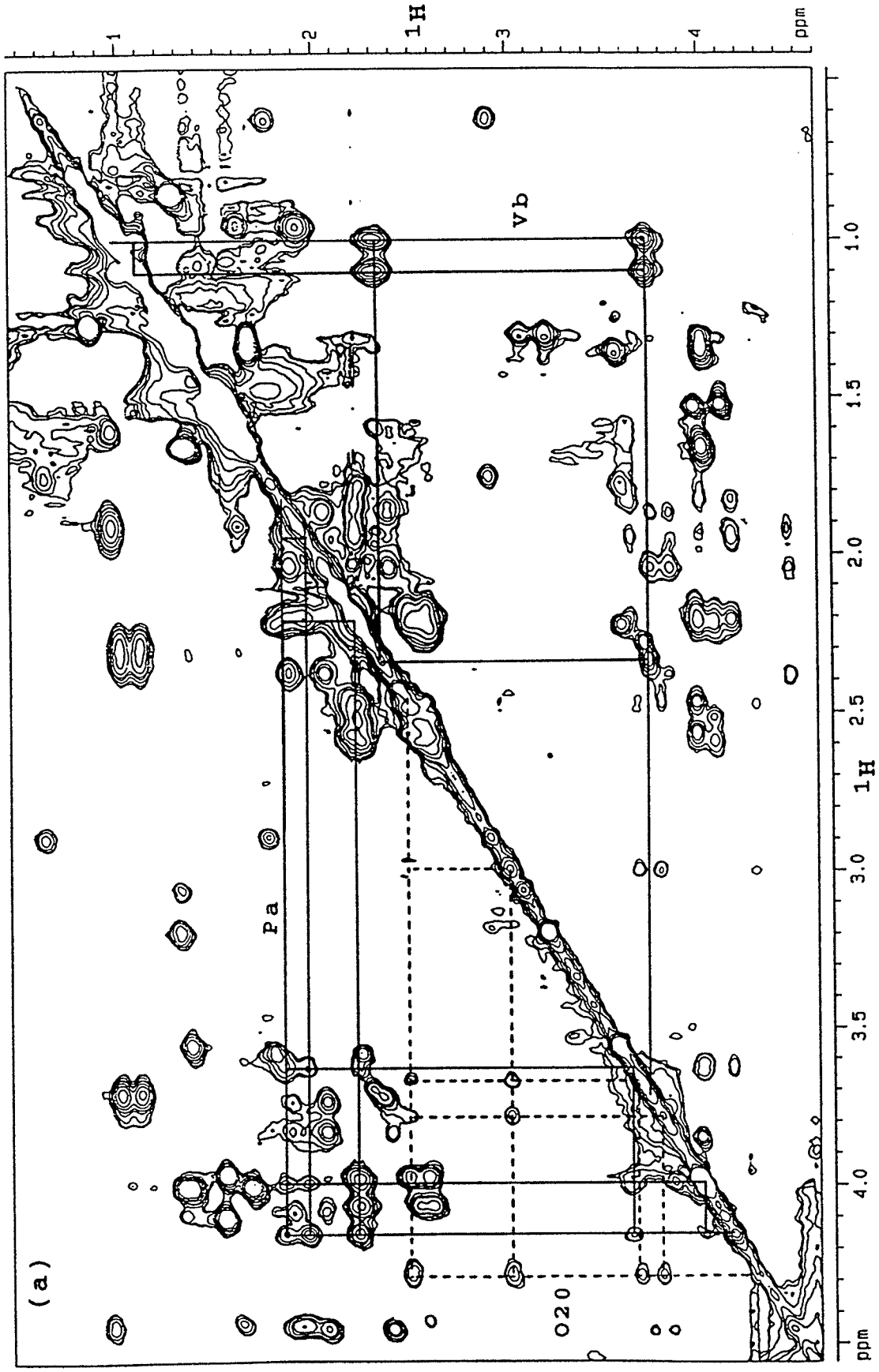
1H
ppm
Vb
Pa
O20
(a)
1H
ppm

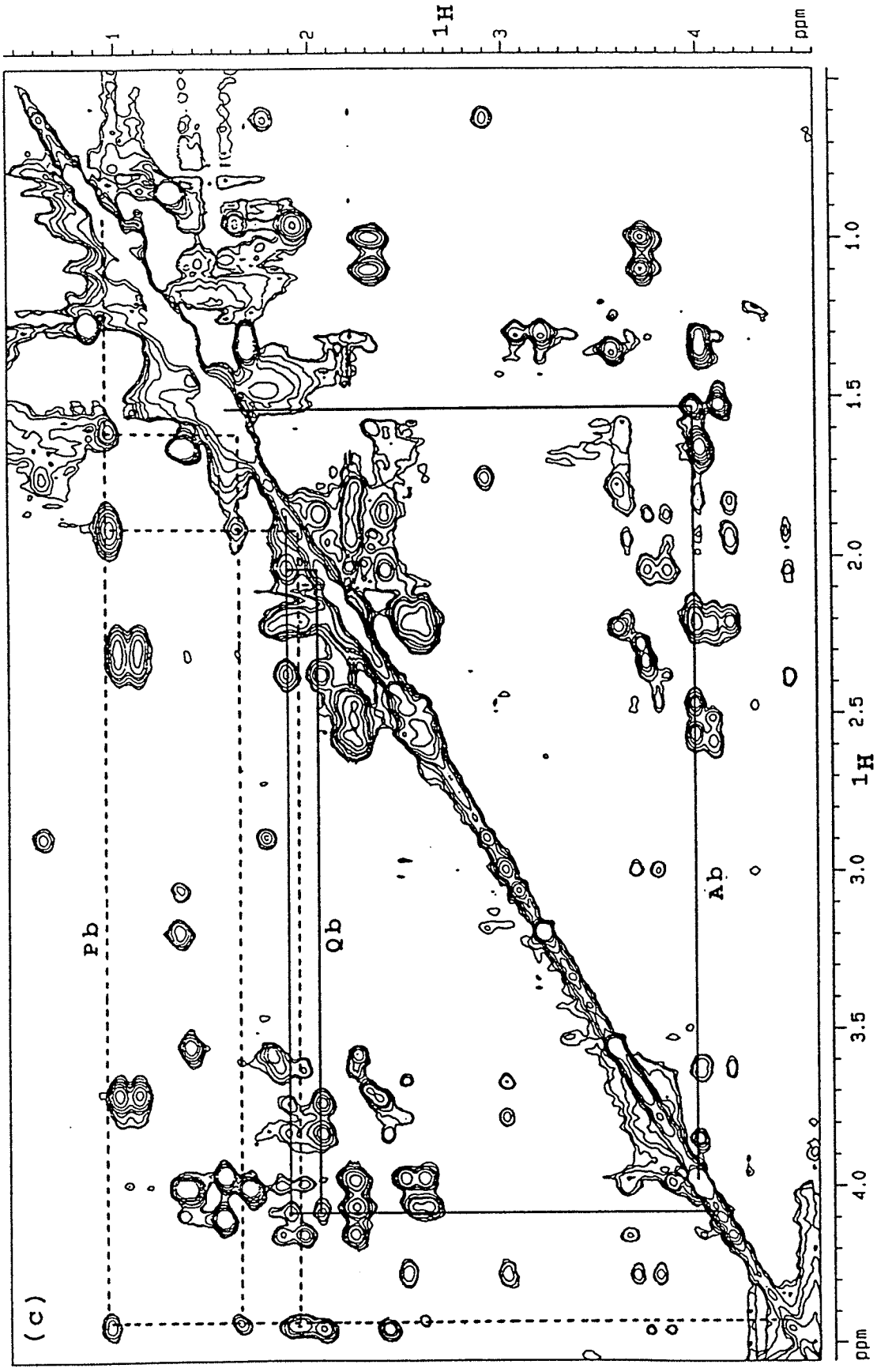
1H
ppm
1
2
3
4
1.0
1.5
2.0
2.5
3.0
3.5
4.0
Pb
Qb
Ab
(c)

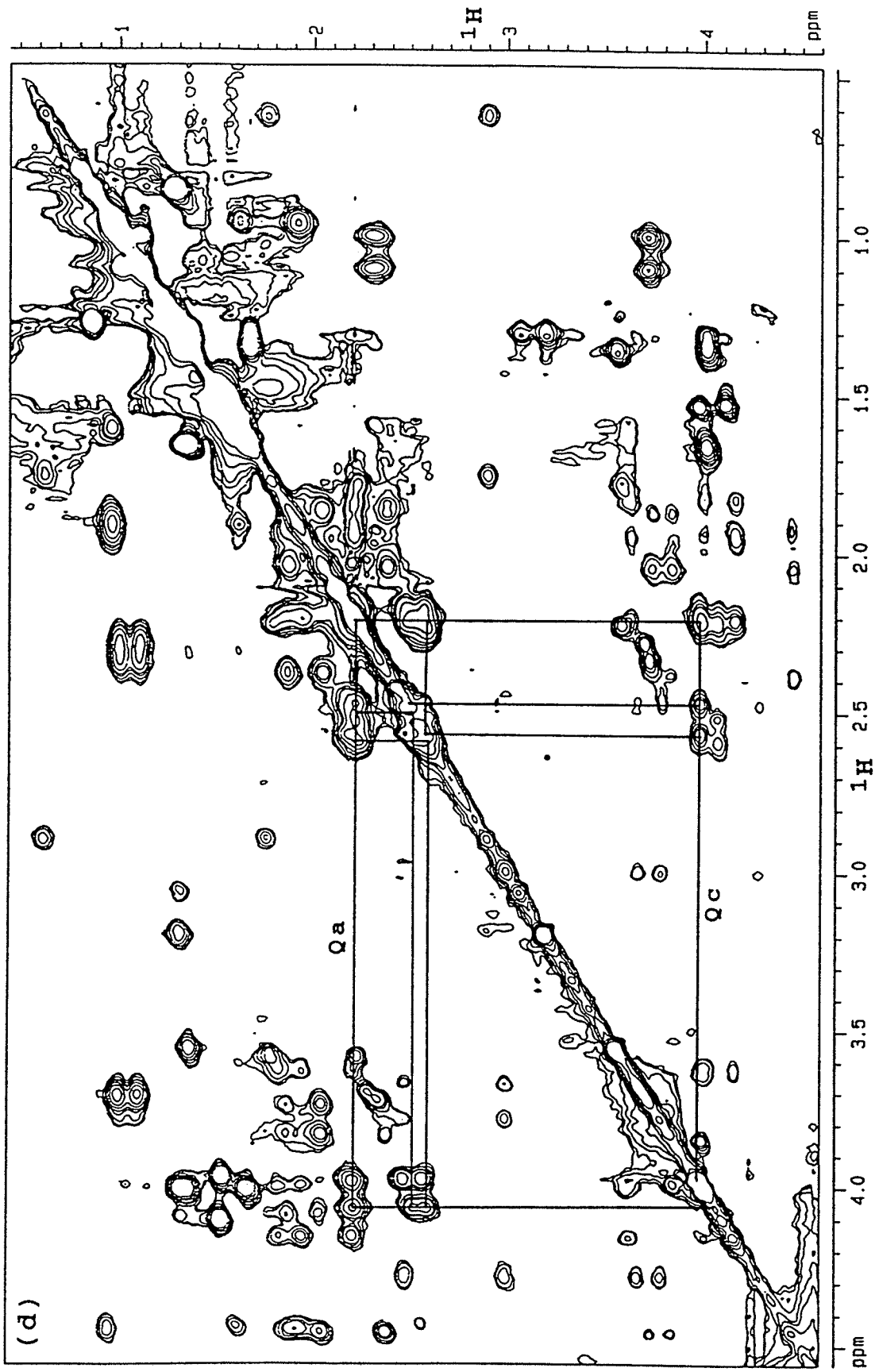
1H
ppm
1
2
3
4
Qa
Qc
(d)
1H
ppm
1.0
1.5
2.0
2.5
3.0
3.5
4.0

Figure 4-8: The amide region of the NOESY-P1$\bar{1}$ spectrum of unlabelled alamethicin in 150 mM SDS-D_{25}, 20 mM Na_2HPO_4 in 95/5 H_2O/D_2O, pH = 5.06. The sequential $H_N(i)$ to $H_N(i+1)$ nOes are traced. The solid line connects H_N resonances from Aib 3 to Aib 13 and the dashed line connects H_N resonances from Val 15 to Phol 20. The number of scans was 96. A total of 512 increments of 2K data points each were acquired. The mixing time was 100 msec. The delay for binomial water suppression (Plateau & Gueron, 1982) was set to 196 μsec. The F_1 dimension was zero filled to 1K, no zero filling was applied to the F_2 dimension and a $\pi/2$-shifted sine-squared filter was applied to both dimensions before fourier transformation.

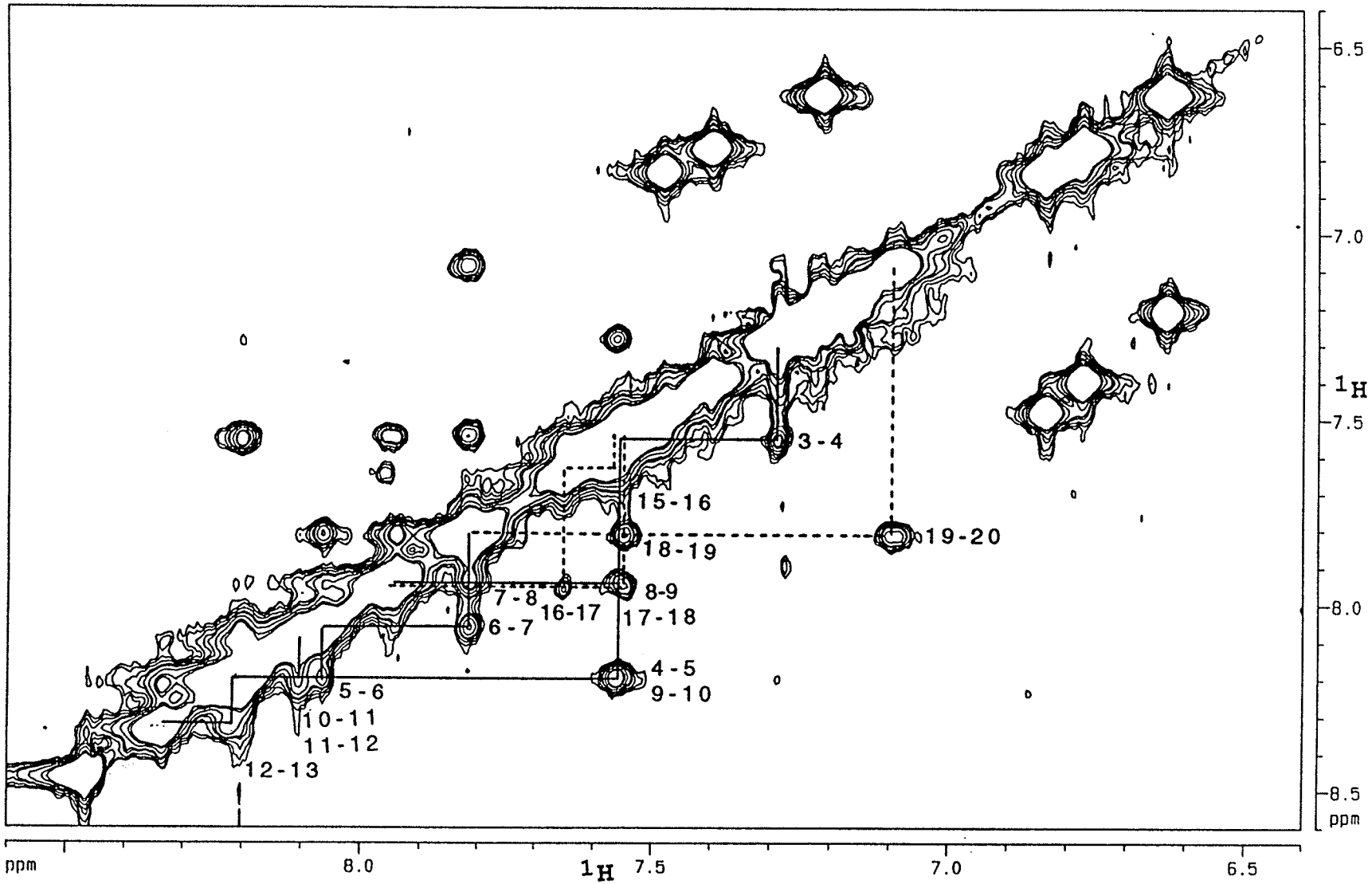
3-4
15-16
18-19
19-20
7-8
16-17
8-9
17-18
6-7
4-5
9-10
5-6
10-11
11-12
12-13
6.5
7.0
1H
7.5
8.0
8.5
ppm
ppm
8.0
1H
7.5
7.0
6.5

of two overlapping Glns (marked Q_b and Q_c in Figure 4-5 and Figure 4-7 c,d) and therefore Q_b was assigned to Gln 19. From Gln 19 there is a crosspeak to 7.55 ppm (Q_a), thus Q_a was assigned to Gln 18. Since there are only three Glns in the alamethicin sequence, Q_c was assigned to Gln 7. Therefore the Gln 7 H_N overlaps with that of Gln 19. From Gln 18, there is a cross peak to 7.94 ppm and this was assigned to Aib 17. The assignment of Aib 16 followed from the cross peak at (7.65, 7.94 ppm). From Aib 16 there appears to be a cross peak very close to the diagonal to a Val H_N which must be Val 15 H_N.

The H_N of Gly 11 at 8.10 ppm has a cross peak to the H_N of Leu 12 at 8.21 ppm which confirms the assignment of both residues. A crosspeak from Leu 12 to an Aib at 8.32 ppm allows the assignment of Aib 13. The only cross peak to Gly 11 is the one from Leu 12, so the Aib 10 H_N may overlap with that of Gly 11, in which case the cross peak is on the diagonal or it may overlap with that of Leu 12, in which case the Gly 11- Leu 12 cross peak is also the Aib 10- Gly 11 cross peak. The residue preceding Aib 10 is Val 9. Both Val resonances overlap at 7.55 ppm and a cross peak between the Val resonances and the peak at 8.21 ppm (Leu 12) was observed but not to the peak at 8.10 ppm (Gly 11). This was therefore assigned to be the (Val 9, Aib 10) cross peak and Aib 10 was assigned to overlap with Leu 12 instead of Gly 11. Thus the (Aib 10, Gly 11) and (Gly 11, Leu 12) cross peaks are superimposed.

The two Ala resonances (A_a and A_b in Figure 4-5) both show cross peaks to Gln 7 and Aib residues so the Ala H_N resonances cannot be assigned unambiguously at this point.

In order to completely assign the ^1H resonances, we used the ^{15}N dimension to resolve the overlap in the H_N region of alamethicin. A simple HMQC (Bax, et al., 1983a,b) spectrum shows correlation cross peaks between the ^{15}N resonances and their attached protons. The HMQC spectrum of alamethicin is shown in Figure 4-9. There are only 23 ^{15}N-^1H_N correlation cross peaks in the HMQC spectrum. We expected 24 cross peaks, 18 from the non-Pro amides and 6 from the three Gln sidechains, therefore two residues overlap in both the ^1H_N and ^{15}N dimensions.

We can now go back to the NOESY spectrum and clear up the ambiguities and overlaps. For instance, the assignment of Aib 10 at 8.2 ppm was confirmed because the HMQC spectrum shows that there are two Aib H_N resonances at 8.2 ppm overlapping with Leu 12 and none at 8.10 ppm (Gly 11). The resonance at 7.28 ppm which overlaps with the phenyl ring proton resonances is one of the missing Aib H_N. It can be assigned to Aib 3 because it only has one cross peak to 7.55 ppm which is one of the Ala H_N (A_a) which is assigned to Ala 4. This leaves the other Ala (A_b) as Ala 6. The cross peak at (7.56, 8.20 ppm) which was assigned to (Val 9, Aib 10) is also (Ala 4, Aib 5) and the HMQC spectrum shows that there are two Aib H_N overlapping at 8.2 ppm. The sequential nOe

Figure 4-9: An HMQC spectrum (Bax, et al., 1983a,b) of ^{15}N-labelled alamethicin in 150 mM SDS-D_{25}, 20 mM Na_2HPO_4 in 95/5 H_2O/D_2O, pH = 5.13. The number of scans was 32. A total of 512 increments of 1K data points each were acquired. The F_1 dimension was zero filled to 1K, no zero filling was applied to the F_2 dimension, and a $\pi/2$-shifted sine-squared filter was applied to both dimensions before fourier transformation.

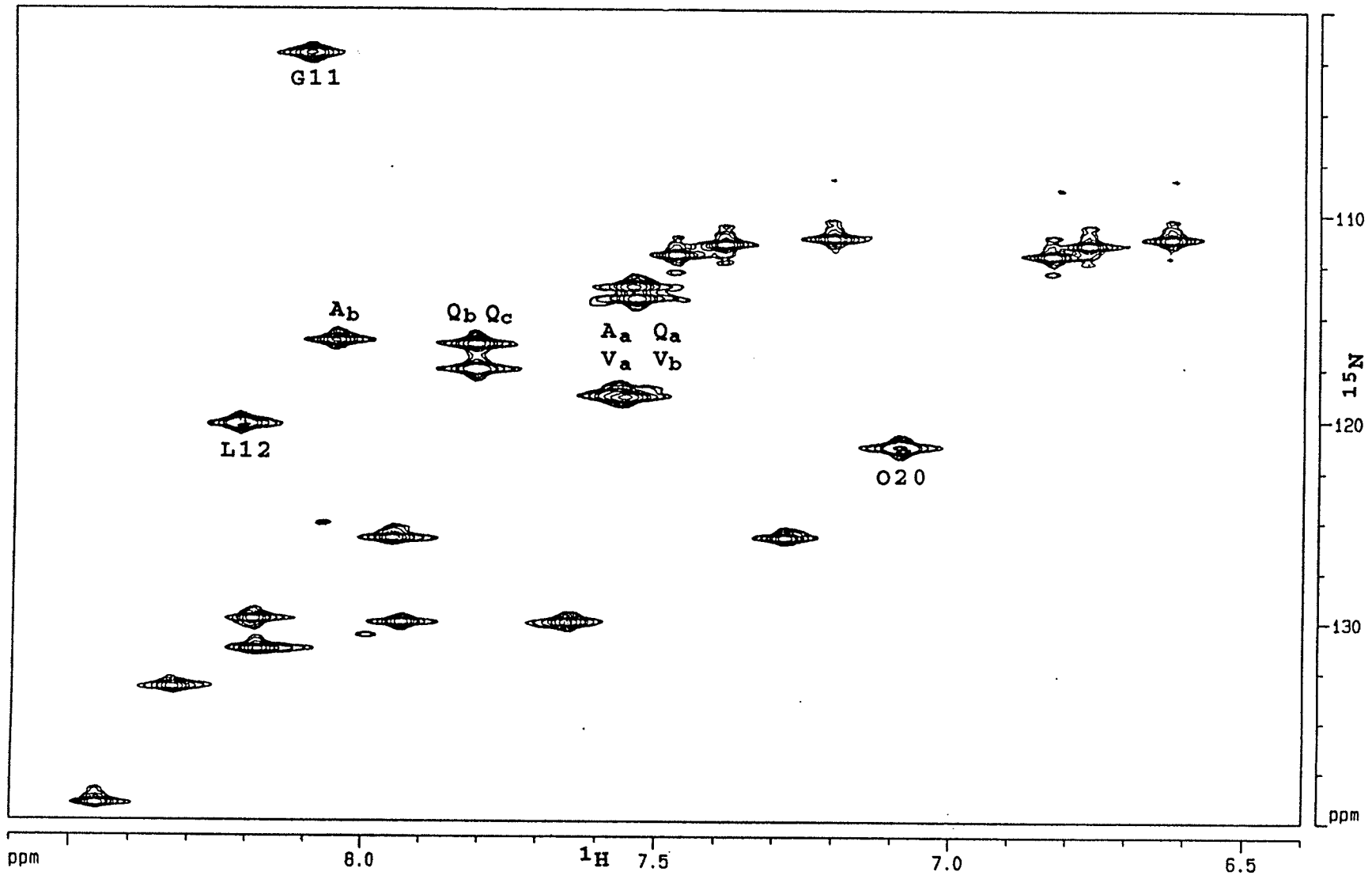
G11
Ab
Qb Qc
Aa Qa
Va Vb
L12
O20
110
120
130
15N
ppm
ppm
8.0
1H
7.5
7.0
6.5

cross peaks were traced from residue 3 to 13 and from 15 to 20 and these are shown in Figure 4-8.

The resonances from the two Pro were assigned based on the nOe from the H_N of Aib 3 to the $H\delta$ of Pro 2 and from the H_N of Aib 13 to the $H\delta$ of Pro 14 (see Figure 4-12j). A summary of the ^1H resonance assignments is given in Appendix A.

4.5.1.3 Assignment of the ^{13}C Resonances

The HSQC spectrum of alamethicin correlating the ^{13}C atoms to their attached protons is shown in Figure 4-10. Since the α and sidechain protons had been assigned previously, the assignment of the ^{13}C resonances was straightforward. The Gly 11 $^{13}C\alpha$ to $H\alpha$ cross peak is barely above the noise level but the presence of two crosspeaks from the two $H\alpha$ of the Gly to a common carbon confirmed this assignment. The $^{13}C\alpha$-$^1H\alpha$ correlations of Leu 12 and Pro 14 are also weaker than the others probably because their ^1H resonances are very close to the water signal and are partially saturated. The assignment of the Leu 12 $^{13}C\gamma$ is ambiguous because the proton at 1.9 ppm shows a correlation to two different carbons at 26.9 ppm and 30.8 ppm. By comparing the crosspeak patterns of the HSQC spectrum of alamethicin acquired in CD_3OH with that obtained in SDS solution, the Leu 12 $^{13}C\gamma$ was tentatively assigned to 26.9 ppm. A summary of the ^{13}C assignments is given in Appendix A.

Unlike the ^{13}C-^1H HSQC spectrum of alamethicin in CD_3OH (Figure 3-4), other ^{13}C-^1H correlations are also observed in

Figure 4-10: The (a) $H\beta$ and $H\gamma$ region and (b) H_α region of the HSQC spectrum (Bodenhausen & Ruben, 1980) with ^{13}C decoupling of unlabelled alamethicin in 150 mM SDS-D_{25}, 20 mM Na_2HPO_4 in 95/5 H_2O/D_2O, pH 5. The number of scans was 48. A total of 512 increments of 1K data points each were acquired. No zero filling was applied to both dimensions and a $\pi/2$-shifted sine-squared filter was applied to both dimensions before fourier transformation.

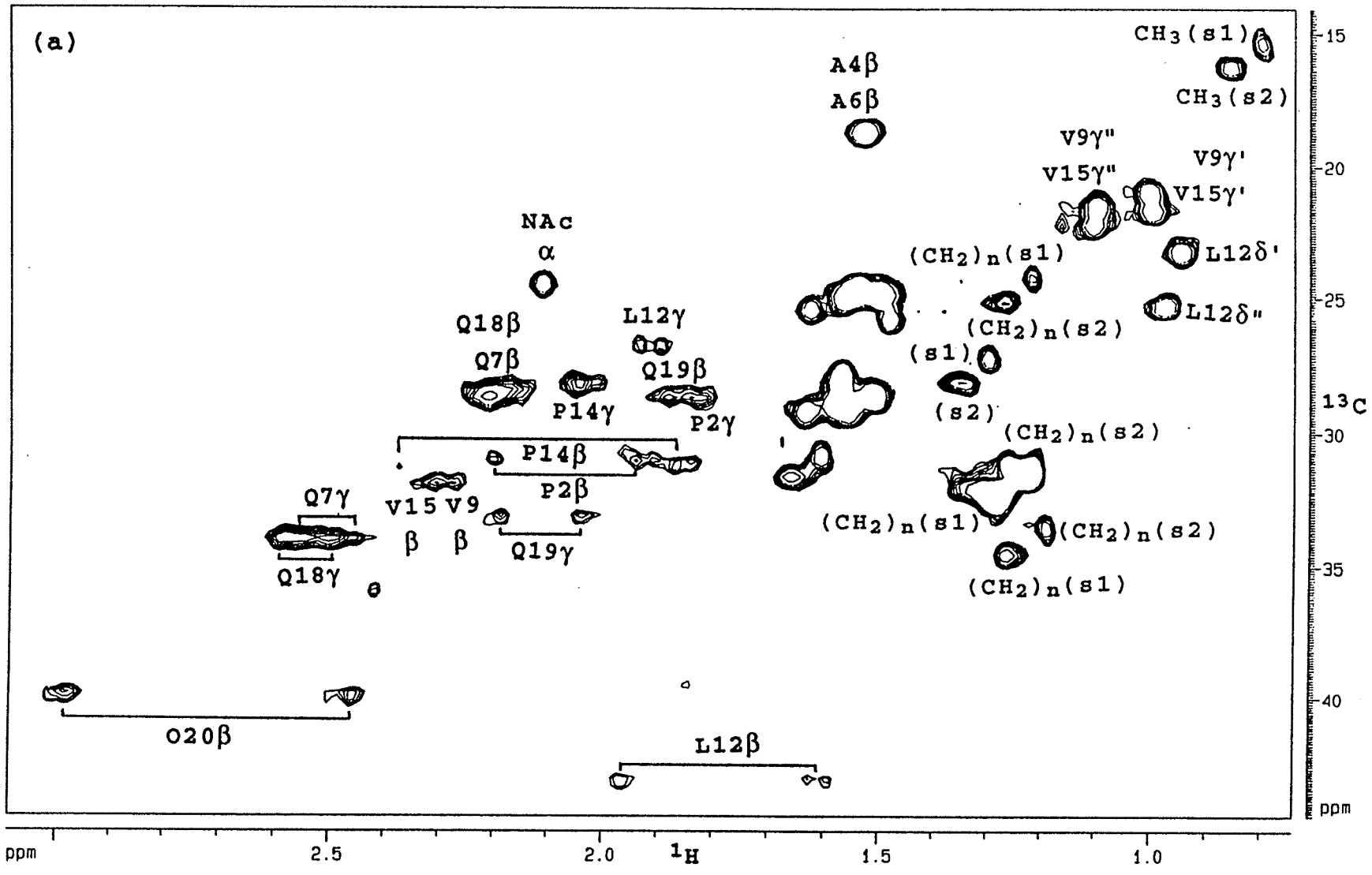
(a)
A4β
A6β
CH3(s1)
CH3(s2)
V9γ"
V15γ"
V9γ'
V15γ'
NAc
α
(CH2)n(s1)
L12δ'
L12δ"
Q18β
Q7β
L12γ
Q19β
P14γ
P2γ
(CH2)n(s2)
(s1)
(s2)
P14β
P2β
Q7γ
V15 V9
β β
Q19γ
Q18γ
(CH2)n(s2)
(CH2)n(s1)
(CH2)n(s2)
(CH2)n(s1)
O20β
L12β
15
20
25
30
35
40
13C
ppm
ppm
2.5
2.0
1H
1.5
1.0

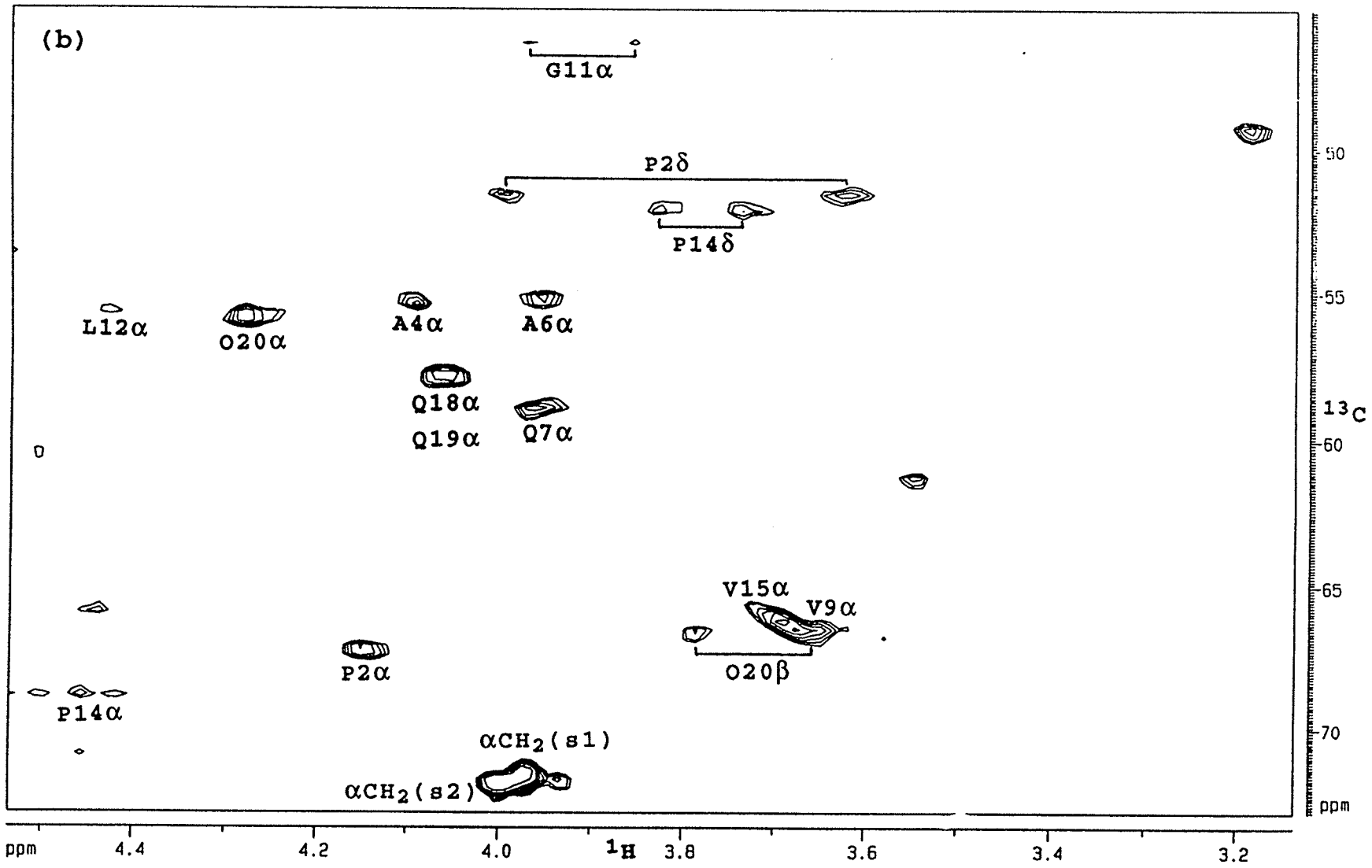
(b)
G11α
P2δ
P14δ
L12α
O20α
A4α
A6α
Q18α
Q19α
Q7α
V15α
V9α
O20β
P2α
P14α
αCH2(s1)
αCH2(s2)
50
55
60
65
70
13C
ppm
ppm
4.4
4.2
4.0
1H
3.8
3.6
3.4
3.2

addition to those arising from alamethicin. Since the SDS used in the experiments is only 98% deuterated, this leaves about 3 mM of the SDS in solution which is protonated. It appears as if there are two sets of SDS peaks labelled s1 and s2 in Figure 4-10. The terminal CH_3 protons of the SDS alkyl chains resonate at 0.82 and 0.86 ppm; the bulk of the methylene protons resonate at 1.15 and 1.35 ppm; and the αCH_2 resonate at 3.97 and 4.00 ppm, respectively. The carbons of the detergent alkyl chain of s1 and s2 resonate at 15.73 and 15.92 ppm for the terminal CH_3, 23.99 to 34.54 ppm for the methylenes, and 71.40 and 71.72 ppm for the αCH_2 resonances, respectively.

4.5.1.4 Assignment of ^{15}N Resonances

Because of the overlaps in the ^1H dimension, unambiguous assignment of the ^{15}N resonances using HMQC alone was not possible (Figure 4-9). For example, the H_N of Gln 7 and Gln 19 overlap at 7.8 ppm, so it is not possible to assign using Figure 4-9 alone which ^{15}N (Gln 7 or Gln 19) resonates at 116.4 ppm and which is at 117.6 ppm. The assignment of the ^{15}N resonances was made possible using the HMQC-NOESY experiment (Shon & Opella, 1989). In this experiment, a mixing time is added at the end of the HMQC sequence to allow for ^1H homonuclear spin exchange to occur. Thus the spectrum not only shows the ^{15}N-^1H correlations but also shows nOe cross peaks between sequential amide protons. The more intense cross peaks are the ^{15}N-^1H correlation peaks and the

less intense peaks are the nOes between amide protons. Some of the H_N to H_α and H_β nOe cross peaks are also observed (Figure 4-11a). The complete ^{15}N resonance assignment was traced as shown in Figure 4-11b and this also confirmed the ^1H_N assignment. The ^1H_N and ^{15}N resonances of Ala 4 and Val 15 resonate at the same frequency in both the ^{15}N and ^1H dimensions. A summary of the ^{15}N assignment is given in Appendix A.

4.5.1.5 Translation of NMR Data into Geometric Constraints

The nOe intensity observed between two protons gives us some idea about how far apart the protons are from each other. When the initial build up of the nOe is linear it is also proportional to the distance between the two protons. The nOe intensity at a given mixing time can be translated into a distance by a proportionality equation, using the intensity of an nOe between two protons of known distance for calibration. An optimum mixing time is one that is long enough for most of the nOe to have built up but short enough so that the initial rate approximation still holds. To find this mixing time, we ran NOESY experiments at three different mixing times, 50, 100, and 200 msecs (Figures 4-12). The cross peaks at (1.87, 2.36), (2.47, 2.98), (7.28, 3.64), and (7.08, 7.81) were integrated at the three different mixing times and plotted against mixing time (Figure 4-13). These cross peaks correspond to the nOes (P14 $H\beta''$, P14 $H\beta'$),

Figure 4-11: HMQC-NOESY spectrum of ^{15}N-labelled alamethicin in 150 mM SDS-D_{25}, 20 mM Na_2HPO_4 in 95/5 H_2O/D_2O, pH 5.13. The mixing time was 200 msec. The number of scans was 64. A total of 512 increments of 1K data points each were acquired. The F_1 dimension was zero filled to 1K, no zero filling was applied to the F_2 dimension, and a $\pi/2$-shifted sine-squared filter was applied to both dimensions before fourier transformation. (a) The aliphatic region showing nOes from the H_N to the H_α and H_β separated by the ^{15}N dimension. (b) The amide region showing nOes from H_N to H_N and also showing H_N to ^{15}N J-correlations. The sequential assignment of the ^{15}N resonances are traced. The solid line connects resonances from Aib 3 to Aib 13, and the dashed line connects resonances from Val 15 to Phol 20.

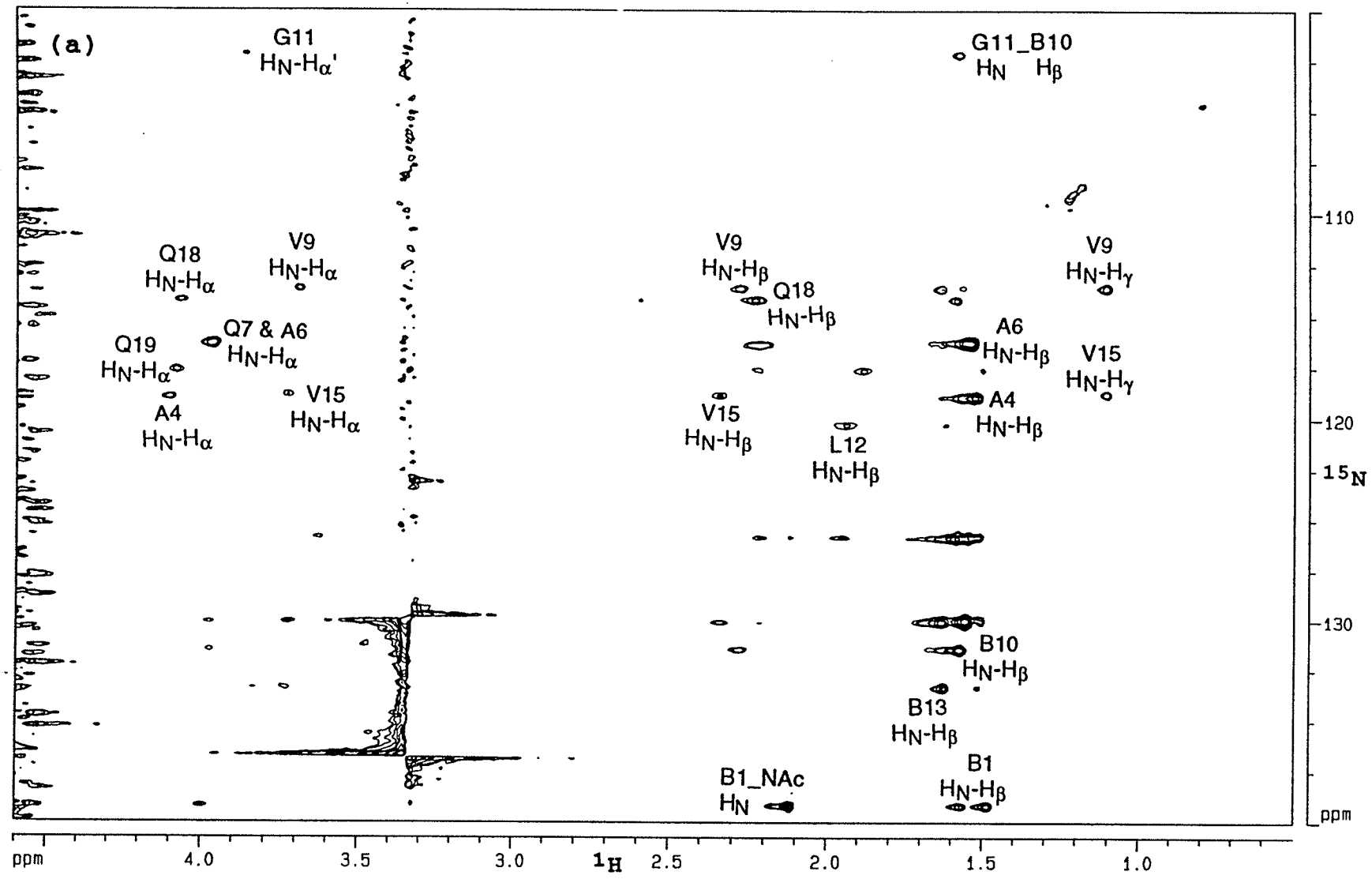
(a)
G11
HN-Hα'
G11_B10
HN Hβ
Q18
HN-Hα
V9
HN-Hα
V9
HN-Hβ
Q18
HN-Hβ
V9
HN-Hγ
Q19
HN-Hα
Q7 & A6
HN-Hα
A6
HN-Hβ
V15
HN-Hγ
A4
HN-Hα
V15
HN-Hα
V15
HN-Hβ
A4
HN-Hβ
L12
HN-Hβ
B10
HN-Hβ
B13
HN-Hβ
B1_NAc
HN
B1
HN-Hβ
110
120
130
15N
ppm
ppm
4.0
3.5
3.0
1H
2.5
2.0
1.5
1.0

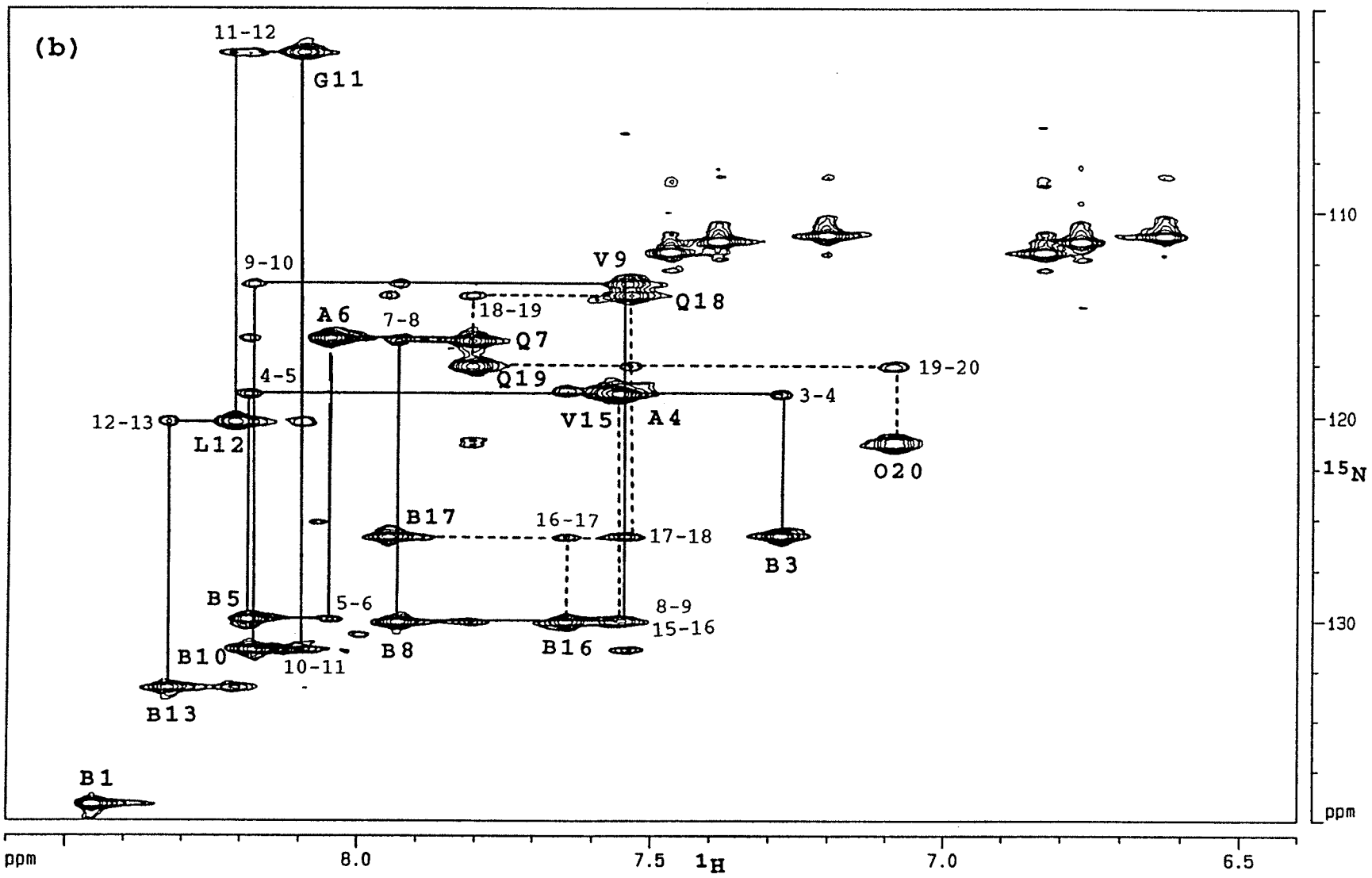
(b)
11-12
G11
9-10
V9
Q18
18-19
A6
7-8
Q7
Q19
19-20
4-5
3-4
12-13
L12
V15
A4
O20
B17
16-17
17-18
B3
B5
5-6
8-9
15-16
B10
10-11
B8
B16
B13
B1
110
120
130
ppm
15N
ppm
8.0
7.5
1H
7.0
6.5

Figure 4-12: NOESY-P1$\bar{1}$ spectra of 1.7 mM unlabelled alamethicin in 150 mM SDS-D_{25}, 20 mM Na_2HPO_4 in 95/5 H_2O/D_2O, pH 5.06 at different mixing times. Solvent was suppressed using a combination of solvent presaturation and the P1$\bar{1}$ sequence (Plateau & Gueron, 1982). Solvent was presaturated for 1 sec. The delay for binomial water suppression was set to 196 μsec. The number of scans was 96. A total of 512 increments of 2K data points each were acquired. The F_1 dimension was zero filled to 1K, no zero filling was applied to the F_2 dimension, and a $\pi/2$-shifted sine-squared filter was applied to both dimensions before fourier transformation. The second and third quadrants are opposite in phase to the first and fourth quadrants. The mixing times are given in the figures. The crosspeaks used in Figure 4-13 are labelled.

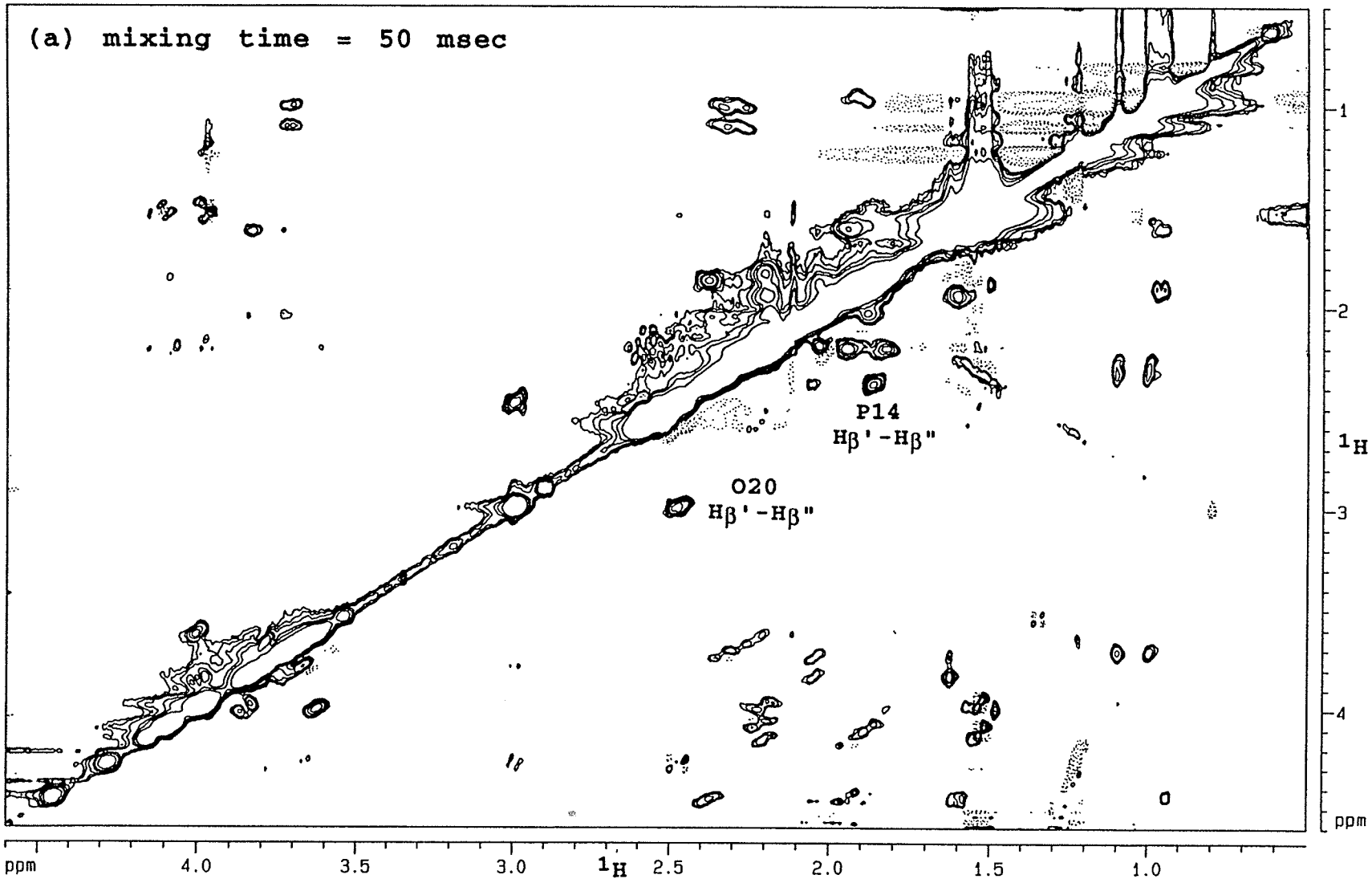
(a) mixing time = 50 msec
P14
Hβ'-Hβ"
O20
Hβ'-Hβ"
ppm
4.0
3.5
3.0
1H
2.5
2.0
1.5
1.0
1
2
3
4
1H
ppm

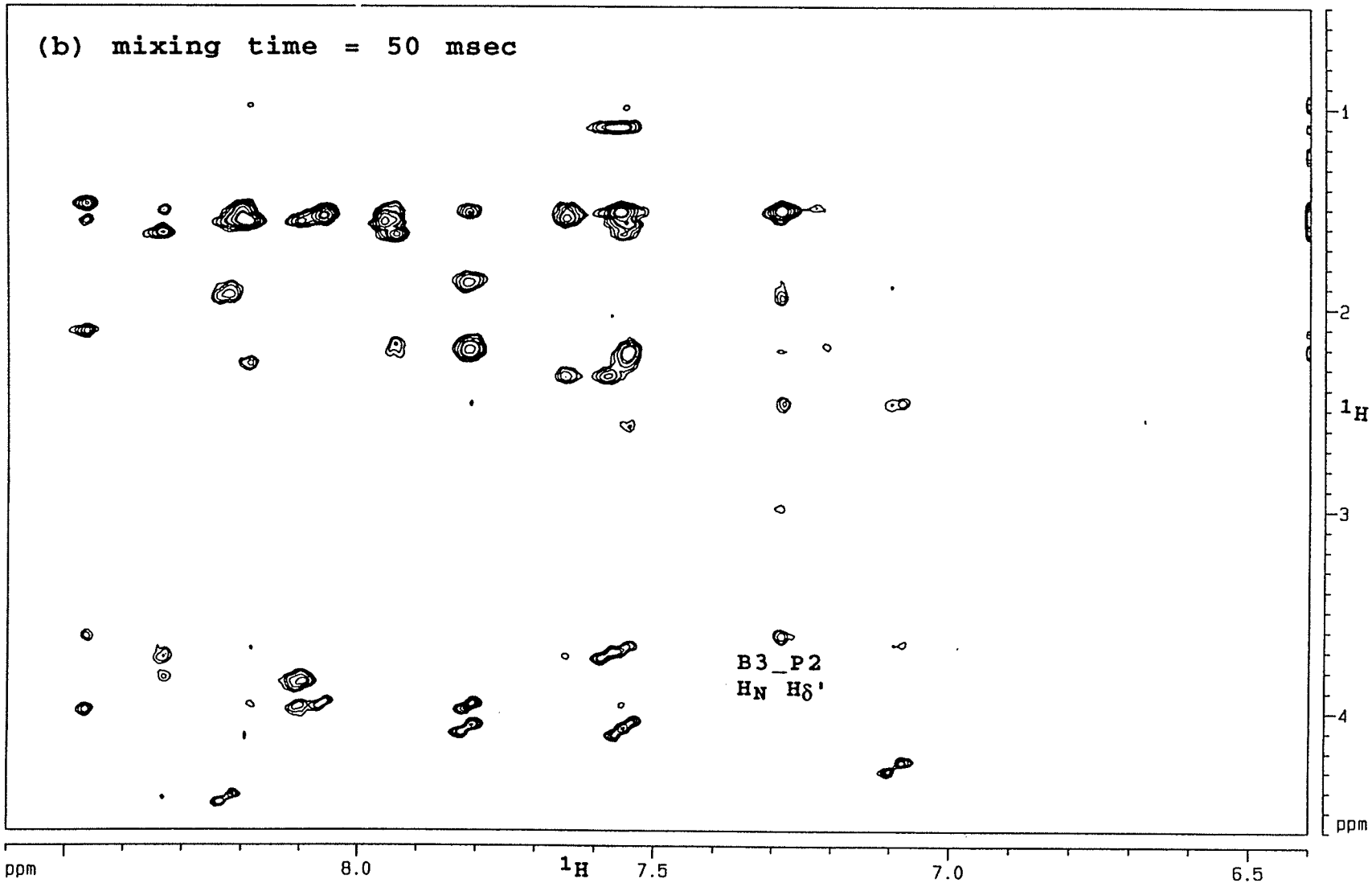
(b) mixing time = 50 msec
B3_P2
H_N H_δ'
ppm
8.0
^1H
7.5
7.0
6.5
1
2
^1H
3
4
ppm

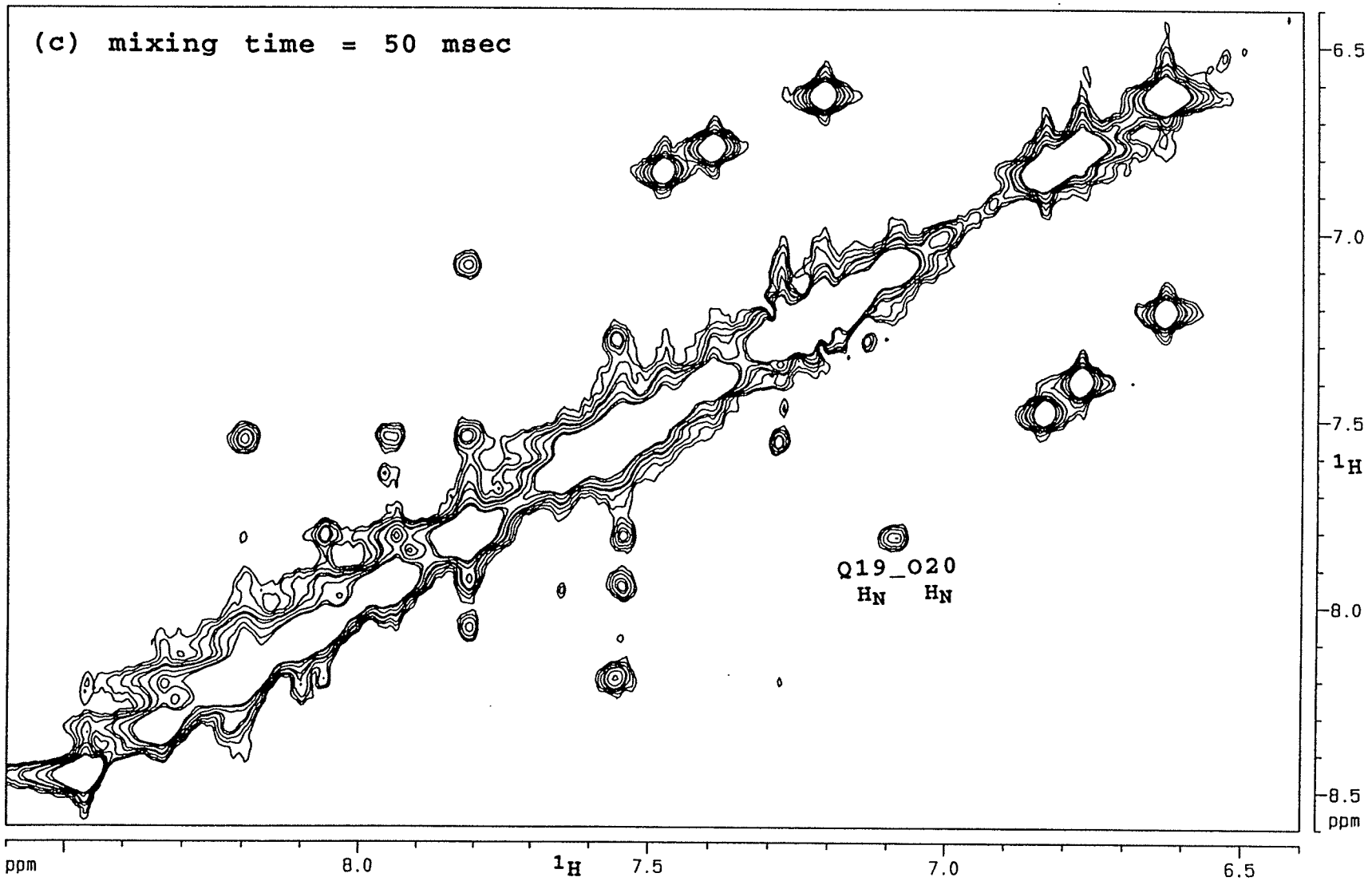
(c) mixing time = 50 msec
Q19_O20
HN HN
6.5
7.0
7.5
1H
8.0
8.5
ppm
ppm
8.0
1H
7.5
7.0
6.5

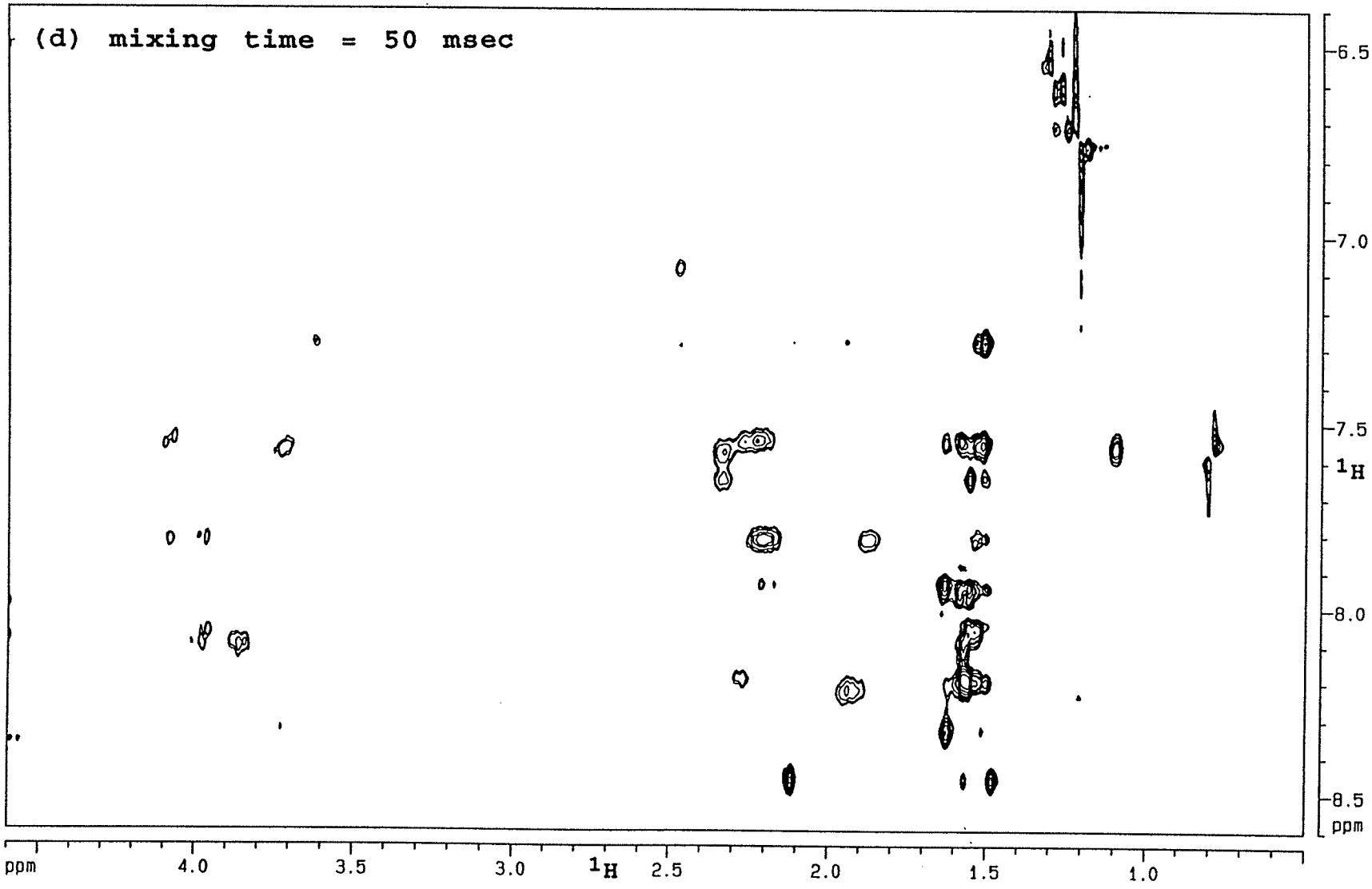
(d) mixing time = 50 msec
6.5
7.0
7.5
^{1}H
8.0
8.5
ppm
ppm
4.0
3.5
3.0
^{1}H
2.5
2.0
1.5
1.0

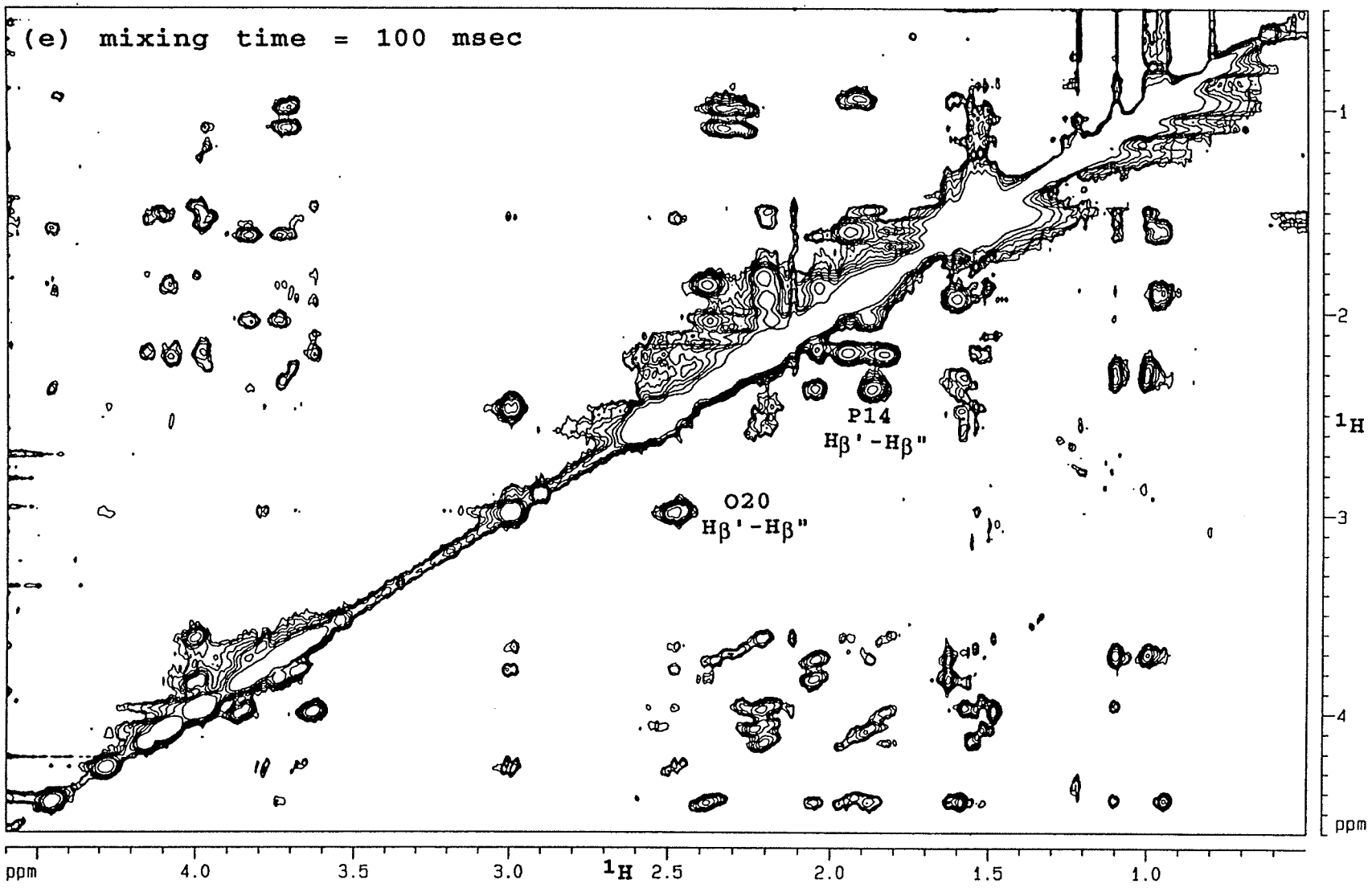
(e) mixing time = 100 msec
P14
Hβ'-Hβ"
O20
Hβ'-Hβ"
ppm
4.0
3.5
3.0
1H
2.5
2.0
1.5
1.0
1
2
1H
3
4
ppm

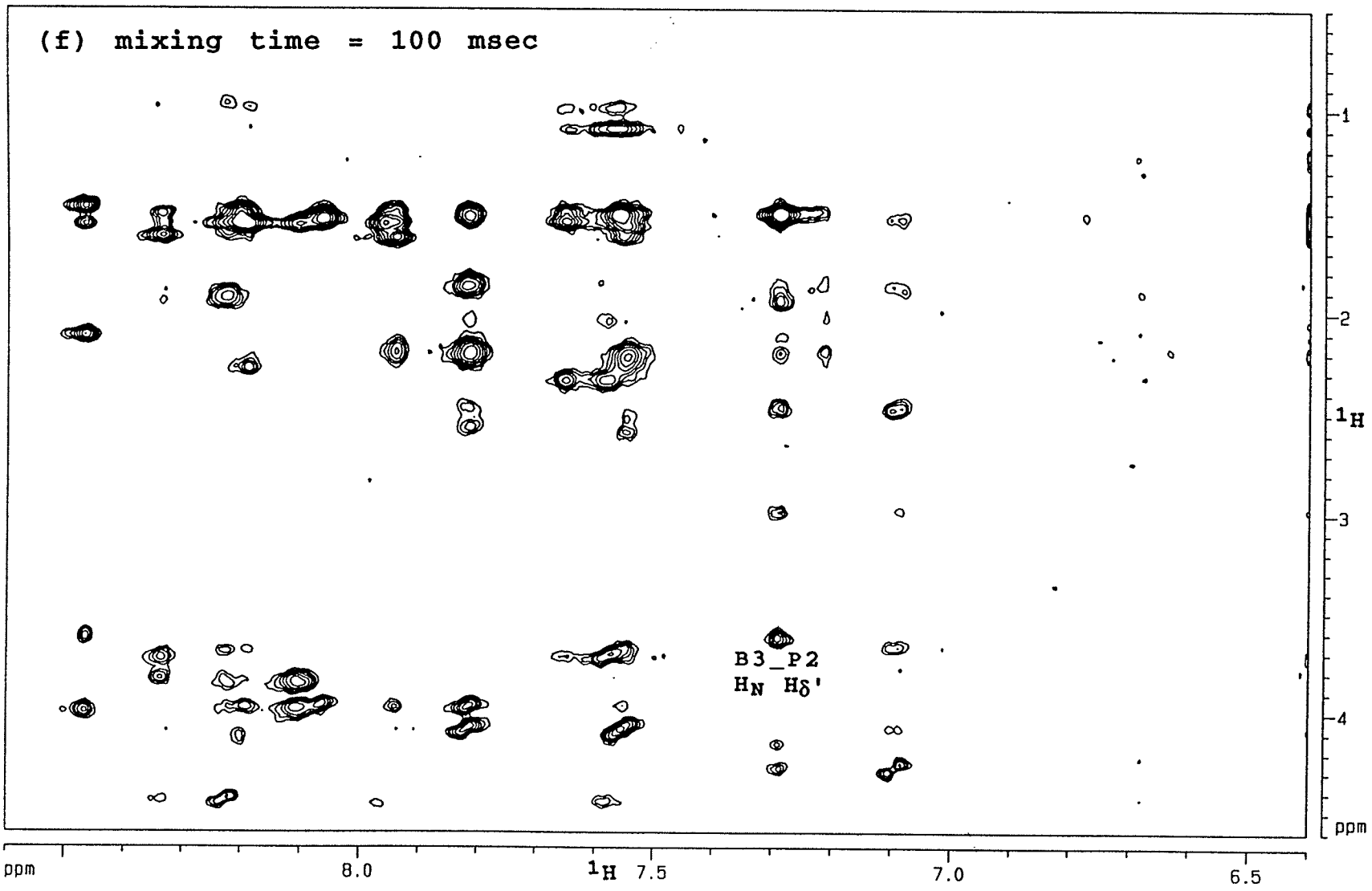
(f) mixing time = 100 msec
B3_P2
H_N $H\delta'$
ppm
8.0
^1H 7.5
7.0
6.5
^1H
ppm

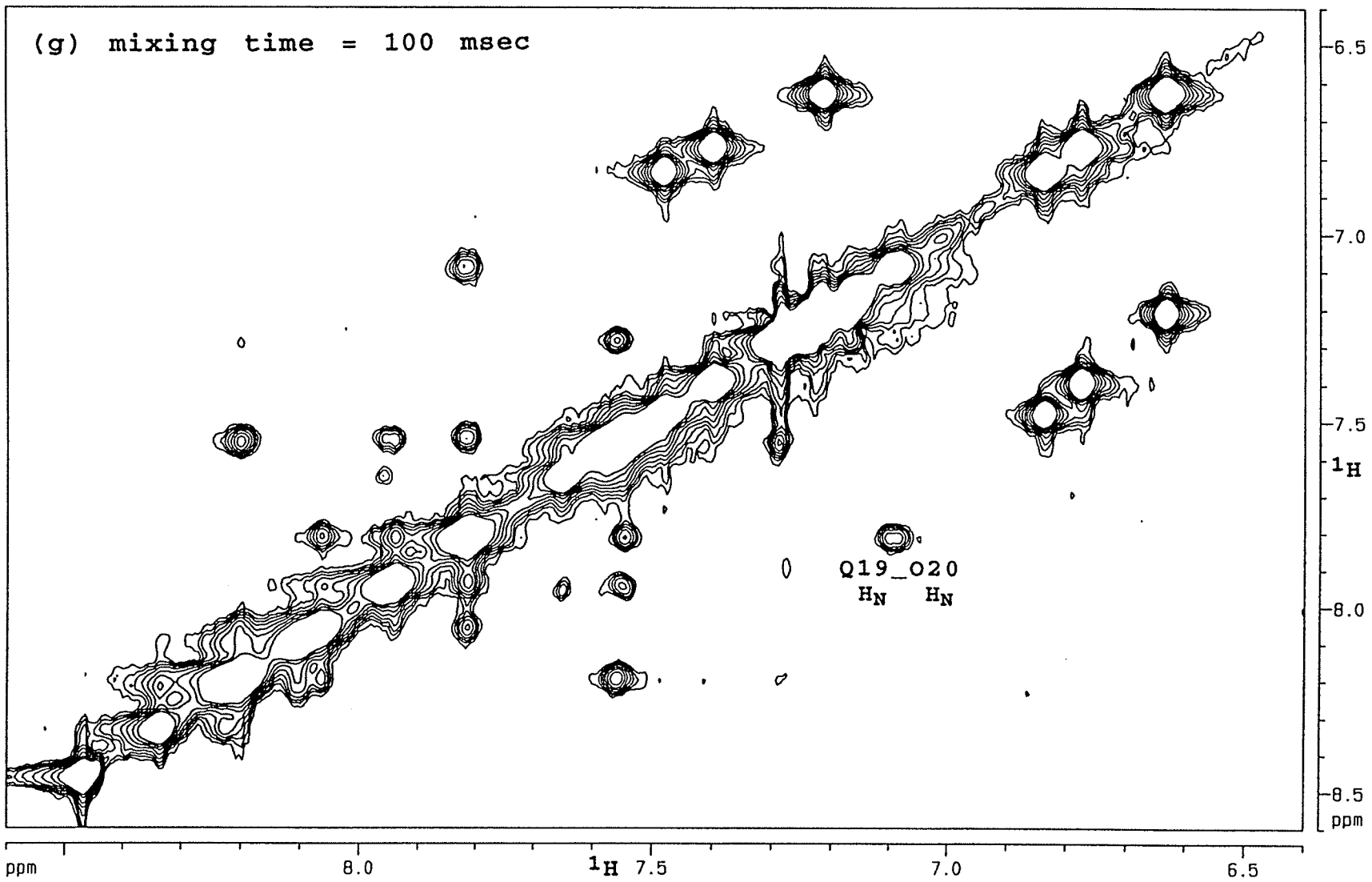
(g) mixing time = 100 msec
Q19_O20
HN HN
6.5
7.0
7.5
1H
8.0
8.5
ppm
ppm
8.0
1H 7.5
7.0
6.5

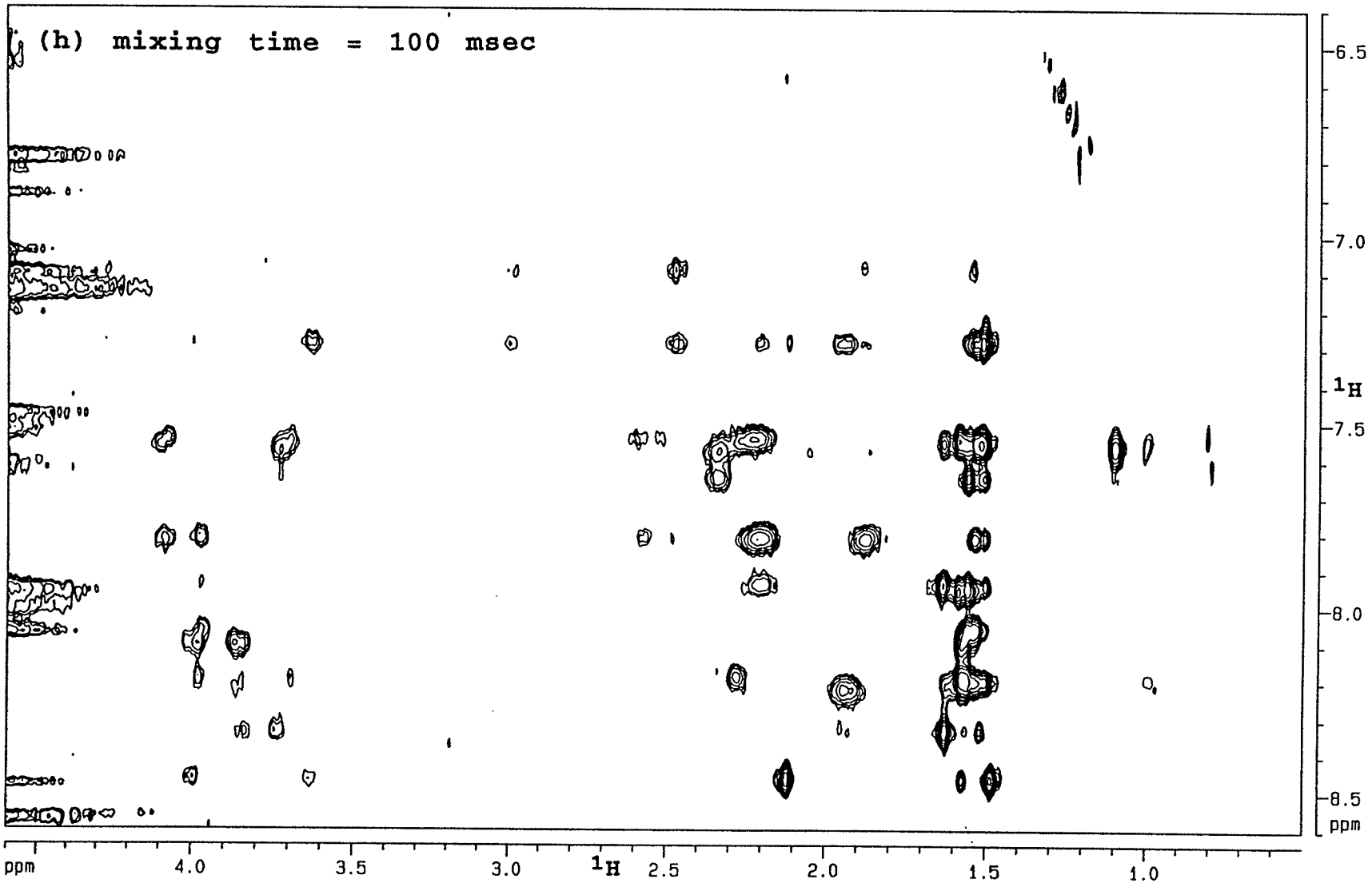
(h) mixing time = 100 msec
6.5
7.0
1H
7.5
8.0
8.5
ppm
ppm
4.0
3.5
3.0
1H
2.5
2.0
1.5
1.0

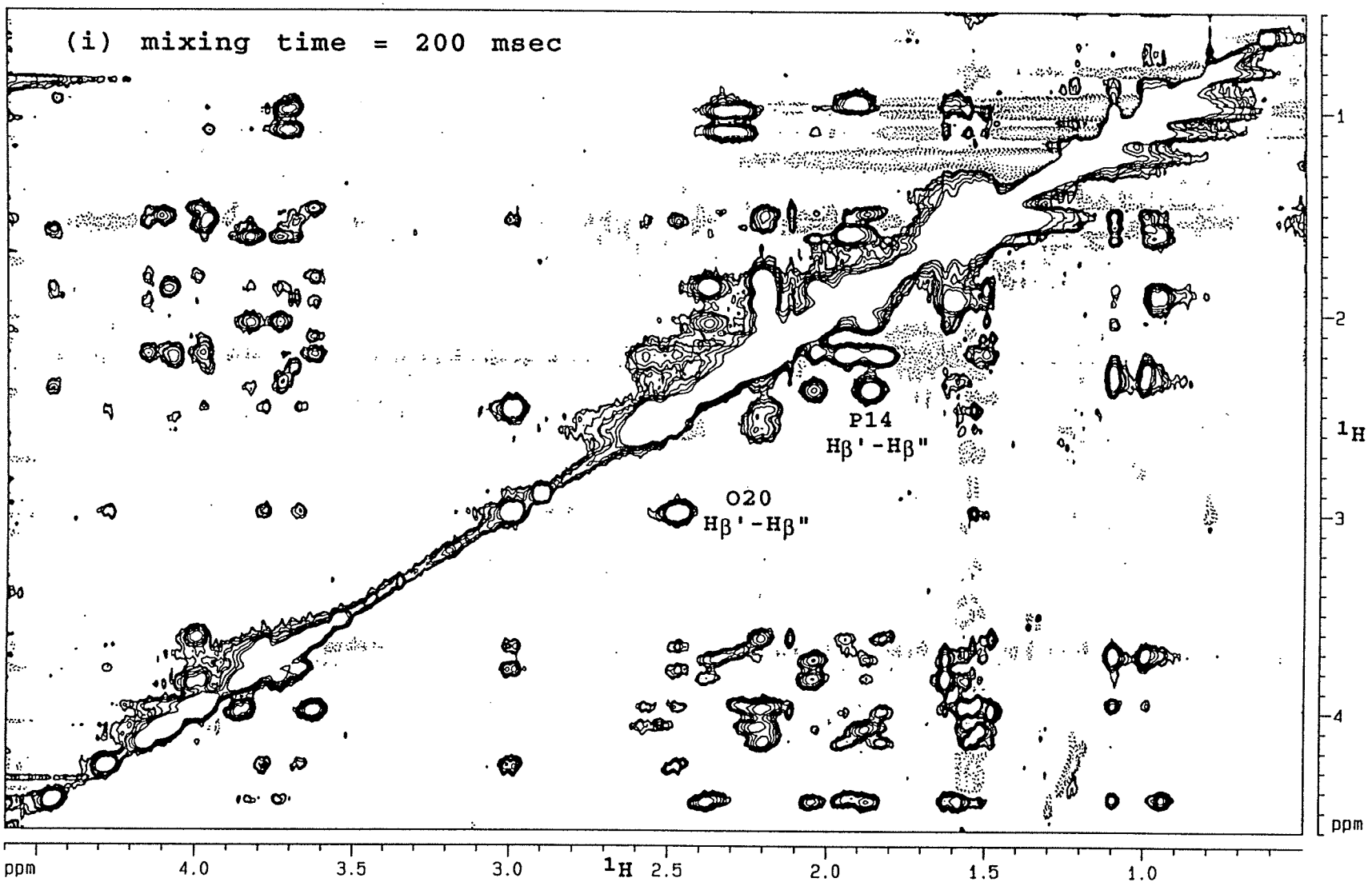
(i) mixing time = 200 msec
P14
Hβ'-Hβ"
O20
Hβ'-Hβ"
ppm
4.0
3.5
3.0
1H
2.5
2.0
1.5
1.0
1
2
3
4
1H
ppm

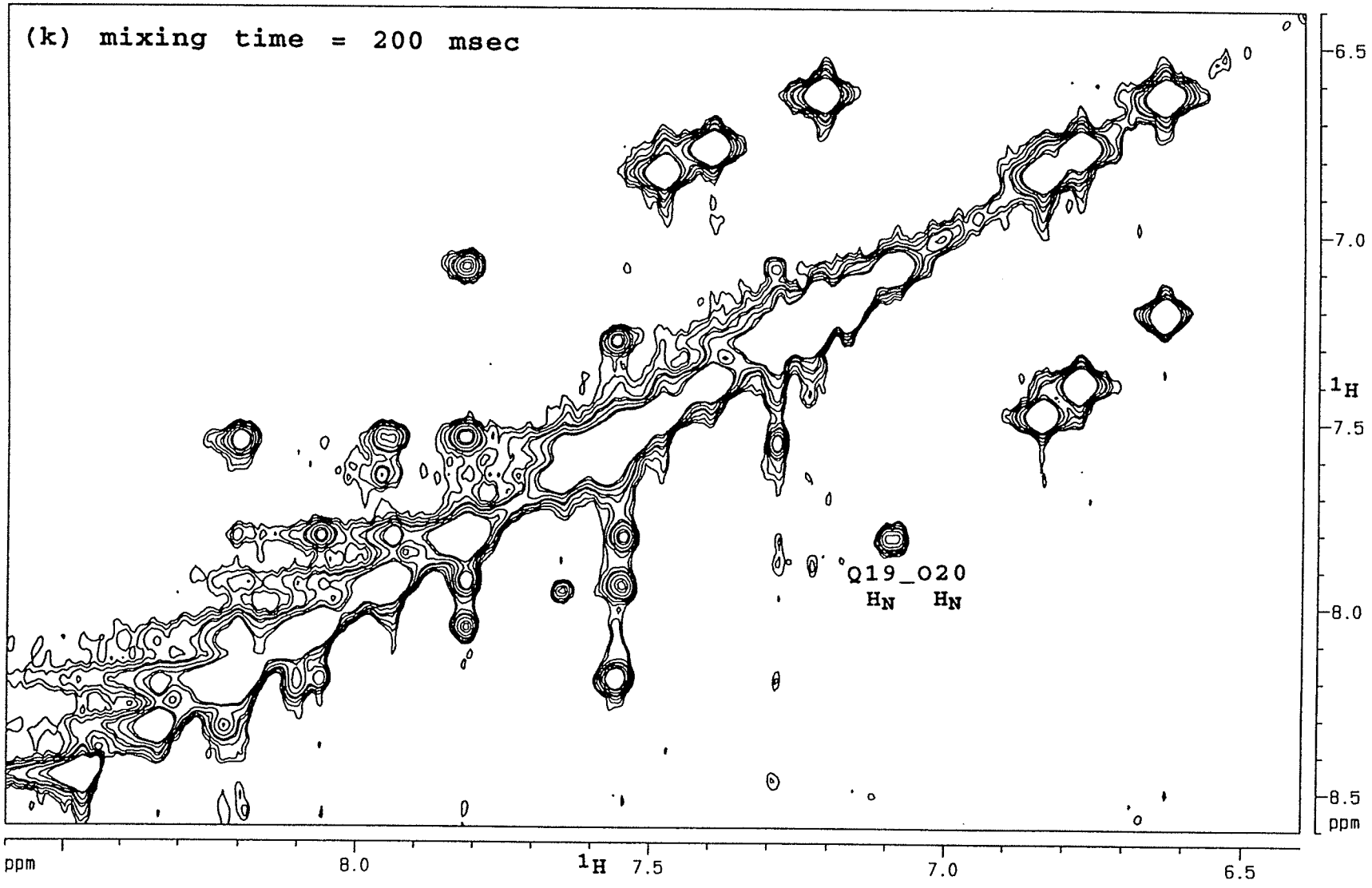
(k) mixing time = 200 msec
Q19_O20
HN HN
6.5
7.0
1H
7.5
8.0
8.5
ppm
ppm
8.0
1H 7.5
7.0
6.5

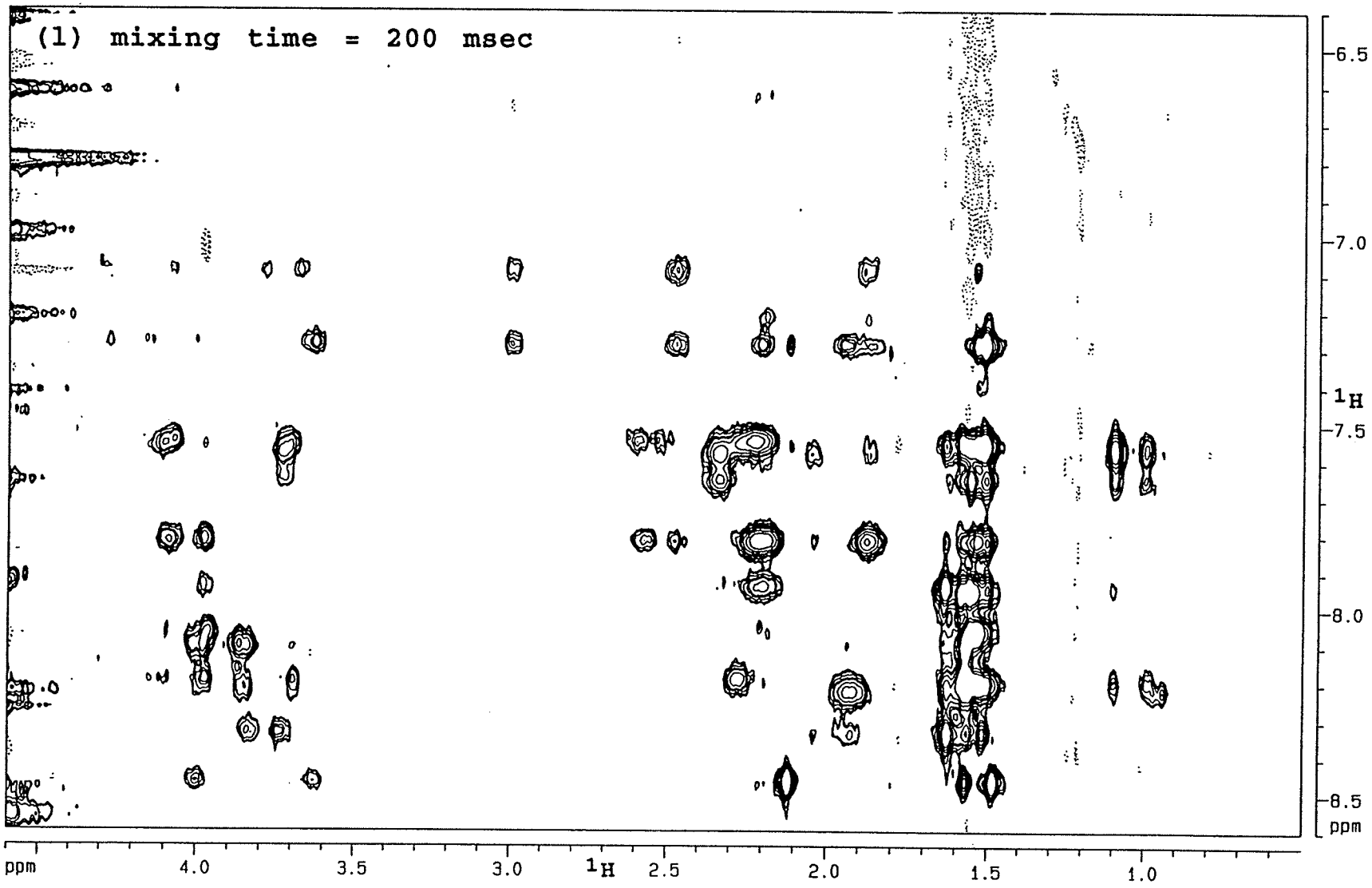
(1) mixing time = 200 msec
6.5
7.0
1H
7.5
8.0
8.5
ppm
ppm
4.0
3.5
3.0
1H
2.5
2.0
1.5
1.0

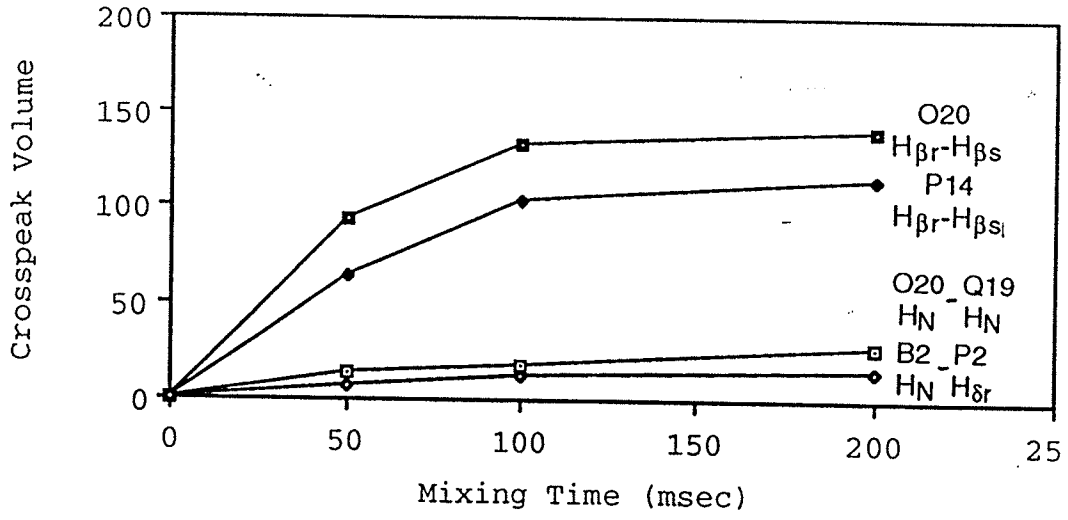

Figure 4-13: A plot of integrated crosspeak volume with mixing time.

(O20 $H\beta'_2$, O20 $H\beta'_1$), (B3 H_N, P2 $H\delta'$), and (O20 H_N, Q19 H_N), respectively. On the basis of the curves in Figure 4-13, we chose the 100 msec mixing time NOESY experiment to be a reasonable compromise between maximum nOe build up and minimum spin diffusion. The distance between the β methylene protons was set to 1.8 Å.

There are a total of 194, 319, and 361 nOe cross peaks observed along both sides of the diagonal in the NOESY spectra acquired with 50, 100, and 200 msec mixing times, respectively. In a perfectly symmetrical NOESY spectrum, the number of cross peaks below and above the diagonal would be the same. Of the 319 cross peaks in the 100 msec mixing time NOESY spectrum, 55 appear only on one side of the diagonal and 132 appear on both sides. Some residues appear only on

one side because the resolution along the F_2 and F_1 dimensions is not the same. Take for example an nOe from an H_N to two βCH_3 resonances, in the second quadrant of the spectrum: The βCH_3 would be along the F_1 dimension and the H_N along the F_2 dimension whereas in the fourth quadrant of the spectrum, it would be the other way around. This nOe would appear as a single cross peak in the second quadrant because the resolution in F_1 is not enough to resolve the small chemical shift separation between the two βCH_3 resonances but this same nOe would appear as two cross peaks (one for each CH_3) in the fourth quadrant because the two βCH_3 are now resolved in the F_2 dimension.

The non-uniform excitation of the P1$\bar{1}$ sequence also contributes to the asymmetry of the NOESY spectrum. In theory, neglecting relaxation during the delay τ, the amplitudes of the transverse magnetization generated by the P11 sequence (90_x-τ-90_{-x}) follows a sine curve as shown in Figure 4-14. A product operator (Sorensen et al., 1984) description of the pulse sequence is given below where Ω is the resonance offset from the carrier frequency and τ is a delay adjusted to give maximum excitation at a desired resonance offset (Cavanagh et al., 1996).

$$I_z \xrightarrow{(\frac{\pi}{2})I_x} -I_y \xrightarrow{(\Omega\tau)I_z} -I_y\cos(\Omega\tau) + I_x\sin(\Omega\tau) \xrightarrow{-(\frac{\pi}{2})I_x} I_z\cos(\Omega\tau) + I_x\sin(\Omega\tau)$$

Figure 4-14 shows that peaks close to the solvent signal will be excited to a smaller extent than those near 7 and 2

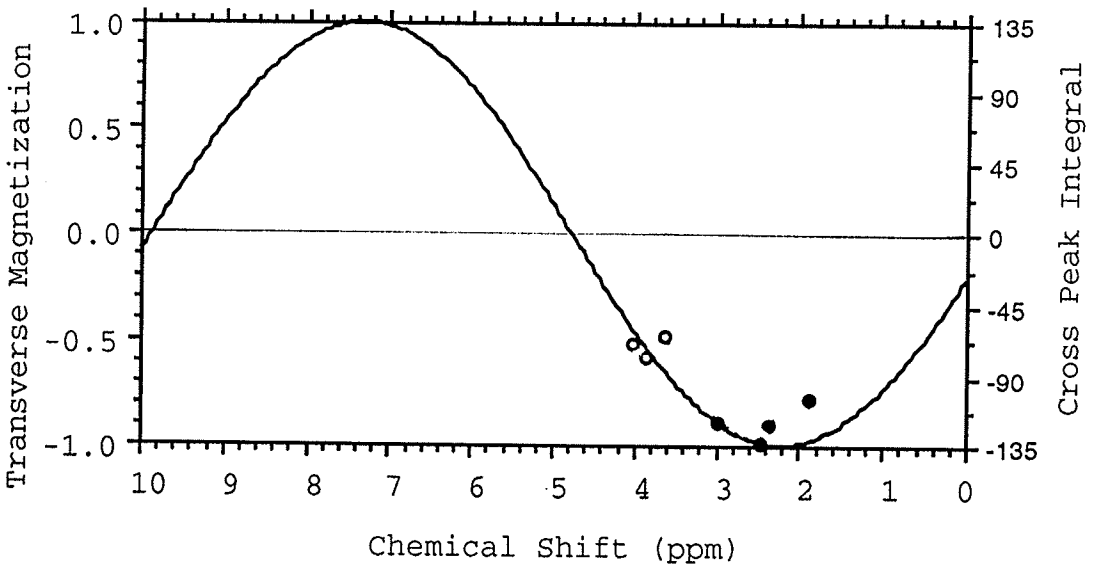

Figure 4-14: Excitation profile calculated for the P1$\bar{1}$ sequence used in the present NOESY experiment. The carrier was set on the solvent resonance at 4.74 ppm and the delay τ was set to 196 usec. Spectrometer frequency is 500.13 MHz. The integrated NOESY cross peak volumes of different methylene pairs for alamethicin dissolved in SDS are plotted. The filled circles are the ones averaged and used in the calibration of distance ranges.

ppm. For example, nOes between methylene proton pairs are expected to show similar intensities (assuming the same correlation times) since they have the same interproton distance. However, as shown in Figure 4-14, nOes between methylene protons resonating close to the solvent are less intense than those resonating close to 2.5 ppm. The non-uniform excitation of the P1$\bar{1}$ sequence is exhibited along the F_2 dimension but not in the F_1 dimension. For example, in the

aliphatic region of the NOESY spectrum (Figure 4-12 i), the cross peaks between the H_α of Leu 12 (4.46 ppm) and Pro 14 (4.38 ppm) and other protons below the diagonal are more intense than those above the diagonal. This is evident in the H_N to H_α region of the same spectrum as well. The cross peaks between the H_α of Leu 12 and Pro 14 and other H_N resonances are more intense in Figure 4-12 j than in Figure 4-12 1. The H_N region is not affected by this non-uniform excitation as much as the H_α region because the H_N resonate from 7.0 to 8.5 ppm which is close to region of maximum excitation (see Figure 4-14).

Of the 187 unique cross peaks, 126 are assigned to a single internuclear distance, 20 are assigned to two or more distances due to cross peak overlaps, and 41 are ambiguous in assignment. The 20 assigned overlaps mostly involve intraresidue nOes. The 41 ambiguous cross peaks mostly involve nOes to the βCH_3 resonances of Aib and Ala resonances and to the Phol 20 ring protons.

The integrated volumes in the 100 msec NOESY spectrum of the nOe cross peaks corresponding to (O20 $H\beta'_1$, O20 $H\beta''_1$) and (P14 $H\beta'$, P14$H\beta''$) were averaged and used to represent the nOe intensity between two protons that are separated by 1.8 Å. These are cross peak numbers 62, 69, 121, and 125 in Appendix B d. No attempts were made to correct for the non-uniform excitation of the P1$\bar{1}$ sequence. As already mentioned above, the P11 sequence would decrease the apparent intensity of a cross peak. Since the calibration intensity used is at the

maximum excitation, the apparent upper distance constraints calculated for diminished cross peaks would be larger than if the peaks were full intensity. The intensities were converted into distances and these were grouped into the following distance ranges: 5.0 Å or less, 4.0 Å or less, 3.5 Å or less, and 3.0 Å or less. For assigned overlapping cross peaks, both distances were given an upper limit of 5 Å to avoid introducing bias into the constraints. The assignment of the nOe crosspeaks in the 100 msec mixing time NOESY experiment and the corresponding distance ranges are given in Appendix B.

Aside from the nOes, the vicinal homonuclear coupling constants ($^3J_{HH}$) also provided some distance constraints (see Section 4.1.2). The $^3J_{HNH\alpha}$ values of alamethicin in detergent solution were obtained from JHH-TOCSY experiments on an ^{15}N-labelled alamethicin (Willker & Leibfrit, 1992) because the ^1H_N resonances were unresolved in the 1D spectrum. Because of the broad linewidths they could not be measured from the separation of the antiphase cross peak in a phase-sensitive experiment like DQF-COSY either. In the JHH-TOCSY experiment, the resonances are separated by the large $^1J_{NH}$ (90 Hz) along the F_1 dimension and the $^3J_{HH}$ can be measured as the displacement of the cross peaks along the F_2 dimension. The sequences were first tested on an ^{15}N-labelled alamethicin dissolved in CD_3OH in order to compare the $^3J_{HH}$ with those measured from the 1D spectrum. The JHH-TOCSY and HX-JHH TOCSY spectra of alamethicin in methanol are shown in Figures 4-15

Figure 4-15: H_N-H_α region of the JHH-TOCSY spectrum (Willker & Leibfrit, 1992) of ^{15}N-labelled alamethicin in CD_3OH. Solvent was presaturated for 1 sec. The number of scans was 64. A total of 512 increments of 4K data points each were acquired. No zero filling was applied and a $\pi/4$-shifted sine filter was applied to both dimensions before fourier transformation. The digital resolution is 1.2 Hz/point along the F_2 dimension. The TOCSY mixing time was 54 msec.

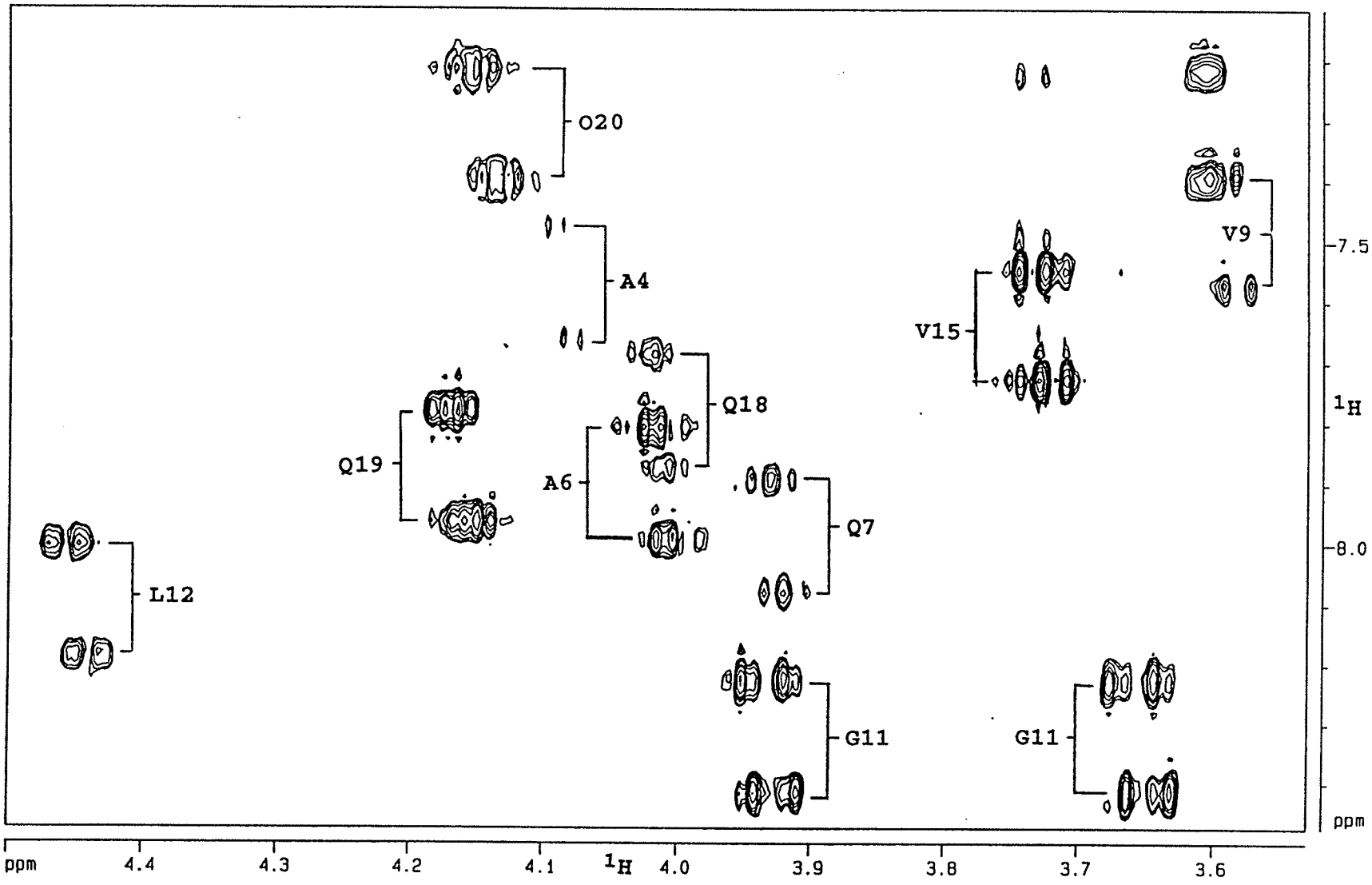
Q20
A4
Q18
Q19
A6
Q7
L12
G11
V15
V9
G11
7.5
8.0
ppm
^{1}H
ppm
4.4
4.3
4.2
4.1
^{1}H
4.0
3.9
3.8
3.7
3.6

and 4-16. In the JHH-TOCSY spectrum, the $^3J_{HNH\alpha}$ were measured from the displacement of the antiphase (H_N, H_α) cross peaks while in the HX-JHH TOCSY spectrum, these were measured from the displacement of the in-phase (^{15}N, H_N) cross peaks. A comparison between the $^3J_{HNH\alpha}$ observed from the 1D spectra and from the TOCSY spectra is presented in Table 4-1. The error to these coupling constants is estimated at ± 1.2 Hz. The comparison shows generally good agreement between the $^3J_{HNH\alpha}$ measured by the three methods. Except for Ala 4 and Leu 12, the conformation deduced from the $^3J_{HNH\alpha}$ is in agreement between all three experiments. However in both cases the $^3J_{HNH\alpha}$ value is close to the boundary between the conformational classes. The HX-JHH TOCSY experiment gave values of $^3J_{HNH\alpha}$ which agree slightly better with the values from the 1D spectrum than the JHH-TOCSY derived values. This is due to more intense cross peaks observed in the HX-JHH TOCSY spectrum.

The $^3J_{HNH\alpha}$ values determined for alamethicin in SDS solution are given in Table 4-2. The H_α of Leu 12 resonates very close to the HOD signal and the $^3J_{HNH\alpha}$ can be measured only from the HX-JHH TOCSY spectrum. The cross peaks for Ala 6 and Gln 7 are overlapped in the HX-JHH TOCSY spectrum (Figure 4-18) but these two are well resolved in the JHH-TOCSY spectrum (Figure 4-17). The cross peak for Ala 4 overlaps with Gln 18 in the JHH-TOCSY spectrum as do the two Val cross peaks. Much better separation of these peaks is achieved in the HX-JHH TOCSY spectrum. Residues 4, 6, 7, 11,

Figure 4-16: HX-JHH TOCSY spectrum (Willker & Leibfrit, 1992) of ^{15}N-labelled alamethicin in CD_3OH. Solvent was presaturated for 1 sec. The number of scans was 64. A total of 128 increments of 4K data points each were acquired. F_1 dimension was zero filled to 256 points and no zero filling was applied to the F_2 dimension. $\pi/2$-shifted sine-squared filter was applied to both dimensions before fourier transformation. The digital resolution is 1.2 Hz/point along the F_2 dimension. The TOCSY mixing time was 54 msec.

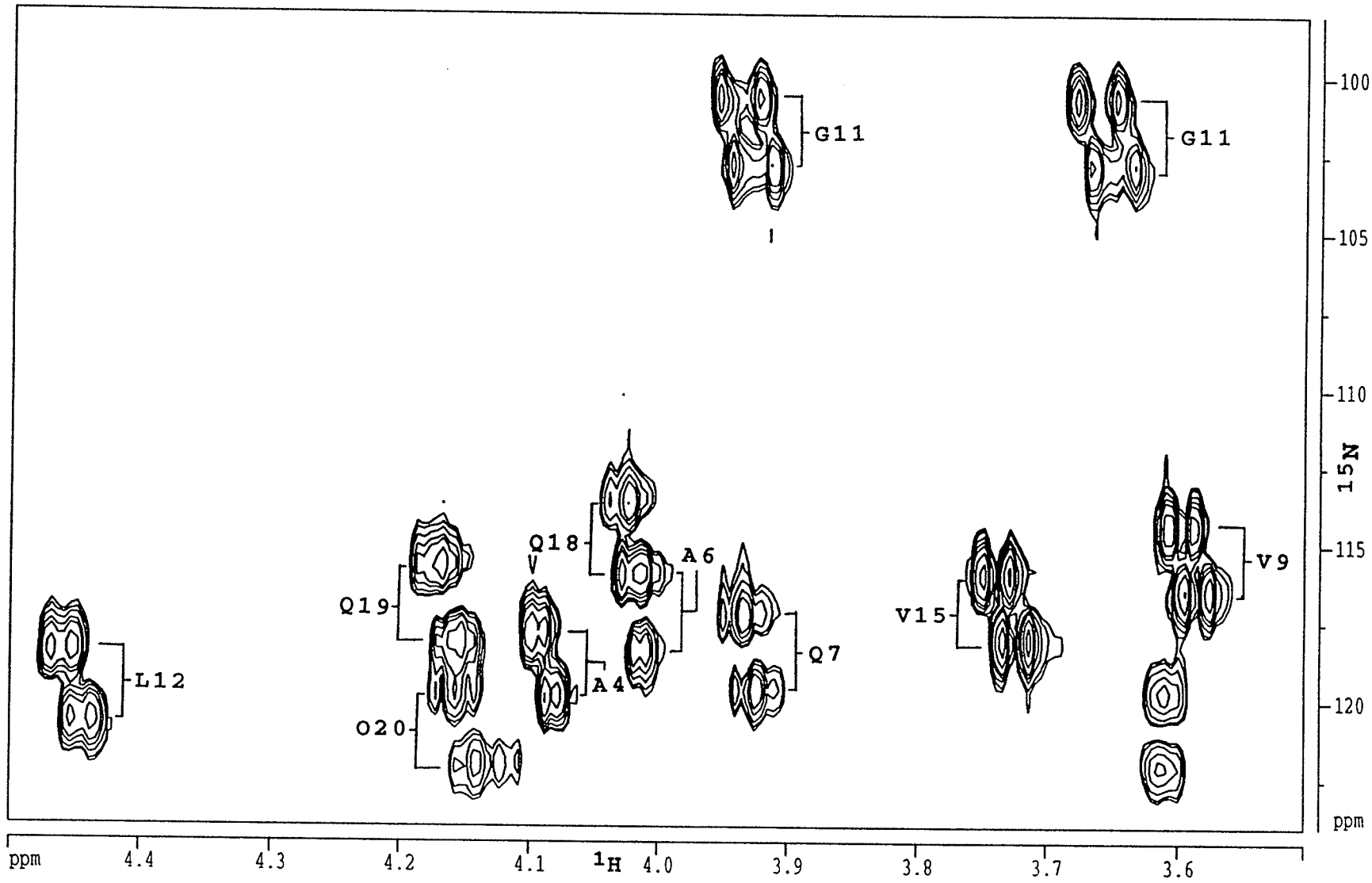
G11
G11
I
L12
Q19
O20
Q18
V
A6
A4
Q7
V15
V9
100
105
110
115
120
15N
ppm
ppm
4.4
4.3
4.2
4.1
1H
4.0
3.9
3.8
3.7
3.6

Table 4-1: Comparison of the $^3J_{HNH\alpha}$ of the non-Aib residues in alamethicin dissolved in CD_3OH measured from a 1D ^1H spectrum and the JHH-TOCSY spectra. All values are given in Hz. The symbol beside the $^3J_{HNH\alpha}$ gives the classification of the ϕ angle according to the following: $^3J_{HNH\alpha}$ < 6.0 Hz is α, $^3J_{HNH\alpha}$ > 8.0 Hz is β, and $^3J_{HNH\alpha}$ between 6.0 Hz and 8.0 Hz is conformationally averaged (Driscoll et al., 1990; Kaptein et al., 1988).

Residue	1D spectra	JHH-TOCSY	HX-JHH TOCSY
A4	5.9 α	6.2 avg	6.3 avg
A6	4.5 α	4.9 α	4.0 α
Q7	5.1 α	5.3 α	5.1 α
V9	5.5 α	4.9 α	5.4 α
G11	5.8 α	5.5 α	5.8 α
L12	7.9 avg	8.6 β	8.0 β
V15	8.5 β	8.6 β	7.9 avg
Q18	5.6 α	4.9 α	5.2 α
Q19	7.5 avg	7.4 avg	7.7 avg
O20	9.9 β	11.7 β	9.2 β

and 18 have $^3J_{HNH\alpha}$ below 6.0 Hz suggesting a helical ϕ conformation, the $^3J_{HNH\alpha}$ for Val 9 is 6.2 Hz which is close to being in the α conformation as well (see results in CD_3OH).

Figure 4-17: H_N-H_α region of the JHH-TOCSY spectrum (Willker & Leibfrit, 1992) of 1.7 mM ^{15}N-labelled alamethicin in 150 mM SDS-D_{25}, 20 mM Na_2HPO_4 in 95/5 H_2O/D_2O, pH 5.1. Solvent was presaturated for 1 sec. The number of scans was 64. A total of 512 increments of 4K data points each were acquired. No zero filling was applied and a $\pi/4$-shifted sine filter was applied to both dimensions before fourier transformation. The digital resolution is 1.2 Hz/point along the F_2 dimension. The TOCSY mixing time was 67 msec.

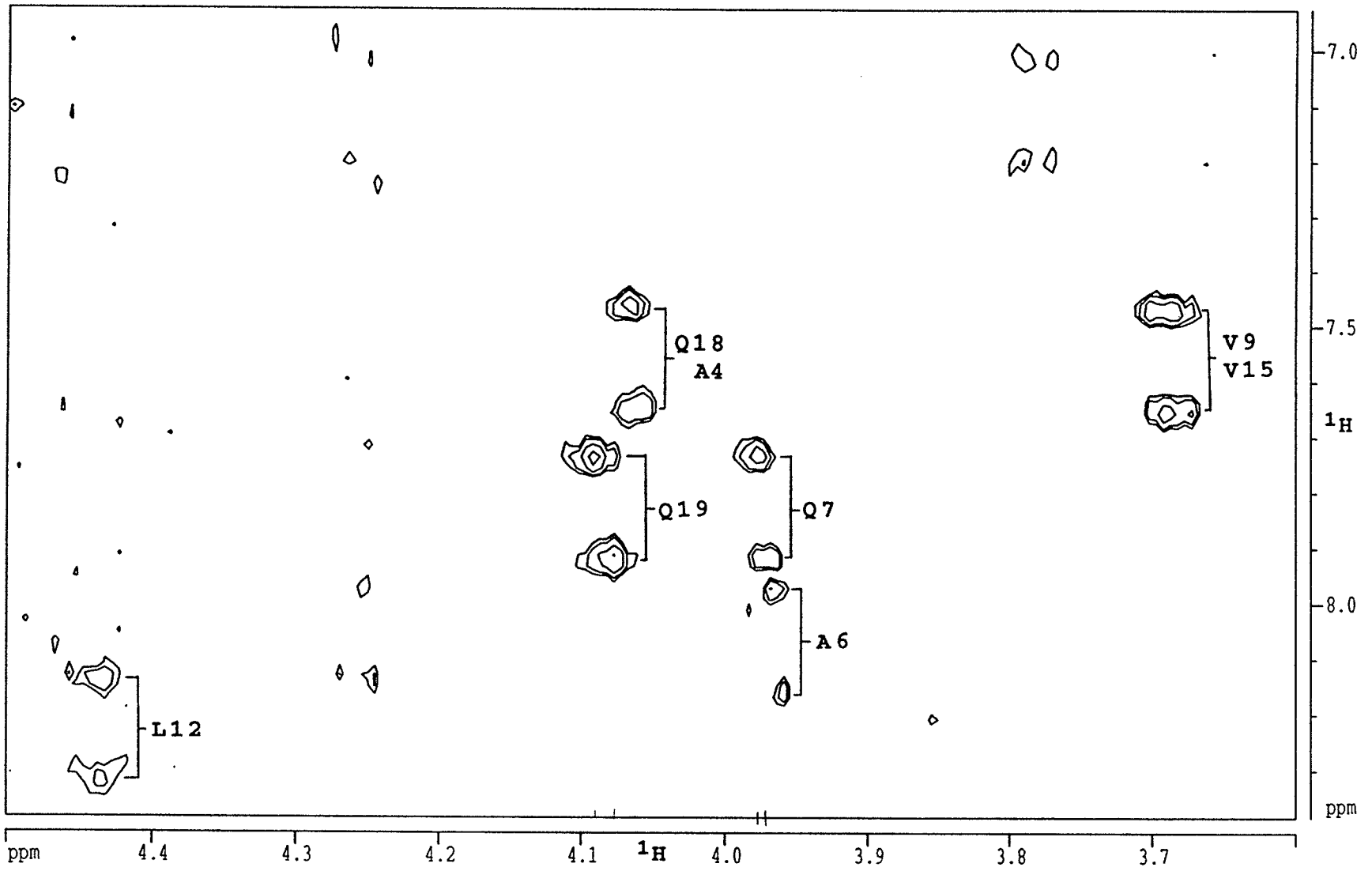
Q18
A4
Q19
Q7
A6
L12
V9
V15
7.0
7.5
8.0
ppm
^{1}H
ppm
4.4
4.3
4.2
4.1
4.0
3.9
3.8
3.7
^{1}H

Figure 4-18: HX-JHH TOCSY spectrum (Willker & Leibfrit, 1992) of 1.7 mM ^{15}N-labelled alamethicin in 150 mM SDS-D_{25}, 20 mM Na_2HPO_4 in 95/5 H_2O/D_2O, pH 5.1. Solvent was presaturated for 1 sec. The number of scans was 64. A total of 128 increments of 4K data points each were acquired. The F_1 dimension was zero filled to 256 points and no zero filling was applied to the F_2 dimension. A $\pi/2$-shifted sine-squared filter was applied to both dimensions before fourier transformation. The digital resolution is 1.2 Hz/point along the F_2 dimension. The TOCSY mixing time was 67 msec.

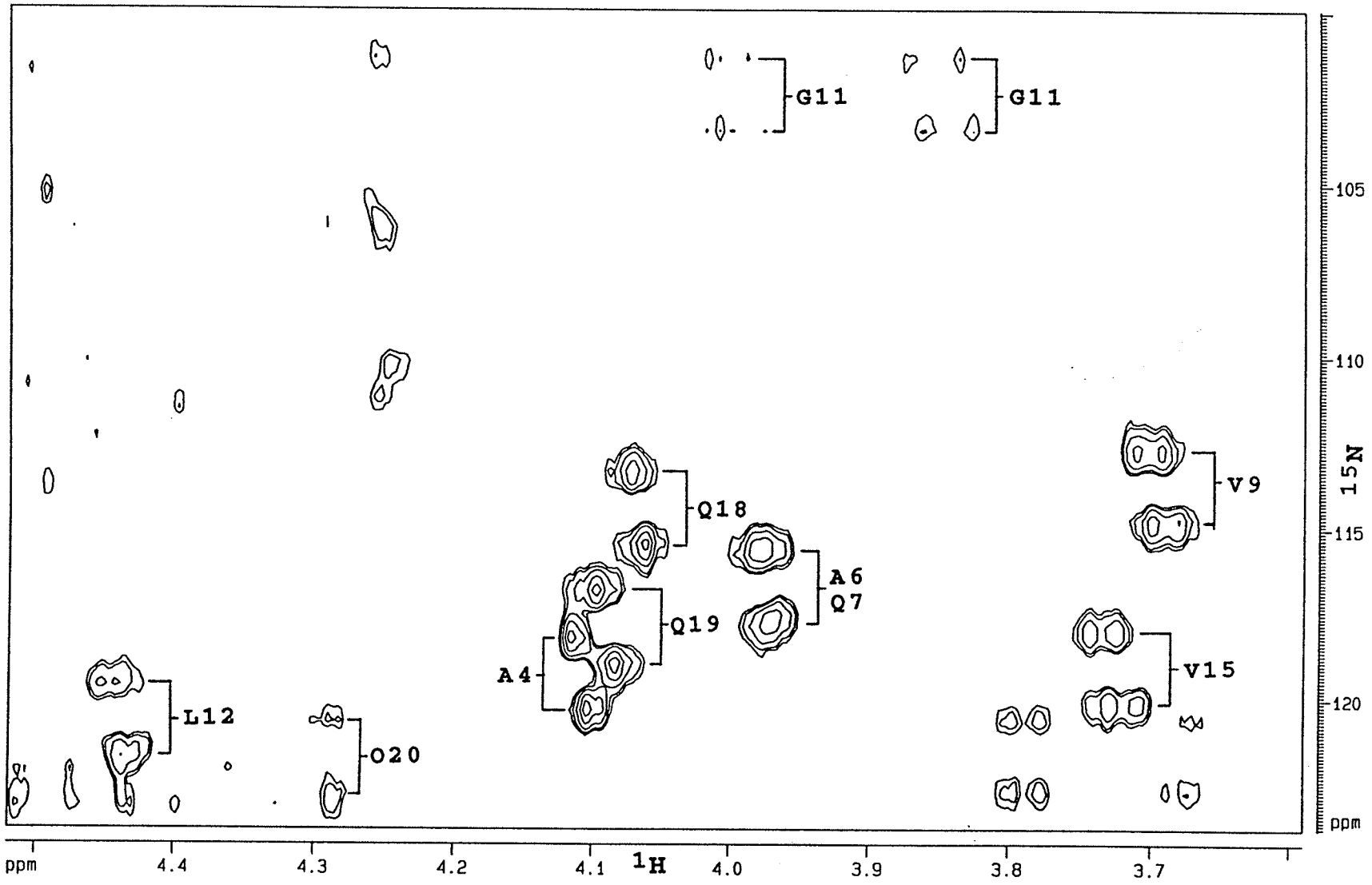
G11
G11
Q18
A6
Q7
Q19
A4
V9
V15
L12
O20
105
110
115
120
ppm
15N
ppm
4.4
4.3
4.2
4.1
1H
4.0
3.9
3.8
3.7

Table 4-2: $^{3}J_{HNH\alpha}$ of 1.7 mM unlabelled alamethicin in 150 mM SDS-D_{25}, 20 mM Na_2HPO_4 in 95/5 H_2O/D_2O, pH 5.06.

Residue	JHH-TOCSY	HX-JHH TOCSY	ϕ conformation
A4	nd	5.9	α
A6	2.7	4.1[a]	α
Q7	3.6	4.1[a]	α
V9	nd	6.2	avg
G11	nd	4.9	α
L12	nd	7.0	avg
V15	nd	7.5	avg
Q18	nd	5.1	α
Q19	7.9	7.0	avg
O20	nd	nd	

[a]overlap; nd, not determined.

Only the $^{3}J_{HNH\alpha}$ which gave a helical conformation were converted into $H_N(i)$ to $H_\alpha(i)$ distance constraints and included in the distance geometry calculations. From Figure 4-1, the α-helical ϕ angles correspond to a distance from 2.60 to 2.85 Å.

A summary of the nOes and $^{3}J_{HNH\alpha}$ are given in Figure 4-19.

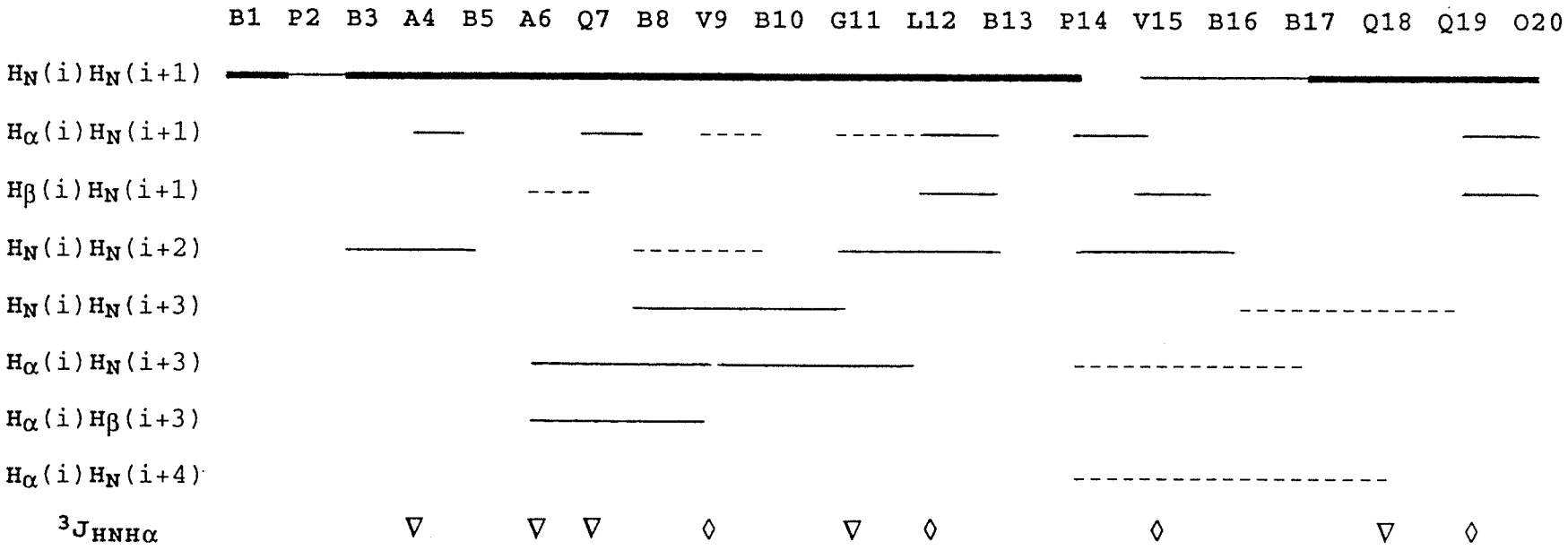

Figure 4-19: Summary of the nOe intensities and $^3J_{HNH\alpha}$ observed for 1.7 mM alamethicin in 150 mM SDS-D_{25}, 20 mM Na_2HPO_4 in 95/5 H_2O/D_2O, pH 5.1. The thickness of the lines indicate the intensity of the nOe as strong (▬▬), medium (——), or weak (-----). The $^3J_{HNH\alpha}$ are indicated by the following symbols: < 6 Hz (∇), > 8 Hz (•), and 6 to 8 Hz (◊). H_δ of Pro residues were used in place of H_N because Pro residues do not have H_N.

4.5.1.6 Calculation of a Molecular Model Using Distance Geometry

Distance geometry calculations were done using the commercial software package DSPACE® (Hare Research Inc.). The minimization and refinement protocols of Blake, et al. (1992) were used. The upper experimental bounds at the start were given a much higher penalty weight compared with the bond angle, bond length, and van der Waals interactions. The whole molecule was annealled by heating and cooling over several steps and then the penalty function was minimized. Several annealling and minimization cycles were done, the penalty weight of the experimental upper bounds was decreased and the penalty weights of all other constraints were increased. The "temperature" at which the molecule was heated during the annealing cycle was decreased with each cycle. Initially, all nOe constraints were put in as 5 Å, and constraints based on nOe to methyl protons and $^{3}J_{HNH\alpha}$ were not included. Sixty randomly embedded structures were generated and annealling and minimization cycles were done against these initial experimental constraints. Of the 60 structures, only 28 passed this initial run based on the penalty. Then the upper bounds constraints were lowered to 4 Å, except those for which the nOe indicated an upper bound of 5 Å. The 28 structures underwent annealling and minimization cycles similar to the one described above except that in this annealling cycle, the molecule was annealled 5 residues at a time. The penalty and constraint violations for each

structure were checked. The upper bound constraints were again lowered by 1 Å until all experimental constraints were in the correct range as presented in Appendix B. The constraints from $^{3}J_{HNH\alpha}$ were added at the last stage of this setting of the upper bounds procedure. With this procedure, misassignment of resonances and over-constrained distances were found and corrected. Over-constrained distances were due to partial overlap of cross peaks and so integration of these gave a higher integration value and therefore shorter distances than can be justified. More details of the constraints are given in Appendix B. Two of the 28 structures were dropped during these cycles of changing the upper experimental bounds because of high penalty. The remaining 26 structures underwent more minimization cycles and the 9 structures with the lowest penalty values were accepted.

The 9 accepted structures were superimposed pairwise along the backbone atoms (N, Cα, C') and gave an average root mean square deviation (RMSD) of 2.95 ± 0.59 Å, suggesting that the calculated structures do not converge to a common conformation. Table 4-3 gives a summary of the structural statistics from these calculations.

An alternative way of looking for convergence in the calculated structures is to superimpose segments of them. The 9 accepted structures were superimposed 5 residues at a time along their entire lengths and the RMSD was calculated (see Figure 4-20). This figure shows that there is convergence of

Table 4-3: Summary of distance constraints used in the DG/SA calculations and the resulting structural information. The errors are 1 standard deviation.

Distance Constraints	
Intraresidue	102
$^3J_{HNH\alpha}$	5
Sequential	46
Medium Range ([i-j] = 2-4)	18
Total	171
Mean constraints/residue	8.5

Structural Statistics for the 9 DG calculated structures	
Mean total penalty	0.8 ± 0.1 Å^2
Max/min penalty	0.9 / 0.5 Å^2
Max individual violation	0.2 Å
Mean pairwise RMSD for N, Cα, and C':	
Residues 1-20	2.9 ± 0.6 Å
Residues 1-11	1.7 ± 0.4 Å
Residues 3-10	1.1 ± 0.3 Å
Residues 13-20	2.0 ± 0.7 Å

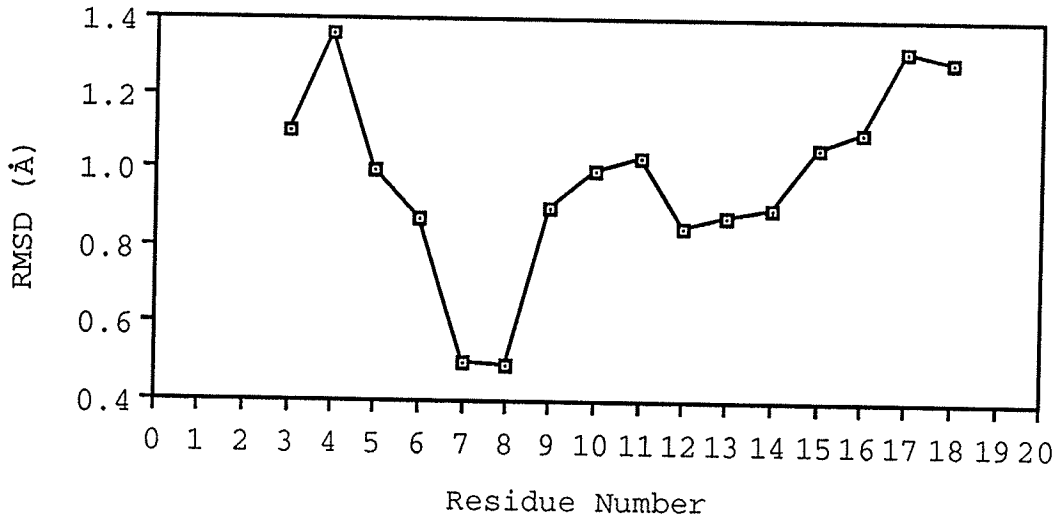

Figure 4-20: Averages of pairwise RMSDs for backbone heavy atoms (N, C_α, C') were calculated over 5 residue segments and plotted in the middle of each segment.

Figure 4-21: The backbone heavy atoms (N, C_α, C') of the 9 calculated structures superimposed from residues 3 to 10. The side chain atoms of Phol 20 are drawn to indicate the C-terminus.

the backbone structures centered at residues 7 and 8. This suggested superimposing the backbone atoms from residues 1 to 11 and this gave an RMSD of 1.75 ± 0.39 Å. Superimposing residues 3 to 10 gave an even better RMSD of 1.12 ± 0.31 Å suggesting that the structures converge in this part of the molecule. For comparison, residues 13 to 20, which have the same number of backbone atoms as residues 3 to 10, were also superimposed and this gave a higher RMSD of 1.99 ± 0.75 Å. Figure 4-21 shows the superimposition of the backbone atoms (N, C_α, C') from residues 3 to 10 of the 9 calculated structures.

As mentioned in the introduction to this thesis (Section 1.2), the non-convergence at the terminals of the structures calculated mainly on the basis of homonuclear nOes is expected in linear peptides because of the lack of medium range nOes beyond the ends of the molecule. The high backbone RMSD values of the calculated structures is consistent with the low average number of constraints per residue of only 8.5, the majority of which are intraresidue and sequential nOes (Gronenborn & Clore, 1994). Also, the distance constraints based on the nOe intensities were not corrected for the non-uniform excitation of the NOESY-P1$\bar{1}$ sequence which would make some distances underestimated and the molecule less constrained. One observation noted in the calculated structures is that the RMSD is lower for the region where there are distance constraints derived from

$^3J_{HNH\alpha}$. This is because the distance bounds from the $^3J_{HNH\alpha}$ are narrower than those derived from nOe measurements.

4.5.2 H_N exchange rates of N-Acetyl-Aib-N'Me

The effect of different side chains on H_N exchange in D_2O has been evaluated relative to alanine for all 20 common amino acids in model dipeptides (Bai et al., 1993). The residue α-aminoisobutyric acid (Aib), commonly found in fungal peptides, differs from the common amino acids in that it has a methyl group in place of a hydrogen on the the α carbon. The effect of the α-methyl on H_N exchange in D_2O was evaluated under the same conditions as those described in Bai et al. (1993) so that protection factors could be calculated for the Aib residues in alamethicin. Figure 4-22 shows the amide region of the Aib dipeptide (N-Ac-Aib-N'Me) at different times of exchange. Figure 4-23 shows sample plots of integrated peak areas versus time and their fits to the monoexponential equation. At lower pHs, the $H_N(R)$ exchanges faster than the $H_N(L)$ and at higher pHs, the $H_N(L)$ exchanges faster than the $H_N(R)$. The exchange rates of $H_N(L)$ and $H_N(R)$ are equal at around pD_{corr} 5.0.

Figure 4-24 shows the pH dependence of H-D exchange for the Aib dipeptide as compared with those of the Ala dipeptide and the Gly dipeptide. The curves through the Ala and Gly dipeptides were calculated from the data of Bai et al. (1993). Note that the current data agree very well with the published results. The H-D exchange curve shows that the

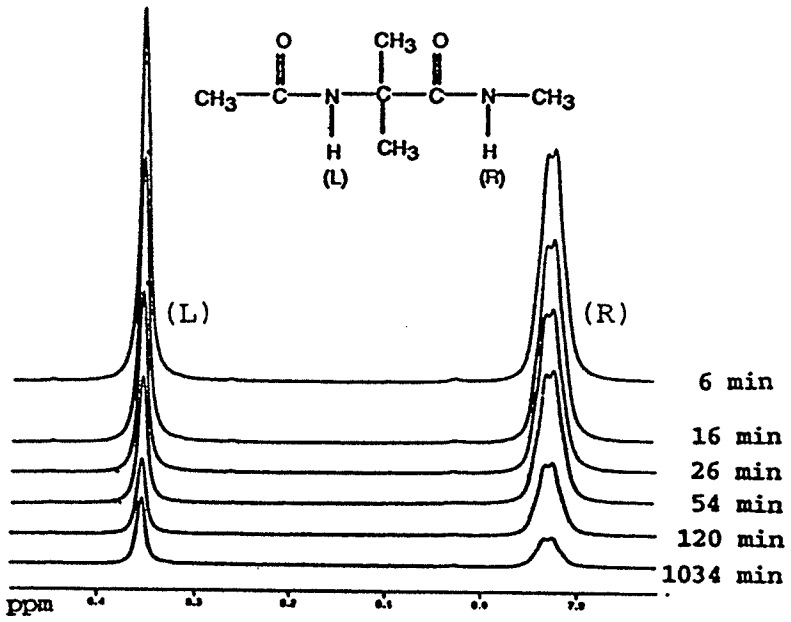

Figure 4-22: The amide regions of ^1H NMR spectra of N-Acetyl-Aib-N'Me in 50 mM succinate, 0.5 M KCl in 87.5 % D_2O and pD_{corr} of 5.2 at different times after dissolution at 5°C.

replacement of the α hydrogen by a methyl group imposes both steric (downward shift of the minima relative to the Ala dipeptide) and inductive effects (rightward shift of the minima relative to the Ala dipeptide) on both the L and R amides. The steric blocking is to be expected since the methyl group is much larger than the hydrogen which is present in all L-amino acids. Similar to other sidechains as reported by Bai et al. (1993), steric blocking was observed to be larger for the L than for the R peptide H_N. Unlike the polar sidechains described in Bai et al (1993), the α methyl is an electron donating substituent and thus increases the

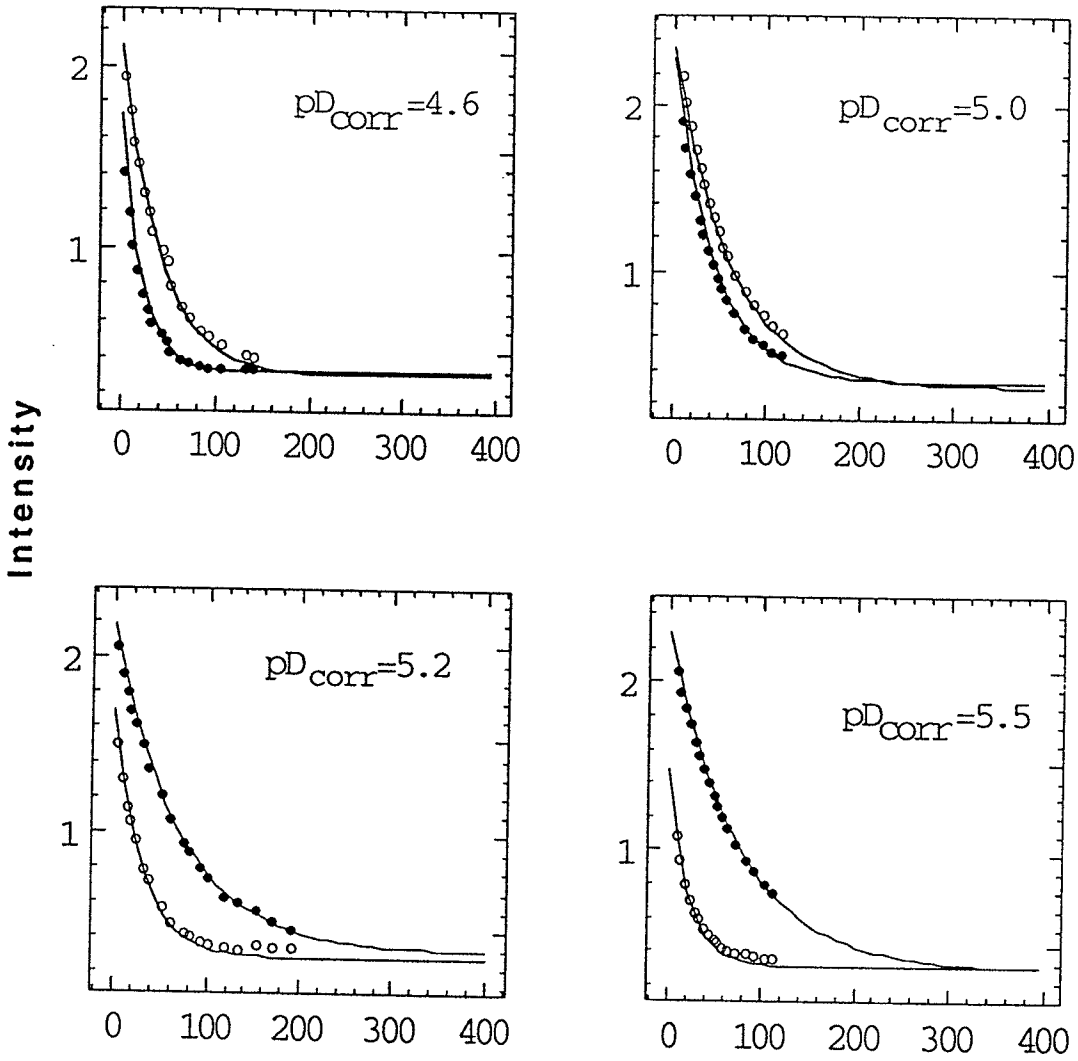

Figure 4-23: The exponential decays of the H_N resonances of N-Acetyl-Aib-N'Me at different pH values. The filled circle (•) is for the $H_N(R)$ and the unfilled circle (o) is for the $H_N(L)$.

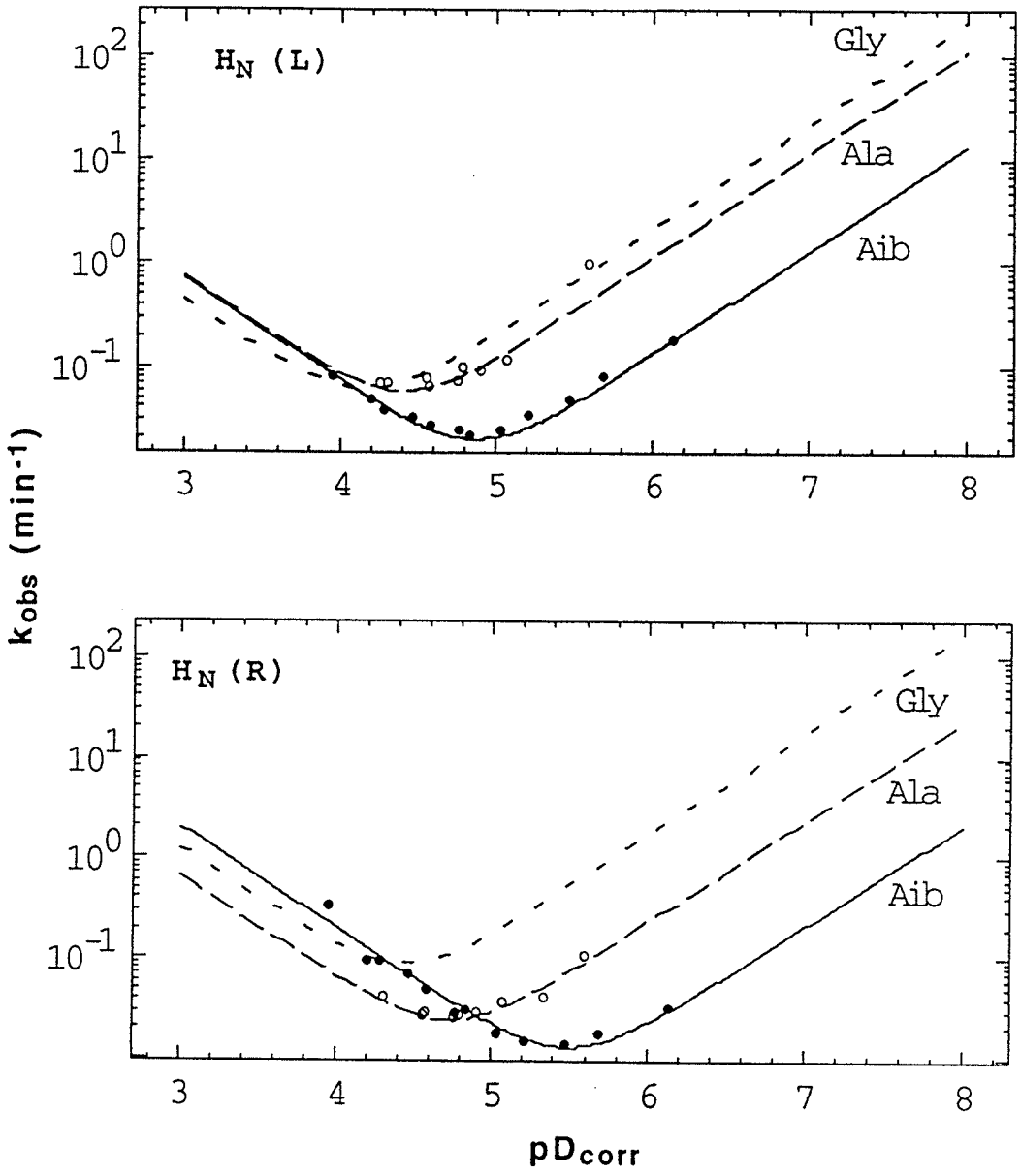

Figure 4-24: The dependence of the H-D exchange rates on pD_{corr} of N-Acetyl-Amino Acid-N'Me. The data for N-Acetyl-Aib-N'Me (•) were fit to eqn 4-11 to give the solid curves. The data for N-Acetyl-Ala-N'Me are indicated by (°). The dashed curves were calculated from the N-Acetyl-Ala-N'Me and N-Acetyl-Gly-N'Me data of Bai et al. (1993).

electron density at the amide making it more basic. A more basic amide is expected to be more rapidly protonated (whether at the N or at the O) and would be expected to have a lower rate of abstraction of the amide hydrogen. These effects result in an increase in the acid catalyzed exchange rate and a decrease in the base catalyzed exchange rate, respectively. The V-shaped rate vs. pD curves are shifted rightward, increasing the pD_{min}. The same trend is observed with alanine relative to glycine (Bai et al., 1993) and the same explanation may be offered for the R amide of the Aib dipeptide relative to the Ala dipeptide.

The inductive effect of the methyl substituent on the pD_{min} parallels the β-effect on the amide ^{15}N chemical shift (Levy & Lichter, 1979) and $^{13}C'$ chemical shift (Stothers, 1972). The ^{15}N of Aib residues resonate at a consistently higher frequency than the other amino acid residues with one α hydrogen, which resonate in turn at a higher frequency than those in Gly residues (Yee, 1991). The $^{13}C'$ chemical shift follows the same trend as the ^{15}N chemical shift (Section 3.4.1). The calculated base and acid catalyzed exchange rates for the Aib dipeptide are given in Table 4-4.

4.5.3 Intrinsic H_N Exchange Rates in Alamethicin

The intrinsic hydrogen exchange rates of peptides in a structureless random coil depend on the inductive and steric effects of the different sidechains in the primary sequence (Molday & Kallen, 1972; Bai et al., 1993). The intrinsic H_N

Table 4-4: Calculated H to D exchange parameters for N-Ac-Aib-N'Me in water at 278°K in 0.5 M KCl.

	log k_H ($M^{-1}min^{-1}$)	log k_{OH} ($M^{-1}min^{-1}$)	k_{min} (min^{-1})	pD_{min}
(L)	2.86	8.77	1.96×10^{-2}	4.87
(R)	3.30	7.97	1.29×10^{-2}	5.49

exchange rates for alamethicin (k_{rc}) were calculated following the procedure of Bai et al. (1993). A sample calculation is given below.

$$\log k_H^{rc} = \log k_H^{ref} + \log A_L + \log A_R$$

$$\log k_{OH}^{rc} = \log k_{OH}^{ref} + \log B_L + \log B_R$$

where k_H^{ref} and k_{OH}^{ref} are the exchange rates of the reference poly D-L alanine peptide; A_L, B_L, A_R, and B_R are the acid and base sidechain correction factors for groups to the left and right of the exchanging H_N. Assuming that k_{H2O} is negligible, the k_{rc} can be calculated as: $k_{rc} = k_H^{rc}\ 10^{-pD} + k_{OH}^{rc}\ 10^{-(pK_D - pD)}$. The constants relevant to the alamethicin calculations are given in Table 4-5. The calculation of k_{rc} for the H_N of Aib 10 of alamethicin at pD 3.0 and 20°C under normal low salt conditions proceeds as follows:

$\log k_H^{rc}$ (Aib 10) = 1.62 + (-0.01) + (-0.30) = 1.31

$\log k_{OH}^{rc}$ (Aib 10) = 10.36 + (-0.94) + (-0.14) = 9.28

Table 4-5: Amino acid sidechain correction factors used for the calculation of the intrinsic H_N exchange rates of alamethicin. Except for the Aib residue the data were obtained from Bai et al. (1993).

	log k_H		log k_{OH}	
PDLA (ref)	1.62		10.36	
Sidechain	A_L	A_R	B_L	B_R
Aib[a]	-0.01	0.49	-0.94	-1.04
Ala	0.00	0.00	0.00	0.00
Gly	-0.22	0.22	0.27	0.17
Gln	-0.47	-0.27	0.06	0.20
Leu	-0.57	-0.13	-0.58	-0.21
Phe	-0.52	-0.43	-0.24	0.06
Pro (trans)		-0.19		-0.24
Val	-0.74	-0.30	-0.70	-0.14
C-term (COOH)	0.05			
C-term (COO-)	0.96		-1.80	

[a]log k_{ex}(Aib)-log k_{ex}(Ala).

$$k_{rc}\ (\text{Aib } 10) = 10^{1.31}\ 10^{-3.0} + 10^{9.28}\ 10^{(3-15.05)}$$

$$= 2.21 \times 10^{-2}\ \text{min}^{-1} \text{ at } 20°C$$

The A_L and B_L values used are for the Aib residue and the A_R and B_R values used are for the Val residue because the exchanging H_N of Aib 10 is to the left of the Aib sidechain and to the right of the Val 9 sidechain (see diagram of the alamethicin fragment below).

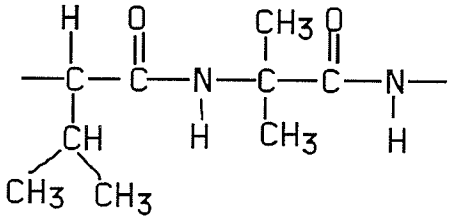

To calculate k_{rc} at 27°C, the temperature at which the actual alamethicin hydrogen exchange experiments were conducted, equation 4-12 was used as follows.

$$k_H^{rc}(\text{at } 27°C) = 10^{1.31} \exp[-14(1/300-1/293)/(1.987 \times 10^{-3})]$$

$$= 35.78 \text{ min}^{-1}$$

$$k_{OH}^{rc}(\text{at } 27°C) = 10^{9.28} \exp[-17(1/300-1/293)/(1.987 \times 10^{-3})]$$

$$= 3.78 \times 10^{9} \text{ min}^{-1}$$

$$k_{rc}(\text{Aib } 10) = 35.78 \times 10^{-3.0} + 3.78 \times 10^{9} \times 10^{(3-15.05)}$$

$$= 3.91 \times 10^{-2} \text{ min}^{-1} \text{ at } 27°C$$

The k_H^{rc} and k_{OH}^{rc} of Phol 20 were calculated as if the C terminus were a neutral carboxylic acid because there is no correction factor available for a neutral alcohol terminal. The k_H^{rc} and k_{OH}^{rc} of Aib 1 were not calculated using the above mentioned method because there is no available correction factor for an N-acetyl terminal. Instead, the k_H^{rc} and k_{OH}^{rc} of Aib 1 were obtained from the k_H and k_{OH} of the

$H_N(L)$ of N-Acetyl-Aib-N'Me (see Figure 4-22 inset). The calculated k_H^{rc} and k_{OH}^{rc} for the amino acids in alamethicin are summarized in Table 4-6.

4.5.4 Observed H_N Exchange Rates in Alamethicin Dissolved in SDS Solution

Figure 4-25 shows examples of HMQC spectra acquired at different time intervals after an aliquot of alamethicin in SDS/H_2O solution was diluted with SDS/D_2O solution. The resolution in the ^{15}N dimension is low because of the time limitation. Compare for example Figure 4-25a which took 20 min. to acquire with that of Figure 4-9 which took 6 hr. to acquire.

The cross peaks of residues 1, 3, 6, 11, 12, 13, 16, and 20 are free from overlap and provide reliable hydrogen exchange data which fit well to monoexponential decay curves (Figure 4-26 a, b, c). Although partially overlapping, the cross peaks of residues 8 and 17 are well enough resolved to provide reliable hydrogen exchange rates for each residue. Note as well that Aib 8 exchanges much more rapidly than Aib 17 at several pH values providing data for the latter which is free of any overlap from the Aib 8 cross peak (see Figure 4-25). The cross peaks for the pairs of residues Val 9/Gln 18 and Ala 4/Val 15 are also well enough resolved to provide reliable hydrogen exchange data for the pairs of amides, however the pairs themselves are not separable. The Val 9/Gln 18 and Ala 4/Val 15 cross peaks were integrated and fit

Figure 4-25: HMQC spectra (Bax, et al., 1983a,b) of ^{15}N-labelled alamethicin in 150 mM SDS-D_{25}, 20 mM Na_2HPO_4 solution, pD_{corr} 6.1. Acquired (a) 10 min. (b) 11 hr. 17 min. (c) 2 days 17 min. (d) 11 days 19 hr. 42 min. after sample in H_2O was diluted with D_2O. The number of scans was 32. A total of 32 increments of 1K data points each were acquired. The F_1 dimension was zero filled to 256 points, no zero filling was applied to the F_2 dimension, and a $\pi/2$-shifted sine-squared filter was applied to both dimensions before fourier transformation.

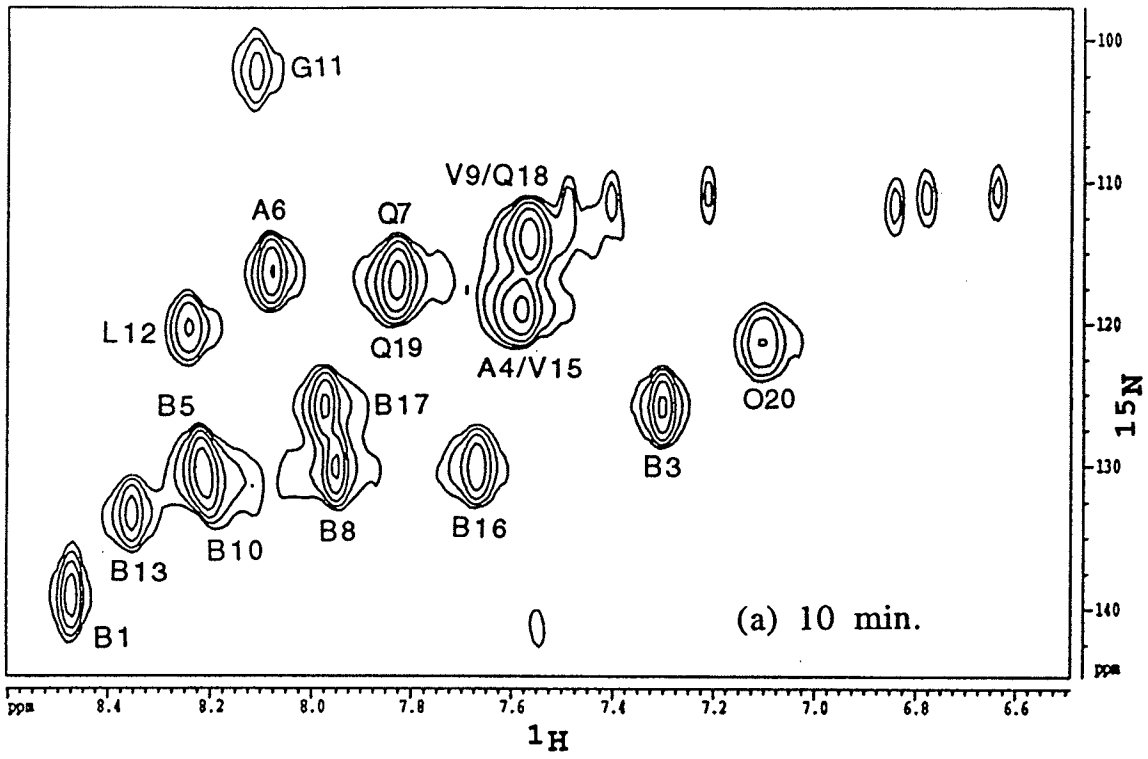
G11
V9/Q18
A6
Q7
L12
Q19
A4/V15
O20
B5
B17
B3
B10
B8
B16
B13
B1
(a) 10 min.
15N
1H

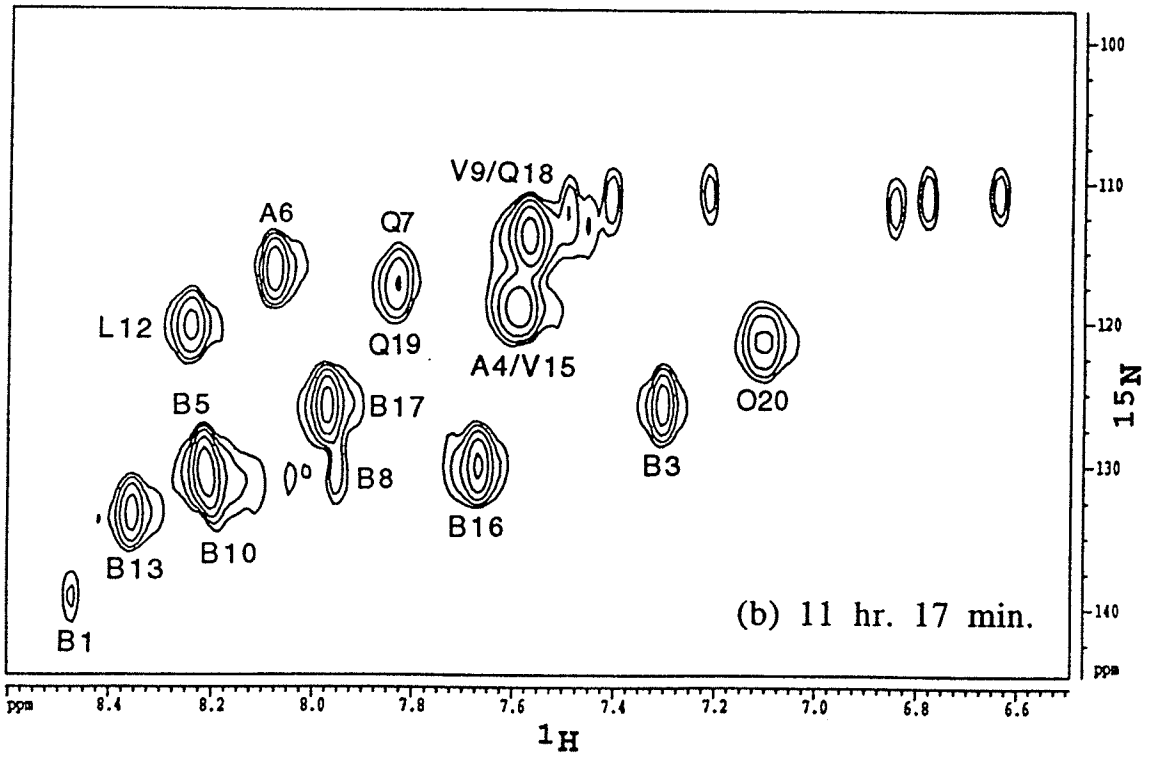
V9/Q18
A6
Q7
L12
Q19
A4/V15
O20
B5
B17
B3
B8
B16
B10
B13
B1
(b) 11 hr. 17 min.
15N
1H

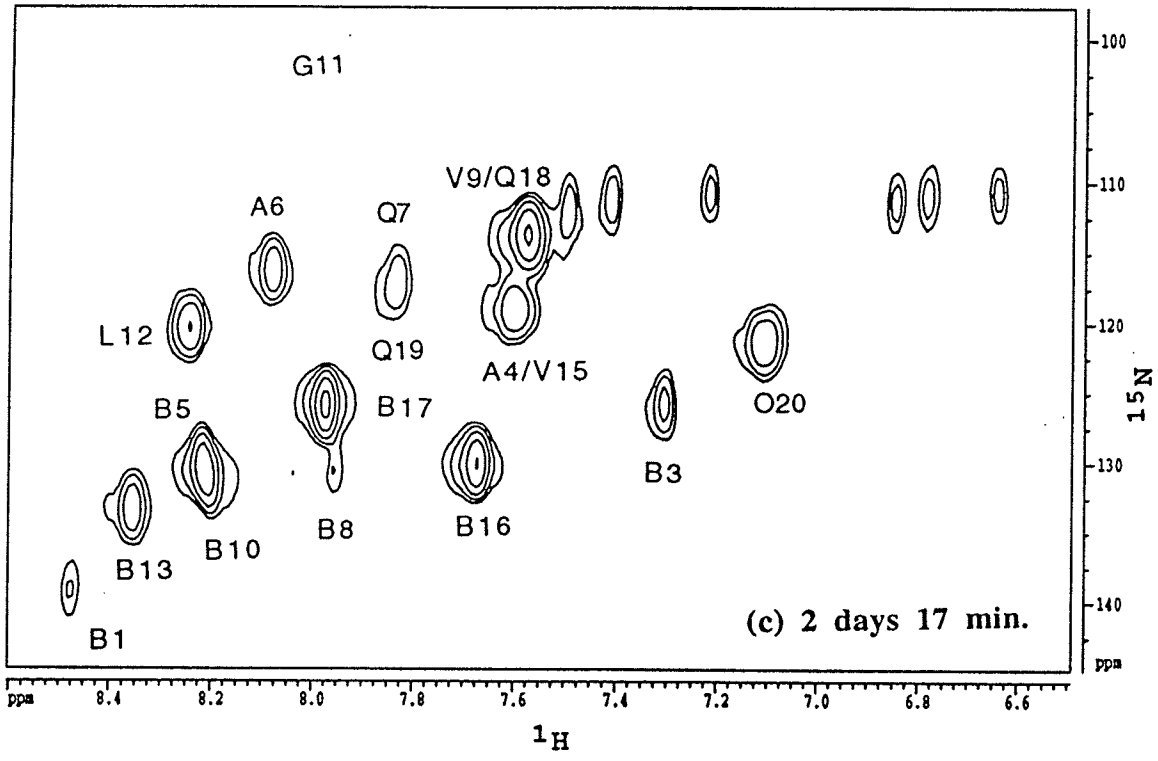
G11
A6
Q7
V9/Q18
L12
Q19
A4/V15
B5
B17
O20
B3
B8
B16
B10
B13
B1
(c) 2 days 17 min.
ppm
8.4
8.2
8.0
7.8
7.6
7.4
7.2
7.0
6.8
6.6
1H
100
110
120
130
140
15N

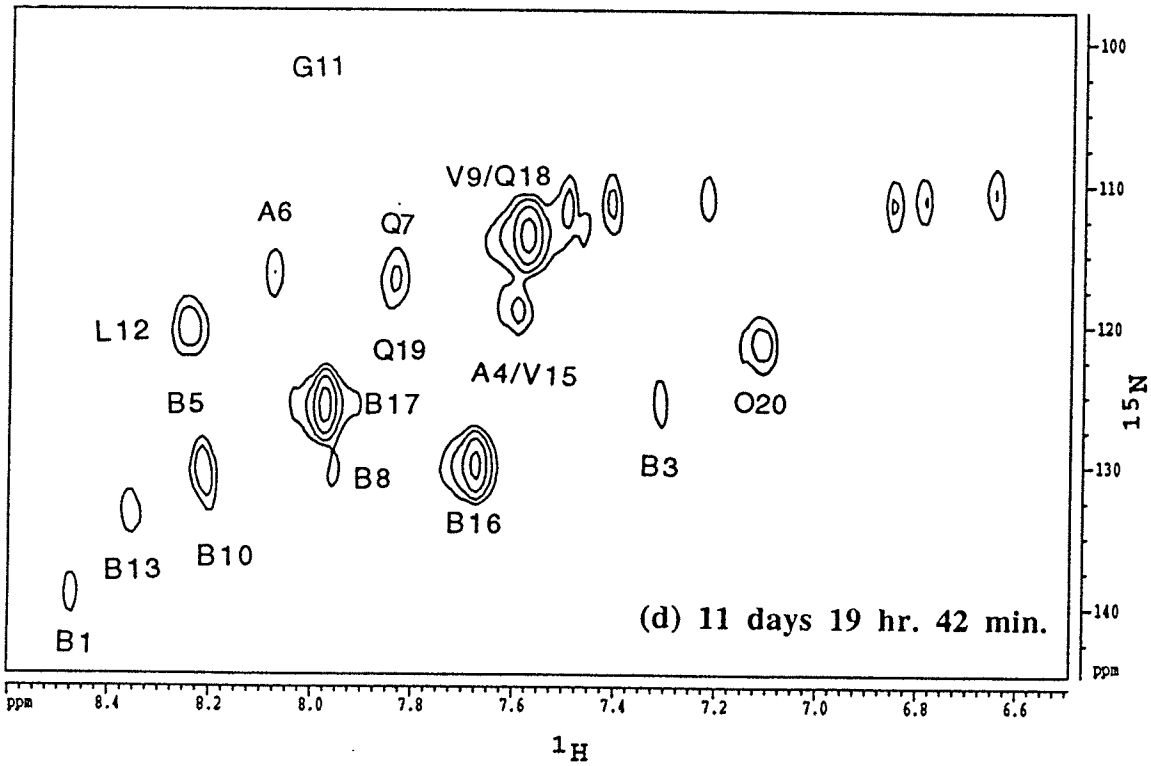
G11
A6
Q7
V9/Q18
L12
Q19
A4/V15
B5
B17
O20
B3
B8
B16
B10
B13
B1
(d) 11 days 19 hr. 42 min.
ppm
8.4
8.2
8.0
7.8
7.6
7.4
7.2
7.0
6.8
6.6
1H
100
110
120
130
140
15N

Figure 4-26: The change in the HMQC cross peak intensities of ^{15}N-labelled alamethicin in 150 mM SDS-D_{25}, 20 mM Na_2HPO_4 solution, pD_{corr} 6.1 as a function of time. (a) Some of the non-overlapping cross peaks fit to a monoexponential decay; (b) Ala 4/ Val 15 cross peaks (•) fitted to a monoexponential decay equation (– – –) and to a biexponential decay equation (———); Ala 6 cross peaks (°) fit to a monoexponential decay (- - - -) is shown for comparison; (c) Val 9/ Gln 18 cross peaks (•) fit to a monoexponential decay (– – –) and to a biexponential decay (———); the preexponential constants are 114 and 129; the Leu 12 cross peaks (°) fit to a monoexponential decay (- - - -) is shown for comparison. (d) Gln 7 cross peaks fitted to a monoexponential decay (———) and a biexponential decay (– –). (e) Gln 7/ Gln 19 cross peaks fit to a monoexponential decay (– – –) and to a biexponential decay (———).

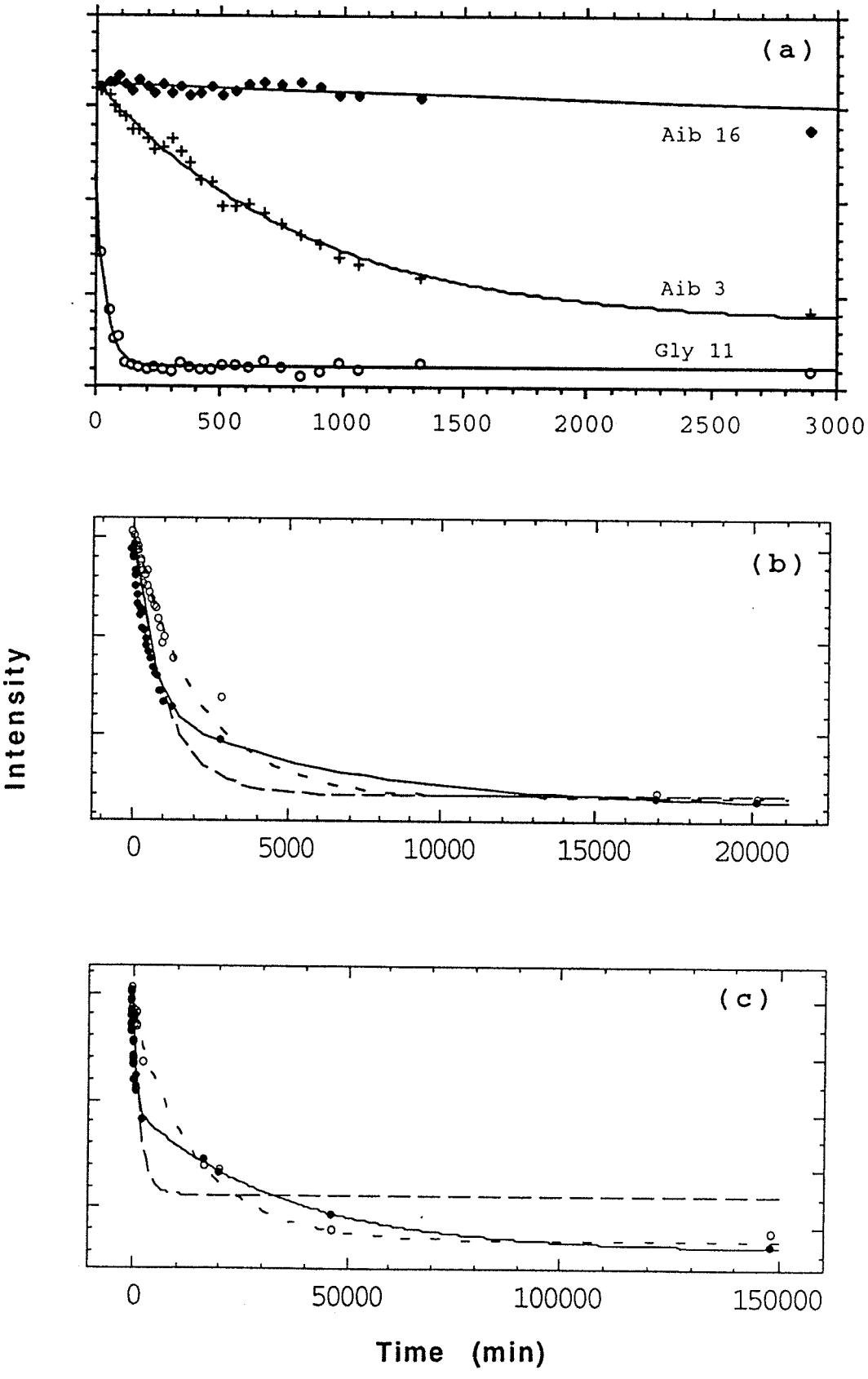
(a)
Aib 16
Aib 3
Gly 11
0
500
1000
1500
2000
2500
3000
(b)
0
5000
10000
15000
20000
(c)
0
50000
100000
150000
Intensity
Time (min)

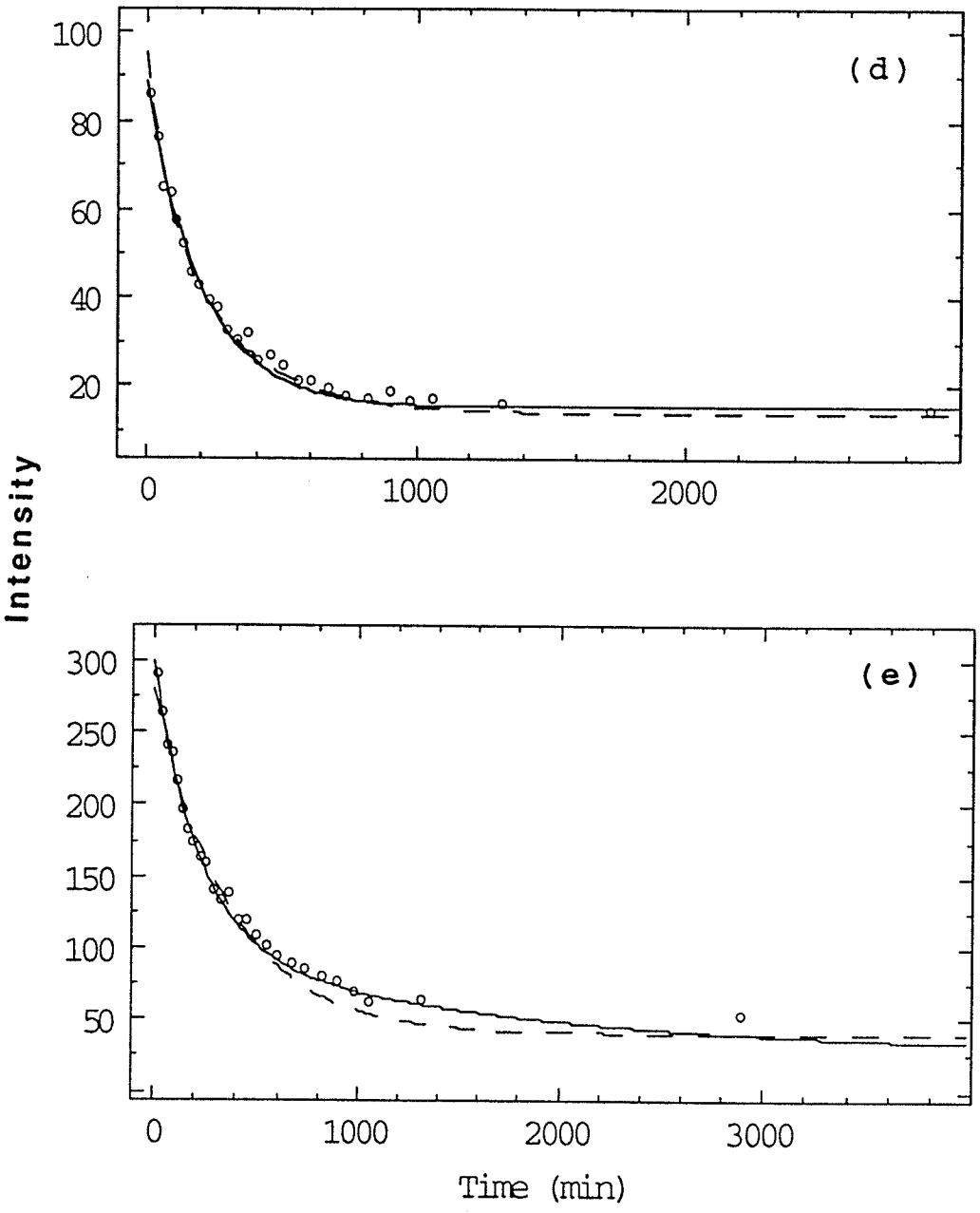
(d)
100
80
60
40
20
0
1000
2000
(e)
300
250
200
150
100
50
0
1000
2000
3000
Intensity
Time (min)

fit well to a monoexponential decay suggesting that Gln 7 and Gln 18 exchange at very similar rates.

The exchange rate constants at different pH are plotted in Figure 4-27 and compared with the predicted exchange rates for an unstructured peptide. With the exception of Aib 1, Aib 3, and Phol 20, the residues show depression of both the acid and base catalyzed exchange rates with the base catalyzed exchange experiencing a larger decrease than the acid catalyzed rates. The acid catalyzed exchange in Aib 3 is the same as that expected for a random coil but the base-catalyzed exchanged rate is depressed. The acid catalyzed exchange rates at Aib 1 and Phol 20 are enhanced but the based catalyzed exchange rates are depressed. The overlapped cross peaks corresponding to Val 9/ Gln 18 and Ala 4/ Val 15 gave a good fit to a biexponential decay equation at most of the pH values above 5, but fit well to a single exponential at low pH values.

The exchange protection factors in alamethicin were calculated three ways: protection from acid catalyzed exchange ($PF(k_H)$), protection from base catalyzed exchange ($PF(k_{OH})$), and protection from exchange at the minimum pH ($PF(k_{min})$). Two $PF(k_H)$ and $PF(k_{OH})$ for the overlapping peaks Ala 4/ Val 15 and Val 9/ Gln 18 were calculated for each residue using the k_{OH} values determined from the data in Figure 4-27. The calculated protection factors are summarized in Tables 4-6 and 4-7.

Figure 4-27: The dependence of H-D exchange rates on pD_{corr} of the H_N in alamethicin in 20 mM Na_2HPO_4, 150 mM SDS-D_{25} solution. The solid curves are the best fit of the data to equation 4-11 and the dashed curves are the predicted exchange rates for the H_N of alamethicin in a structureless conformation. The predicted exchange rates were calculated following the methods of Bai et al.(1993).

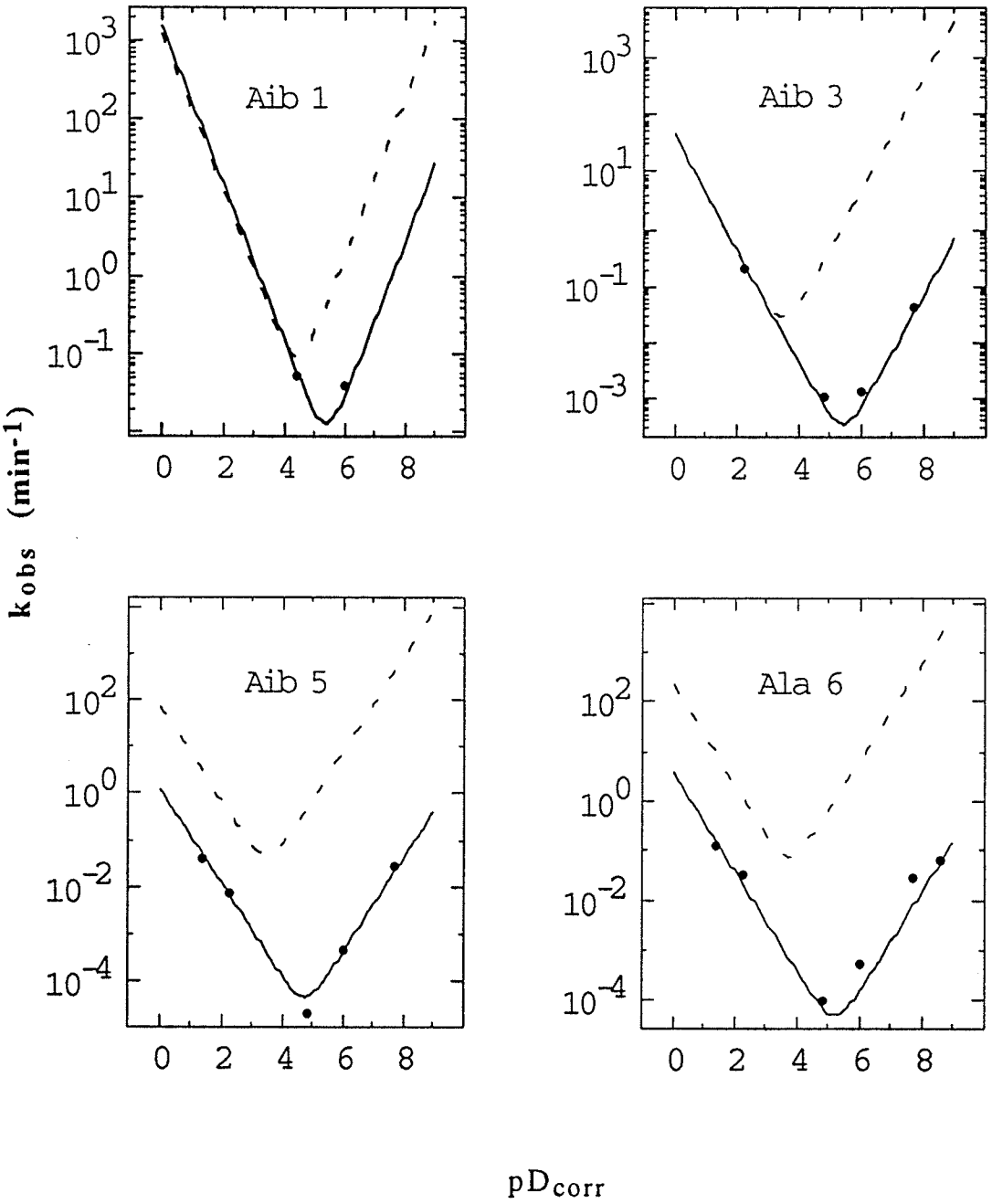
Aib 1
Aib 3
Aib 5
Ala 6
k_{obs} (min^{-1})
pD$_{corr}$

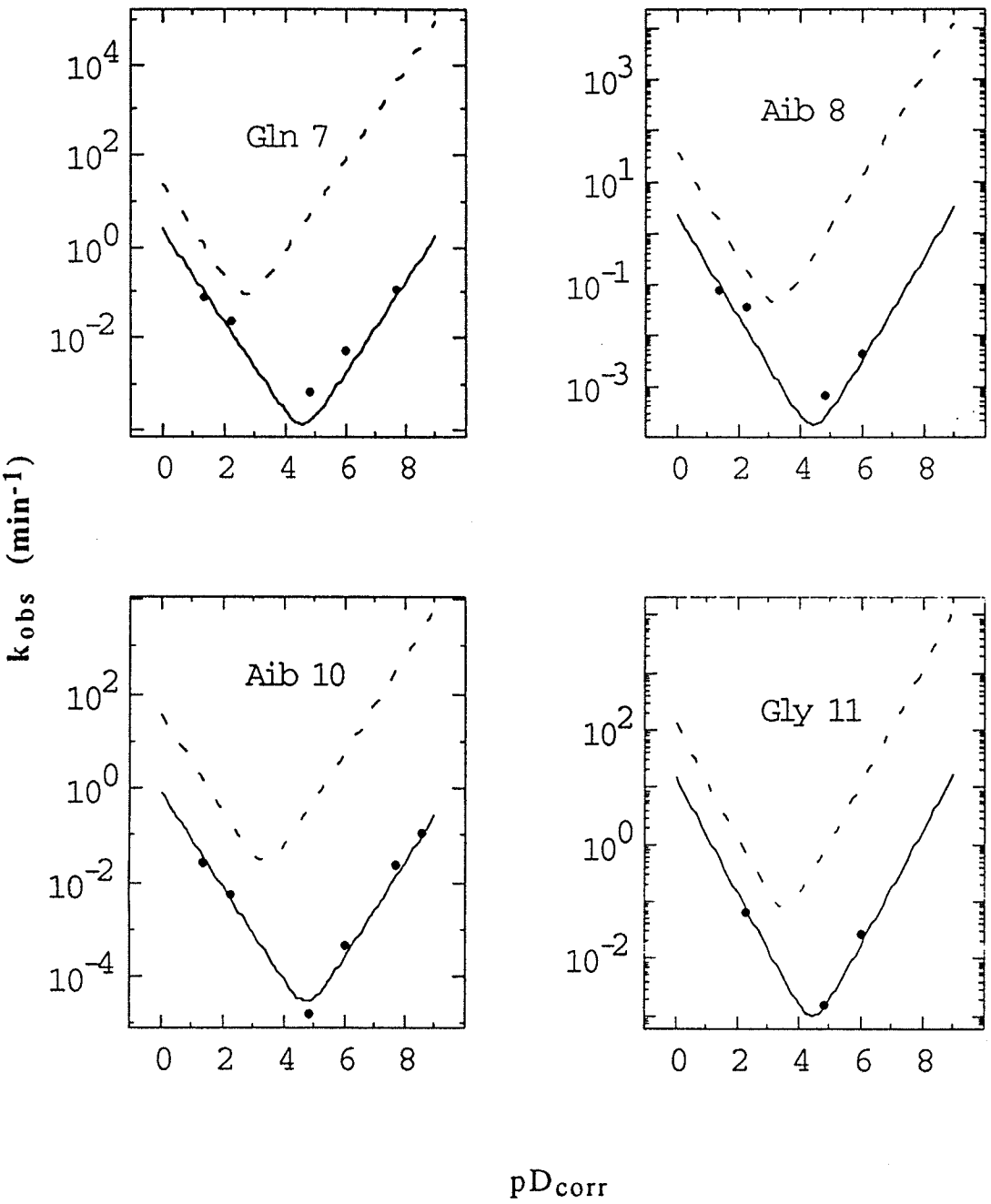
Gln 7
Aib 8
Aib 10
Gly 11
k_{obs} (min^{-1})
pD$_{corr}$

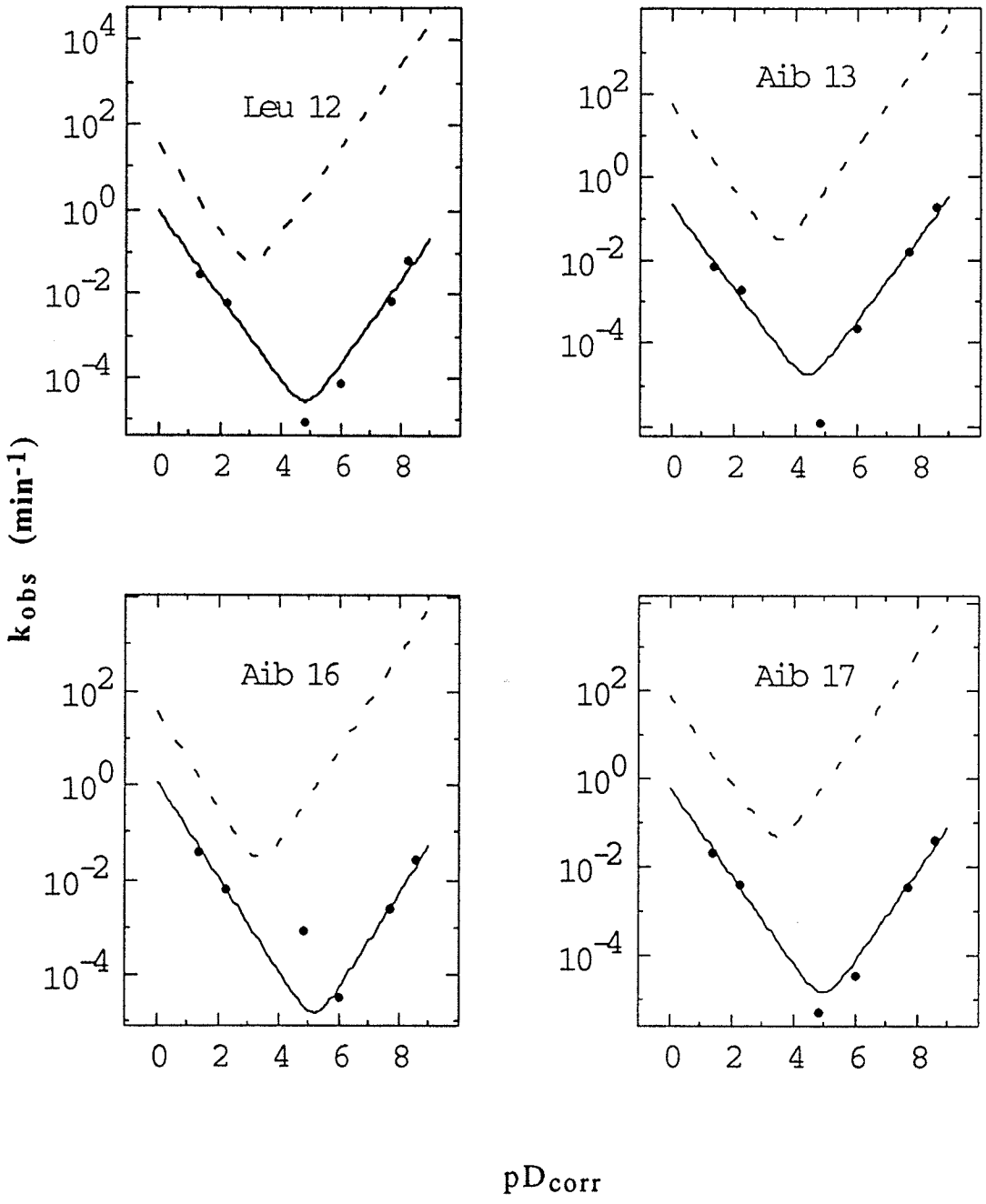
Leu 12
Aib 13
Aib 16
Aib 17
k_{obs} (min^{-1})
pD$_{corr}$

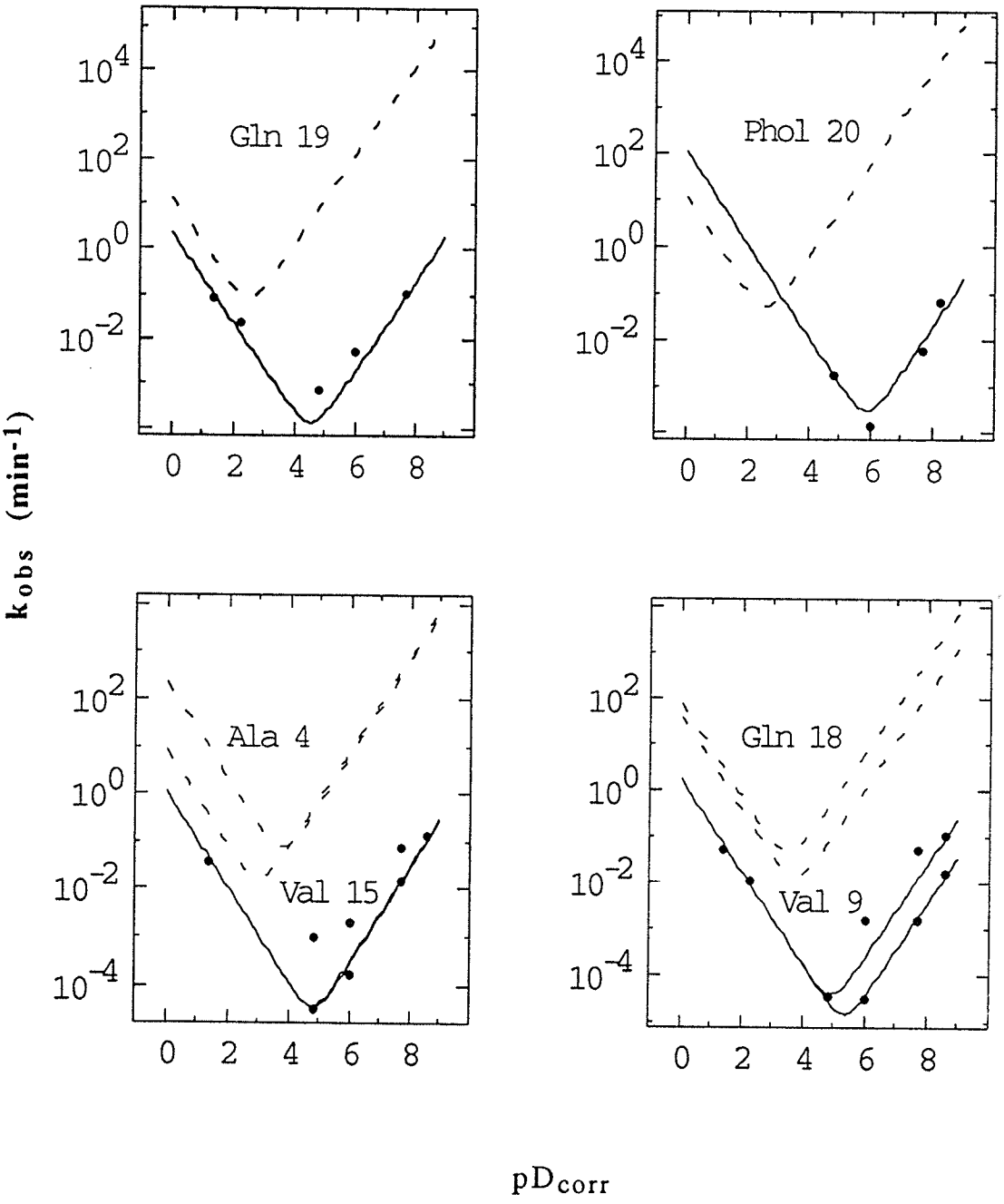
Gln 19
Phol 20
Ala 4
Val 15
Gln 18
Val 9
k_{obs} (min^{-1})
pD$_{corr}$

Table 4-6: H_N exchange protection factors for alamethicin in SDS solution in D_2O at 27°C.

Residue	k_H^{rc} ($M^{-1}min^{-1}$)	k_H^{obs} ($M^{-1}min^{-1}$)	$PF(k_H)$	k_{OH}^{rc} ($M^{-1}min^{-1}$)	k_{OH}^{obs} ($M^{-1}min^{-1}$)	$PF(k_{OH})$
Aib 1	1269.64	1587.13	0.80	1.16×10^9	1.77×10^7	65.5
Pro 2						
Aib 3	46.10	46.59	0.99	2.99×10^9	4.34×10^5	6886.7
Ala 4[a]	225.78	1.11	203.41	4.13×10^9	1.69×10^5	24437.9
					1.92×10^5	21510.4
Aib 5	71.40	1.25	57.09	5.20×10^9	2.67×10^5	19477.6
Ala 6	225.78	3.98	56.74	4.13×10^9	9.59×10^4	43049.9
Gln 7	24.76	2.43	10.18	5.20×10^{10}	1.11×10^6	46975.3
Aib 8	38.34	2.40	15.98	8.24×10^9	2.06×10^6	4005.6
Val 9[a]	41.08	1.79	22.95	8.24×10^8	2.30×10^4	35826.1
					1.61×10^5	5118.0
Aib 10	35.78	0.84	42.58	3.77×10^9	1.65×10^5	22811.4
Gly 11	136.04	9.16	4.46	7.69×10^9	1.13×10^7	680.4

Leu 12	32.63	0.92	35.35	1.76×10^{10}	1.36×10^{5}	129176.0
Aib 13	52.93	0.23	226.47	3.20×10^{9}	2.23×10^{5}	14401.7
Pro 14						
Val 15[a]	8.58	1.11	7.73	5.20×10^{9}	1.69×10^{5}	30769.2
					1.92×10^{5}	27083.3
Aib 16	35.78	1.22	29.39	3.77×10^{9}	3.34×10^{4}	112763.0
Aib 17	220.64	0.63	349.78	4.74×10^{8}	4.67×10^{4}	10104.7
Gln 18[a]	76.50	1.79	42.74	4.74×10^{9}	2.30×10^{4}	206087.0
					1.61×10^{5}	29441.0
Gln 19	13.29	2.30	5.77	8.24×10^{10}	1.19×10^{6}	69373.4
Phol 20	13.29	114.35	0.12	4.13×10^{10}	1.24×10^{5}	331928.0

[a]Ala 4 overlaps with Val 15, Val 9 overlaps with Gln 18.

Table 4-7: Comparison of the observed and expected H_N exchange parameters at the pD of minimum exchange.

Residue	pD_{min}^{rc}	pD_{min}^{obs}	ΔpD_{min}	k_{min}^{rc} (min^{-1})	k_{min}^{obs} (min^{-1})	$PF(k_{min})$
Aib 1	4.42	5.38	0.96	9.67×10^{-2}	1.33×10^{-2}	7.2
Pro 2						
Aib 3	3.49	5.41	1.92	2.95×10^{-2}	3.58×10^{-4}	82.4
Ala 4[a]	3.77	4.81	1.04	7.68×10^{-2}	3.44×10^{-5}	2233.9
		4.78	1.01		3.67×10^{-5}	2093.7
Aib 5	3.47	4.74	1.27	4.84×10^{-2}	4.59×10^{-5}	1054.4
Ala 6	3.77	5.21	1.44	7.68×10^{-2}	4.91×10^{-5}	1562.8
Gln 7	2.74	4.57	1.83	9.02×10^{-2}	1.30×10^{-4}	691.4
Aib 8	3.23	4.43	1.20	4.47×10^{-2}	1.77×10^{-4}	253.0
Val 9[a]	3.75	5.35	1.60	1.46×10^{-2}	1.61×10^{-5}	905.0
		4.54	0.79		6.00×10^{-5}	243.3
Aib 10	3.39	4.75	1.36	2.92×10^{-2}	2.96×10^{-5}	985.7

Gly 11	3.52	4.90	0.94	8.13×10^{-2}	1.39×10^{-3}	79.0
Leu 12	3.03	4.81	1.78	6.03×10^{-2}	2.82×10^{-5}	2137.0
Aib 13	3.51	4.41	0.90	3.28×10^{-2}	1.81×10^{-5}	1806.1
Pro 14						
Val 15[a]	3.01	4.81	1.80	1.68×10^{-2}	3.44×10^{-5}	488.4
		4.78	1.77		3.67×10^{-5}	457.8
Aib 16	3.39	5.18	1.79	2.92×10^{-2}	1.60×10^{-5}	1820.6
Aib 17	4.23	4.96	0.73	2.57×10^{-2}	1.37×10^{-5}	1879.8
Gln 18[a]	3.50	5.35	1.85	4.79×10^{-2}	1.61×10^{-5}	2969.2
		4.54	1.04		6.00×10^{-5}	798.3
Gln 19	2.50	4.54	2.04	8.32×10^{-2}	1.31×10^{-4}	632.7
Phol 20	2.63	5.88	3.25	5.56×10^{-2}	3.00×10^{-4}	185.4

[a]Ala 4 overlaps with Val 15, Val 9 overlaps with Gln 18.

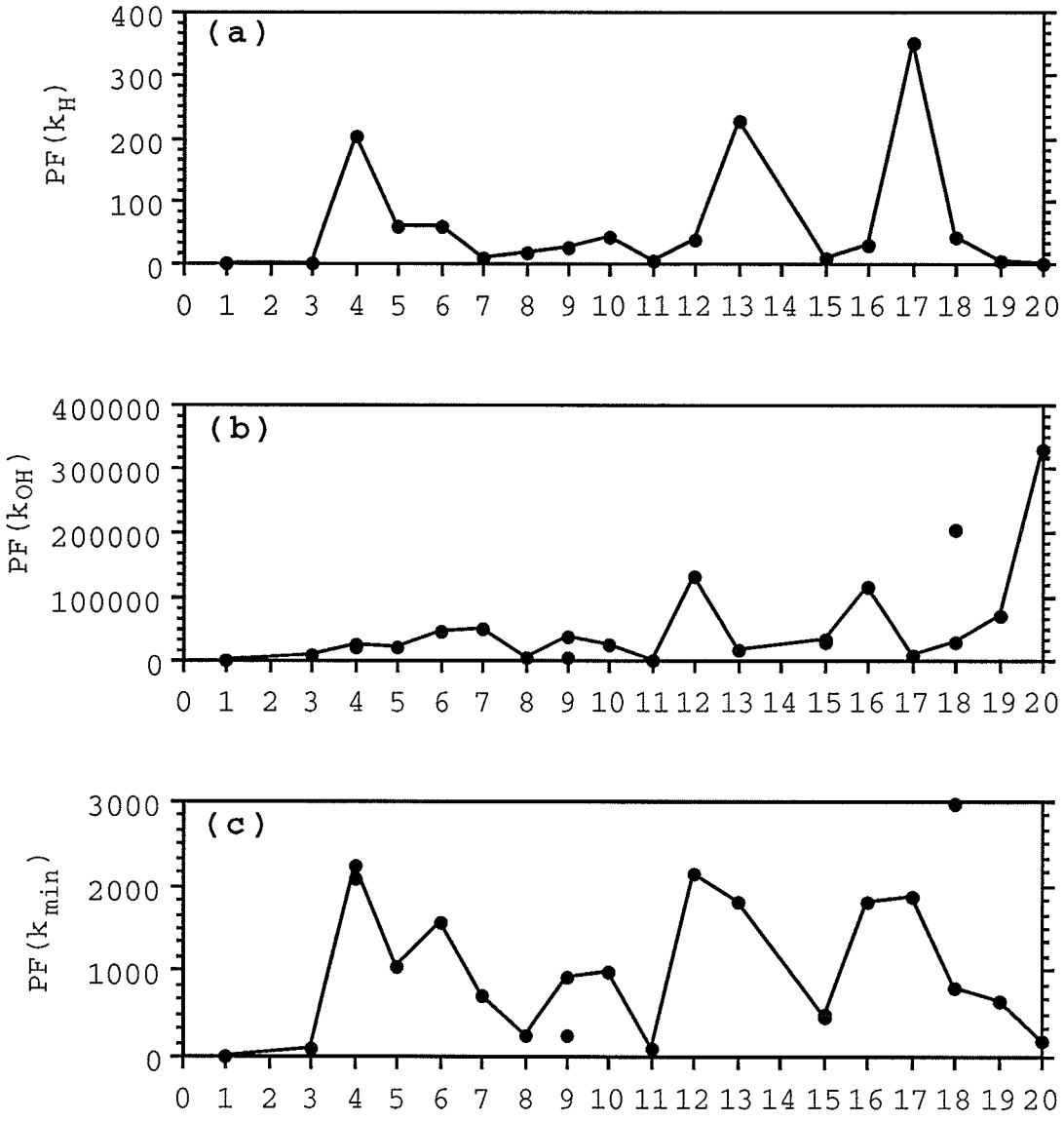

Figure 4-28: Summary of the calculated protection factors of the amide hydrogens of residues in alamethicin dissolved in 150 mM SDS-D_{25}, 20 mM Na_2HPO_4 in water. (a) Protection from acid-catalyzed exchange, (b) protection from base-catalyzed exchange, (c) protection at the pD of minimum exchange.

The lowest observed acid catalyzed protection factor was for Phol 20 at 0.1 followed by Aib 1 at 0.8 suggesting that both are deprotected ($PF(k_H) < 1.0$). Aib 3 has the same acid catalyzed exchange rate as that predicted for an unstructured peptide so the protection factor is 1. The largest protection factors for acid catalyzed exchange are observed for Ala 4, Aib 13 and Aib 17 at around 200 to 300. The rest have protection factors from 10 to 50.

The base catalyzed protection factors are very much larger than the acid catalyzed protection factors. The smallest calculated value was for Aib 1 followed by Gly 11 which has a protection factor of 680; Aib 3 and Aib 8 have protection factors on the order of 10^3; Leu 12, Aib 16, Gln 18, and Phol 20 have protection factors on the order of 10^5; and the rest are on the order of 10^4. The smallest protection factor at the pD_{min} is observed at Aib 1 followed by Gly 11 and Aib 3. The largest observed is for Leu 12 which is 2000.

4.6 Discussion

4.6.1 Conformation of Alamethicin in Detergent Based on C_α and H_α Chemical Shift Index

Figure 4-29 shows the chemical shifts of the $^{13}C_\alpha$ and $^{1}H_\alpha$ resonances of the non-Aib residues of alamethicin in detergent relative to their random coil chemical shifts calculated from the data compiled by Wishart and coworkers (Wishart et al., 1992; Wishart & Sykes, 1994). All the $^{13}C_\alpha$

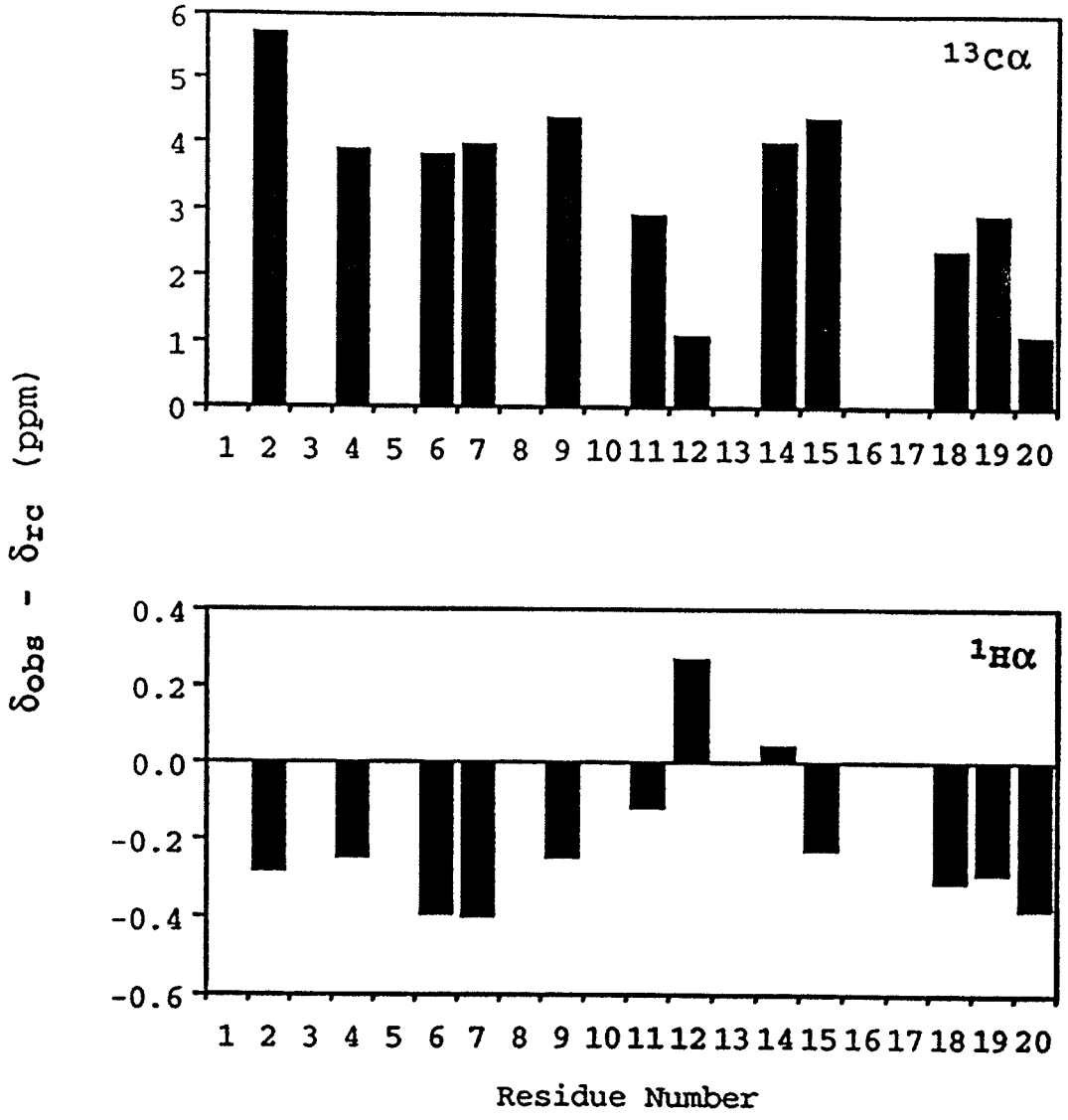

Figure 4-29: The chemical shifts of the non-Aib residues in alamethicin in SDS solution relative to their random coil values used in the chemical shift indexing (CSI) as described by Wishart & Sykes (1994). Before indexing 1.6 ppm was added to the ^{13}C chemical shifts reported in Appendix A to account for the difference in the TMS reference used for the sample shifts and the DSS reference used for the random coil values.

resonate at a higher frequency than their random coil values by more than 0.7 ppm suggesting that all of these residues are in a helical conformation. The H_α of Leu 12 resonates at a higher frequency than its random coil value by more than 0.1 ppm suggesting that it is in the extended conformation. The H_α of Pro 14 resonates at a higher frequency than its random coil value by 0.04 ppm suggesting that this is in a random coil conformation. All other H_α resonate at a lower frequency than their random coil values by more than 0.1 ppm suggesting that they are all in a helical conformation. At present, unlike the situation in methanol, the $^{13}C'$ resonances of alamethicin in SDS solution are not assigned, so the ambiguity between the $^{13}C_\alpha$ and $^{1}H_\alpha$ CSI values of Leu 12 and Pro 14 cannot be resolved by the concensus CSI method (Wishart & Sykes, 1994). The $^{3}J_{HNH\alpha}$ of Leu 12 suggest that it is in neither a helical nor an extended conformation. There are no $^{3}J_{HNH\alpha}$ data for Pro 14 because this residue is lacking H_N. The chemical shift difference between the $^{13}C_\beta$ resonances of each Aib are at least 3.5 ppm (see Figure 4-10) suggesting that these residues are also in a helical conformation (see discussion in section 3.5.1). Taken together with the CSI data, it can be concluded that alamethicin in SDS solution is helical from Aib 1 to Phol 20 but that the Leu 12 and Pro 14 conformation is undetermined.

4.6.2 Conformation of Alamethicin in Detergent Based on Homonuclear NOes

In an ideal helical conformation, the $H_N(i)$ to $H_N(i+1)$ distances range from 2.6 to 2.8 Å and the $H_\alpha(i)$ to $H_N(i+1)$ distances range from 3.4 to 3.5 Å, so the $H_N(i)$ to $H_N(i+1)$ nOe should be stronger than the $H_\alpha(i)$ to $H_N(i+1)$ nOe (Wuthrich, 1986). In an ideal β sheet conformation, the $H_N(i)$ to $H_N(i+1)$ distances range from 4.2 to 4.3 Å and the $H_\alpha(i)$ to $H_N(i+1)$ distances are around 2.2 Å, so the reverse would be observed (Wuthrich, 1986). Figure 4-19 shows that the measured nOe between sequential H_N are stronger than those between sequential H_α and H_N from Aib 3 to Pro 14 and from Aib 17 to Phol 20 suggesting that these segments of the peptide are helical. In addition, nOes from residue i to i+3 are observed extending from Ala 6 to Leu 12 and from Pro 14 to Gln 19, further evidence that these segments are in a helical conformation. The presence of a very weak $H_\alpha(i)$ to $H_N(i+4)$ nOe from Pro 14 to Gln 18 suggests that the helix in this segment is an α helix as opposed to a 3_{10} helix. The nOe pattern shows that evidence for a helical structure is strongest between residues 6 to 12.

There is one $H_\beta(i)$ to $H_N(i+3)$ nOe and seven $H_\alpha(i)$ to $H_N(i+3)$ nOes observed in alamethicin in methanol (Yee, 1991; Yee & O'Neil, 1992). In SDS solution, there is one $H_\beta(i)$ to $H_N(i+3)$ nOe but only three $H_\alpha(i)$ to $H_N(i+3)$ nOes are observed, possibly due to spectral overlap in SDS solution. For example, the $H_\alpha(2)$ to $H_N(5)$ nOe that was observed in methanol

may be overlapping with the $H_\alpha(4)$ to $H_N(5)$ nOe in the SDS solution because the $^1H_\alpha$ of Pro 2 and Ala 4 are very close to each other. (This is peak number 23 in Appendix B b.) In Figure 4-19 we have taken a conservative approach and assigned the nOe to $H_\alpha(4)$ to $H_N(5)$ because they are closer to each other in sequence. Likewise the $H_\alpha(4)$ to $H_N(7)$, $H_\alpha(7)$ to $H_N(10)$, and $H_\alpha(12)$ to $H_N(15)$ nOes that were observed in methanol may be overlapping with the $H_\alpha(19)$ to $H_N(19)$, $H_\alpha(11)$ to $H_N(10)$, and $H_\alpha(14)$ to $H_N(15)$ nOes, respectively, in SDS solution, and these are all assigned as the latter in Figure 4-19. (These are peak numbers 19, 26, and 1 in Appendix B b.) The only i to i+4 nOe observed in the SDS solution is from Pro 14 to Gln 18, whereas in methanol solution, an nOe is observed between Ala 4 and Aib 8. The latter i to i+4 nOe was observed in the SDS solution at the 200 msec mixing time NOESY experiment but not in the 100 msec mixing time experiment (peak number 21 in Appendix B b). This probably indicates that the nOe is very weak in SDS solution, which is to be expected even in an α helix, and likely does not arise by spin diffusion. That being the case this nOe may reflect a small fraction of molecules in the α-helical state with short (i, i+4) distances or it may reflect dynamic flexibility of the α-helical conformation of the entire population.

4.6.3 Conformation of Alamethicin in Detergent Based on $^3J_{HNH\alpha}$

The $^3J_{HNH\alpha}$ for residues 4, 6, 7, and 11 are all less than 6 Hz suggesting that these residues in the N-terminal part of the peptide are helical. This agrees with the pattern of nOe results. The $^3J_{HNH\alpha}$ of residue 9 is 6.2 Hz which is very close to the cut off value between the helical and averaged conformations. Of the five measured $^3J_{HNH\alpha}$ of the non-Aib residues in the C-terminal half of the peptide, only residue 18 is in a helical conformation, the rest are neither in a helical nor in an extended conformation. The $^3J_{HNH\alpha}$ for alamethicin in SDS solution are very similar to those determined in methanol except at residues 9 and 20. As already mentioned above, residue 9 may be in a helical conformation because its $^3J_{HNH\alpha}$ is very close to 6 Hz, similar to the $^3J_{HNH\alpha}$ for Ala 4 in methanol (Table 4-1). Residue 20 is in an extended conformation in methanol but the $^3J_{HNH\alpha}$ suggests an averaged conformation in SDS solution.

The distance geometry calculated structure based on the nOe and $^3J_{HNH\alpha}$ distance constraints showed convergence only from residue 3 to 10. This would suggest a very flexible C-terminal half of alamethicin as reflected by the $^3J_{HNH\alpha}$. However, as mentioned in Section 1.3, the non-convergence at the terminals of a linear peptide may be due to lack of medium range nOe constraints at the ends and the lack of $^3J_{HNH\alpha}$ for Pro and Aib residues. The P1$\bar{1}$ read pulse used in the present NOESY experiment may also contribute to the low

convergence of the structures as described in Section 4.5.2.1. In the present distance geometry calculations, no constraints were derived from the $^{1}H_{\alpha}$, $^{13}C_{\alpha}$ CSI and $^{13}C_{\beta}$ of Aib residues, all of which suggest that the C-terminus from residue 13 to 20 are in a helical conformation (see Section 4.6.1). Likewise, hydrogen exchange experiments suggest hydrogen bonding of all the H_N except for that of Aib 1 (see Section 4.6.6) but no hydrogen bonding constraints were imposed on the structures.

4.6.4 Effects of Hydrogen Bonding on H_N Exchange Rates

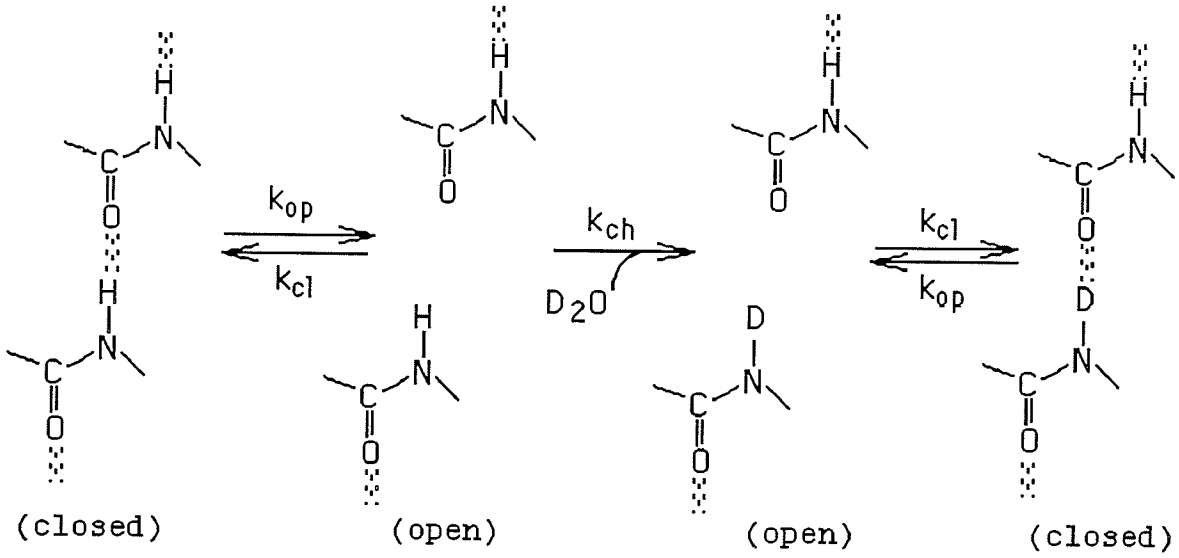

In the breathing model of protein hydrogen exchange (see diagram above), exchange protection factors are usually interpreted in terms of the stability of intramolecular hydrogen bonding since this has to be broken first before hydrogen exchange can proceed (see Section 4.3). In alanine-based peptides in water, the acid- and base-catalyzed

protection factors were interpreted as due to hydrogen bonding at the amide hydrogen and/or the carbonyl oxygen by Rohl & Baldwin (1994). The effects of hydrogen bonding at the amide hydrogen and at the carbonyl oxygen on the pH-dependent hydrogen exchange curve (V-curve) are illustrated in Figure 4-30.

In an aqueous solvent and if acid catalyzed exchange were to occur via N-protonation or O-protonation, hydrogen bonding at the amide hydrogen will retard both the acid- and base-catalyzed exchange to almost the same extent (effect a in Figure 4-30). In this case PF(k_H) is the same as PF(k_{OH}) and also PF(k_{min}). In an aqueous solvent when acid-catalyzed exchange occurs via O-protonation, hydrogen bonding at the carbonyl oxygen retards acid catalyzed exchange but not base-catalyzed exchange (effect b in Figure 4-30). In this case the PF(k_H) is slightly larger than PF(k_{min}) and PF(k_{OH}) is one. However, when acid-catalyzed exchange occurs via N-protonation, hydrogen bonding at the carbonyl oxygen will not affect acid- or base-catalyzed exchange. In this case the PF(k_H) is the same as the PF(k_{min}) and PF(k_{OH}) are all equal to one.

4.6.5 Effects of SDS Detergent on H_N Exchange Rates

The presence of detergent makes the interpretation of the protection factors in alamethicin not as straightforward as in the case of peptides dissolved in aqueous solution. Catalysis and inhibition of organic reactions by detergent

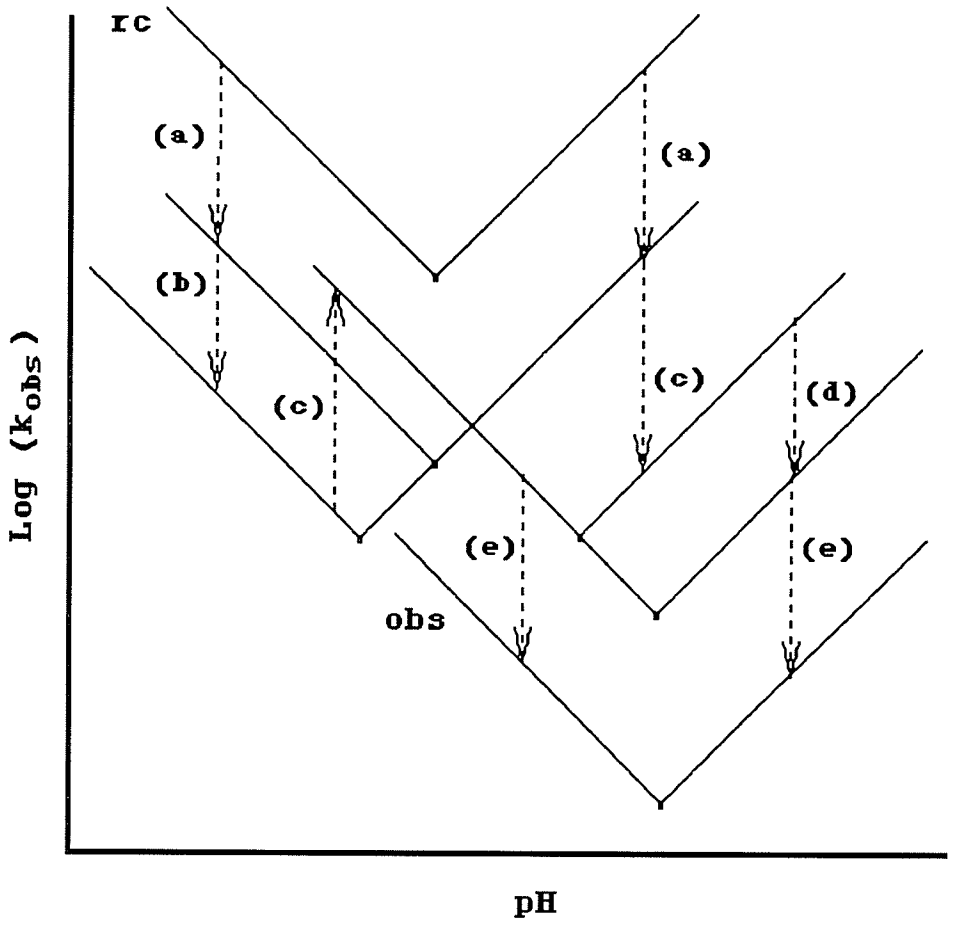

Figure 4-30: Effects of hydrogen bonding and SDS on peptide H_N exchange rate as a function of pH (V-curve). The hypothetical V-curve marked rc is that predicted for a structureless peptide. The curve marked obs is a hypothetical curve where several mechanisms affect the final measured exchange rate. The dashed arrows indicate the direction of the following effects: (a) Hydrogen bonding is at the amide H and acid-catalyzed exchange is via N- or O-protonation. (b) Hydrogen bonding is at the carbonyl O and acid-catalyzed exchange is via O-protonation. (c) Micelle surface condenses H^+ onto the micelle surface. (d) Micelle core increases the pK_a of the amide group. (e) Micelle core excludes catalysts.

micelles in water has been attributed to either electrostatic or solubilizing effects (Myers, 1992).

The concentration of SDS used in the present study is above the critical micelle concentration (cmc) of SDS which is 8 mM in the absence of salt and decreases as the salt concentration increases (Emerson & Holtzer, 1965). Figure 4-10 shows two sets of resonances corresponding to SDS. The possibility that the shifts are due to an isotope effect of random deuteration of the SDS molecules was considered but deemed unlikely because if it were an isotope effect, then the terminal methyl group would show three signals instead of two; one for each carbon in CD_2H, CDH_2, and CH_3. The possibility that the two SDS signals belong to the micelle form and the monomer form was also considered since the reported differences in ^1H chemical shifts between micelle and monomer are 0.03 ppm for the terminal CH_3, 0.02 ppm for $(CH_2)_n$, and 0.04 ppm for the αCH_2 (Oakes, 1974). The observed differences between the two SDS resonances in the presence of alamethicin are 0.04 ppm for terminal CH_3 and 0.03 ppm for the αCH_2. If this were the case then the cross peaks from the monomers would be less intense than those from the micelles since the concentration of SDS in the monomer form (< 8 mM) is a lot less than the concentration of SDS in the micelle form (> 142 mM). However, the intensities of the two peaks in Figure 4-10 are almost equal. Alternative possibilities include the following: (1) The number of SDS molecules per molecule of peptide is not uniform. This is based on the

observation that the ^1H chemical shifts of SDS have been reported to shift to higher frequencies as the number of SDS molecules per peptide increases in a bovine serum albumin-SDS denaturation study (Oakes, 1974). (2) SDS associated with the peptide resonates at a different frequency than that associated with another SDS molecule. Either of these possibilities suggest that the peptide is associated with the detergent. The larger overall correlation times for alamethicin in SDS solution (5.7 nsec) compared with that in methanol (1.1 nsec) also suggests an alamethicin-SDS interaction (Spyracopoulos, 1996). So before protection factors can be interpreted in terms of structural stability of alamethicin, the influence of SDS on the hydrogen exchange chemistry has to be considered.

4.6.5.1 Electrostatic Effect of SDS on Hydrogen Exchange

The polar head of SDS is negatively charged and this could affect hydrogen exchange in three ways. First, the negative charge on the surface of the SDS micelle could depress the k_{OH} and enhance or have little effect on the k_H by stabilizing or destabilizing, respectively, the reaction intermediates. In the base catalyzed exchange chemistry (equation 4-2), the reaction intermediate is negative and this would be destabilized by the negative SDS head groups so the forward reaction would be slowed down. In the acid catalyzed exchange chemistry (equations 4-6 and 4-7), the

reaction intermediate in the N-protonation mechanism is positive which would be stabilized by the negative SDS head groups so the forward reaction would be enhanced. In the O-protonation mechanism, the reaction intermediate is neutral so that the negative SDS head groups would have a smaller effect on k_H. In proteins and peptides, evidence suggests that acid catalyzed exchange proceeds via the O-protonation mechanism (Tuchsen & Woodward, 1985; Rohl & Baldwin, 1994), so the electrostatic enhancement of k_H is expected to be smaller than the depression of k_{OH}. The net effect of this on the V-curve would be to shift the pH_{min} to a higher pH and depress the k_{min}. In hydrogen exchange studies on unstructured hydrophobic tripeptides dissolved in aqueous SDS solution, only an elevation of pH_{min} and not a depression of k_{min} was observed suggesting that the effect of the SDS head groups on the reaction intermediates is not significant (O'Neil & Sykes, 1989).

Second, the negatively charged SO_4^- of the SDS could act as a general base catalyst and enhance the k_{OH} so that the observed k_{OH} is actually the sum of k_b $[SO_4^-]$ and k_{OH} $[OH^-]$. In hydrogen exchange studies on unstructured hydrophobic tripeptides dissolved in aqueous SDS solution, the k_{OH} was depressed and not enhanced suggesting that general base catalysis by the detergent SO_4^- is not significant (O'Neil & Sykes, 1989 and references therein). Third, the negative charge on the surface of the SDS micelle could condense hydronium ions making the pH near the surface of the micelle

lower than the measured bulk pH. This would make it appear as if the k_{OH} at the measured bulk pH is depressed while the k_H is enhanced to the same extent. The net effect of this on the exchange rate versus pH curve (V-curve) would be to shift the pH_{min} to a higher pH without affecting the k_{min} (effect c in Figure 4-30).

4.6.5.2 Hydrophobic Effect of SDS

The core of an SDS micelle is hydrophobic and this could influence the H_N exchange rate in two ways. First, the micelle core is less polar than water so the pK_{NH} in the core of the micelle may be higher than the pK_{NH} in water; this would result in a decrease in k_{obs} by decreasing the base-catalyzed exchange with little change in the acid-catalyzed exchange (Zhang et al., 1995). The net effect on the V-curve is to increase the pH_{min} and decrease the k_{min} (effect d in Figure 4-30). Second, the amount of water and charged catalysts in the core may be limited. For hydrophobic model amides, this solvent exclusion in the core was shown to result in a decrease in k_{obs} by decreasing both k_H and k_{OH} (Spyracopoulos & O'Neil, 1994). The net effect of this on the V-curve is to decrease the k_{min} without changing the pH_{min} (effect e in Figure 4-30).

Overall, the electrostatic and hydrophobic effects of detergent are expected to depress k_{OH} more than they will enhance k_H resulting in an increase of the pH_{min} and a

decrease of the k_{min}. This is the trend observed in all of the measured V-curves in alamethicin (Figure 4-27).

4.6.6 H_N Protection Factors in Alamethicin

One notable difference between the hydrogen exchange properties of the model amides in detergent (O'Neil & Sykes, 1989; Spyracopoulos & O'Neil, 1994) and those for alamethicin is in the protection factors for the acid catalyzed exchange. All calculated protection factors are summarized in Figure 4-28. With the exception of Aib 1, Aib 3, and Phol 20, all the H_N in alamethicin are protected from acid catalyzed exchange relative to the predicted random coil values ($PF(k_H) > 1$) whereas in the model amides, k_H is enhanced ($PF(k_H) < 1$). Even for the most hydrophobic amide, which was calculated to have a fractional residence time of 0.9 in the micellar core (Spyracopoulos & O'Neil, 1994), the k_H in detergent solution is enhanced compared to its value in water ($PF(k_H) = 0.14$) (i.e., for the model amides, effect e is not large enough to counter effect c in Figure 4-30). This difference between the model compounds and alamethicin can be attributed to the presence of hydrogen bonding in alamethicin which is absent in the model studies as follows. Hydrogen bonding at the amide H of the peptide would result in added protection from both acid- and base-catalyzed exchange. Hydrogen bonding at the carbonyl O would result in protection from acid-catalyzed exchange if this exchange occurs via O-protonation. The depression of k_H by hydrogen bonding more than offsets

the enhancement of k_H due to the SDS micelle for all but three of the amides. Helical alanine-based peptides in D_2O (Rohl & Baldwin, 1994) and alamethicin in methanol (Dempsey, 1995) also showed PF(k_H) greater than 1 indicative of hydrogen bonding.

The PF(k_H) for Aib 1 and Aib 3 are very close to 1 whereas at Phol 20, it is 0.12. The deprotection observed at Phol 20 suggests either of the following: (1) The predicted random coil k_H and k_{OH} for Phol 20 using the Molday correction for Phe may not be appropriate (see Section 4.5.3). The peptide fragment below shows the difference between C-terminal Phe and Phol.

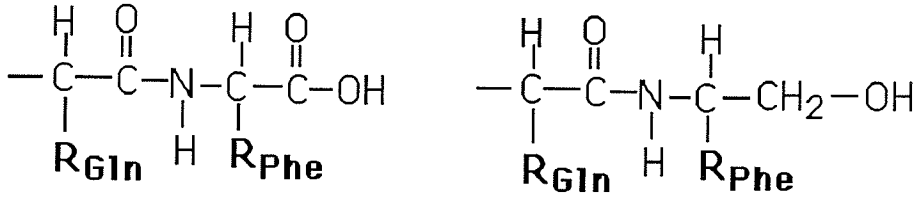

No Molday effect correction factor is available for an amino alcohol. As mentioned in Section 4.5.3, the predicted random coil k_H and k_{OH} values for Phol 20 were calculated as if the C-terminus is a neutral Phe residue. The carboxylic acid terminal is a stronger electron withdrawing group than the alcohol moiety. Electron withdrawing groups will increase the k_{OH} and decrease the k_H, so it is possible that the correct k_{OH}^{rc} (or k_H^{rc}) for Phol 20 is lower (or higher) than what is given in Table 4-5. Consequently, the true PF(k_{OH}) (or PF(k_H)) will be lower (or higher) than what is given in Table

4-5. The Molday correction factor for an ionized carboxylate terminal is available so the protection factors may be calculated assuming that the C-terminus is a negatively charged carboxylate group. The calculated PF(k_H) is 0.94 and the PF(k_{OH}) is 5261. The neutral alcohol group is a weaker electron donor compared with the negatively charged carboxylate group. This is supported by the lower pKa values reported for amino alcohols compared with their amino acid counterparts (Jencks & Regenstein, 1976).

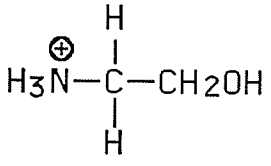

pKa = 9.50

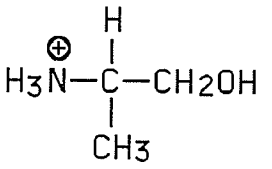

pKa = 9.43

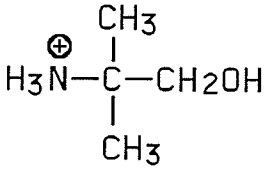

pKa = 9.71

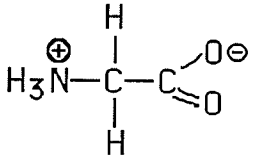

pKa_1 = 2.34
pKa_2 = 9.60

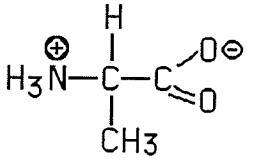

pKa_1 = 2.34
pKa_2 = 9.69

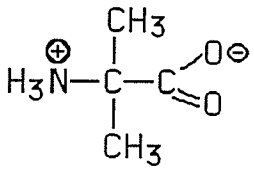

pKa_1 = 2.36
pKa_2 = 10.21

Thus, the correct PF(k_H) for the Phol terminal will be between 0.12 and 0.94 and the correct PF(k_{OH}) will be between 5×10^3 and 3×10^5. At this point, it is difficult to speculate whether the PF(k_H) for Phol terminal is closer to 0.12 or to 0.94. Nevertheless this still shows that the acid-catalyzed H_N exchange of Phol 20 is enhanced. (2) In hydrophobic model amides in SDS solution where there is no hydrogen bonding to depress the k_H, the reported PF(k_H) are

less than one (O'Neil & Sykes, 1989; Spyracopoulos & O'Neil, 1994). So the enhancement of k_H for Phol 20 may suggest the absence of hydrogen bonding similar to the model amides. This is supported by the fact that even in a 3_{10} or α helical conformation, the C'O of Phol 20 will not be hydrogen bonded. However, the PF(k_{OH}) of Phol 20 is much larger than that observed in the model amides (PF(k_{OH}) = 3000) and one possibility is that there is hydrogen bonding, at least to the amide H of Phol 20. Similar to Phol 20, no hydrogen bonding to the carbonyl O is expected for Gln 19 but the PF(k_H) for Gln 19 is greater than one suggesting that the depression of k_H by hydrogen bonding at the amide H alone is enough to counter the enhancement of k_H effected by the SDS. Among the factors that affect the k_H and k_{OH} in peptides described above, only the electrostatic effect due to SO_4^- works to enhance k_H (Figure 4-30). Hydrogen bonding and the hydrophobic effect all work to depress k_H. Thus one way that the Phol 20 k_H can be enhanced is by close association with the negative surface of the SDS micelle. The association with the negative surface will work to depress the k_{OH}, so this could explain the added depression of k_{OH} for Phol 20 as well.

As the peptide is dissolved with the aid of SDS detergent, it is expected that k_{OH} will be depressed due to one or more effects of the detergent micelle. Therefore, it is difficult to interpret the PF(k_{OH}) values solely in terms of hydrogen bonding to the H_N (see Section 4.6.5.1). There is a wide distribution of PF(k_{OH}) values observed in alamethicin

in SDS solution ranging from 65 to 3 x 10^5. This compares with the values reported for the model alanine-based peptides dissolved in water, and alamethicin and mellitin dissolved in methanol which are all less than 2000. One explanation of the large PF(k_{OH}) in detergent solubilized alamethicin is that the effects of hydrogen bonding and the detergent micelle work together to produce the large observed depression of the k_{OH}.

The differences in PF(k_{OH}) among the residues may be interpreted in terms of static or dynamic alamethicin-SDS interaction models. In a static model, the differences in protection factors between residues may be viewed as due to different residues' interaction with different parts of the SDS micelle. For example those residues interacting closely with the surface of the micelle would experience a large enhancement of k_H, a large suppression of k_{OH} and a large ΔpD_{min}. In a simple dynamic model where alamethicin adopts the same conformation inside and outside the micellar core, the differences in protection factors between residues may be viewed as due to different residence times in the micellar core of different residues. In a more complicated dynamic model where alamethicin either adopts different conformations or has a different stability inside and outside of the micellar core, the differences in protection factors between residues may be viewed as due to both the differential residence time and the differential hydrogen bonding stability among the residues. At present, no hydrogen exchange data are available for alamethicin either in water

or in a low dielectric constant solvent like n-hexane (to approximate the core environment). The only hydrogen exchange data available are from methanol. So interpretation of $PF(k_{OH})$ in terms of the more complicated dynamic model is simply impossible at this point.

The $PF(k_{OH})$ of some C-terminal residues are at least ten times larger than in the rest of the peptide. As described above, from the $PF(k_H)$ values it is reasonable to conclude that Phol 20 is associated with the surface of the micelle. A possible static model interpretation of the $PF(k_{OH})$ values is that the C-terminus of the peptide is associated with the surface of the micelle. The $^{13}C_\alpha$ and $^1H_\alpha$ CSI suggest that the C-terminus is helical. Figure 4-31 is an α helical wheel depiction of alamethicin which shows that except for Gln 18 the three residues with the largest $PF(k_{OH})$ (residues 12, 16, and 20) are all located on one face of the helix. This suggests that one face of the C-terminal helix is located close to the surface of the SDS micelle. If this is the case, then the $PF(k_{OH})$ for Gln 18 is most likely 2×10^4 rather than 2×10^5 (see Figure 4-32). Therefore, the $PF(k_{OH})$ for Val 9 will be 3×10^4 instead of 5×10^3. Unlike Phol 20, the k_H of Aib 16 and Leu 12 are not enhanced, which may be explained by hydrogen bonding at their C'O is which is absent in Phol 20. Residues Val 9 and Aib 5 are on the same face of the putative helix as Phol 20- Aib 16- Leu 12 in an ideal α-helical arrangement but the magnitude of their $PF(k_{OH})$ are not as large as the three C-terminal residues. This suggests a

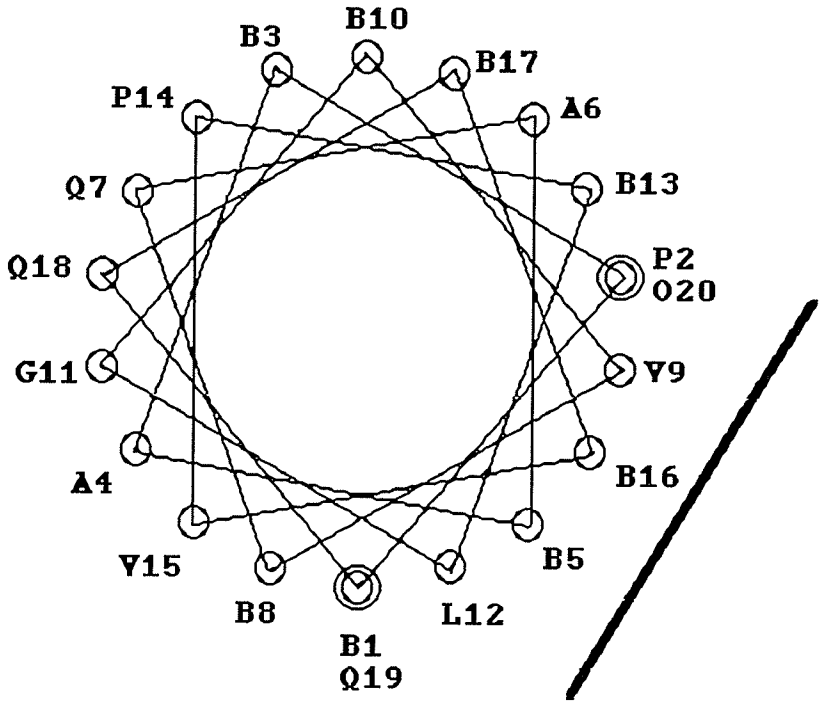

Figure 4-31: Distribution of the amino acids in an ideal α helical alamethicin. The line drawn shows the face of the helix suggested to be associated with the negative surface of the SDS micelle based on the hydrogen exchange data.

possible small distortion from an ideal α helix in the N-terminus. Figure 4-32 correlates the observed $PF(k_{OH})$ with each residue's distance from the arbitrarily chosen reference of Aib 16 if alamethicin were an ideal α helix.

Because consecutive residues have very different $PF(k_{OH})$ it is difficult to explain the observed $PF(k_{OH})$ in terms of any other simple dynamic model. For example, in the C-terminus, residues 12 and 16 have large $PF(k_{OH})$ whereas residues 13 and 15 have small $PF(k_{OH})$, so it is difficult to reconcile how residues 12 and 16 can reside longer in the

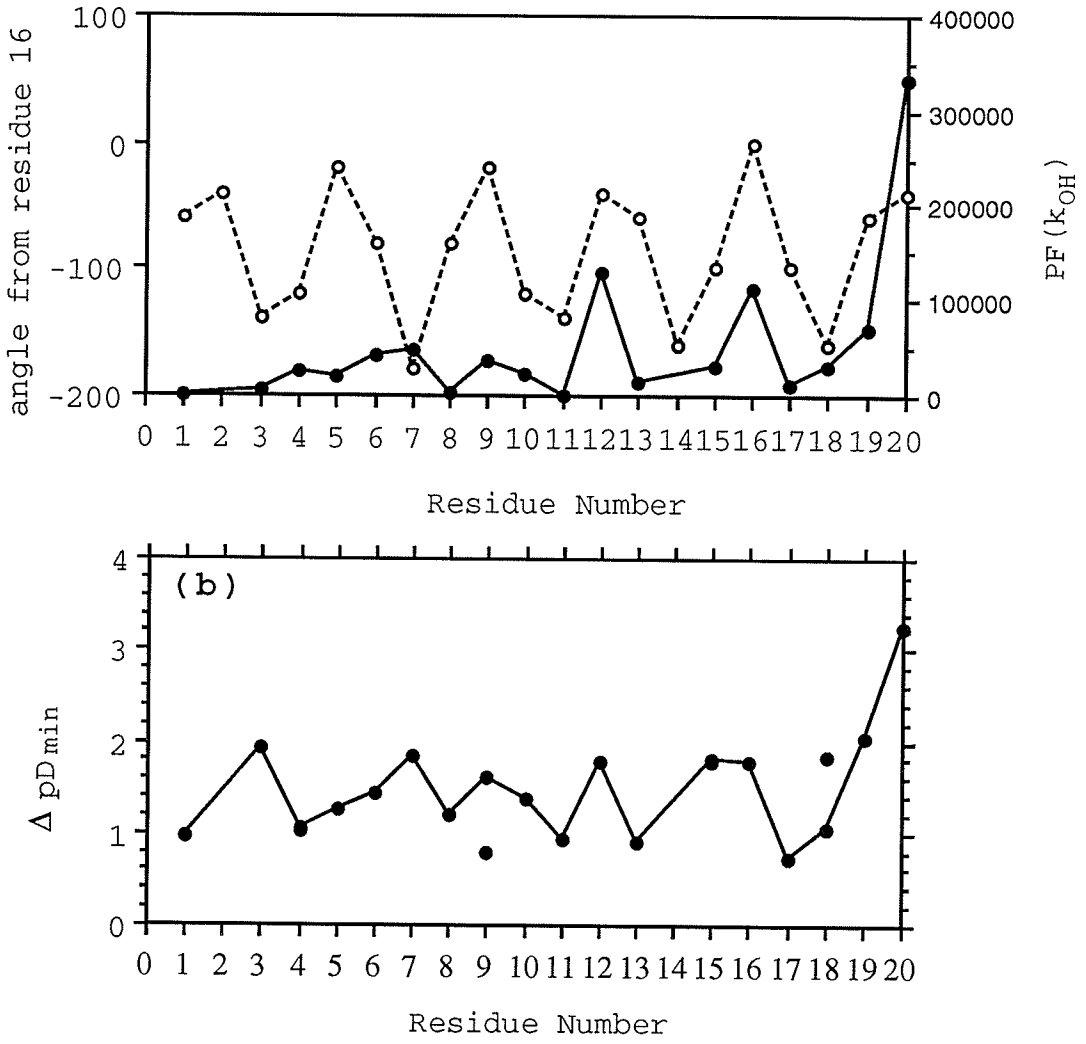

Figure 4-32: (a) The correlation between the observed amide hydrogen protection factors from base-catalyzed exchange and the angular distance of each residue from Aib 16 in an ideal α helical alamethicin. (b) The change in pD of minimum exchange relative to those predicted for a random coil alamethicin.

core of the micelle than residues 13 and 15 when they are all covalently bonded together. Such a simple dynamic model would

be a good fit to data where one region of the peptide, say, the residues at the N-terminal half, shows consistently larger protection factors than those at the C-terminal half but this is not what we observe for alamethicin. This is not to say that the present alamethicin-SDS complex is static since we know that SDS micelles are dynamic and constantly breaking/forming in equilibrium with SDS monomers. The conformation of the alamethicin molecule is also dynamic because if it were static, hydrogen exchange would not occur. The present interpretation of the PF(k_{OH}) of alamethicin merely suggests that the majority of the time, the Phol 20- Aib 16- Leu 12 face of the C-terminal helix of alamethicin preferentially interacts with the surface of the SDS micelle.

As discussed in Section 4.6.4, in aqueous solution, hydrogen bonding at the H_N would depress k_H and k_{OH} to the same extent and leave the pD_{min} unchanged. Hydrogen bonding at the C'O depresses the k_H but not the k_{OH} and so the pD_{min} is shifted to lower pD. As discussed in Section 4.6.5.2, in SDS solution, in the absence of hydrogen bonding, the hydrophobic and electrostatic effects of SDS enhance the k_H and depress k_{OH} and so the pD_{min} is shifted to higher pD. For peptide dissolved in SDS solution, the change in pD_{min} (ΔpD_{min}) would be a balance between the shift caused by hydrogen bonding and by the electrostatic effect of detergent. As long as the shift caused by hydrogen bonding along the peptide is uniform, the ΔpD_{min} would reflect the specific residue's proximity to the surface of the micelle. The pattern of ΔpD_{min}

supports the interpretation given to the $PF(k_{OH})$ data regarding which surface of the peptide interacts with the surface of the micelle (Figure 4-32 b).

4.6.7 Hydrogen Bonding in Alamethicin Deduced from Protection from Hydrogen Exchange

Some of the effects of detergent on calculated protection factors may be circumvented by comparing the exchange rates at the pD_{min} (Dempsey, 1992; 1995; 1988). This is because model studies show that the main electrostatic effect of SDS is that it changes the k_H and k_{OH} to the same extent but in opposite directions, so the observed k_{min} are unaffected. In the absence of a hydrophobic effect, i.e., the peptide is associated only with surface of the micelle, the $PF(k_{min})$ reflects the relative stability of the hydrogen bonding at the H_N or the C'O (effects a and b in Figure 4-30). If the peptide is associated with the core of the micelle, then the $PF(k_{min})$ reflects the relative stability of the hydrogen bonding at the H_N and C'O and the extent of burial in the core (in a static model) or the extent of residence in the core (in a simple dynamic model).

Table 4-7 summarizes the exchange parameters at the pD_{min}. The magnitudes of the $PF(k_{min})$ are about the same as those reported for melittin, [Ala-14]melittin, and alamethicin in methanol (Dempsey, 1992; 1995; 1988) and these are all about two orders of magnitude larger than those reported for model alanine-based peptides in D_2O (Rohl &

Baldwin, 1994). It is evident that the smallest PF(k_{min}) is that of Aib 1, which reflects the fact that there is no hydrogen bonding at the H_N.

From the interpretation of the PF(k_H) (page 24), it was suggested that Phol 20 is associated with the surface of the micelle. From the interpretation of the PF(k_{OH}) (page 251), it was suggested that Leu 12, Aib 16, and Phol 20 are associated with the surface of the micelle. However, the PF(k_H) of Leu 12 and Aib 16, unlike Phol 20, are greater than one. The larger PF(k_{min}) observed for Leu 12 and Aib 16 than for Phol 20 supports the suggestion that the depression of k_H for Leu 12 and Aib 16 may be due to stronger hydrogen bonding of the H_N of Leu 12 and Aib 16 compared with Phol 20 and perhaps an added hydrogen bonding at the C'O of Leu 12 and Aib 16 which is absent in Phol 20.

All the PF(k_{min}) are larger than that for Aib 1 by at least a factor of 10 suggesting that all the other H_N are hydrogen bonded. Hydrogen bonding at the H_N of Aib 3 suggests a 3_{10} interaction with the N-acetyl terminal similar to that observed in methanol by hydrogen exchange (Dempsey, 1995) and the temperature dependence of H_N (Babiuk, 1995; Yee et al., 1995).

4.6.8 Conformation of Alamethicin Based on Hydrogen Exchange Data

The calculated protection factors suggest that the amide hydrogens throughout the entire length of the peptide are

hydrogen bonded except for Aib 1. In the N-terminal half of the peptide, Aib 3 forms a 3_{10} hydrogen bond presumably with the carbonyl of the N-acetyl and the rest of the N-terminal region is in a helical conformation. It is difficult to say for sure whether it is an α or 3_{10} helix based on the amide exchange data alone. The C-terminal region, from Leu 12 up to Phol 20, is in an α helical conformation. The Leu 12- Aib 16- Phol 20 face of the C-terminal helix is associated with the surface of the detergent micelle.

Figure 4-33 shows the possible alamethicin-SDS micelle complexes that would satisfy the data presented herein (observed hydrogen exchange) and data from the literature. It is difficult, based on the hydrogen exchange data alone, to differentiate between the three possible models in Figure 4-33.

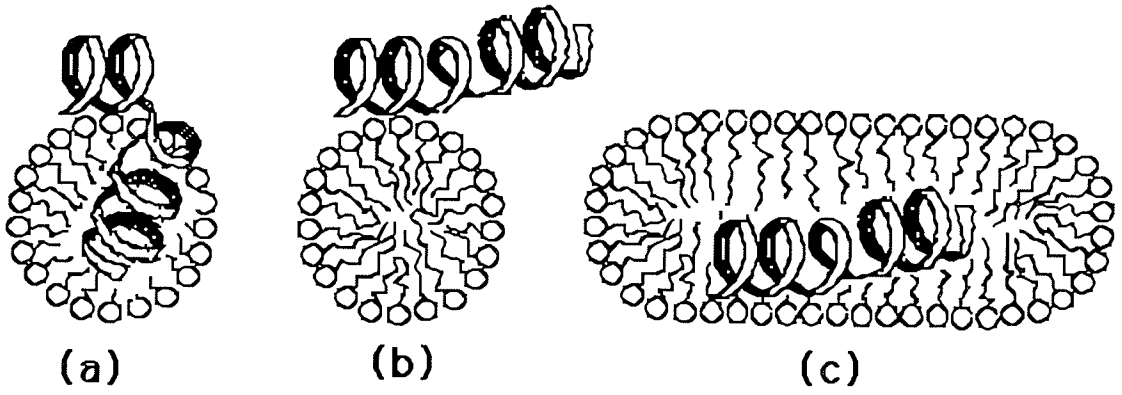

Figure 4-33: Cartoon of possible models of an alamethicin-SDS micelle complex that would satisfy the hydrogen exchange data. The sizes and shapes of the molecules are not drawn to scale.

Franklin et al. (1994) suggested that alamethicin is uniformly buried in the SDS micelle. They arrived at this conclusion based on the effect of paramagnetic probes on the ^1H NMR linewidths and on hydrogen exchange data obtained at only one pH. They reported that the exchange rates of all the amide hydrogens, with the exception of Phol 20 and Aib 1, are on the order of $10^{-4}s^{-1}$ at pH 4. They also reported that the paramagnetic probe (gadolinium(III) diethylenetriaminepentaacetate, Gd[DTPA]) reduces the intensities of COSY cross peaks on average by a factor of 4 and they did not observe any region of the peptide that was selectively more or less affected.

Model a in Figure 4-33 does not agree with the paramagnetic probe results of Franklin et al. (1994) which showed the absence of selective protection from the Gd[DTPA]. Franklin et al. (1994) used their hydrogen exchange result from one pH to rule out model b. As we have discussed in the previous sections, the presence of SDS and the primary sequence of the peptide will greatly alter the observed exchange rates at one particular pH. To interpret the hydrogen exchange rates without considering their pH dependence could lead to erroneous conclusions, so model b cannot be rejected.

In the globular protein ubiquitin, the effect of the paramagnetic probes Gd[DTPA] and 4-hydroxy-2,2,6,6-tetramethylpiperidinyl-1-oxy (HyTEMPO) on the line broadening

of the ^1H NMR resonances was correlated with the accessible surface area calculated from the crystal structure of ubiquitin (Petros et al., 1990). The effect of the paramagnetic probes was quantified by measuring the ratio of the integrated DQF-COSY cross peak volume in the presence (V) and the absence (V_o) of the paramagnetic probe. The results showed that hydrogens with large calculated surface areas gave small V/V_o. From these observations, it was suggested that a V/V_o of 0.6 can be taken as an arbitrary cutoff value to suggest probe-exposed hydrogens. The results of Franklin et al. (1994) give a V/V_o of 0.25 suggesting that the entire molecule is probe-exposed. This suggests that their conclusion that alamethicin is entirely buried is wrong (Franklin et al., 1994).

So based on my interpretation of the paramagnetic data of Franklin et al. (1994) and my present hydrogen exchange data, models a and c in Figure 33 are not likely to be correct. I therefore conclude that the alamethicin is solvent exposed and is associated with the SDS micelle surface at the Phol 20- Aib 16- Leu 12 face of the C-terminal helix in a manner similar to that drawn in Figure 4-33 b.

Chapter 5
Summary

If some understanding of the voltage-gating mechanism of alamethicin is to be deduced from its structure, it is best that the structure of the peptide be determined in the native membrane environment. Unfortunately, the NMR resonances of peptides incorporated into bilayer membranes or liposomes are often very broad which makes structure determination by NMR spectroscopy very difficult if not impossible to perform. An alternative is to study peptides in a membrane-mimetic environment. Alcohols are used as membrane-mimetic environments because of their low dielectric constants (Jackson & Mantsch, 1992). For example methanol has a dielectric constant of 32.6 compared with water which has a dielectric constant of 78.5 (Weast, 1987). The dielectric constant of biological membranes is estimated at about 1 and for n-hexane is 1.9 (Jackson & Mantsch, 1992). Detergent micelles are used as membrane-mimetic environments because they offer an amphiphatic environment with a low dielectric interior similar to that found in biological membranes.

5.1 Comparison of Alamethicin Conformations in Methanol and in SDS solution

ROe and $^{3}J_{HNH\alpha}$ data suggest that the conformation of the N-terminus of alamethicin in methanol is a stable helix whereas the C-terminus is a less stable helix (Yee, 1991; Yee

& O'Neil, 1992). The chemical shifts reported herein suggest that the peptide is helical from Aib 1 up to Gly 11 and from Aib 13 up to Gln 19 (Section 3.6.1). The carbonyl of the N-terminal acetyl forms a 3_{10} hydrogen bond with the amide hydrogen of Aib 3. It is also suggested that Gly 11/Leu 12 forms a flexible hinge joining the two helices and that Phol 20 is in an extended conformation (Section 3.6.1). The hydrogen exchange data reported for alamethicin in methanol (Dempsey, 1995) show that the residues with the highest protection factors are concentrated in the N-terminus from Ala 4 to Aib 13 except for Gly 11. These data support the idea that in methanol, the N-terminal helix of the peptide is more stable than the C-terminal helix and they agree well with the rOe data which show that most of the i to (i+3) rOes are concentrated in the N-terminal helix. The temperature dependence of carbonyl carbons suggests that alamethicin is more stable than alanine-based peptides and that the folding/unfolding of alamethicin is quite different from that of alanine-based peptides. The idea of a flexible hinge near Gly 11/ Leu 12 in methanol is partially supported by the low PF(k_{min}) at Gly 11 (Dempsey, 1995).

Chemical shift data suggest that the conformation of alamethicin in SDS solution is helical from Aib 1 to Gly 11 and from Aib 13 to Phol 20. The Leu 12 conformation is undetermined due to a lack of consensus in the $^{1}H_{\alpha}$ and $^{13}C_{\alpha}$ CSI (Section 4.6.1). The conformation of alamethicin in SDS solution calculated using distance geometry only shows

convergence from Aib 3 to Aib 10 (Section 4.5.1.6). The hydrogen exchange data for alamethicin in SDS solution show that all the amide hydrogens are protected except for that of Aib 1, suggesting that the peptide is helical throughout its length (Section 4.6.6). The acid- and base-catalyzed protection factors fit a model in which the Leu 12 to Phol 20 region forms an α helix associated with the surface of the micelle. The hydrogen exchange data of alamethicin in SDS show that the protection factors in the C-terminus and the N-terminus have about the same magnitude suggesting that the C-terminal helix is just as stable as the N-terminal helix. Figure 5-1 shows a comparison between the measured hydrogen exchange protection of alamethicin in methanol (Dempsey, 1995) and in SDS solution (this study) and also those of an alanine-based model peptide (Rohl and Baldwin, 1994). Comparison of the stability of alamethicin in methanol and in SDS shows that the C-termini are of similar stability but that the N-terminus is more stable than the C-terminus in methanol but not in SDS. Comparison of the protection factors between alamethicin in SDS solution and the alanine-based peptide in water suggests that alamethicin is considerably more stable. The temperature dependence of the molar ellipticity and of the $^{13}C'$ chemical shift of alamethicin also support this unusual conformational stability of alamethicin. This is likely due to the presence of the Aib residues. This stability is especially striking when we consider that alamethicin contains a helix breaking Gly and Pro near its

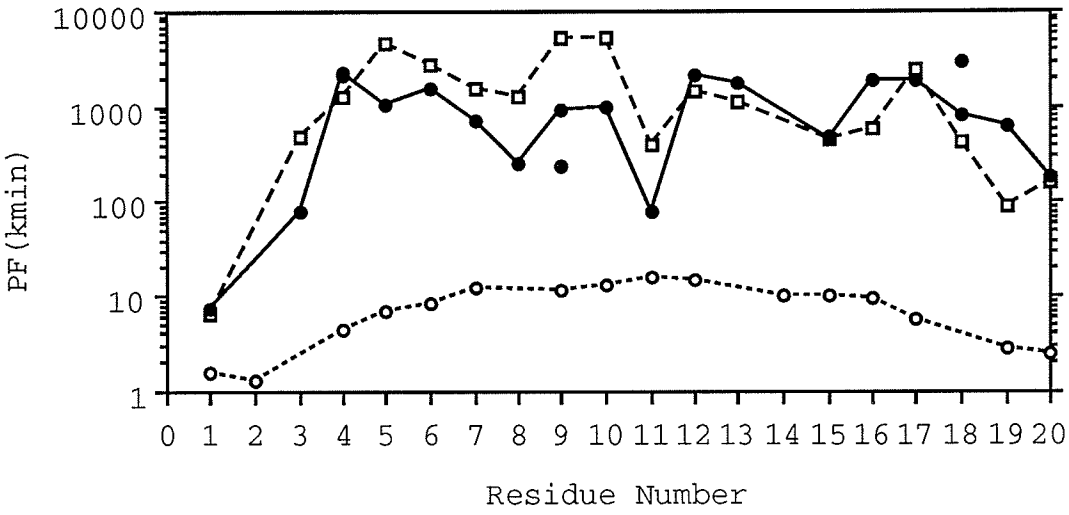

Figure 5-1: A comparison of the protection from hydrogen exchange of alamethicin amide hydrogens in methanol and in SDS solution with that of an alanine-based peptide in water. Protection factors in methanol (--▫--) are those reported by Dempsey (1995). Protection factors in SDS solution (—●—) are from Table 4-6; both values are given for the overlapping peaks Ala 4/Val 5 and Val 9/ Gln 18. Protection factors for the alanine-based peptide in water (----o----) are those reported by Rohl and Baldwin (1994).

middle and a Pro at residue 2. In alanine-based peptides, a single Gly or Pro in the middle is enough to disrupt helix formation.

5.2 Implications for the Alamethicin Conformation in SDS Solution to Voltage-Gating Models

The current models for the voltage-gating mechanism of alamethicin suggest that the peptide is either in a rigid helical conformation (Latorre & Alvarez, 1981; Mathew & Balaram, 1983; Boheim et al., 1983) or in a hinged conformation (Fox & Richards, 1982; Hall et al., 1984). The two-layered barrel model requires that the C-terminus be in a β conformation (Hall et al., 1983). However, since the evidence presented in this thesis suggests that the C-terminus of alamethicin in SDS solution is α-helical, the two-layered barrel model can be discounted as a possible explanation for voltage-gating.

In the funnel-like model of Fox and Richards (1982), the C-terminal portion of the molecule is modelled as either a random coil associated with the head group region of the membrane or projecting into the solvent, or as an α-helical segment interacting with the surface of the membrane. The present results suggest that the C-terminus may well interact with the surface of the membrane, but as a helix rather than a random coil. Their model of the α-helical segment is such that the side chain of Gln 18 is fully exposed to the aqueous phase. Gln 18 is on the opposite side of the helix to the Phol 20- Aib 16- Leu 12 helical face suggesting that this face interacts with the lipid when the molecule inserts into the bilayer. This agrees very well with the model of the C-terminal helix-detergent micelle interaction deduced from the

present amide hydrogen exchange data (Figure 4-33). However, the funnel-like model is not supported by the paramagnetic relaxation results of Franklin et al. (1994) which did not show any indication of selective protection of the N-terminus from the paramagnetic probe. In addition, our measurement of protection factors of the amide hydrogens suggests that the molecule is stably hydrogen bonded throughout the helix. The hinged alamethicin in the funnel-like model does agree with the hinged conformation of alamethicin in methanol.

The present data on alamethicin in SDS fit better to the voltage-gating model of Latorre and Alvarez (1981) which involves a reorientation of rigid helices upon application of voltage. Given the preferred interaction of one face of the helix with the surface of the micelle, it is reasonable to speculate that in the absence of an applied voltage, alamethicin, or at least its C-terminus, is likely adsorbed onto the surface of the lipid membrane. Of course, the surface of an SDS micelle may interact quite differently with alamethicin compared to the surface of a lipid bilayer owing to the difference in head group structure. However, this idea is in agreement with the reported oriented circular dichroism (OCD) results which suggest that, at a high lipid to peptide ratio, the majority of alamethicin molecules are on the membrane surface in the absence of an applied voltage (Huang & Wu, 1991). The X-ray diffraction of alamethicin in dioleoylphosphatidylcholine (DOPC) oriented multibilayers

gave reflections consistent with alamethicin molecules parallel to the lipid bilayer (Woolley & Wallace, 1993).

5.3 Proposed Experiments for Further Research

A molecular mechanics calculation of alamethicin at a simulated lipid-water interface showed that a fully helical alamethicin is oriented so that the axis of the helix is perpendicular to the phase boundary in the absence of an applied field (Galaktionov & Marshall, 1993). The OCD results of Huang and Wu (1991) also showed that at low lipid to peptide ratio, alamethicin inserts into the membrane. At high detergent to peptide ratios we find that alamethicin interacts with the surface of the micelle. An NMR study of alamethicin at very low SDS concentrations might be able to complement the low detergent to peptide studies. At the present SDS to alamethicin ratio, the terminal methyl protons of the SDS alkyl chain resonate at 0.8 ppm while the lowest frequency proton resonance of alamethicin is at 0.9 ppm. If alamethicin inserts into the micelle at low SDS to alamethicin ratios, then an nOe from the SDS alkyl terminal to any of the alamethicin protons would be easily observed and would confirm such an interaction.

Structural data on alamethicin in a membrane environment have been obtained mostly with the use of FTIR spectroscopy (Harris & Chapman, 1988) and circular dichroism (CD) spectropolarimetry (Cascio & Wallace, 1988). If an NMR study of alamethicin in small unilamellar vesicles (SUV) can be

conducted, it might provide higher resolution structural information than can be obtained from IR or CD. One foreseeable difficulty in such a study is the long rotational correlation time of the peptide-vesicle complex which would give rise to short relaxation times and broad lines. An attempt to circumvent this might be to use ^{13}C-, ^{15}N-labelled and partially deuterated peptides. Some of the advantages of using deuterated molecules include simplifying the ^{1}H resonance spectra (Markley et al., 1968; Arrowsmith et al., 1990), increasing the sensitivity of 3D and 4D heteronuclear experiments used for sequential backbone assignments (Grzesiek et al., 1993; Farmer & Venters, 1995), and increasing the sensitivity of ^{1}H NOESY experiments (Arrowsmith et al., 1990; Grzesiek et al., 1995). Deuteration simplifies the ^{1}H spectra because ^{2}H does not resonate near the ^{1}H frequency (Markley et al., 1968). One of the advantages of working with alamethicin is that we do not anticipate as much ^{1}H spectral overlap as observed in larger proteins since alamethicin is only 20 amino acids long. Deuteration enhances the efficiency of magnetization transfer from the ^{13}C to a neighboring heteroatom in 3D and 4D heteronuclear J correlated experiments because it decreases the ^{13}C linewidth. The magnetogyric ratio of ^{2}H (4.11×10^{-7} rad $T^{-1}s^{-1}$) is lower than that of ^{1}H (26.75×10^{-7} rad $T^{-1}s^{-1}$) so the T_2 is longer for deuterium-attached ^{13}C. Deuteration increases the sensitivity of ^{1}H NOESY experiments because it decreases the homonuclear dipolar interactions.

Since we have already defined the minimum medium required for the production of alamethicin, then random deuteration of alamethicin could probably be attained by simply growing the fungus in deuterated water.

Appendix A: Assignment of ^{1}H, ^{15}N, and ^{13}C resonances of alamethicin in methanol and SDS solution. All chemical shifts are in ppm. The internal ^{1}H reference is DSS; external ^{15}N reference is 2.9 M $^{15}NH_4Cl$ in 1M HCl which resonates at 24.93 ppm relative to $NH_{3(l)}$; the internal ^{13}C reference is the solvent $^{13}CD_3OH$ which resonates at 49.0 ppm relative to TMS. Some of the assignments in methanol are taken from Yee (1991).

Residue	Atom	methanol	SDS solution
N-Acetyl	$C\alpha$	22.21	24.36
	$H\alpha$	2.05	2.11
	C'	172.55	
	O		
Aib 1	N	138.7	139.16
	H_N	8.61	8.47
	$C\alpha$	57.46	
	C'	175.64	
	O		
	$C\beta r$	23.64	
	$H\beta r$	1.54	1.56
	$C\beta s$		
	$H\beta s$	1.46	1.48
Pro 2	N	131.0	
	$C\alpha$	65.68	67.09
	$H\alpha$	4.24	4.16

Residue	Atom	methanol	SDS solution
	C'	175.74	
	O		
	Cβ	29.84	30.89
	Hβr	1.79	1.94
	Hβs	2.34	2.21
	Cγ	26.93	28.62
	Hγr	2.07	1.83
	Hγs	1.95	1.83
	Cδ	49.74	51.20
	Hδr	3.95	3.99
	Hδs	3.49	3.63
Aib 3	N	126.0	125.78
	H_N	7.62	7.28
	Cα	57.48	
	C'	178.51	
	O		
	Cβr		
	Hβr	1.54	1.50
	Cβs		
	Hβs		
Ala 4	N	118.9	118.91
	H_N	7.56	7.56
	Cα	53.87	54.77
	Hα	4.09	4.10

Residue	Atom	methanol	SDS solution
	C'	177.21	
	O		
	Cβ	16.72	18.35
	Hβ	1.49	1.52
Aib 5	N	129.5	129.97
	H_N	7.92	8.20
	Cα	57.29	
	C'	177.86	
	O		
	Cβr		
	Hβr	1.55	1.56
	Cβs		
	Hβs	1.48	
Ala 6	N	117.2	116.22
	H_N	7.90	8.06
	Cα	53.72	54.72
	Hα	4.02	3.96
	C'	178.05	
	O		
	Cβ	16.72	18.35
	Hβ	1.52	1.52
Gln 7	N	118.6	116.37
	H_N	7.98	7.82
	Cα	58.04	58.59

Residue	Atom	methanol	SDS solution
	H_α	3.92	3.97
	C'	175.82	
	O		
	C_β	27.05	28.71
	$H_\beta r$	2.15	2.22
	$H_\beta s$	2.28	
	C_γ	32.70	33.99
	$H_\gamma r$	2.36	2.47
	$H_\gamma s$	2.53	2.57
	C_δ		
	O_δ		
	N_ε		
	$H_\varepsilon E$	6.74	
	$H_\varepsilon Z$	7.42	
Aib 8	N	129.22	130.04
	H_N	8.06	7.94
	C_α	57.67	
	C'	178.24	
	O		
	$C_\beta r$		
	$H_\beta r$	1.52	1.54
	$C_\beta s$		
	$H_\beta s$	1.59	1.62
Val 9	N	115.5	113.53

Residue	Atom	methanol	SDS solution
	H_N	7.48	7.54
	$C\alpha$	65.64	65.78
	$H\alpha$	3.58	3.70
	C'	175.28	
	O		
	$C\beta$	30.41	31.88
	$H\beta$	2.23	2.28
	$C\gamma r$	19.39	21.1
	$H\gamma r$	0.99	0.98
	$C\gamma s$	20.61	21.74
	$H\gamma s$	1.13	1.08
Aib 10	N	131.4	131.46
	H_N	8.20	8.21
	$C\alpha$	57.65	
	C'	179.01	
	O		
	$C\beta r$		
	$H\beta r$	1.56	1.56
	$C\beta s$		
	$H\beta s$		
Gly 11	N	101.7	102.09
	H_N	8.33	8.10
	$C\alpha$	44.78	46.30
	$H\alpha r$	3.67	3.85

Residue	Atom	methanol	SDS solution
	$H_{\alpha}s$	3.93	3.98
	C'	173.01	
	O		
Leu 12	N	119.6	120.25
	H_N	8.09	8.22
	C_{α}	53.82	55.17
	H_{α}	4.46	4.44
	C'	175.90	
	O		
	C_{β}	41.57	43.15
	$H_{\beta}r$	1.59	1.60
	$H_{\beta}s$	1.92	1.96
	C_{γ}	25.47	26.92
	H_{γ}	1.92	1.92
	$C_{\delta}r$	21.27	22.98
	$H_{\gamma}r$	0.91	0.93
	$C_{\delta}s$	23.41	25.27
	$H_{\delta}s$	0.94	0.96
Aib 13	N	134.7	133.41
	H_N	8.38	8.32
	C_{α}	58.11	
	C'	175.00	
	O		
	$C_{\beta}r$		

Residue	Atom	methanol	SDS solution
	$H\beta r$	1.53	1.51
	$C\beta s$	23.70	
	$H\beta s$	1.61	1.62
Pro 14	N	132.3	
	$C\alpha$	64.65	65.33
	$H\alpha$	4.38	4.48
	C'	176.43	
	O		
	$C\beta$	29.87	31.08
	$H\beta r$	1.80	1.87
	$H\beta s$	2.31	2.37
	$C\gamma$	26.93	28.03
	$H\gamma r$	1.98	2.04
	$H\gamma s$	2.07	2.04
	$C\delta$	50.44	51.60
	$H\delta r$	3.73	3.74
	$H\delta s$	3.87	3.84
Val 15	N	117.0	118.91
	H_N	7.63	7.58
	$C\alpha$	64.10	65.78
	$H\alpha$	3.73	3.72
	C'	175.36	
	O		
	$C\beta$	30.21	31.88

Residue	Atom	methanol	SDS solution
	Hβ	2.32	2.34
	Cγr	20.05	21.10
	Hγr	0.96	0.99
	Cγs	19.31	21.74
	Hγs	1.07	1.09
Aib 16	N	131.0	130.04
	H_N	7.59	7.64
	C_α	57.58	
	C'	177.65	
	O		
	Cβr		
	Hβr	1.50	1.51
	Cβs		
	Hβs	1.55	1.55
Aib 17	N	126.0	125.86
	H_N	7.80	7.96
	C_α	57.70	
	C'	178.76	
	O		
	Cβr		
	Hβr	1.53	1.56
	Cβs		
	Hβs		
Gln 18	N	114.8	114.12

Residue	Atom	methanol	SDS solution
	H_N	7.78	7.54
	C_α	56.95	57.51
	H_α	4.02	4.06
	C'	175.46	
	O		
	C_β	27.82	28.71
	$H_\beta r$	2.23	2.21
	$H_\beta s$		
	C_γ	33.12	33.94
	$H_\gamma r$	2.43	2.52
	$H_\gamma s$	2.62	2.59
	C_δ		
	O_δ		
	N_ε		
	$H_\varepsilon E$	6.76	
	$H_\varepsilon Z$	7.42	
Gln 19	N	116.9	117.56
	H_N	7.87	7.81
	C_α	55.56	57.51
	H_α	4.16	4.08
	C'	174.02	
	O		
	C_β	27.92	28.67
	$H_\beta r$	2.02	1.87

Residue	Atom	methanol	SDS solution
	Hβs		
	Cγ	32.80	33.19
	Hγr	2.19	2.21
	Hγs	2.33	2.03
	Cδ		
	Oδ		
	Nε	107.8	
	HεE	6.60	6.62
	HεZ	7.31	7.21
Phol 20	N	120.8	121.30
	HN	7.29	7.08
	Cα	54.31	55.22
	Hα	4.14	4.28
	Cβs	64.84	66.28
	Hβsr	3.61	3.67
	Hβss		3.78
	O		
	HO		
	Cβr	37.83	39.35
	Hβrr	2.73	2.47
	Hβrs	2.94	2.98
	Cγ	130.16	
	Hγ		7.16
	Cδ	128.84	

Residue	Atom	methanol	SDS solution
	H_δ		
	C_ε	126.79	
	H_ε		

Appendix B: Constraints list used in the calculation of the alamethicin structure.

The following list gives the integrated volumes of the cross peaks in the 100 msec mixing time NOESY-P1$\bar{1}$ experiment of 1.7 mM alamethicin in 150 mM SDS-D_{25}, 20 mM Na_2HPO_4, in 95/5 H_2O/D_2O, pH 5.06. The region of integration of cross peaks from the 200 msec mixing time experiment was used in the 100 msec mixing time experiment so that very weak cross peaks would be distinguished from noise cross peaks. Real cross peaks would intensify with mixing time whereas noise cross peaks would not. The total spectrum was divided into four quadrants namely, (a) the amide to amide region; (b and c) the two amide to aliphatic regions on both sides of the diagonal; and (d) the aliphatic to aliphatic region. The format of the table is as follows: The first column gives the cross peak number as found in the spectrum preceding the table. The second and third columns give the coordinates of the regions of integration; this is the "box" that encloses the cross peak; the coordinates are given in terms of chemical shift. The fourth column gives the integral of the volume. A "+" or "-" means that the positive or negative region of the spectrum was integrated, respectively. The amide to aliphatic and the amide to amide regions are in opposite phase with that of the aliphatic to aliphatic and aliphatic to amide regions of the spectrum because of the P1$\bar{1}$ sequence at the end of the NOESY sequence. The fifth column gives the assignment of the cross peak. An "R" means that the

cross peak is a repeat of another cross peak; only one cross peak from both sides of the diagonal was considered since theoretically, they should be identical. The choice of which of the two cross peaks to be used was based on the resolution (see main text Section 4.5.1.5). The nomenclature used in this assignment was the same as that used in the DSPACE® software in order to facilitate transfer into a constraint file. The name of the hydrogen is followed by the residue number enclosed in a square bracket "[]". The nomenclature of the different hydrogens are as follows: the first letter is h; followed by the position of the hydrogen, e.g., n for amide, a for α, b for β, g for γ, and so on; this is followed by the stereoassignment, either r or s. As an example, one of the β protons of Leu 12 will be named hbr[12]. The methyl groups are represented as a pseudoatom using the symbol m. In cases where two assignments are given, the "&" means that the cross peak is assigned to overlapping cross peaks while "or" means an ambiguous assignment. In cases where the nOe is to an unassigned methyl of an Aib, the residue number is simply given as [B]. Proton resonances of the phenyl sidechain of Phol 20 were not assigned and were written as r*[20]. The sixth column gives the distance range used in the calculation. An "x" means that the cross peak was observed in the 200 msec mixing time spectrum but not in the 100 msec mixing time spectrum. The "#" in the distance range meant that the lower bound was set to the sum of the van der Waals radii.

For Figure 4-19, integrated cross peak volumes greater than 10 were considered strong, integrated cross peak volumes greater than 1.8 but smaller than 10 were considered medium, and integrated cross peak volumes greater than 1.0 but smaller than 1.8 were considered weak.

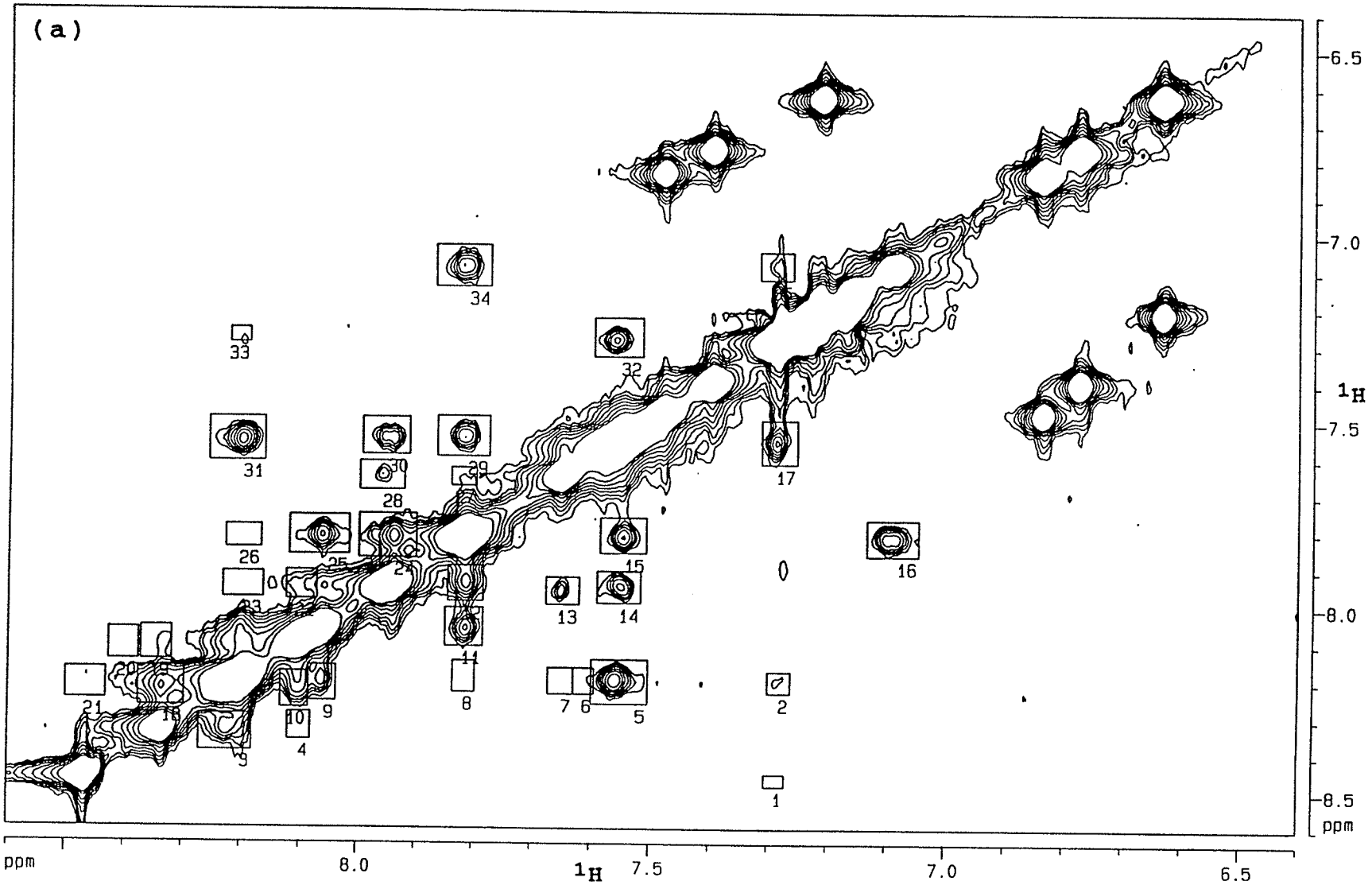
(a)
6.5
7.0
7.5
8.0
8.5
ppm
^{1}H
ppm
8.0
7.5
7.0
6.5
^{1}H
34
33
32
31
30
29
28
17
26
25
24
16
15
13
14
11
8
7
6
5
2
21
10
9
4
1

peak no.	row1(ppm) col1(ppm)	row2(ppm) col2(ppm)	Integral	Assignment	Distance Range
1	8.48323	8.44864	-0.29345	hn[1]-hn[3]	x
	7.30632	7.27181			
2	8.22818	8.17198	-1.2683	hn[3]-hn[5]	# 4.0
	7.30200	7.26318			
3	8.38812	8.28870	-32.615	hn[12]-hn[13]	# 3.0
	8.27248	8.18190			
4	8.35786	8.28438	-0.70769	hn[11]-hn[13]	x
	8.12152	8.08270			
5	8.25844	8.14172	-30.376	hn[4]-hn[5] &	# 5.0
	7.59962	7.50472		hn[9]-hn[10]	# 5.0
6	8.23250	8.16333	-0.85257	unassigned	x
	7.62981	7.59530			
7	8.23250	8.16333	-0.20046	hn[10]-hn[16] or	x
	7.67294	7.62981		hn[12]-hn[16]	
8	8.22818	8.14604	-0.82044	hn[5]-hn[7]	x
	7.83684	7.79802			
9	8.25412	8.15901	-16.591	hn[5]-hn[6]	# 3.0
	8.08701	8.03957			
10	8.27141	8.17630	-20.154	hn[10]-hn[11] &	# 5.0
	8.13446	8.08701		hn[11]-hn[12]	# 5.0
11	8.10714	8.00339	-15.409	hn[6]-hn[7]	# 3.0
	7.84978	7.78508			
12	7.98610	7.89099	-33.445	hn[7]-hn[8]	# 3.0

	7.84547	7.78508				
13	7.99474	7.92125	-4.0801	hn[16]-hn[17]	#	3.5
	7.67725	7.62118				
14	7.99042	7.90396	-10.804	hn[8]-hn[9] &	#	5.0
	7.59099	7.51766		hn[17]-hn[18]	#	5.0
15	7.85641	7.76131	-13.693	hn[18]-hn[19]	#	3.0
	7.58668	7.50904				
16	7.86073	7.76563	-16.933	hn[19]-hn[20]	#	3.0
	7.13379	7.04752				
17	7.61433	7.49761	-18.169	hn[3]-hn[4]	#	3.0
	7.31494	7.25456				
18	8.26708	8.16333	-46.804	R		
	8.37600	8.29836				
19	8.14604	8.05526	-3.5027	hn[11]-hn[13]	#	3.5
	8.37168	8.31993				
20	8.14604	8.05958	-0.21623	unassigned	x	
	8.42776	8.37600				
21	8.24979	8.16766	-2.0488	hn[1]-hn[5]	#	3.5
	8.50108	8.43207				
22	7.98177	7.90396	-8.3122	hn[8]-hn[11]	#	3.5
	8.12583	8.07407				
23	7.97745	7.90828	-1.6419	hn[8]-hn[5] or		
	8.23366	8.16465		hn[8]-hn[10]	#	4.0
24	7.86938	7.75266	-41.857	R		
	8.00075	7.90154				
25	7.86073	7.75698	-17.657	R		
	8.12152	8.01800				

26	7.84344	7.78292	-0.46401	R	
	8.22935	8.16896			
27	7.67485	7.62730	-1.6648	hn[16]-hn[19]	# 4.0
	7.84116	7.79802			
28	7.68782	7.61001	-3.6534	R	
	8.00075	7.92311			
29	7.59704	7.48897	-14.423	R	
	7.86704	7.77646			
30	7.59271	7.49329	-10.247	R	
	7.99643	7.91448			
31	7.61001	7.49329	-25.894	R	
	8.25954	8.16465			
32	7.32902	7.22527	-12.821	R	
	7.59962	7.51766			
33	7.29444	7.25553	-0.60407	R	
	8.22503	8.19053			
34	7.14314	7.03074	-18.952	R	
	7.87135	7.77646			
35	7.12152	7.04803	-3.5253	hn[20]-r*[20]	
	7.31925	7.26318			

The crosspeak between hn[15]-hn[16] was very close to the diagonal and was not integrated, this distance was assigned the upper bound of 4.0. Cross peak numbers 5, 10, and 14 were given an upper bound of 5 Å because of overlap. Cross peak number 22 was first given an upper bound of 3.0 based on the volume but was later changed to 3.5 (see Section 4.5.1.6)

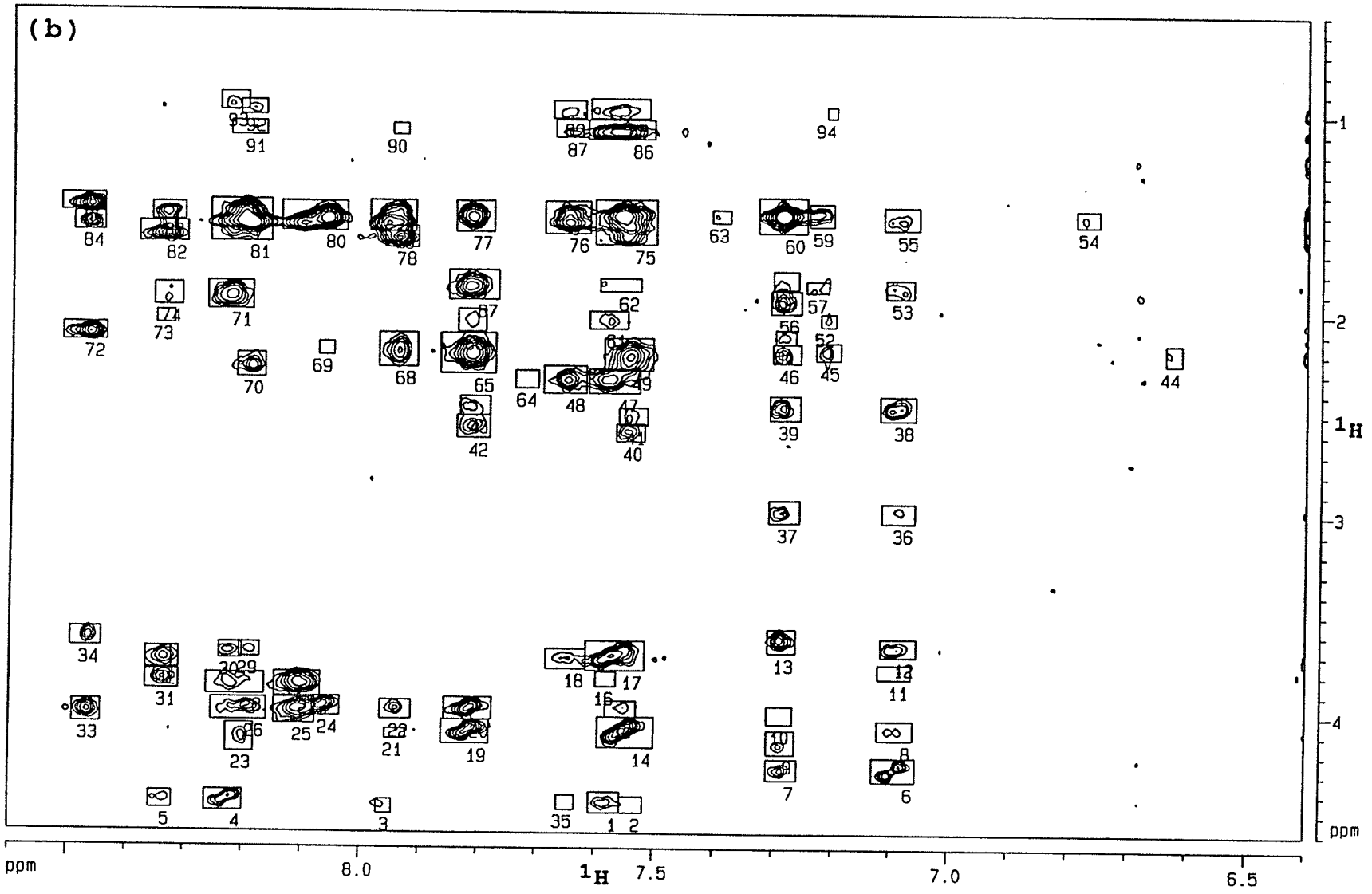
(b)
ppm
8.0
^{1}H
7.5
7.0
6.5
ppm
^{1}H

peak no.	row1(ppm) col1(ppm)	row2(ppm) col2(ppm)	Integral	Assignment	Distance Range
1	4.49610 7.60824	4.39174 7.55648	-4.8641	hn[15]-ha[14]	# 3.5
2	4.49610 7.55648	4.41582 7.51766	-1.2214	hn[18]-ha[14]	# 4.0
3	4.50413 7.97055	4.43188 7.94467	-1.458	hn[17]-ha[14]	# 4.0
4	4.49610 8.26385	4.39174 8.19915	-8.1039	hn[12]-ha[12]	# 3.0
5	4.48808 8.35874	4.39977 8.31993	-2.4065	hn[13]-ha[14] or hn[13]-ha[12]	# 3.5
6	4.33554 7.12947	4.21512 7.05615	-9.9768	hn[20]-ha[20]	# 3.0
7	4.32751 7.31063	4.22315 7.25887	-4.2995	r*[20]-ha[20]	
8	4.12681 7.12085	4.03047 7.06046	-2.9123	hn[20]-ha[19]	# 3.5
9	4.19906 7.31063	4.07864 7.26318	-2.2225	hn[3]-ha[4]	# 3.5
10	4.04652 7.31063	3.95821 7.26750	-1.1036	hn[3]-hds[2]	# 4.0
11	3.82173 7.12085	3.74948 7.06477	-1.4952	hn[20]-hs[20]	# 4.0
12	3.70934	3.62103	-5.8234	hn[20]-hr[20]	# 3.0

	7.11653	7.05615			
13	3.69328	3.57286	-10.751	hn[3]-hdr[2]	# 4.0
	7.31063	7.26318			
14	4.16695	4.01441	-30.64	hn[4]-ha[4] &	# 3.0
	7.59530	7.50041		hn[18]-ha[18]	# 3.0
15	4.01441	3.93413	-3.1297	hn[9]-ha[6]	# 3.5
	7.58236	7.53060			
16	3.86188	3.78962	-1.7212	hn[15]-hds[14]	x
	7.59962	7.56511			
17	3.78159	3.63709	-30.831	hn[15]-ha[15] &	# 3.0
	7.61687	7.51766		hn[15]-hdr[14] &	
				hn[9]-ha[9]	# 3.0
18	3.77357	3.67723	-5.385	hn[16]-hdr[14]	# 3.0
	7.68588	7.61687			
19	4.15089	4.03047	-21.909	hn[19]-ha[19]	# 3.0
	7.86272	7.78077			
20	4.03047	3.91807	-18.839	hn[7]-ha[7]	# 3.0
	7.85841	7.77646			
21	4.12681	4.07864	-0.85747	hn[8]-ha[4]	x
	7.95761	7.92311			
22	4.03047	3.93413	-4.0308	hn[8]-ha[7] or	# 3.5
	7.96624	7.91448		hn[8]-ha[6]	
23	4.19906	4.05455	-4.2373	hn[5]-ha[4]	# 3.5
	8.22935	8.18190			
24	4.01441	3.91807	-13.37	hn[6]-ha[6]	# 3.0
	8.08270	8.03525			
25	4.05455	3.92610	-22.825	hn[11]-has[11]	# 3.0

	8.14740	8.07838		
26	4.03850	3.92610	-10.195	hn[12]-has[11] & # 5.0
	8.25523	8.16034		hn[10]-has[11] # 5.0
27	3.91807	3.79765	-33.692	hn[11]-har[11] # 3.0
	8.14740	8.06976		
28	3.91004	3.80568	-9.1801	hn[12]-har[11] or # 3.5
	8.26385	8.16465		hn[10]-har[11] or
				hn[10]-ha[7]
29	3.72540	3.65314	-1.7691	hn[10]-ha[9] # 4.0
	8.20778	8.17327		
30	3.73342	3.65314	-3.1511	hn[12]-ha[9] # 3.5
	8.24229	8.20347		
31	3.88596	3.78962	-8.1845	hn[13]-hds[14] # 3.0
	8.36737	8.31130		
32	3.78159	3.67723	-11.131	hn[13]-hdr[14] # 3.0
	8.36737	8.31130		
33	4.05455	3.94216	-9.745	hn[1]-hds[2] # 3.0
	8.49245	8.44501		
34	3.67723	3.58089	-5.1679	hn[1]-hdr[2] # 3.0
	8.49677	8.44501		
35	4.48005	4.40779	-0.89646	hn[16]-ha[14] x
	7.66431	7.63412		
36	3.04300	2.94666	-1.96	hn[20]-hbs[20] # 3.5
	7.11653	7.06046		
37	3.04300	2.93060	-5.1404	r*[20]-hb[20]
	7.31063	7.25887		
38	2.52919	2.40877	-10.43	hn[20]-hbr[20] # 3.0

	7.12085	7.06046		
39	2.52919	2.40877	-8.4388	r*[20]-hb[20]
	7.31063	7.25887		
40	2.64159	2.55328	-5.91	hn[18]-hgr[18] # 3.0
	7.56942	7.52198		
41	2.56131	2.47300	-4.2721	hn[18]-hgs[18] # 3.5
	7.56511	7.51766		
42	2.62553	2.51314	-8.8424	hn[7]-hgr[7] # 3.0
	7.84116	7.78508		
43	2.51314	2.41680	-5.7928	hn[7]-hgs[7] # 3.0
	7.83684	7.78508		
44	2.24821	2.14384	-1.4964	he[Q]-hb[Q] x
	6.63776	6.61189		
45	2.23215	2.14384	-3.8366	r*[20]-hbr[18]
	7.23299	7.18986		
46	2.24821	2.15187	-4.7801	r*[20]-hbr[18] or
	7.30632	7.25887		hn[3]-hbr[7] # 3.5
47	2.40074	2.28032	-30.35	hn[15]-hb[15] # 3.0
	7.61687	7.53060		
48	2.40074	2.26426	-16.46	hn[16]-hb[15] # 3.0
	7.69451	7.62118		
49	2.28835	2.12778	-51.862	hn[18]-hbr[18] # 3.0
	7.59099	7.50904		
50	2.15187	2.07961	-2.0092	hn[3]-m[0] # 4.0
	7.30200	7.26750		
51	2.15187	2.07961	-2.0092	identical to 50
	7.30200	7.26750		

52	2.06356	1.99933	-1.5893	r*[20]-hgr[19]
	7.22436	7.19848		
53	1.91905	1.83074	-4.8079	hn[20]-hbs[19] # 3.5
	7.11222	7.06477		
54	1.55778	1.47750	-1.7214	he[Q]-mb[B]
	6.78873	6.74991		
55	1.58186	1.46947	-4.8175	hn[20]-mb[B]
	7.11653	7.05615		
56	1.99933	1.88694	-10.719	hn[3]-hg[12] or
	7.31063	7.25887		r*[20]-hg[12]
57	1.89497	1.83877	-2.4212	r*[20]-hb[19] x
	7.25024	7.21142		
58	1.87891	1.79060	-2.9063	R
	7.30632	7.26318		
59	1.56581	1.45341	-7.6193	r*[20]-mb[B]
	7.24593	7.20280		
60	1.59792	1.42130	-69.608	hn[3]-mbr[3] & # 3.5
	7.33219	7.25024		hn[3]-mbs[3]
61	2.07961	1.99130	-4.5348	hn[15]-hgr[14]or # 3.5
	7.61687	7.55217		hn[15]-hgr[19]
62	1.89497	1.83074	-1.3228	R
	7.59962	7.53060		
63	1.54975	1.48553	-0.92491	he[Q]-mb[B]
	7.40983	7.37964		
64	2.37666	2.28835	-0.63109	unassigned x
	7.74195	7.70313		
65	2.30440	2.10370	-61.325	hn[7]-hbr[7] # 3.0

	7.87135	7.77646		
66	2.09567	1.98328	-4.7517	hn[19]-hgr[19] # 3.5
	7.84116	7.79371		
67	1.93511	1.79060	-32.623	hn[19]-hbs[19] # 3.0
	7.85841	7.77214		
68	2.27229	2.10370	-17.351	hn[8]-hbr[7] # 3.0
	7.97487	7.91017		
69	2.21609	2.15187	-0.099767	hn[6]-hgr[7] x
	8.07838	8.05250		
70	2.32849	2.20807	-10.009	hn[10]-hb[15] # 3.0
	8.21641	8.16896		
71	1.99130	1.85482	-24.395	hn[12]-hg[12] & # 5.0
	8.26817	8.19053		hn[12]-hbr[12] # 5.0
72	2.15187	2.06356	-22.035	hn[1]-m[0] # 3.5
	8.51402	8.44070		
73	2.06356	1.99933	-0.5803	hn[13]-hgr[14] x
	8.35443	8.32424		
74	1.97525	1.86285	-3.0997	R
	8.35874	8.31130		
75	1.66215	1.43736	-119.1	R
	7.60824	7.50472		
76	1.60595	1.44539	-37.994	R
	7.69451	7.61687		
77	1.59792	1.44539	-24.958	hn[7]-mb[6] & # 5.0
	7.84547	7.78077		hn[19]-mb[B]
78	1.67820	1.57384	-46.635	R
	7.96624	7.91017		

79	1.59792	1.44539	-59.91	R
	7.99212	7.91448		
80	1.59792	1.45341	-81.143	hn[11]-mb[B] &
	8.14308	8.03094		hn[6]-mb[6] # 3.5
81	1.65412	1.44539	-127.65	R
	8.26385	8.16034		
82	1.66215	1.55778	-24.361	R
	8.38462	8.30267		
83	1.54975	1.46144	-8.3027	R
	8.36306	8.30698		
84	1.60595	1.51764	-8.6182	hn[1]-mbs[1] # 3.5
	8.49677	8.44501		
85	1.50961	1.42130	-24.753	hn[1]-mbr[1] # 3.5
	8.51833	8.44501		
86	1.13229	1.03595	-32.836	hn[9]-mgr[9] & # 5.0
	7.62118	7.50904		hn[15]-mgr[15] # 5.0
87	1.12426	1.03595	-3.743	hn[16]-mgr[15] # 4.0
	7.67725	7.62118		
88	1.02792	0.93158	-9.127	hn[9]-mgs[9] & # 5.0
	7.61687	7.51766		hn[15]-mgs[15] # 5.0
89	1.02792	0.93961	-3.9325	hn[16]-mgs[15] # 4.0
	7.68157	7.62549		
90	1.11623	1.06003	-0.6754	hn[8]-mgr[9] x
	7.95330	7.92742		
91	1.12426	1.05200	-1.6449	hn[10]-mgr[9] # 4.0
	8.22935	8.16896		
92	1.01989	0.94764	-2.4729	hn[10]-mgs[9] # 4.0

	8.21209	8.16896		
93	0.99581	0.90750	-3.4638	hn[12]-mdr[12] # 4.0
	8.24660	8.19915		
94	1.01989	0.96369	-0.34622	r*[20]-mgs[15] x
	7.21574	7.19848		

The upper bounds of cross peak numbers 13, 18, and 28 were increased from 3.0 to 4.0, 3.5, and 3.5, respectively (see Section 4.5.1.6)

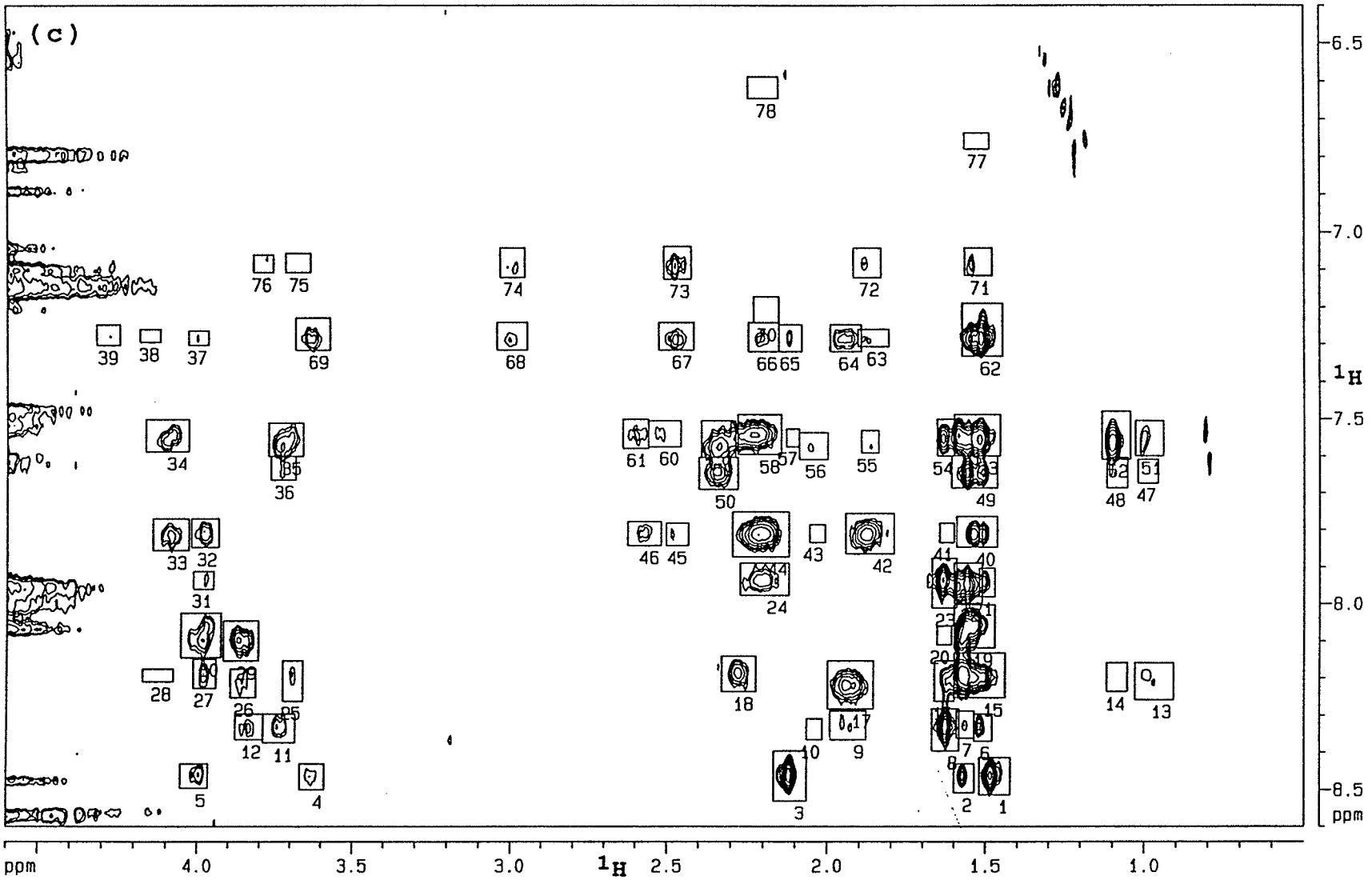
(c)
78
77
76 75
74
73
72
71
39 38 37
69
68
67
66 65
64 63
62
34
36
61 60
58 57
56
55
54
49
48 47
50
33 32
31
46 45
43
42
24
28
27
26
12 11
18
10
9
15
14
13
5
4
3
2 1
ppm
4.0
3.5
3.0
1H
2.5
2.0
1.5
1.0
6.5
7.0
1H
7.5
8.0
8.5
ppm

peak no.	row1(ppm) col1(ppm)	row2(ppm) col2(ppm)	Integral	Assignment	Distance Range
1	8.51349	8.41406	28.887	R	
	1.51859	1.42225			
2	8.50916	8.43135	5.8675	R	
	1.59887	1.53464			
3	8.53078	8.39677	35.855	R	
	2.16887	2.06450			
4	8.50052	8.43135	4.2339	R	
	3.67015	3.58986			
5	8.49620	8.43135	6.1259	R	
	4.05550	3.96719			
6	8.37083	8.29734	4.6275	hn[13]-mbs[13]	# 4.0
	1.53464	1.47845			
7	8.36219	8.28870	2.0851	hn[13]-mb[B]	
	1.59084	1.53464			
8	8.39677	8.28438	26.781	hn[13]-mbr[13]	# 3.5
	1.67112	1.58281			
9	8.36651	8.28870	4.5485	hn[13]-hbr[12] or	# 3.5
	1.99225	1.87986		hn[13]-hg[12]	
10	8.36651	8.31031	0.71462	hn[13]-hgr[14]	x
	2.06450	2.01634			
11	8.37516	8.29734	7.7615	R	
	3.79057	3.68620			
12	8.36651	8.29734	4.8956	R	

	3.87888	3.79057				
13	8.25844	8.15901	5.4029	R		
	1.02887	0.90844				
14	8.23682	8.15901	1.1872	R		
	1.11718	1.05295				
15	8.25412	8.13307	116.22	hn[12]-mb[B]		
	1.59887	1.43830				
16	8.26276	8.15469	10.584	hn[12]-mbr[13]	#	3.5
	1.66309	1.59887				
17	8.28438	8.15469	32.988	R		
	2.00028	1.85577				
18	8.23682	8.14172	13.144	R		
	2.32944	2.22507				
19	8.12011	8.00339	74.9	R		
	1.59887	1.47042				
20	8.11146	8.05958	0.44581	hn[11]-mb[13]	x	
	1.65507	1.60690				
21	7.98177	7.90396	6.4748	hn[8]-mbr[8]	#	3.5
	1.51859	1.47042				
22	7.99906	7.89099	46.998	hn[17]-mbr[17]	#	3.5
	1.59887	1.51056		hn[17]-mbs[17]		
23	8.01203	7.87802	35.438	hn[8]-mbs[8]	#	3.5
	1.67112	1.59084				
24	7.97745	7.89099	16.391	R		
	2.27324	2.12070				
25	8.26276	8.15469	4.6945	R		
	3.72634	3.66212				

26	8.25412	8.17630	5.5204	R	
	3.89494	3.81465			
27	8.22818	8.15037	5.7153	R	
	4.01536	3.94310			
28	8.21089	8.17630	2.0882	R	
	4.17592	4.07958			
29	8.15469	8.04662	18.678	R	
	3.91902	3.80662			
30	8.14604	8.02500	18.097	R	
	4.05550	3.92705			
31	7.96016	7.91261	1.8415	R	
	4.01536	3.95113			
32	7.84776	7.76995	8.7939	R	
	4.02339	3.93508			
33	7.85641	7.76995	9.988	R	
	4.14381	4.03141			
34	7.58839	7.50193	11.637	R	
	4.16789	4.03141			
35	7.60136	7.51058	17.225	R	
	3.77451	3.66212			
36	7.66620	7.60136	5.2594	R	
	3.76648	3.68620			
37	7.30308	7.26417	1.1235	hn[3]-hdr[2]	# 4.0
	4.03141	3.96719			
38	7.29444	7.25985	0.69394	hn[3]-ha[4]	x
	4.18395	4.11973			
39	7.30308	7.24688	2.3744	R	

	4.32043	4.24818			
40	7.84776	7.76563	16.089	R	
	1.59084	1.46239			
41	7.83480	7.78292	0.26654	hn[7]-mb[8]	x
	1.64704	1.59887			
42	7.86506	7.75698	30.44	R	
	1.94408	1.79155			
43	7.83480	7.78724	1.268	R	
	2.05648	2.00831			
44	7.87370	7.75266	54.046	R	
	2.29732	2.12070			
45	7.84344	7.78292	2.7651	R	
	2.50606	2.43380			
46	7.84344	7.77860	5.8537	R	
	2.62648	2.52211			
47	7.67485	7.61001	1.2928	R	
	1.02084	0.95661			
48	7.68782	7.60568	4.6781	R	
	1.11718	1.05295			
49	7.68782	7.60136	35.015	hn[16]-mbr[16] & # 3.5	
	1.60690	1.46239		hn[16]-mbs[16] # 3.5	
50	7.69214	7.60568	20.611	R	
	2.40169	2.28127			
51	7.60136	7.50626	6.3479	R	
	1.02887	0.94055			
52	7.61001	7.48032	25.837	R	
	1.13323	1.04492			

53	7.60136	7.48897	83.914	hn[4]-mb[B] or		
	1.59887	1.45436		hn[9]-mb[B] or		
				hn[18]-mb[B]		
54	7.60136	7.50193	12.052	hn[4]-mb[B] or		
	1.65507	1.59887		hn[9]-mb[B] or		
				hn[18]-mb[B]		
55	7.59271	7.53219	1.8898	hn[18]-hbr[19]	#	3.5
	1.89591	1.83971				
56	7.61001	7.53652	2.7763	R		
	2.08859	2.00028				
57	7.57542	7.52787	0.27263	hn[4]-m[0]	x	
	2.12873	2.08859				
58	7.59704	7.48897	41.315	R		
	2.28127	2.14479				
59	7.60568	7.50626	25.642	R		
	2.39366	2.28929				
60	7.57542	7.50626	4.1309	R		
	2.56225	2.45789				
61	7.57975	7.50193	6.3239	R		
	2.64253	2.56225				
62	7.33334	7.19069	59.71	R		
	1.57478	1.44633				
63	7.30740	7.25985	3.3706	r*[20]-hbr[19]		
	1.90394	1.80760				
64	7.32037	7.24688	10.405	R		
	1.99225	1.89591				
65	7.32037	7.24688	2.4552	hn[3]-m[0]	#	4.0

	2.15282	2.08056		
66	7.32037	7.24256	5.2082	R
	2.24915	2.15282		
67	7.31605	7.24256	8.0258	R
	2.53014	2.41775		
68	7.31605	7.24256	4.2678	R
	3.04395	2.94761		
69	7.31605	7.22959	8.8942	R
	3.68620	3.57381		
70	7.24256	7.17340	2.8888	R
	2.23310	2.15282		
71	7.11720	7.04371	3.3775	R
	1.56676	1.47845		
72	7.12152	7.04371	3.5958	R
	1.92000	1.83169		
73	7.12584	7.03939	9.1082	R
	2.51408	2.42577		
74	7.12152	7.04371	3.6366	R
	3.03592	2.95564		
75	7.10855	7.05668	2.1783	R
	3.71831	3.63803		
76	7.10855	7.06100	1.141	R
	3.82268	3.75846		
77	6.78001	6.73678	1.9066	R
	1.56676	1.48647		
78	6.64600	6.58981	2.8176	R
	2.24915	2.15282		

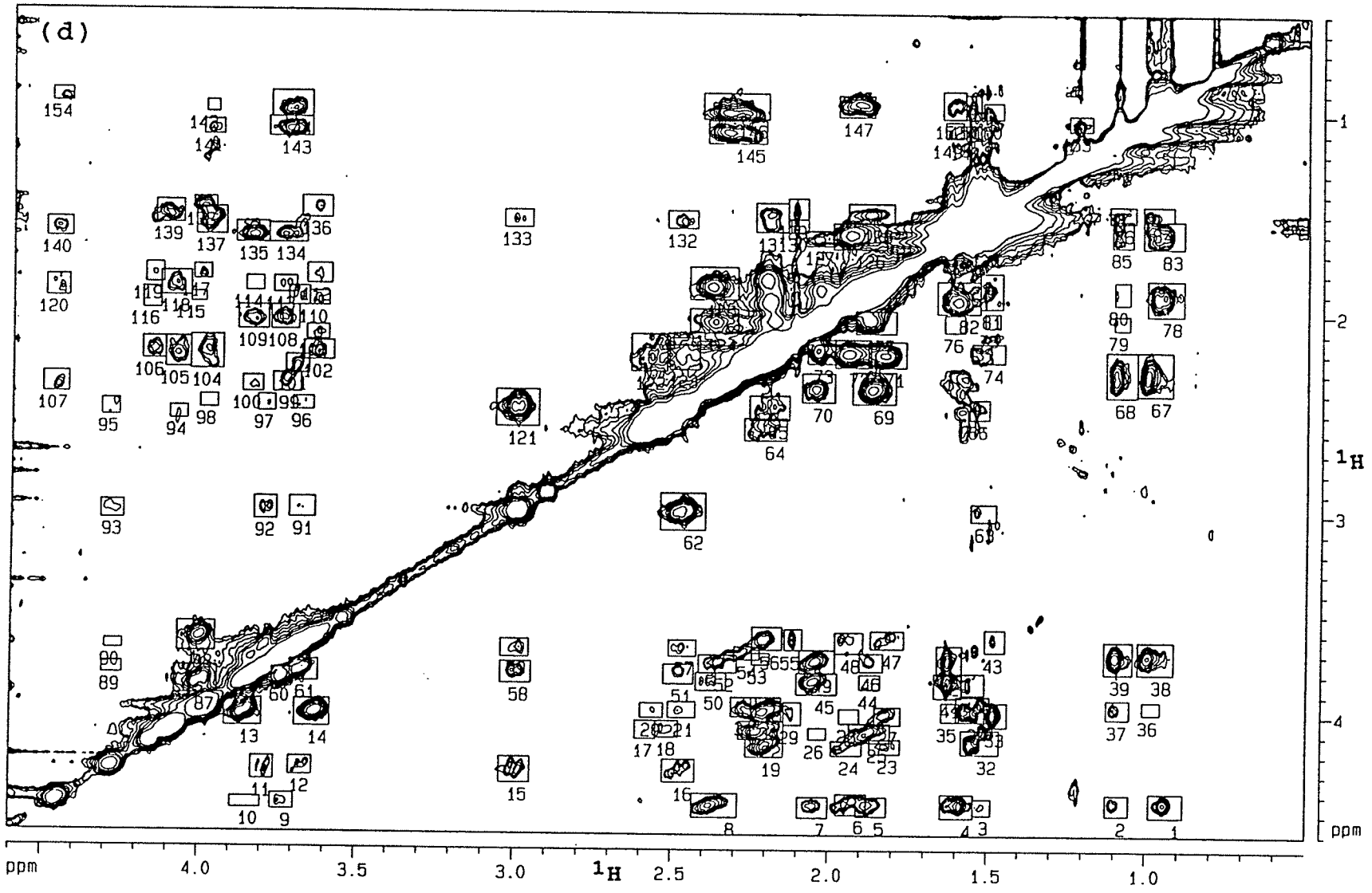
(d)
ppm
4.0
3.5
3.0
^{1}H
2.5
2.0
1.5
1.0
ppm
^{1}H

peak no.	row1(ppm) col1(ppm)	row2(ppm) col2(ppm)	Integral	Assignment	Distance Range
1	4.50413 0.98872	4.38371 0.88436	18.748	ha[12]-mdr[12]	# 3.5
2	4.49610 1.12520	4.39174 1.05295	6.0198	ha[14]-mgr[15]	# 3.5
3	4.49610 1.54267	4.41582 1.48647	3.3696	ha[12]-mb[B] or ha[14]-mb[B]	
4	4.51216 1.64704	4.39174 1.54267	36.244	ha[12]-hbs[12]	# 3.0
5	4.50413 1.91197	4.40779 1.81563	20.981	ha[14]-hbs[14]	# 3.0
6	4.49610 1.97619	4.39174 1.87986	23.265	ha[12]-hbr[12] or ha[12]-hg[12]	# 3.0
7	4.51216 2.09662	4.40779 2.00028	10.384	ha[14]-hgr[14]	# 3.0
8	4.51216 2.43380	4.39174 2.28929	44.37	ha[14]-hbr[14]	# 3.0
9	4.48808 3.76648	4.40779 3.69423	4.7222	ha[14]-hdr[14]	# 3.5
10	4.48005 3.89494	4.42385 3.79860	2.9517	R	
11	4.33554 3.83071	4.22315 3.75846	6.6573	ha[20]-hs[20]	# 3.0
12	4.31145	4.22315	4.7448	ha[20]-hr[20]	# 3.5

	3.71029	3.63803		
13	4.07061	3.93413	77.575	har[11]-has[11] # 3.0
	3.91902	3.79860		
14	4.07061	3.93413	63.904	hdr[2]-hds[2] # 3.0
	3.69423	3.58184		
15	4.34357	4.21512	17.109	ha[20]-hbs[20] # 3.0
	3.04395	2.94761		
16	4.33554	4.22315	12.069	ha[20]-hbr[20] # 3.0
	2.53014	2.42577		
17	4.11878	4.03047	2.9804	ha[18]-hgr[18] # 3.5
	2.61845	2.55422		
18	4.11075	4.03047	6.6295	ha[18]-hgs[18] # 3.0
	2.55422	2.48197		
19	4.20709	4.11878	35.5	ha[2]-hbr[2] # 3.0
	2.26521	2.14479		
20	4.01441	3.94216	2.6683	ha[7]-hgr[7] # 3.5
	2.60239	2.53014		
21	4.01441	3.93413	4.3405	ha[7]-hgs[7] # 3.5
	2.51408	2.42577		
22	4.11878	4.03047	52.457	ha[18]-hbr[18] # 3.0
	2.28929	2.14479		
23	4.19103	4.11878	5.5746	ha[2]-hgr[2] # 3.0
	1.87183	1.77549		
24	4.19906	4.12681	9.3568	ha[2]-hbs[2] # 3.0
	1.99225	1.89591		
25	4.13483	4.03850	35.709	ha[19]-hbr[19] # 3.0
	1.93605	1.80760		

26	4.11878	4.06258	0.33642	ha[7]-hgr[7] x
	2.06450	2.00831		
27	4.04652	3.95821	11.678	hgr[2]-hds[2] # 3.0
	1.85577	1.77549		
28	4.03850	3.96624	1.238	R
	1.96817	1.90394		
29	4.04652	3.93413	5.1139	m[0]-hds[2] # 3.5
	2.14479	2.08859		
30	4.03047	3.91004	46.336	ha[7]-hbr[7] # 3.0
	2.24915	2.15282		
31	4.00638	3.91004	16.169	ha[6]-hb[9] # 3.5
	2.31338	2.23310		
32	4.19103	4.07061	60.848	ha[4]-mb[4] # 3.5
	1.58281	1.46239		
33	4.05455	3.93413	34.528	hds[2]-mb[B]
	1.51056	1.43830		
34	4.03047	3.90202	71.246	ha[6]-mb[6] # 3.5
	1.59887	1.49450		
35	4.03047	3.93413	2.9415	R
	1.64704	1.59084		
36	3.99033	3.92610	1.1878	R
	1.01281	0.95661		
37	4.01441	3.91807	5.9517	ha[6]-mgr[9] or # 4.0
	1.12520	1.05295		ha[7]-mgr[9]
38	3.78962	3.62906	42.771	ha[9]-mgr[9] & # 5.0
	1.02887	0.91647		ha[15]-mgr[15] # 5.0
39	3.78962	3.62906	42.011	ha[9]-mgs[9] & # 3.5

	1.13323	1.04492		ha[15]-mgs[15] # 3.5
40	3.89399	3.78962	6.6555	hdr[14]-mb[B]
	1.58281	1.51056		
41	3.91004	3.78962	47.032	hdr[14]-mb[B]
	1.67112	1.58281		
42	3.79765	3.65314	30.316	hds[14]-mb[B]
	1.66309	1.58281		
43	3.68526	3.57286	3.0302	hdr[2]-mb[B]
	1.51056	1.44633		
44	3.86990	3.79765	1.9658	R
	1.90394	1.83971		
45	3.89399	3.78962	27.008	hds[14]-hgr[14] # 3.0
	2.10465	1.97619		
46	3.78159	3.69328	7.1798	hdr[14]-hbs[14] # 3.0
	1.90394	1.83169		
47	3.66920	3.58089	8.9613	hdr[2]-hgr[2] # 3.0
	1.87183	1.76746		
48	3.69328	3.58892	9.0719	hdr[2]-hbs[2] # 3.0
	1.98422	1.89591		
49	3.78962	3.67723	28.8	hdr[14]-hgr[14] # 3.0
	2.09662	1.98422		
50	3.87793	3.78962	7.3997	hds[14]-hbr[14] # 3.0
	2.42577	2.32944		
51	3.84582	3.74948	7.1233	hbr[20]-hs[20] # 3.0
	2.53014	2.43380		
52	3.78962	3.70131	18.868	ha[15]-hb[15] # 3.0
	2.41775	2.29732		

53	3.74948	3.69328	1.8381	R
	2.24915	2.19296		
54	3.72540	3.66117	11.648	ha[9]-hb[9] # 3.0
	2.30535	2.22507		
55	3.67723	3.57286	6.7673	m[0]-hdr[2] # 3.5
	2.14479	2.08859		
56	3.67723	3.56483	18.779	hdr[2]-hbr[2] # 3.0
	2.24915	2.15282		
57	3.70934	3.62906	5.3762	hbr[20]-hr[20] # 3.0
	2.51408	2.42577		
58	3.84582	3.74145	10.858	hbs[20]-hs[20] # 3.0
	3.04395	2.94761		
59	3.71737	3.62906	7.4133	hbs[20]-hr[20] # 3.0
	3.04395	2.95564		
60	3.86188	3.78159	78.286	hdr[14]-hds[14] # 3.0
	3.76648	3.70226		
61	3.84582	3.74145	81.231	hr[20]-hs[20] # 3.0
	3.71029	3.62198		
62	3.08314	2.89849	133.27	hbr[20]-hbs[20] # 3.0
	2.54620	2.40169		
63	3.03497	2.94666	5.466	R
	1.55873	1.47845		
64	2.63356	2.52116	28.19	hbr[7]-hgr[7] & # 3.0
	2.28127	2.14479		hbr[18]-hgr[18] # 3.0
65	2.52919	2.40877	26.397	hbr[7]-hgs[7] & # 3.0
	2.26521	2.13676		hbr[18]-hgs[18] # 3.0
66	2.52116	2.42483	12.372	R

	1.56676	1.50253		
67	2.40074	2.18398	69.232	hb[9]-mgr[9] & # 3.5
	1.03689	0.92450		hb[15]-mgr[15] # 3.5
68	2.40877	2.18398	55.222	hb[9]-mgs[9] & # 3.5
	1.13323	1.03689		hb[15]-mgs[15] # 3.5
69	2.44891	2.28835	103.77	hbs[14]-hbr[14] # 3.0
	1.93605	1.79957		
70	2.44088	2.29638	27.051	hbr[14]-hgr[14] # 3.0
	2.09662	1.99225		
71	2.26426	2.13581	104.1	hgr[2]-hbr[2] # 3.0
	1.88788	1.76746		
72	2.26426	2.12778	125.06	hgr[2]-hbs[2] # 3.0
	1.99225	1.87986		
73	2.24821	2.12778	85.523	hgr[14]-hbr[18] # 3.0
	2.08056	1.99225		hgr[14]-hbr[7]
74	2.24018	2.14384	17.296	hgr[2]-mb[B]
	1.55873	1.45436		
75	2.06356	1.99130	0.068631	unassigned
	1.51859	1.47042		
76	2.08764	1.99933	1.2769	R
	1.64704	1.58281		
77	2.09567	1.98328	101.1	hgr[14]-hbs[14] # 3.0
	1.92803	1.79957		
78	1.99933	1.82271	60.608	mgr[12]-hg[12] & # 5.0
	1.00478	0.89239		mgr[12]-hbr[12] # 5.0
79	2.07159	1.99933	1.4086	R
	1.10915	1.06098		

80	1.94314	1.83074	2.7206	R
	1.10915	1.06098		
81	1.96722	1.79060	18.285	unassigned
	1.53464	1.46239		
82	1.99130	1.83074	119.34	hbs[12]-hbr[12] # 3.0
	1.67112	1.53464		hbs[12]-hg[12]
83	1.66215	1.52567	47.936	hbs[12]-mdr[12] # 3.5
	1.02084	0.89239		
84	1.52567	1.45341	10.038	hgr[9]-mb[B]
	1.02084	0.92450		hgr[15]-mb[B]
85	1.65412	1.52567	12.726	hgs[9]-mb[B]
	1.11718	1.05295		hgs[15]-mb[B]
86	1.53370	1.45341	8.9579	hgs[9]-mb[B]
	1.12520	1.04492		hgs[15]-mb[B]
87	3.91004	3.77357	119.85	R
	4.07958	3.94310		
88	3.70131	3.55680	67.96	R
	4.07156	3.95113		
89	3.81371	3.75751	1.7329	x
	4.31240	4.24818		
90	3.69328	3.64511	0.3079	x
	4.30437	4.24818		
91	3.03497	2.93060	3.2984	R
	3.71831	3.63803		
92	3.04300	2.93060	6.2477	R
	3.83071	3.75846		
93	3.04300	2.95469	6.168	R

	4.32043	4.24818		
94	2.54525	2.48102	2.8214	R
	4.10367	4.04747		
95	2.52919	2.44891	3.8864	R
	4.32043	4.26423		
96	2.49708	2.43285	2.7301	R
	3.71029	3.64606		
97	2.50511	2.42483	2.4617	R
	3.82268	3.76648		
98	2.48905	2.42483	1.8298	ha[19]-hgs[19] # 5.0
	4.00733	3.95113		
99	2.40877	2.31243	10.677	R
	3.77451	3.68620		
100	2.40877	2.32849	4.3372	R
	3.87085	3.80662		
101	2.31243	2.22412	8.9735	R
	3.73437	3.66212		
102	2.24821	2.15187	11.387	R
	3.67817	3.58184		
103	2.14384	2.07159	4.6724	R
	3.67015	3.59789		
104	2.29638	2.12778	22.725	R
	4.03944	3.93508		
105	2.28835	2.13581	18.763	R
	4.11973	4.03944		
106	2.24821	2.13581	9.6785	R
	4.19198	4.11973		

107	2.41680	2.31243	6.343	R
	4.50508	4.42480		
108	2.09567	1.97525	15.407	R
	3.78254	3.69423		
109	2.09567	1.97525	15.303	R
	3.88691	3.79057		
110	1.97525	1.90299	4.9017	R
	3.66212	3.59789		
111	1.97525	1.87891	5.0944	R
	3.72634	3.66212		
112	1.86285	1.76651	5.1155	R
	3.67015	3.58986		
113	1.91102	1.83074	4.8671	R
	3.77451	3.70226		
114	1.90299	1.83074	1.4731	hdr[14]-hbs[14] # 5.0
	3.86282	3.80662		
115	1.95919	1.91102	0.20978	hdr[2]-hbr[2] x
	4.03944	3.99127		
116	1.99130	1.88694	1.9446	ha[2]-hbr[2] # 4.0
	4.19198	4.13578		
117	1.84680	1.77454	3.8433	R
	4.03141	3.97522		
118	1.92708	1.80666	13.494	R
	4.13578	4.03944		
119	1.86285	1.76651	2.4452	R
	4.18395	4.12775		
120	1.93511	1.83074	5.4291	R

	4.49705	4.42480		
121	2.56933	2.38469	120.15	R
	3.06803	2.93155		
122	2.28835	2.10370	62.413	R
	2.64253	2.53014		
123	2.28032	2.11976	74.556	R
	2.52211	2.42577		
124	2.09567	1.97525	55.938	R
	2.45789	2.30535		
125	1.92708	1.76651	122.16	R
	2.45789	2.30535		
126	1.67017	1.54172	175.23	R
	2.00028	1.83169		
127	1.65412	1.58186	12.436	mdr[12]-hgr[14] # 3.5
	2.08859	1.99225		
128	1.54172	1.44539	35.037	R
	1.95211	1.80760		
129	1.52567	1.42130	7.5507	m[0]-mb[B]
	2.14479	2.08056		
130	1.58989	1.52567	4.457	m[0]-mb[B]
	2.13676	2.08056		
131	1.58989	1.44539	22.414	R
	2.24915	2.14479		
132	1.57384	1.48553	7.8775	hr[20]-mb[B]
	2.53014	2.43380		
133	1.57384	1.48553	4.6214	hbs[20]-mb[B]
	3.04395	2.95564		

134	1.66215	1.56581	16.729	R
	3.79057	3.67015		
135	1.66215	1.55778	31.309	R
	3.89494	3.79057		
136	1.53370	1.42933	6.7805	R
	3.68620	3.58986		
137	1.62201	1.48553	43.955	R
	4.02339	3.92705		
138	1.49355	1.43736	12.986	R
	4.03141	3.95916		
139	1.56581	1.45341	22.363	R
	4.15184	4.06353		
140	1.63806	1.54172	7.266	R
	4.49705	4.41677		
141	1.12426	1.05200	4.2915	R
	3.99930	3.93508		
142	1.01186	0.95566	0.8873	unassigned
	3.99127	3.95113		
143	1.13229	1.03595	35.226	R
	3.79057	3.65409		
144	1.03595	0.90750	31.718	R
	3.78254	3.65409		
145	1.14834	1.03595	92.96	R
	2.40169	2.21704		
146	1.02792	0.89947	105.8	R
	2.41775	2.20901		
147	1.01186	0.90750	63.236	R

	1.98422	1.87183		
148	1.12426	1.05200	15.356	R
	1.58281	1.53464		
149	1.11623	1.03595	1.0777	R
	1.64704	1.59084		
150	1.01989	0.93961	11.156	R
	1.52661	1.46239		
151	1.01989	0.89947	19.774	R
	1.58281	1.53464		
152	1.01989	0.88341	13.89	R
	1.65507	1.58281		
153	1.07609	1.00383	14.606	unassigned
	1.25365	1.18140		
154	0.96369	0.89947	3.2751	R
	4.48100	4.41677		

Distance constraints from cross peak numbers 46, 48, 50, 114, and 116 were removed from the contraints file because these distort the Pro ring giving a very high penalty.

Appendix C: Standard IUPAC nomenclature for dihedral angles in peptides.

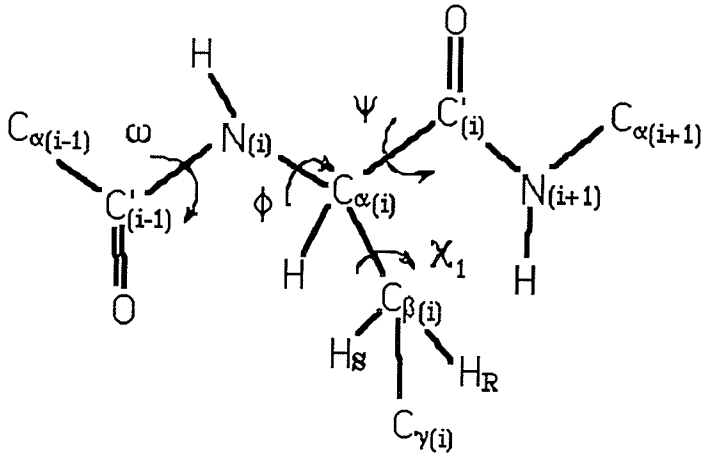

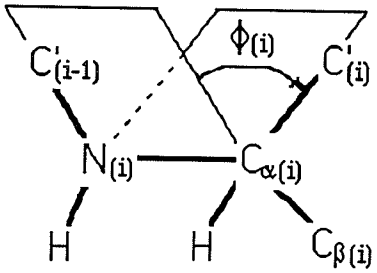

e.g., $\phi_{(i)} = -57°$

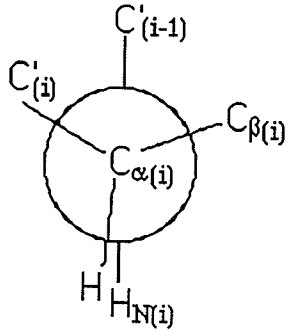

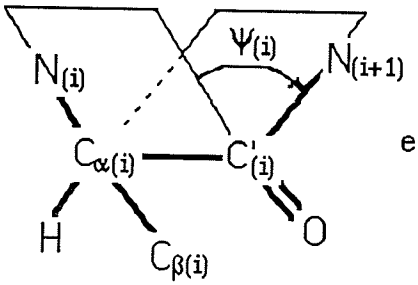

e.g., $\Psi_{(i)} = -47°$

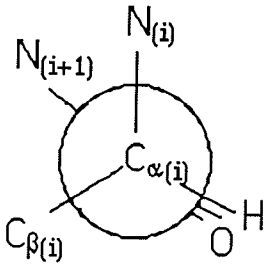

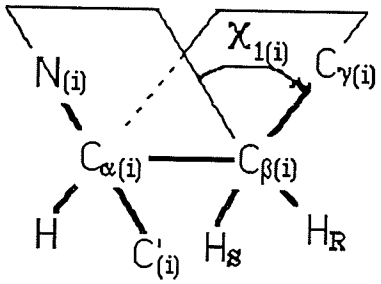

e.g., $\chi_{1(i)} = 60°$

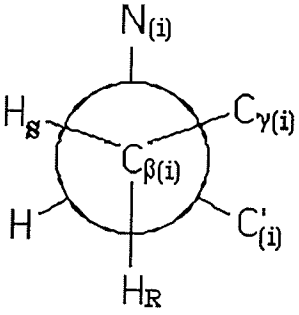

References

Ando, S., Ando, I., Shoji, A., & Ozaki, T. (1988) *J. Am. Chem. Soc. 110*, 3380-3386.

Arrowsmith, C.H., Pachter, R., Altman, R.B., Iyer, S.B., & Jardetzky, O. (1990) *Biochemistry 29*, 6332-6341.

Asakawa, N., Kuroki, S., Kurosu, H., Ando, I., Shoji, A., & Ozaki, T. (1992) *J. Am. Chem. Soc. 114*, 3261-3265.

Augsperger, J.D., Bindra, V.A., Scheraga, H.A., & Kuki, A. (1995) *Biochemistry 34*, 2566-2576.

Babiuk, R. (1995) M.Sc. Thesis, University of Manitoba.

Bai, Y., Milne, J.S., Mayne, L. & Englander, S.W. (1993) *Proteins: Struct., Funct., and Genet. 17*, 75-86.

Balasubramanian, T.M., Kendrick, N.C.E., Taylor, M., Marshall, G.R., Hall, J.E., Vodyanoy, I., & Reusser, F. (1981) *J. Am. Chem. Soc. 103*, 6127-6132.

Baleja, J.D., Moult, J., & Sykes, B.D. (1990) *J. Magn. Reson. 87*, 375-384.

Banerjee, U. & Chan, S.I. (1983) *Biochemistry 22*, 3709-3713.

Banerjee, U., Tsui, F.P., Balasubramanian, T.N., Marshall, G.R., & Chan, S.I. (1983) *J. Mol. Biol. 165*, 757-775.

Barksdale, A.D. & Rosenberg, A. (1982) *Methods Biochem. Anl. 28*, 1-113.

Basu, G. & Kuki, A. (1993) *Biopolymers 33*, 995-1000.

Bax, A. & Davis, D.G. (1985) J. Magn. Reson. 65, 355-545.

Bax, A. & Freeman, R. (1981) *J. Magn. Reson. 44*, 542-545.

Bax, A. & Freeman, R. (1982) *J. Am. Chem. Soc. 104*, 1099-

1100.

Bax, A., Griffey, R.H., & Hawkins, B.L. (1983a) *J. Am. Chem. Soc. 105*, 7188-7190.

Bax,A, Griffey, R.H., & Hawkins, B.L. (1983b) *J. Magn. Reson. 55*, 301-315.

Bax, A. & Grzesiek, S. (1993) *Acc. Chem. Res. 26*, 131-138.

Bax, A., Sparks, S.W., & Torchia, D.A. (1988) *J. Am. Chem. Soc. 110*, 7926-7927.

Berger, S. (1978) *Tetrahedron 34*, 3133-3136.

Berger, A., Loewenstein, A., & Meiboom, S. (1959) *J. Am. Chem. Soc. 81*, 62-67.

Binsch, G., Lambert, J.B., Roberts, B.W., & Roberts, J.D. (1964) *J. Am. Chem. Soc. 86*, 5564-5570.

Blake, P.R., Park, J.B., Zhou, Z.H., Hare, D.R., Adams, M.W.W., & Summers, M.F. (1992) *Protein Science 1*, 1508-1521.

Bodenhausen, G., Freeman, R., & Turner, D.L. (1977) *J. Magn. Reson. 27*, 511-514.

Bodenhausen, G. & Ruben, O.J. (1980) *Chem. Phys. Lett. 69*, 185-189.

Bodenhausen, G. & Turner, D.L. (1980) *J. Magn. Reson. 41*, 200-205.

Boelens, R., Griesinger, C., Kay, L.E., Marion, D., and Zuiderweg, E.R.P. (1991) In *Computational Aspects of the Study of Biological Macromolecules by Nuclear Magnetic Resonance Spectroscopy*, Hoch, J.C., Ed., Plenum Press: New York, 127-149.

Boheim, G., Hanke, W., & Jung, G. (1983) *Biophysics of Structure and Mechanism 9*, 181-191.

Breitmaier, E. & Voelter, W. (1987) *Carbon-13 NMR Spectroscopy* 3rd Ed. VCH Publishers: New York.

Brewer, D., Mason, F.G., & Taylor, A. (1987) *Can. J. Microbiol. 33*, 619-625.

Brunger, A.T. (1992) *X-Plor 3.1 A System for X-ray Crystallography and NMR*, Yale University Press: New Haven.

Burgess, A.W. & Leach, S.J. (1973) *Biopolymers 12*, 2599-2605.

Bystrov, V.F. (1976) *Prog. NMR Spec. 10*, 41-81.

Bystrov, V.F., Gavrilov, Y.D., & Solkan, V.M. (1975) *J. Magn. Reson. 19*, 123-129.

Cantor, C.R. & Schimmel, P.R. (1980) *Biophysical Chemistry Part III: The Behavior of Biological Macromolecules*. W.H. Freeman and Co.: New York.

Cascio, M. & Wallace, B.A. (1988) *Proteins: Struct., Funct., Genet. 4*, 89-98.

Catterall, W.A. (1988) *Science 242*, 50-61.

Cavanagh, J., Fairbrother, W.J., Palmer, A.G. III, Skelton, N.J. (1996) *Protein NMR Spectroscopy, Principles and Practice*, Academic Press, Inc.: San Diego.

Chakrabartty, A., Doig, A.J., & Baldwin, R.L. (1993) *Proc. Natl. Acad. Sci. USA 90*, 11332-11336.

Connelly, G.P., Bai, Y., Jeng, M.F., & Englander, S.W. (1993) *Proteins: Struct., Funct., Genet. 17*, 87-92.

Crippen, G.M. & Havel, T.F. (1978) *Acta Cryst. A 34*, 282-284.

Davis, D.G., Agosta, W.C., & Cowburn, D. (1983) *J. Am. Chem. Soc. 105*, 6189-6190.

de Dios, A.C., Pearson, J.G., & Oldfield, E. (1993a) *Science 260*, 1491-1496.

de Dios, A.C., Pearson, J.G., & Oldfield, E. (1993b) *J. Am. Chem. Soc. 115*, 9768-9773.

de Dios, A.C. & Oldfield, E. (1994) *J. Am. Chem. Soc. 116*, 5307-5314.

Delaglio, F., Torchia, D.A., & Bax, A. (1991) *J. Biomolecular NMR 1*, 439-446.

DeMarco, A., Llinas, M., & Wuthrich, K. (1978) *Biopolymers, 17*, 2727-2742.

Dempsey, C.E. (1988) *Biochemistry 27*, 6893-6901.

Dempsey, C.E. (1992) *Biochemistry 31*, 4705-4712.

Dempsey, C.E. (1995) *J. Am. Chem. Soc. 117*, 7526-7534.

Derome, A.E. (1987) *Modern NMR Techniques for Chemistry Research* 1st Ed., Pergamon Press: Toronto.

Deslauriers, R., & Smith, I.C.P. (1980) In *Biological Magnetic Resonance*; Berliner, L.J., Reuben, J., Eds., Plenum Press: New York. 286-288.

Ditchfield, R. & McKinney, R.E. (1976) *Chem. Phys. 13*, 187-194.

Driscoll, P.C., Gronenborn, A.M., Wingfield, P.T., & Clore, G.M. (1990) *Biochemistry 29*, 4668-4682.

Eigen, M. (1964) *Angew. Chem. Int. Ed. Engl. 3*, 1-19.

Emerson, M.F. & Holtzer, A. (1965) *J. Phys. Chem. 69*, 3718-3721.

Englander, S.W., Downer, N.W., & Teitelbaum, H. (1972) *Annu. Rev. Biochem. 41*, 903-924.

Englander, S.W. & Kallenbach, N.R. (1984) *Q. Rev. Biophys. 16*, 521-655.

Englander, S.W. & Poulsen, A. (1969) *Biopolymers 7*, 379-393.

Esposito, G., Carver, J.A., Boyd, J., & Campbell, I.D. (1987) *Biochemistry 26*, 1043-1050.

Farmer, B.T.II & Venters, R.A. (1995) *J. Am. Chem. Soc. 117*, 4187-4188.

Fox, R.O. & Richards, F.M. (1982) *Nature 300*, 325-330.

Franklin, J.C., Ellena, J.F., Jayasinghe, S., Kelsh, L.P., & Cafiso, D.S. (1994) *Biochemistry 33*, 4036-4045.

Freifelder, D. (1976) *Physical Biochemistry: Applications to Biochemistry and Molecular Biology*, W.H. Freeman & Co.: San Francisco.

Galaktionov, S.G. & Marshall, G.R. (1993) *Biophys. J. 65*, 608-617.

Gellman, S.H., Dado, G.P., Liang, G., & Adams, B.R. (1991) *J. Am. Chem. Soc. 113*, 1164-1173.

Gisin, B.F., Davis, D.G., Borowski, Z.K., Hall, J.E., & Kobayashi, S. (1981) *J. Am. Chem. Soc. 103*, 6373-6377.

Glasel, J.A. (1974) *Water: A Comprehensive Treatise, Vol 1*; Franks, F., Ed., Plenum Press: New York. 215-254.

Glasoe, P. & Long, F. (1960) *J. Phys. Chem. 64*, 188-190.

Griffey, R.H., Redfield, A.G., Loomis, R.E., & Dahlquist, F.W. (1985) *Biochemistry 24*, 817-822.

Grzesiek, S., Anglister, J., Ren, H., & Bax, A. (1993) *J. Am.*

Chem. Soc. 115, 4369-4370.

Grzesiek, S., Wingfield, P., Stahl, S., Kaufman, J.D., & Bax, A. (1995) *J. Am. Chem. Soc. 117,* 9594-9595.

Grzesiek, S. & Bax, A. (1992) *J. Am. Chem. Soc. 114,* 6291-6293.

Gronenborn, A.M. & Clore, G.M. (1994) *Proteins: Structure, Function, and Genetics 19,* 273-276.

Guntert, P., Braun, W., Billeter, M., & Wuthrich, K. (1989) *J. Am. Chem. Soc. 111,* 3997-4004.

Hagler, A.T., Leiserowitz, L., & Tuval, M. (1976) *J. Am. Chem. Soc. 98,* 4600-4612.

Hall, J.E., Vodyanoy, I., Balasubramanian, T.M., & Marshall, G.R. (1984) *Biophysical J.* 45, 233-247.

Hansen, P.E. (1988) *Prog. NMR Spectrosc. 20,* 207-255.

Hansen, P.E., Kawecki, R., Krowczynski, A., & Kozerski, L. (1990) *Acta Chem. Scand. 44,* 826-832.

Hansen, P.E., Kolonicny, A., & Lycka, A. (1992) *Magn. Reson. Chem. 30,* 786-795.

Harris, P.I. & Chapman, D. (1988) *Biochim. Biophys. Acta 943,* 375-380.

Howarth, O.W. and Lilley, D.M. (1978) *Progr. NMR Spectrosc. 12,* 1-40.

Huang, H.W. & Wu, Y. (1991) *Biophys. J. 60,* 1079-1087.

Hvidt, A. (1973) In *Dynamic Aspects of Conformational Changes in Macromolecules,* Sadron, C., Ed., Holland: Reidel.

Ikura, M., Kay, L.E., & Bax, A. (1990) *Biochemistry 29,* 4659-4667.

Jackson, M. & Mantsch, H.H. (1991) *Biochim. Biophys. Acta 1118*, 139-143.

Jackson, M. & Mantsch, H.H. (1992) *Vibrational Spectrosc. 3*, 323-326.

James, T.L., Gochin, M., Kerwood, D.J., Pearlman, D.A., Schmitz, U., & Thomas, P.D. (1991) In *Computational Aspects of the Study of Biological Macromolecules by Nuclear Magnetic Resonance Spectroscopy*, Hoch, J.C., Ed., Plenum Press: New York, 331-347.

Jameson, C.J. (1980) *Bull. Magn. Reson. 3*, 3-28.

Jameson, C.J. & Osten, H.J. (1986) *Ann. Reports NMR Spectrosc. 17*, 1-78.

Jardetzky, O., Clore, G.M., Hare, D., & Torda, A. (1991) In *Computational Aspects of the Study of Biological Macromolecules by Nuclear Magnetic Resonance Spectroscopy*, Hoch, J.C., Ed., Plenum Press: New York, 375-389.

Jeener, J. (1971) *Ampere International Summer School*, Basko Polje, Yugoslavia.

Jeffrey, G.A. & Saenger, W. (1991) *Hydrogen Bonding in Biological Structures*, Springer-Verlag, New York.

Jencks, W.P. & Regenstein, J. (1976) In *CRC Handbook of Biochemistry and Molecular Biology - Physical and Chemical Data I*, 3rd Ed., Fasman, G.D., Ed., CRC Press Inc.: Ohio, 305-351.

Jiao, D., Barfield, M., & Hruby, V.J. (1993) *J. Am. Chem. Soc. 115*, 10883-10887.

Jung, G., Bosch, R., Katz, E., Schmitt, H., Voges, K.P., & Winter, W. (1983) *Biopolymers 22*, 241-246.

Juranic, N., Ilich, P.K., & Macura, S. (1995) *J. Am. Chem. Soc. 117*, 405-410.

Kakuda, Y., Perry, N., & Mueller, D>D. (1971) *J. Am. Chem. Soc. 93*, 5992-5998.

Kaptein, R., Boelens, R., Scheek, R.M., & van Gunsteren, W.F. (1988) *Biochemistry 27*, 5389-5395.

Katz, B. (1966) *Nerve, Muscle, and Synapse*, McGraw-Hill Book Co.: Toronto.

Kelsh, L.P., Ellena, J.F., & Cafiso, D.S. (1992) *Biochemistry 31*, 5136-5144.

Khaled, M.A., Sugano, H., and Urry, D.W. (1979) *Biochim. Biophys. Acta 577*, 273-284.

Klotz, I.M. & Frank, B.H. (1965) *J. Am. Chem. Soc. 87*, 2721-2728.

Kopple, K.D., Ohnishi, M., & Go, A. (1969) *J. Amer. Chem. Soc. 91*, 4264-4272.

Kuntz, I.D., Crippen, G.M., & Kollman, P.A. (1979) *Biopolymers 18*, 939-957.

Latorre, R. & Alvarez, O. (1981) *Physiol. Rev. 61*, 78-150.

Le, H., Pearson, J.G., de Dios, A.G., & Oldfield, E. (1995) *J. Amer. Chem. Soc. 117*, 3800-3807.

Lee, B. & Richards, F.M. (1971) *J. Mol. Biol. 55*, 379-400.

Leibfritz, D., Mayr, W., Oekonomopulos, R., & Jung, G. (1978) *Tetrahedron 34*, 2045-2050.

Leichtling, B.H. & Klotz, I.M. (1966) *Biochemistry 5*, 4026-

4037.

Levy, G.C. & Lichter, R.L. (1979) *Nitrogen-15 Nuclear Magnetic Resonance Spectroscopy*, John-Wiley & Sons: New York.

Linderstrom-Lang, K.U. (1955) *Spec. Publ.-Chem. Soc. 2*, 1-20.

Linderstrom-Lang, K.U. & Schellman, J.A. (1959) *Enzymes*, 2nd Ed. 1, 443-510.

Lippert, E. (1976) in *The Hydrogen Bond/I Theory*, Schuster, P., Zundel, G., & Sandorfy, C. Eds. North-Holland Publishing Co.: New York, 1-22.

Llinas, M., Wilson, D.M., & Neilands, J.B. (1977) *J. Am. Chem. Soc. 99*, 3631-3637.

Mandels, G.R. & Darby, R.T. (1953) *J. Bact. 65*, 16-26.

Marion, D., Driscoll, P.C., Kay, L.E., Wingfield, P.T., Bax, A., Gronenborn, A.M., & Clore, G.M. (1989) *Biochemistry 28*, 6150-6156.

Marion, D. & Wuthrich, K. (1983) *Biochem. Biophys. Res. Commun. 113*, 967-974.

Markley, J.L., Putter, I., & Jardetzky, O. (1968) *Science 161*, 1249-1250.

Martin, R.H., Morau, J., & Defay, N. (1974) *Tetrahedron 30*, 179-185.

Mathew, M.K. & Balaram, P. (1983) *FEBS Letters 157*, 1-5.

Matthews, G.G. (1991) *Cellular Physiology of Nerve and Muscle*, Blackwell Scientific Publications: Boston.

Means, G.E. & Feeney, R.E. (1971) *Chemical Modification of Proteins*, Holden-Day, Inc.: Toronto.

Meyer, C.E. & Reusser, F. (1967) *Experentia 23*, 85-86.

Molday, R.S., Englander, S.W., & Kallen, R.G. (1972) *Biochemistry 11*, 150-158.

Molday, R.S. & Kallen, R.G. (1972) *J. Am. Chem. Soc. 94*, 6739-6745.

Montelione, G.T., Winkler, M.E., Rauenbuehler, P., & Wagner, G. (1989) *J. Magn. Reson. 82*, 198-204.

Mooberry, E.S., Oh, B., & Markley, J.L. (1989) *J. Magn. Reson. 85*, 147-149.

Moore-Landeker, E. (1990) *Fundamentals of the Fungi* 2nd Ed., Prentice-Hall, Inc., New Jersey.

Mueller, P. & Rudin, D.O. (1968) *Nature 217*, 713-719.

Muller, N. & Reiter, R.C. (1965) *J. Chem. Phys. 42*, 3265-3269.

Myers, D. (1992) *Surfactant Science and Technology* 2nd ed. VCH Publishers, Inc.: New York, 155-158.

Neuhaus, D. & Williamson, M.P. (1989) *The Nuclear Overhauser Effect - Structural and Conformational Analysis*, VCH Publishers, Inc.: New York.

Oakes, J. (1974) *J. Chem. Soc. Faraday Trans. I 70*, 2200-2209.

Ohnishi, M. & Urry, D.W. (1969) *Biochem. Biophys. Res. Commun. 36*, 194-201.

O'Neil, J.D.J. & Sykes, B.D. (1989) *Biochemistry 28*, 699-707.

Pardi, A., Billeter, M., & Wuthrich, K. (1984) *J. Mol. Biol. 180*, 741-751.

Pardi, A., Wagner, G., & Wuthrich, K. (1983) *Eur. J. Biochem.*

137, 445-454.

Plateau, P. & Gueron, M. (1982) *J. Am. Chem. Soc. 104*, 7310-7311.

Perrin, C.L. (1994) *Science 266*, 1665-1668.

Perrin, C.L. & Arrhenius, G.M.L. (1982) *J. Am. Chem. Soc. 104*, 6693-6696.

Petros, A.M., Mueller, L., & Kopple, K.D. (1990) *Biochemistry 29*, 10041-10048.

Poppe-Schriemer, N. (1995) Ph.D. Thesis, University of Manitoba.

Ramsey, N.F. (1952) *Phys. Rev. 87*, 1075-1079.

Reuben, J.(1986) *J. Am. Chem. Soc. 108*, 1735-1738.

Reuben, J.(1987) *J. Am. Chem. Soc. 109*, 316-321.

Reusser, F. (1967) *J. Biol. Chem. 242*, 243-247.

Rindfleisch, H. & Kleinkauf, H. (1976) *FEBS Lett. 62*, 276-280.

Robertson, A.D. & Baldwin, R.L. (1991) *Biochemistry 30*, 9907-9914.

Rohl, C.A. & Baldwin, R.L. (1994) *Biochemistry 33*, 7760-7767.

Rohl, C.A., Scholtz, J.M., York, E.J., Stewart, J.M., & Baldwin, R.L. (1992) *Biochemistry 31*, 1263-1269.

Rohling, C.M., Allen, L.C., & Ditchfield, R. (1983) *J. Chem. Phys. 79*, 4958-4966.

Sailer, M., Helms, G.L., Henkel, T., Niemczura, W.P., Stiles, M.E., & Vederas, J.C. (1993) *Biochemistry 32*, 310-318.

Schmitt, H. & Jung, G. (1985) *Liebigs Ann. Chem. 1985*, 321-344.

Shaka, A.J., Keeler, J., Frenkiel, T., & Freeman, R. (1983) *J. Magn. Reson. 52*, 334-338.

Shaka, A.J., Barker, P.B., & Freeman, R. (1985) *J. Magn. Reson. 64*, 547-552.

Shalongo, W., Dugad, L., & Stellwagen, E. (1994) *J. Am.Chem. Soc. 116*, 2500-2507.

Shalongo, W., Dugad, L., & Stellwagen, E. (1994) *J. Am. Chem. Soc. 116*, 8288-8293.

Shon, K. & Opella, S.J. (1989) *J. Magn. Reson. 82*, 193-197.

Slomczynska, U., Zabrocki, J., Kaczmarek, K., Leplawy, M.T., Beusen, D.D., & Marshall, G.R. (1992) *Biopolymers 32*, 1461-1470.

Solomon, I. (1955) *Phys. Rev. 99*, 559-565.

Song, S.C., Akaike, T., & Hatanaka, K. (1994) *Polymer Journal 26*, 387-391.

Sorensen, O.W., Eich, G.W., Levitt, M.H., Bodenhausen, G., & Ernst, R.R. (1984) *Prog. NMR Spectrosc. 16*, 163-192.

Spera, S. & Bax, A. (1991) *J. Am. Chem. Soc. 113*, 5490-5492.

Spyracopoulos, L. (1996) Ph.D. Thesis, University of Manitoba.

Spyracopoulos, L. & O'Neil, J.D.J. (1994) *J. Am. Chem. Soc. 116*, 1395-1402.

Sternberg, U. & Brunner, E. (1994) *J. Magn. Reson. A 108*, 142-150.

Stothers, J.B. (1972) *Carbon-13 NMR Spectroscopy Vol. 24*, Academic Press: New York.

Stuhmer, W. (1991) *Annu. Rev. Biophys. Chem. 20*, 65-78.

Sulzbach, H.M., Schleyer, P.R., & Schaefer, H.F. (1995) *J. Am. Chem. Soc. 117*, 2632-2637.

Tonelli, A.E. (1984) *Biopolymers 23*, 819-829.

Tuchsen, E. & Hansen, P.E. (1988) *Biochemistry 27*, 8568-8576.

Tuchsen, E. & Woodward, C. (1985) *J. Mol. Biol. 185*, 421-430.

Urry, D.W., Mitchell, L.W., and Ohnishi, T. (1974) *Proc. Nat. Acad. Sci. USA 71*, 3265-3269.

Urry, D.W., Mitchell, L.W., and Ohnishi, T. (1975) *Biochim. Biophys. Acata 393*, 296-306.

Venters, R.A., Calderone, T.L., Spicer, L.D., & Fierke, C.A. (1991) *Biochemistry 30*, 4491-4494.

Wagner, G. (1983) *Q. Rev. Biophys. 16*, 1-57.

Wagner, G. (1990) *Prog. Nucl. Magn. Reson. Spectrosc. 22*, 101-139.

Wagner, G. & Wuthrich, K. (1982) *J. Mol. Biol. 160*, 343-361.

Wagner, G., Hyberts, S.G., & Havel, T.F. (1992) *Annu. Rev. Biophys. Biomol. Struct. 21*, 167-198.

Walter, J.A. & Wright, J.L.C. (1979) *Tetrahedron Lett. 41*, 3909-3912.

Weast, R.C. (1987) Ed. *CRC Handbook of Chemistry and Physics, 1st Student Ed.*, CRC Press: Florida, D103-D104.

Willker, W. & Leibfritz, D. (1992) *J. Magn. Reson. 99*, 421-425.

Wishart, D.S. & Sykes, B.D. (1994) *J. Bio. NMR 4*, 171-180.

Wishart, D.S., Sykes, B.D., & Richards, F.M. (1991) *J. Mol. Biol. 222*, 311-333.

Wishart, D.S., Sykes, B.D., & Richards, F.M. (1992)

Biochemistry 31, 1647-1651.

Woodward, C.K. (1977) *J. Mol. Biol. 11*, 509-515.

Woodward, C.K. & Hilton, B.D. (1979) *A. Rev. Biophys. Bioengng 8*, 99-127.

Woolley, G.A. & Wallace, B.A. (1993) *Biochemistry 32*, 9819-9825.

Wuthrich, K. (1986) *NMR of Proteins and Nucleic Acids*, John-Wiley and Sons: New York.

Yee, A.A. (1991) M.Sc. Thesis, University of Manitoba.

Yee, A.A. & O'Neil, J.D.J. (1992) *Biochemistry 31*, 3135-3143.

Yee, A.A., Babiuk, R.P., & O'Neil, J.D.J. (1995) *Biopolymers 36*, 781-792.

Zhang, Y., Paterson, Y., & Roder, H. (1995) *Protein Sci. 4*, 804-814.